

6.3.3 Drift-Scale Unsaturated Zone Flow

Water contacting DSs and WPs is expected to originate from two sources: (1) seepage of groundwater from the UZ above the repository into the emplacement drifts (SNL 2007 [DIRS 181244], Section 1) and (2) water-vapor condensate dripping from the walls of the drifts (SNL 2007 [DIRS 181648] Sections 6.3, 8.3, 6[a], and 8[a]). Percolation flux at the base of the PTn is used as the source of water for both drift seepage and drift-wall condensation. However, in this analysis no water balance is applied between the percolation flux, drift seepage, and drift-wall condensation. Note that even though the drift seepage and drift-wall condensation could possibly add up to more than the percolation flux, the approach chosen of not applying a water balance is considered conservative. The TSPA-LA Model calculates drift seepage and drift-wall condensation flow rates using the Drift Seepage Submodel (Section 6.3.3.1) and the Drift Wall Condensation Submodel (Section 6.3.3.2), respectively. These two flow rates are combined in the EBS Flow Submodel (Section 6.3.6) to yield a total dripping rate. Section 6.3.3.1 discusses the Drift Seepage Submodel (SNL 2007 [DIRS 181244], Section 6 and Section 6[a]), and Section 6.3.3.2 presents the Drift Wall Condensation Submodel (SNL 2007 [DIRS 181648], Section 6 and Section 6[a]).

6.3.3.1 Drift Seepage

Drift seepage refers to the flow of liquid water from the UZ above the repository into waste emplacement drifts. The Drift Seepage Submodel calculates two quantities: (1) the fraction of WP locations that experience seepage and (2) the average seepage flow rate for WP locations that have seepage (Section 6.3.3.1.3). The calculations are performed for each WP type in each percolation flux subregion (MSTHM Abstraction, Section 6.3.2.2.1). Figure 6.3.3-1 illustrates the flow of information for the Drift Seepage (SNL 2007 [DIRS 181244], Section 6) and Drift Wall Condensation Submodels (SNL 2007 [DIRS 181648], Section 6). Figure 6.3.3-2 shows the connections between the Drift Seepage Submodel and the EBS Flow Submodel (Section 6.3.6). Figure 6.3.3-2 shows inputs to and outputs from the Drift Seepage Submodel and indicates the principal features of the Drift Seepage Submodel and the foundation for confidence in the model.

6.3.3.1.1 Conceptual Model

Numerical modeling, natural analogues, and field tests summarized in (SNL 2007 [DIRS 181244], Sections 6.4.1, 6.4.2, 6.4.3, 7.3.1, and 7.3.2) indicate that seepage flux into emplacement drifts will be less than the local percolation flux. This difference results from two main processes: (1) the formation of capillary barriers at drift walls that are active during the thermal and ambient postclosure periods, and (2) the formation of dry-out zones helping to prevent percolation from reaching the repository during the thermal period. The effectiveness of these processes depends on the strength of the capillary pressure in the fractures close to the drift, the host rock's permeability close to the drift, the local percolation flux above the drift, the temperature of the rock near the drift wall, and the shape of the drift opening.

Figure 6.3.3-3 shows TH effects and the dry-out zone in the vicinity of the emplacement drifts due to repository heating. As water approaches a waste emplacement drift, conditions near the drift wall affect the amount of water that eventually seeps into the drifts. For preclosure conditions, the water may first encounter a dry-out zone caused by drift ventilation. During the

first several hundreds of years of the postclosure period, the dry-out zone may also develop from an increase in temperature due to decay heat from the emplaced waste, and where temperatures are high enough, may reach several meters from the drift wall due to boiling of rock water in the drift vicinity. Under boiling conditions, water will not enter the emplacement drifts (BSC 2005 [DIRS 172232], Section 6.1.2). The dry-out zone, indicated by the red shading around the drifts, is shown on Figure 6.3.3-3. The zone around the emplacement drift affected by TH processes is characterized by boiling, vapor transport, condensation, and migration of water back toward the heat source, either by capillary forces or gravity drainage (SNL 2007 [DIRS 181244], Section 6.3.2, p. 6-12). If liquid water approaches the immediate vicinity of the drift wall after the repository cools, a zone of increased saturation is expected to develop as a result of the capillary-barrier effect of the drift opening (Figure 6.3.3-4). Most of this water cannot seep into the drift because of capillary suction, which retains water in the pore space of the rock. If the permeability and capillarity of the fracture network are sufficiently high, some or all of the water is diverted around the drift under partially saturated conditions. Locally, however, the water potential in the formation could become great enough to allow seepage from the formation into the drifts, as described in *Seepage Model for PA Including Drift Collapse* (BSC 2004 [DIRS 167652], Section 6.2.1).

Emplacement drifts may degrade with time as a result of thermal stress, seismic ground motion, and time-dependent degradation of rock strength. These effects may lead to partial or complete drift collapse, with rock material filling the enlarged drifts and changing their shape and size. Depending upon the intensity of these effects, damage to drifts may be small, with local rockfall at the ceiling of otherwise intact drift openings, or in extreme cases, may result in partial or complete drift collapse, with rubble rock material filling the enlarged drifts. These changes alter the potential for drift seepage (SNL 2007 [DIRS 181244], Sections 6.2[a], 6.3.1 and 6.3.2). Local breakouts in the drift ceiling may also lead to geometry changes that may reduce or prevent flow diversion around the drifts and thus increase the seepage into drifts. The larger size and potentially altered shape of collapsed drifts can also bring about reduction in flow diversion. In addition, the larger footprint of collapsed drifts causes an increase in the percolation flux arriving at the drifts, which increases seepage into the drifts. Further, drift degradation may lead to fracture dilation that would promote flow diversion around the drifts, but at the same time decrease fracture capillary strength and cause less flow diversion around the drifts. Thus, the seepage into a collapsed drift may be different from that into an intact drift.

6.3.3.1.2 TSPA-LA Model Abstraction

As described in Section 6.1.4.3, water seepage into emplacement drift segments on the scale of a WP is a process that is modeled outside of the TSPA-LA Model, and the results are then abstracted (SNL 2007 [DIRS 181244]) for use in the TSPA-LA Model simulations. The abstracted results are based on drift-seepage simulations conducted for both ambient (BSC 2004 [DIRS 167652]) and thermal periods (BSC 2005 [DIRS 172232]).

The Drift Seepage Abstraction calculations differ for collapsed and noncollapsed drifts, as explained below. Drift collapse is not considered in Nominal or Early Failure Modeling Cases. In the 1,000,000 year Seismic GM Modeling Case, drift collapse can occur in both lithophysal and nonlithophysal units. Partial collapse is considered in the lithophysal units, by comparing the cumulative rubble volume generated by seismic events to a lower and an upper threshold to

determine whether to: (1) use the intact seepage model, (2) interpolate between intact-drift seepage model and collapsed drift seepage model, or (3) use the collapsed-drift seepage model (SNL 2007 [DIRS 181244], Section 6.2.2[a]). In the nonlithophysal units, once a specified degree of drift collapse has occurred, the intact-drift seepage model is no longer appropriate. The cumulative rubble volume generated by seismic events is compared to a threshold rubble volume to determine whether: (1) the intact-drift seepage model is used or (2) the percolation fluxes are used (SNL 2007 [DIRS 181244], Sections 6.2.3[a]). For the Seismic FD Modeling Case drift collapse in lithophysal units and drift degradation in the nonlithophysal units always occurs at the same time as an event. After an event, seepage rates in lithophysal units are estimated using the collapsed-drift seepage model (SNL 2007 [DIRS 181244], Section 6.2.2[a]). In nonlithophysal units, seepage rates per unit area are set equal to percolation fluxes after an event (SNL 2007 [DIRS 181244]). Drift collapse is not considered for the Igneous Scenario Class, as the drifts are filled with basalt by the intrusive event. For a detailed understanding of the rationale for the abstraction decisions, refer to *Abstraction of Drift Seepage* (SNL 2007 [DIRS 181244], Sections 6.5.1.5 and 6.5.1.7).

Ambient seepage process model simulations were conducted for a range of representative local percolation fluxes ($q_{perc,ff}$), ranges of local permeability (k) and capillary strength ($1/\alpha$), nondegraded and degraded drift profiles and multiple realizations of the small-scale heterogeneous fracture-permeability field (BSC 2004 [DIRS 167652], Sections 6.3, 6.4, and 6.6). The local percolation fluxes ($q_{perc,ff}$) are derived from the fluxes at the base of the PTn from the MSTHM Abstraction (q_{perc}) (Section 6.3.2) by multiplication with flow-focusing factors (f_{ff}). The flow-focusing factors account for intermediate-resolution heterogeneity (SNL 2007 [DIRS 181244], Section 6.6.5.2) (on the spatial resolution of a few drift diameters) that is not accounted for in the MSTHM Process Model. In addition, it is possible that the initially circular-shaped emplacement drifts degrade with time principally as a result of seismic ground motion. These changes affect the potential for drift seepage (SNL 2007 [DIRS 181244], Sections 6.2[a], 6.3.1 and 6.3.2). The Seepage Model for Performance Assessment simulations (SNL 2007 [DIRS 181244], Section 6.4.2) produce, for both nondegraded and degraded drifts, response surfaces in the form of look-up tables for a seepage rate into a 5.1-m long drift section and a seepage rate standard deviation (SD) that are functions of $q_{perc,ff}$, $\log(k)$, and $1/\alpha$ (DTN: LB0702PASEEP01.001_R0 [DIRS 179511]). Note that the output from *Seepage Model for PA Including Drift Collapse* (BSC 2004 [DIRS 167652]) is extended in *Abstraction of Drift Seepage* (SNL 2007 [DIRS 181244], Section 6.1[a]) and its output DTN: LB0702PASEEP01.001 [DIRS 179511].

Probability distributions were developed to represent the spatial variability in flow-focusing factor (f_{ff}), $\log(k)$, and $1/\alpha$, and the uncertainty in $\log(k)$ and $1/\alpha$ (SNL 2007 [DIRS 181244], Section 6.3[a] and Section 6.7.1.1).

Four different methods were identified to derive statistical parameters that describe spatial variability and uncertainty in $1/\alpha$ with respect to the geologic units present around the drifts (SNL 2007 [DIRS 181244], Sections 6.3[a] and 6.6.2.2). However, as discussed in *Abstraction of Drift Seepage*, the overall seepage results do not significantly differ between methods (SNL 2007 [DIRS 181244], Section 6.8.2). Therefore, the probability distributions for spatial variability and uncertainty in $1/\alpha$, defined in Table 6.3.3-1, are used (DTN: LB0407AMRU0120.001_R0 [DIRS 173280]). Spatial variability and uncertainty for

$\log(k)$ are dependent on the geologic units present around the drifts. The distributions for spatial variability and uncertainty in $\log(k)$ in the nonlithophysal and lithophysal repository units are defined in Table 6.3.3-2. Local percolation flux values in the vicinity of the drifts are determined from percolation fluxes at the base of the PTn. These are provided at each repository subdomain, r , by the MSTHM Abstraction which obtains the information from the Site-Scale UZ Flow Process Model (Figure 6.3.1-1), as described in Section 6.3.2. The percolation fluxes in the UZ are time dependent (represented by four different climate periods), spatially variable (because of nonuniform infiltration and nonuniform flow in the UZ), and uncertain (as represented by four different infiltration cases) as discussed in Section 6.3.1. As discussed in (SNL 2007 [DIRS 181244], Section 6.5.1.1), these percolation fluxes, q_{perc} , are adjusted for intermediate-scale heterogeneity, which is not represented in the distributions of fluxes provided by the MSTHM Abstraction. This adjustment uses a spatial distribution of flow-focusing factors (f_{ff}). Multiplication of the q_{perc} from the MSTHM Abstraction by the f_{ff} gives the local percolation flux, $q_{perc,ff}$, to be used in the TSPA-LA Model calculations. The spatial variability distribution for the flow-focusing factor is defined as a cumulative probability distribution in the following form (SNL 2007 [DIRS 181244], Section 6.7.1.1 and DTN: LB0407AMRU0120.001_R0 [DIRS 173280]).

The equation can be written as:

$$Y = -0.3137 f_{ff}^4 + 5.4998 f_{ff}^3 - 35.66 f_{ff}^2 + 102.3 f_{ff} - 11.434 \quad (\text{Eq. 6.3.3-1})$$

where Y is the cumulative probability in percent (SNL 2007 [DIRS 181244], Section 6.7.1.1).

The values of local percolation flux ($q_{perc,ff}$), the sampled values of local permeability ($\log(k)$), and capillary strength parameters (l/α) are used to interpolate from the look-up tables for the mean seepage rate into a 5.1-m-long drift section and the seepage rate SD. The value of SD is used to account for uncertainty in the estimation of seepage rates.

The estimation uncertainty in the calculated seepage rates is accounted for by a uniform distribution with a mean of zero and a range defined by the seepage rate SD (-1.7321 SD, 1.7321 SD) (SNL 2007 [DIRS 181244], Section 6.7.1.1 and DTN: LB0407AMRU0120.001_R0 [DIRS 173280]).

For noncollapsed drifts, the ambient seepage is increased by 20 percent to account for additional uncertainty due to partial drift degradation, such as breakouts in the drift ceiling that do not lead to complete drift collapse. However, for collapsed drifts, this increase is not implemented because this extreme degree of damage and its impact on seepage is represented by the seepage response surface for a collapsed drift, which includes sufficient conservatism (SNL 2007 [DIRS 181244], Section 6.7.2).

Analyses performed with the TH Seepage Process Model for noncollapsed drifts have shown that thermal seepage (seepage that is influenced by heat generated by the WP) will always be less than ambient seepage and that thermal seepage never occurs when there is boiling in the rock close to the emplacement drifts (BSC 2005 [DIRS 172232], Section 6.2.4). The recommended abstraction sets the thermal seepage equal to zero during the period of above-boiling temperatures at the crown of the drift. The threshold temperature that defines when seepage can

occur is set to 100°C (SNL 2007 [DIRS 181244], Sections 6.5.2.2 and 6.7.1.2). After the temperature falls below 100°C, thermal seepage is set equal to the estimated ambient seepage.

For collapsed drifts, the thermal seepage abstraction conservatively sets the seepage equal to the estimated ambient seepage at all times in the TSPA period. This is based on the results of analyses that found that with the expanded drift opening, the rock temperature at the crown, is always below 100°C, or nearly so (SNL 2007 [DIRS 181244], Section 6.4.3.4). Thus there is no vaporization barrier in the intact rock to prevent water flow into a rubble-filled drift (SNL 2007 [DIRS 181244], Section 6.5.3).

For the Igneous Intrusion Modeling Case, the abstraction considers setting the seepage percentage to 100 percent, where the seepage rate is equal to the local percolation rate (L/t) at the base of the PTn multiplied by the footprint area (L²) of the considered drift segment. It is applied from the time at which the igneous event occurs.

6.3.3.1.3 TSPA-LA Model Implementation

The TSPA-LA Model implementation of drift seepage is primarily accomplished through the use of an external DLL. When drift-seepage submodel calculations are required by the TSPA-LA Model, the Seepage DLL (STN: 11076-1.3-00 [DIRS 181058]) is called, and a total of 35 inputs are passed by the TSPA-LA Model to the Seepage DLL (refer to Table 6.3.3-3 for a list of these inputs).

The output of the Seepage DLL is a set of tables of seepage flow rate versus time. Each table corresponds to a WP type and percolation flux subregion (e.g., CSNF subregion 1; see Section 6.3.2.2.1 for a description of how the subregions are defined). The timesteps in the tables are related to the climate periods and to the timesteps used in the MSTHM. These tables are then interpolated to determine the seepage flow rate at each TSPA-LA Model timestep. Note, the tables were developed for two units only, the Ttptll and Ttptmn units (BSC 2004 [DIRS 167652], Section 1). Based on current repository design, a small fraction of the emplacement drifts would also be located in the Ttptul and Ttptln units at Yucca Mountain. As noted in *Abstraction of Drift Seepage* (SNL 2007 [DIRS 181244], Sections 6.3.1 and 6.6.4), the Ttptul unit makes up about 4.5 percent and the Ttptln unit makes up about 2.6 percent of the repository area. In the TSPA-LA analysis the tables developed for the Ttptll and Ttptmn units are also applied to the Ttptul and Ttptln units. In addition, because of a paucity of data for the Ttptul and Ttptln units, capillary strength and permeability parameter distributions from the Ttptll and Ttptmn units are used for the Ttptul and Ttptln units, respectively.

In addition to these inputs passed directly from TSPA-LA Model to the Seepage DLL, the Seepage DLL reads a set of PREWAP (STN: 10939-1.1-00 [DIRS 181053]) output files and a set of seepage look-up tables. The PREWAP output files (DTN: MO0707PREWAPMS.000_R0 [DIRS 183002]) contain the output results from the MSTHM in a format that can be used by both the WP and DS Degradation Submodels (Section 6.3.5) for WP and DS failure calculations and by the Seepage DLL. There are 120 PREWAP files, one for each of the five percolation subregions, two WP types, four infiltration scenarios, and three TH uncertainty cases. The inputs that the Seepage DLL reads from these files are the percolation flux at the base of the PTn at each MSTHM subdomain location, the drift-wall temperature for each WP at that subdomain

location, and the fraction of lithophysal rock at that location. Two files containing seepage look-up tables, one for noncollapsed drifts and one for collapsed drifts, are provided by DTN: LB0702PASEEP01.001_R0 [DIRS 179511]. These files contain three-dimensional tables of mean seepage rate and seepage rate SD as functions of percolation flux, capillary strength, and fracture permeability.

The Seepage DLL uses these inputs to implement the calculations outlined in *Abstraction of Drift Seepage* (SNL 2007 [DIRS 181244], Section 6.7.1) to obtain the fraction of WPs that is expected to experience seepage and the seepage rate (m^3/yr per WP) onto those WPs that experience seepage. The DLL also adjusts the calculated ambient seepage rates for thermal and drift degradation effects, as necessary, as follows: (1) the ambient seepage rates are increased by 20 percent to account for drift degradation for the noncollapsed drift locations, and (2) seepage is set to zero for noncollapsed drift locations if the drift-wall temperature exceeds 100°C . The results of the Seepage DLL's seepage rate calculations (seepage rate versus time) are passed to the TSPA-LA Model in the form of 10 one-dimensional tables, one table for each WP type in each percolation subregion. The DLL also passes to GoldSim the fraction of WPs that experience seepage for each percolation subregion and WP type, and the fraction of each percolation subregion that is in nonlithophysal rock. The EBS Flow Submodel (Section 6.3.6) uses the results for seepage rate, the fraction of WPs that experiences seepage, and the fraction of each percolation subregion that is in nonlithophysal rock. The Waste Package Localized Corrosion Submodel uses the results for the fraction of WPs that experiences seepage. The Drift Wall Condensation Submodel (Section 6.3.3.2) uses the results for the fraction of each percolation subregion that is in nonlithophysal rock.

The remainder of this section describes the drift-seepage implementation in more detail. Figure 6.3.3-5 illustrates the procedure for the probabilistic calculation of seepage in the TSPA-LA Model. The seepage DLL is applied for each WP (i.e., six CSNF or two CDSP WPs; Section 6.3.2.3) at each of the 3,264 repository subdomains, r , identified by the MSTHM Abstraction comprehensive data set (Engineered Barrier System Thermal-Hydrologic Environment, Section 6.3.2). For each WP at each repository subdomain, r , the calculation of drift seepage involves two main steps: (1) evaluate ambient seepage rate from seepage look-up tables, and (2) adjust ambient seepage rate for thermal and drift degradation effects. As shown on Figure 6.3.3-5, these two steps are implemented for each probabilistic TSPA-LA Model realization and repository location.

Step 1: Ambient Seepage—Step 1 involves three main activities. The first activity deals with random sampling of spatial variability and uncertainty distributions, and the application of spatial variability and uncertainty to arrive at values for the capillary-strength parameter ($1/\alpha$), fracture permeability ($\log(k)$), and local percolation flux ($q_{perc,ff}$). The sampling and calculations are performed as follows:

- The uncertainty distributions specified in Tables 6.3.3-1 and 6.3.3-2 are sampled once per TSPA-LA Model realization, R , to determine $\Delta\log(k)$ and $\Delta 1/\alpha$. The seepage rate uncertainty is sampled from a uniform distribution. At each subdomain, r , the following steps are completed:

- The spatial variability distributions specified in Tables 6.3.3-1 and 6.3.3-2 and Equation 6.3.3-1 are sampled randomly for $\log(k)$, $1/\alpha$, and f_{ff} at the subdomain, r , for each WP (six CSNF and two CDSP WPs).
- The $\log(k)$ and $1/\alpha$ values are adjusted, using the values for $\Delta\log(k)$ and $\Delta 1/\alpha$ that are sampled in each realization, R , to arrive at the values of $\log(k)$ and $1/\alpha$ that account for both spatial variability and uncertainty.
- The mountain-scale percolation flux at each subdomain, r , for each WP (six CSNF and two CDSP WPs) (from the MSTHM Abstraction as obtained from the Site-Scale UZ Flow Process Model), provided by the PREWAP_LA files, is adjusted by multiplying it by f_{ff} to yield a local percolation flux, $q_{perc,ff}$.

It is possible, but unlikely, that the parameter ranges for $1/\alpha$, $\log(k)$, and $q_{perc,ff}$ covered by the seepage look-up tables are exceeded for parameter values sampled from the unbounded distributions of permeability and percolation flux. To avoid sampling values outside the parameter's ranges, the following constraints on $1/\alpha$, $\log(k)$, and $q_{perc,ff}$ (based on the range limits presented in *Abstraction of Drift Seepage* (SNL 2007 [DIRS 181244], Section 6.1[a]), are imposed:

- If $1/\alpha$ is larger than 1,000 Pa, set it to 1,000 Pa.
- If local percolation flux is less than 0.01 mm/yr, set it to 0.01 mm/yr.
- If local percolation flux is more than 5,000 mm/yr, set it to 5,000 mm/yr.
- If $\log(k)$ is less than -14, set it to -14.
- If $\log(k)$ is larger than -10, set it to -10.

The second activity in Step 1 is to extract (by linear interpolation between the three independent input parameters) at each subdomain, r , the ambient mean seepage rate and SD of ambient seepage rate from the appropriate seepage look-up tables originally from the *Seepage Model for Performance Assessment Including Drift Collapse* (BSC 2004 [DIRS 167652], Section 6.6.1) but extended as noted in *Abstraction of Drift Seepage* [DIRS 181244], Section 6.1[a]. The lookup tables are contained in the files *ResponseSurfaceSMPA_Collapsed_ExtendedFlux.dat* and *ResponseSurfaceSMPA_ExtendedFlux.dat* (DTN: LB0702PASEEP01.001_R0 [DIRS 179511]). The TSPA-LA Model selects the appropriate look-up tables, depending on the host geologic unit and the selected Scenario Class. For the Nominal Scenario Class, look-up tables for noncollapsed drifts are selected because extensive roof collapse is not expected. The selection of the appropriate table for the Seismic Scenario Class depends on the character of the host-rock unit (SNL 2007 [DIRS 181244], Sections 6.2.2[a] and 6.2.3[a]). In the lithophysal zone, the appropriate tables correspond to the choice of noncollapsed or collapsed drift look-up tables. In the nonlithophysal zone, the appropriate tables correspond to the choice of the noncollapsed table or percolation rates (100 percent seepage). In the Seismic Scenario Class, multiple implementations of the Seepage DLL are utilized to simulate the effects of drift collapse (see Step 4).

The third activity in Step 1 is to calculate the local seepage rate; that is, the volumetric flow rate. Note that for this calculation, the density of water is assumed to be 960 kg/m^3 for water at 100°C and 1 atm (Incropera and DeWitt 2002 [DIRS 163337], Appendix A.6). The calculation

considers a footprint of 5.1 m × 5.5 m, representing a WP length of 5.1 m (SNL 2007 [DIRS 181244], Sections 6.7.1 and 4.1[a] and (BSC 2004 [DIRS 167652], Section 6.3.1)), and a drift diameter of 5.5 m (SNL 2007 [DIRS 181244], Section 6.4.2.1 and (BSC 2004 [DIRS 167652], Section 6.3.1)). The results, obtained from DTN: LB0310AMRU0120.002_R0 [DIRS 166116], are the mean seepage values and SDs. The SDs represent the estimation of uncertainty in the seepage results and are different for each sampled set of parameters. The mean seepage rates are, therefore, adjusted by applying a uniform distribution, with a mean of zero and upper and lower bounds, respectively, of +/-1.7321 times the seepage rate SD (SNL 2007 [DIRS 181244], Section 6.5.1.3). The sampled value from this uniform distribution is then added to the mean seepage value to obtain the ambient seepage rate. Note that the WP length of 5.1 m is based upon an average WP length of 5.0 m, which was the rounded length of the 44-BWR and 21-PWR WPs considered in previous designs (SNL 2007 [DIRS 181244], 4.1[a]). The additional 0.1 m represents 0.1-m spacings between packages. The 5.1 m length was the basis for the model domain length used in the Seepage Model for Performance Assessment seepage simulations and the resultant seepage look-up tables. The addition of the transportation, aging, and disposal (TAD) canisters for CSNF increased the average length of all WPs to 5.614 m (DTN: MO0702PASTREAM.001_R0 [DIRS 179925]). This longer average length increases the probability that an individual WP may encounter seepage (SNL 2007 [DIRS 181244], 4.1[a]). The increased WP length will have a direct influence on seepage rates since the seepage rates are per WP ($\text{m}^3/\text{yr}/\text{WP}$) and a function of the WP length. The influence on seepage fraction is not straightforward, since the increase in rate will not affect the locations that are already considered (in seepage calculations) to be seepage locations for the shorter WP. In addition, since some areas are prone to seepage and some not, increasing the WP length in areas not prone to seepage may have little effect on seepage fraction. The TSPA-LA Model does not account for this updating of the WP length in its seepage calculations. The impact on model results is quantified in an analysis in Appendix P (see P13).

Before Step 1 is completed, the results are checked for consistency. If the resulting seepage rates are less than zero, they are set to zero. If the resulting seepage rates correspond to a value higher than the local percolation flux applied to the footprint of 5.1 m × 5.5 m, the seepage rates are set to a rate corresponding to the local percolation flux.

For each TSPA-LA realization, R , the result from Step 1 of the seepage calculation is an ambient seepage rate for the four climate states in the TSPA-LA Model simulation for each WP (six CSNF and two CDSP WPs) at 3,264 MSTHM Abstraction locations (MSTHM Abstraction comprehensive data set as discussed in Section 6.3.2). Note that temporal changes in percolation flux through the UZ and, therefore, ambient seepage rate occur instantaneously when the climate state changes (Assumption 5.1.1). During a climate state, percolation flux and ambient seepage rate are at steady state.

Step 2: Seepage Adjusted for Thermal Effects and Drift Degradation Uncertainty—The ambient seepage rates calculated in Step 1 are adjusted to account for additional uncertainty due to the effects of some partial degradation (roof breakouts) of noncollapsed drifts and for thermal perturbations where the drift-wall temperature is at or above 100°C (determined for each repository location). The following adjustments are implemented:

- For all collapsed drift cases, uncertainty is already accounted for by using the look-up tables for fully collapsed drifts and taking into consideration uncertainty in the estimation of rubble volumes in the Seismic Submodel (see Step 4). For noncollapsed cases, the ambient seepage rates are increased by 20 percent to account for uncertainty associated with the seepage evaluation for these cases. This uncertainty stems in part from the limited number of simulation cases studied for moderately degraded drifts, but is mainly related to the large estimation differences between the stochastic realizations conducted for those cases (SNL 2007 [DIRS 181244], Section 6.7.1.2).
- Two abstraction approaches for thermal seepage are implemented: (1) for collapsed drifts, thermal seepage is set equal to the adjusted ambient seepage, and (2) for noncollapsed drifts, thermal seepage is set to zero for the period of above-boiling temperature, using a 100°C threshold temperature at the drift wall (SNL 2007 [DIRS 181244], Section 6.7.1.2).

Seepage in the Igneous Intrusion Modeling Case is discussed in Section 6.5.

Step 3: Determination of Seepage Fraction—The seepage fraction is calculated as the ratio of WPs experiencing seepage to all WPs in a percolation subregion by WP type for a given realization. WPs with seepage at any time during the 20,000-year simulation period are counted as WPs in a location with drift seepage (for 20,000-year simulations) and any time during the 1,000,000-year simulation period (for 1,000,000-year simulations). The seepage fraction is calculated using a threshold seepage rate of 0.1 kg/yr per WP. WP locations with less than this threshold rate are counted as locations where seepage does not occur because such small values are considered to be the result of the interpolation procedure (SNL 2007 [DIRS 181244], Section 6.8). WPs with seepage at any time are in a seep environment, and those without seepage are in a non-seep environment.

Step 4: Seismic Scenario Class—Separate implementations for collapsed and noncollapsed conditions are used. In addition, separate collapsed condition implementations are utilized for lithophysal and nonlithophysal rock. Composite tables are then generated within GoldSim to account for the change from noncollapsed to collapsed conditions. For lithophysal rock (SNL 2007 [DIRS 181244], Section 6.2.2[a]) if rockfall volumes into the drift are less than or equal to 5 m³/m of drift length, the intact-drift look-up table is utilized. If rockfall volumes into drifts are greater than 60 m³/m of drift length, the collapsed-drift look-up table is utilized. If rockfall volumes (per unit drift length) into the drift are between 5 m³/m and 60 m³/m, seepage values are linearly interpolated between a Seepage DLL analysis based on the intact-drift look-up table and a Seepage DLL analysis based on the collapsed-drift look-up table. In the nonlithophysal zone (SNL 2007 [DIRS 181244], Section 6.2.3[a]), if rockfall volumes into the drift are less than or equal to 0.5 m³/m, the intact-drift look-up table is utilized; if not, the percolation rates are utilized. The above criteria based on rockfall volumes are described in

Abstraction of Drift Seepage [DIRS 181244], Section 6.1[a] and DTN: LB0702PASEEP02.001_R0 [DIRS 181635]. Note that since both collapsed and noncollapsed seepage analyses are used for the Seismic Scenario Class, the seismic threshold data and seismic event frequencies are now used only as control parameters for controlling the multiple calls to the Seepage DLL (Table 6.3.3-3).

6.3.3.2 Drift-Wall Condensation

Condensate dripping from drift walls affects TSPA-LA Model calculations by adding additional water to the drift seepage volumetric flow rate (which may be zero in the non-seep environments). This combined condensate and seepage flows through the invert and, in some scenarios, through the DSs, WPs, and the waste forms. The Drift Wall Condensation Submodel calculates a probability of condensation on the drift walls at any location and, if condensation occurs, the rate of condensation. The source of condensation water is evaporated water from the invert and evaporated seepage water from the drift wall. Water vapor is transported axially by convective mixing from hotter drift regions to cooler drift regions where it can then condense. The axial movement of the water vapor, the saturated vapor pressure at the drift wall and in the invert, and temperature differences along the drifts are important factors that drive the occurrence of condensation (SNL 2007 [DIRS 181648], Section 6.3.1.1). The probability of drift-wall condensation occurrence and the condensation rate are abstracted as functions of the percolation flux at the base of the PTn (Section 6.3.3.1.2) and simulation time, as described in *In-Drift Natural Convection and Condensation* (SNL 2007 [DIRS 181648], Section 8.1[a]).

Information flow and connections between the EBS TH Environment Submodel (Section 6.3.2) and the Drift Seepage Submodel (Section 6.3.3.1), Drift Wall Condensation Submodel (Section 6.3.3.2.1), and EBS Flow Submodel (Section 6.3.6) are shown on Figure 6.3.3-1. Figure 6.3.3-6 shows the inputs and outputs to the Drift Wall Condensation Submodel and indicates the principal features of the submodel and the bases for confidence in the submodel.

6.3.3.2.1 Conceptual Model

The Drift Wall Condensation Process Model (SNL 2007 [DIRS 181648], Section 6.3) is used to calculate the occurrence and quantity of water vapor condensation at WP locations along the entire lengths of seven drifts selected to characterize the expected range of axial temperature gradients (see discussion below). The Drift Wall Condensation Process Model includes heat transfer from WPs through EBS components to the drift walls, evaporation of water vapor at the drift walls, radial vapor flux from drift walls, axial water vapor movement along the drift by convection, and condensation on the drift walls where the wall temperature is less than the condensation temperature. Probabilities of condensation at any location are calculated as the ratio of the drift length over which condensation occurs to total drift length.

Temperature at drift locations where water evaporation or condensation may occur is based on heat transfer calculations. Heat transfer between surfaces (WPs and DSs, WPs and inverts, DSs and drift walls, drift walls and inverts, and DSs and inverts) is based on literature references for correlations of natural convection heat and mass transfer for representative geometry. Thermal radiation is calculated from surface-to-surface radiation with appropriate radiation view factors. Only heat transferred in the radial direction is considered. The effects of axial heat transfer are

assumed to be minimal, as described in *In-Drift Natural Convection and Condensation* (SNL 2007 [DIRS 181648], Sections 5.3, 6.3.3.2.6, and Executive Summary).

Evaporative water vapor sources include the drift wall and the invert at each WP location (Figure 6.3.3-7). The local water vapor partial pressure is the saturation pressure at the calculated temperature. The rate at which water evaporates from a surface depends on the local difference between the saturation vapor pressure at the evaporating surface and the local gas-phase partial pressure, using the corresponding mass-transfer correlation. The condensation rate is limited by the available water vapor, which, in turn, is limited by the rate of water transfer to the drift by capillary wicking and percolation through the host rock.

Condensation is modeled with a lumped parameter approach using standard heat and mass transfer processes within the drift. The Drift Wall Condensation Process Model considers the entire length of each of seven drifts. The seven drifts are chosen to represent the range of thermal conditions in the repository (SNL 2007 [DIRS 181648], Section 6.3.5.1). Figure 6.3.3-8 illustrates the locations of the seven drifts. Drift-wall temperature boundary conditions are derived from analytical heat line-source solutions. The amount and location of water vapor depend on the availability of water and the axial transport properties. Axial and radial mass transport equations and radial heat transport equations are solved to estimate the water vapor distribution and condensation on various surfaces along each of the seven selected drifts at six selected times of 1,000; 3,000; 10,000; 30,000; 100,000; and 300,000 years. The selection of the first three analysis times is based on when the wall temperature drops below the saturation temperature (boiling temperature—approximately 96°C at the repository elevation) and the rate at which the waste-form decay heat declines during the first 10,000 years after repository closure. The remaining three analysis times span the remainder of the TSPA modeling period. Note here that the Drift Wall Condensation Model uses 96°C as the boiling temperature of water at the repository elevation and the Seepage Abstraction sets a threshold of 100°C as the temperature for thermal seepage in the TSPA-LA Model (Section 6.3.3.3.1).

The calculated results for the seven drifts at the selected times are used to estimate the location and rate of condensation on the drift walls, under the DSs, and on individual WPs. The TSPA-LA Model uses only the condensation abstraction for condensation on drift walls. Condensation under DSs and on WPs is calculated by the model, but is not significant and is not recommended for inclusion in the TSPA-LA (SNL 2007 [DIRS 181648], Section 8.1[a] and DTN: MO0706SPAFEPLA.001_R0 [DIRS 181613], FEP Number 2.1.08.14.0A)). The condensation model defines three stages for the occurrence of condensation. Stage 1 is when the drift wall temperature is above the boiling temperature of water at all locations in the drift. No condensation occurs during Stage 1. Stage 2 is for times between when the first location in a drift drops below the boiling temperature and the last location drops below the boiling temperature. A separate part of the Drift Wall Condensation Abstraction (SNL 2007 [DIRS 181648], Section 6.2[a]) describes the Stage 2 condensation occurrence and rate. Stage 3 occurs after all WPs (and thus the drift wall) drop below the boiling temperature. The abstraction for Stage 2 uses a reasonable-bound approach for the occurrence and rate of condensation.

6.3.3.2.2 TSPA-LA Model Abstraction

The Drift Wall Condensation Abstraction (SNL 2007 [DIRS 181648], Section 8.1[a]) calculates a probability of condensation occurrence on the drift walls at a WP location and, if condensation occurs, a rate of condensation for all locations in the drift that are below the boiling temperature. Lower- and upper-bounding cases for axial dispersion coefficients are provided. Lower-bound values for the axial dispersion coefficients are computed without any axial gradients in the process model boundary temperatures, whereas the upper bound on the axial dispersion coefficients is computed using an axial gradient in the boundary temperature (SNL 2007 [DIRS 181648], Section 6.3.7.1). Additionally, high- and low-invert transport cases are computed, but only low-invert cases are recommended for use in the TSPA-LA (SNL 2007 [DIRS 181648], Section 6.1.2[a]). The low-invert transport case assumes that the partial pressure at the bottom of the invert surface is the saturation vapor pressure at the drift-wall temperature. The high-invert transport case assumes that the partial pressure at the invert surface underneath the DS is the saturation vapor pressure for the invert surface temperature (SNL 2007 [DIRS 181648], Section 6.3). Finally, ventilated and unventilated (alternatively, mixed and unmixed) DS cases are provided (SNL 2007 [DIRS 181648], Section 8.1[a]). This gives eight possible cases for drift-wall condensation. After further analysis, the high-invert transport case is determined to be unrealistic, so it is not included in the TSPA abstraction (SNL 2007 [DIRS 181648], Section 6.1.2[a]).

The Drift Wall Condensation Abstraction results are determined through 144 different steady-state simulations, with results for each of the seven drifts being produced for each of the 144 runs ((two axial dispersion coefficients) \times (two invert transport properties) \times (two DS ventilation cases) \times (three infiltration cases) \times (six simulation times)) (SNL 2007 [DIRS 181648], Section 6.1.1[a] and Section 6.1.2[a]). These three infiltration cases were chosen to cover the range of infiltration. Specifically, the 10th, 30th, and 90th percentiles were used to produce the regressions for the TSPA-LA Model abstraction. The actual infiltration values used between the upper and lower bounds are not as important as the range of values used to produce the regression (SNL 2007 [DIRS 181648], Section 6.1.1[a]). These results are reduced to four distinct cases because the three different infiltration case results for each of these 48 cases are combined and used to create functional relationships in which condensation flux and condensation fraction are dependent upon percolation flux. That is, the four cases are composed of eight simulations at each of the six output times of 1,000, 3,000, 10,000, 30,000, 100,000, and 300,000 years. The eight simulations include the possible combinations of two values of dispersion coefficient (low and high), two values of invert transport properties (low and high), and two values for DS ventilation (ventilated and unventilated). By performing linear regressions between the probability of condensation on the drift wall and the mean percolation fluxes for the chosen drifts at the given time as $\ln[1 - P_w]$ and $\ln(\bar{p})$, and between the condensation rate and the percolation flux, as CW and \bar{p} (time-dependent percolation rate), functional relationships are developed in which condensation flux and condensation fraction are dependent on average percolation flux. These functional relationships are developed for each of the 48 simulation cases. The following mathematical relationship was developed (SNL 2007 [DIRS 181648], Section 8.3.1.1, Equation 8.3.1.1-3) from the linear regression analysis to approximate the probability of condensation on the drift walls:

$$\hat{P}_w = 1 - e^{a \ln(\bar{p}) + b} \quad (\text{Eq. 6.3.3-2})$$

where the parameters a and b are the slope and y-intercept of the linear regressions. As mentioned previously, the high invert transport case is not included in the abstraction for TSPA. Also, the analysis showed that condensation only occurs at 1,000 years. The parameters for the regressions for 1,000 years are found in DTN: MO0702PALOVERT.000_R2 [DIRS 180377] and DTN: MO0702PALV010K.000_R2 [DIRS 180376]. There are four non-zero values for a and four non-zero values for b .

Uncertainty in \hat{P}_w is captured using the standard error on the linear regression coefficients. They are found in DTN: MO0702PALOVERT.000_R2 [DIRS 180377]. Plus/minus one standard error is used as uncertainty ranges around the slope and intercept parameters. Uncertainty in the slope and intercept parameters are modeled as normally distributed about the computed value for each parameter, with the SD equal to the standard error. The parameter values are sampled independently (SNL 2007 [DIRS 181648], Section 8.3.1.1, Equation 8.3.1.1-4).

The equation:

$$CW = c\bar{p} + d \quad (\text{Eq. 6.3.3-3})$$

approximates the rate of condensation on the wall, CW , where the parameters c and d are the slope and y-intercept of the linear regression and are found in DTN: MO0702PALOVERT.000_R2 [DIRS 180377] and DTN: MO0702PALV010K.000_R2 [DIRS 180376]. There are four non-zero values for c and four non-zero values for d .

Uncertainty in CW is captured using the standard error on the linear regression coefficients, which are also found in DTN: MO0702PALOVERT.000_R2 [DIRS 180377] and DTN: MO0702PALV010K.000_R2 [DIRS 180376]. The standard errors are used as uncertainty ranges around the slope and intercept parameters. Uncertainty in the slope and intercept parameters are modeled as normally distributed about the computed value for each parameter, with SD equal to the standard error. The parameter values are sampled independently (SNL 2007 [DIRS 181648], Section 8.3.1.1).

Table 6.3.3-4 (DTN: MO0702PALOVERT.000_R2 [DIRS 180377]) shows one of the four tables containing values and standard errors for coefficients a , b , c , and d used in Equations 6.3.3-2 and 6.3.3-3. The R -squared values for each regression are also provided to indicate how well each linear regression model fits the results. Table 6.3.3-5 shows the values for the parameter distributions, which are sampled independently in the TSPA-LA Model for each TSPA-LA realization.

For condensation rate correlations at 1,000 years and for high axial dispersion, the correlation models have a larger standard error. The correlation uncertainty is applied by sampling a normal distribution with the SD equal to the standard error (SNL 2007 [DIRS 181648], Section 8.3 and Appendix H). Applying the uncertainty to the correlation coefficients produces a range of possible values covering, and in some cases exceeding, the Drift Wall Condensation Abstraction

output that was used to develop the correlation model. The TSPA-LA Model uses zero as the lower bound on the condensation rate and condensation probability.

The Drift Wall Condensation Abstraction (SNL 2007 [DIRS 181648]), Section 6.2.2[a]) describes a reasonable-bound approach for the condensation rate during Stage 2. Ultimately, the Stage 2 condensation rate is a single reasonably bounding value with rate in kg/m/yr. Only CDSP WPs have non-zero Stage 2 condensation. Stage 2 begins at a particular WP location when the drift wall cools to the boiling temperature of water. The Stage 2 CDSP WP condensation rate is in DTN: MO0703PAEVSIIIC.000_R2 [DIRS 181990]. No probability is given for Stage 2 condensation. In other words, the Stage 2 condensation rate is applied to all CDSP WPs during Stage 2.

TSPA-LA Model Implementation

The TSPA-LA Model implementation of the Drift Wall Condensation Submodel uses the abstracted probability of condensation on the drift wall (Equation 6.3.3-2) and an abstracted rate of condensation (Equation 6.3.3-3) whenever condensation occurs for Stage 3 condensation. The four cases corresponding to the four combinations of the two values for axial dispersion coefficient and two values of DS ventilation are treated as four equally likely cases and are sampled with equal frequency in the TSPA-LA Model (SNL 2007 [DIRS 181648], Section 8.1[a]). The CSNF and CDSP WPs are treated equally in terms of drift-wall condensation. The abstraction for the fraction of WPs that experience condensation and the corresponding condensation flow volume, apply equally to CSNF and CDSP WPs. In the Drift Wall Condensation Abstraction, the average percolation flux \bar{p} , represents the average of the MSTHM Abstraction percolation fluxes along the length of each of the seven simulated drifts. In the TSPA-LA Model, \bar{q}_{perc} represents the average of the percolation flux over a TSPA-LA Model percolation subregion (EBS TH Environment, Section 6.3.2). This average characterizes the percolation flux for that subregion (SNL 2007 [DIRS 181648], Section 8.3.1.1). In the TSPA-LA Model, \bar{q}_{perc} is used for \bar{p} in the Drift Wall Condensation Submodel. The TSPA-LA Model implementation does not include condensation under the DSs (SNL 2007 [DIRS 181648], Section 6.1.2[a]).

Inputs to the Drift Wall Condensation Submodel include slope, intercept, and standard error values for the slope and intercept. These inputs are provided for each combination of the invert transport properties, axial dispersion coefficient, and time. In addition, the average percolation rate is for each percolation subregion. For the Seismic Scenario Class, drift collapse is not expected in the nonlithophysal units, so condensation can only occur on drift walls above DSs in the nonlithophysal units. In contrast, there is no condensation in the lithophysal units after drift collapse (SNL 2007 [DIRS 181648], Section 8.1[a]). Consequently, the fraction of WPs in the nonlithophysal region is used in the implementation of the Drift Wall Condensation Submodel for the Seismic Scenario Class in the TSPA-LA Model.

The Drift Wall Condensation Abstraction provides correlations to calculate the condensation rate and probability of condensation as a function of time and percolation rate (SNL 2007 [DIRS 181648], Section 8[a], Appendix A[a], and Appendix B[a]). The Drift Wall Condensation Abstraction is divided into three stages: Stage 1 is the initial stage when all WPs

in the drift are above boiling; Stage 2 is the middle stage after the first WP in the drift cools to below boiling, but before the last WP in the drift cools to below boiling; and Stage 3 is the final stage after all WPs in the drift are below boiling. During Stage 1, before the first WP location in the drift drops below boiling, the condensation rate everywhere in the drift is zero because all WPs are boiling. Recall that the TSPA-LA Model uses a “representative WP” to represent the thermal and flow properties for the percolation subregion. (See Section 6.1.5 for a discussion of the percolation subregions). The temperature of the representative WP drops below boiling some time during Stage 2, after the first location in the drift drops below boiling, but before the last location drops below boiling. The Stage 2 condensation rate is used until the time when Stage 3 starts, which is the time when the last location in the drift drops below boiling. For Stage 3, the 1,000-year condensation rate and probability are used until 2,000 years. After 2,000 years, the 3,000-year rate and probability would be used, but because they are zero, the Stage 3 condensation rate is zero. The condensation rate remains zero for the remainder of the simulation up to 1,000,000 years because the process model gives a condensation rate equal to zero for times beyond 2,000 years.

The TSPA-LA drift-wall condensation implementation also requires a stochastic parameter, `Seepage_Condensation_Prob_a`, a $U[1,0]$ that is used to determine whether the first failed WP in a percolation subregion is in a location with condensation or not. `Seepage_Condensation_Prob_a` is an epistemic parameter sampled once per realization. The TSPA-LA treats WPs with seepage separately from WPs with no seepage. Drift-wall condensation is added to the seepage flux, or becomes the only advective flux in a non-seep environment. The drift-wall condensation fraction for Stage 3 is independent of the seepage fraction, so some of the WPs in both the seep and non-seep environments will potentially have condensation and some will not. Thus, the very first WP to fail in a percolation subregion can potentially have condensation or not. If `Seepage_Condensation_Prob_a` is less than or equal to the drift-wall condensation fraction, the first failed WP is assumed to be in an environment that can potentially have condensation. After more than one WP has failed in a percolation subregion, the drift-wall condensation flux is multiplied by the drift-wall condensation fraction to give an average condensation rate for the percolation subregion. This technique preserves the mass balance of condensing water and properly treats the percolation subregion as an average of WPs. It also properly applies the full condensation flux to a single failed WP in a percolation subregion during Stage 3. During Stage 2, no seepage fraction is applied and every CDSP WP receives the full condensation flux.

The output of the Drift Wall Condensation Submodel is the fraction of WPs exposed to condensation and the condensation rate as functions of percolation flux for each WP type (SNL 2007 [DIRS 181648], Section 8[a], Appendix A[a], and Appendix B[a]). These outputs are used in the EBS Flow Submodel to determine the average flow rate in the drift above a DS and WP and also below the WP in the invert. The EBS Flow Submodel calculations include effects of both drift seepage and drift-wall condensation. Specifically, the EBS Flow Submodel directly adds the drift seepage rate and the drift-wall condensation rate to obtain the total flow rate into the drift.

6.3.3.3 Model Component Consistency and Conservatism in Assumptions and Parameters

To enhance understanding of the complex interactions within the TSPA-LA Model, a discussion of consistency among model components and among submodels, and identification of conservative assumptions in abstractions, process models, and parameter sets supporting seepage and drift-wall condensation are discussed below.

6.3.3.3.1 Consistency of Assumptions

In-Drift Evaporation—In-drift evaporation of seepage flow is not included in the Drift Seepage Submodel in any of the scenario classes at temperatures less than 100°C, even though below-boiling evaporation is a process that is modeled in the MSTHM Process Model (Section 6.3.2), Drift Wall Condensation Submodel (Section 6.3.3.2), and the EBS Chemical Environment Submodel (Section 6.3.4).

Effect on TSPA—Not including evaporation of seepage flux (Section 5.1.4) leads to an overestimate in TSPA-LA Model of: (1) the water present at any point in time; (2) the amount of water flux through the invert and/or WP; and, therefore, (3) the radionuclide mass released.

Repository Boiling Temperature—The thermal seepage model conservatively uses 100°C for the boiling temperature of water while the drift wall condensation model uses 96°C, which is the actual boiling temperature at the repository horizon.

Effect on TSPA—The 100°C threshold for thermal seepage means that seepage starts sooner and water is available for transport sooner. This approach is conservative and can lead to earlier doses to the RMEI.

Water Balance—There is no water balance (liquid or vapor) between the MSTHM, drift seepage, and drift-wall condensation models.

Effect on TSPA—It is assumed for each model that there is sufficient water to support the predicted flow rates. This results in an over-prediction of flow rates, as well as an over-prediction of the number of WPs that are in an advective environment. This results in higher rates of radionuclide transport, which lead to higher doses to the RMEI. Therefore, this approach is conservative.

Thermal-Hydrologic Behavior of the Rock Mass—The condensation model does not explicitly consider the thermal-hydrologic behavior of the rock mass. The inclusion of rock characteristics in the condensation model is expected to affect the predicted condensation distributions. For example, the presence of the capillary behavior of the rock would tend to reduce the evaporation rate and increase the imbibition rate, both of which would decrease the net condensation rate.

Effect on TSPA—The different responses arising from these differing model assumptions tend to decrease with time as the repository cools. This difference in assumptions does not affect the thermal-hydrologic response following an igneous intrusion event or seismic event, which are the dominant contributors of dose to the RMEI. Therefore, the approach is conservative and would have little effect on dose.

6.3.3.2 Identification of Conservatism in Submodels and Abstractions

Ambient Seepage—For drift-wall temperatures less than 100°C, the thermal seepage model implemented into the TSPA-LA Model conservatively uses ambient drift seepage instead of taking credit for thermal effects (SNL 2007 [DIRS 181244], Section 6.7.1.2). Ambient seepage, which does not account for thermal effects, is always greater than the thermal seepage as shown in *Abstraction of Drift Seepage* (SNL 2007 [DIRS 181244], Figure 6.4-15). In the TSPA-LA Model, rather than the seepage rate, the presence or absence of flowing water in the drift is the more dominant factor controlling radionuclide releases when the DSs are intact. Reducing the seepage slightly to account for thermal effects may have a slight impact on the radionuclide release from the EBS for WPs with breached DSs.

Flow Focusing—Two models for flow focusing have been developed for the Drift Seepage Model. The model implemented in the TSPA-LA Model is based on a fine grid resolution and the flow focusing factor distribution for the base model is described by a polynomial regression curve with a maximum factor of between five and six (SNL 2007 [DIRS 181244], Section 6.6.5.2). The model was selected because it is expected to be more conservative and generate considerably larger average seepage rates with only a small decrease in seepage fraction when compared to the ACM (SNL 2007 [DIRS 181244], Section 6.6.5.2.3).

Igneous Seepage Model—The base-case igneous seepage model is based on a conceptualization that after the event the waste may be encapsulated by solidified magma with few cooling joints, and water contact with the waste being limited by the small permeability of the solidified magma (SNL 2007 [DIRS 181244], Section 6.5.1.7). This conceptual model assumes that the solidified magma has the same hydrologic properties as the surrounding rock. To represent this conceptual model, the seepage flux is set equal to the percolation flux (SNL 2007 [DIRS 181244], Section 6.5.1.7).

6.3.3.4 Alternative Conceptual Model(s) for Drift Seepage and Drift-Wall Condensation

Section 6.2 outlines the general consideration and treatment of ACMs used to support the TSPA-LA Model. A brief description of the ACMs for the Drift Seepage and Drift Wall Condensation Submodels summarized in Table 6.3.3-6 is presented below.

Drift Seepage ACMs—Five ACMs for drift seepage were considered: (1) flow through discrete fractures; (2) episodic-preferential flow in superheated rock; (3) an alternative flow-focusing model and (4, 5) two alternative igneous seepage models.

The most important ACM for ambient seepage is one that simulates flow through discrete fractures rather than through a stochastic porous continuum. It was concluded that conceptual model uncertainty is small compared to other sources of uncertainty that are explicitly accounted for by the base-case conceptual model, its numerical implementation, and the associated uncertainty estimates, which are propagated through the TSPA-LA Model (SNL 2007 [DIRS 181244], Section 6.4.1.2).

The effectiveness of the vaporization barrier was examined with an ACM representing episodic-preferential flow into a superheated rock environment (SNL 2007 [DIRS 181244],

Section 6.4.3.2). In this ACM, the thermally perturbed downward flux from the condensation zone toward the superheated rock zone is conceptualized to form episodic preferential-flow patterns. The effectiveness of the vaporization barrier was then tested for these extreme conditions where downward flux is fast and large in magnitude compared to average flow. A semi-analytical solution was employed to simulate the complex flow processes of episodic fingerflow in a superheated fracture. With this solution, the maximum penetration distance into the superheated rock was determined for specific episodic flow events and thermal conditions. In addition, the amount of water arriving at the drift crown and the impact of capillary diversion were calculated. It was concluded that the thermal seepage process model results are reasonably consistent with the ACM (SNL 2007 [DIRS 181244], Section 6.4.3.2).

Two flow-focusing models were developed for the Drift Seepage Model. The base-case model was based on a fine grid resolution of < 1 m. The ACM was based on a coarser resolution of scale at which the flow-focusing factors were averaged over 5-meter long sections at the bottom of the model (SNL 2007 [DIRS 181244], Section 6.6.5.2). The flow-focusing factor distribution for the base model is described by a polynomial regression curve with a maximum factor of between five and six. The ACM flow-focusing factor distribution is described by a normal distribution with a maximum of 2.4. The base model is expected to be more conservative because it generates large increase in average seepage rates and only a small decrease in seepage fraction when compared to the ACM (SNL 2007 [DIRS 181244], Section 6.6.5.2.3).

The two ACMs for evaluating drift seepage after an igneous event are based on a conceptual model where thermal contraction gives rise to numerous fractures and joints in the cooling process filling the drift with fractured magma of relatively high permeability and low capillary strength (SNL 2007 [DIRS 181244], Section 6.5.1.7). If the capillary strength of the solidified magmas is much lower than the capillary strength of the surrounding rock, the capillary barrier and flow diversion at the interface would be preserved (SNL 2007 [DIRS 181244], Section 6.5.1.7). It is also possible for the magma to drain out of the drift, leaving an air space which would generate a capillary barrier (SNL 2007 [DIRS 181244], Section 6.5.1.7). The two ACMs that consider this conceptual model are based on the use of (1) the nondegraded drift seepage table which would provide a reasonable estimate of seepage rates or (2) the degraded drift seepage table which would account for the considerable uncertainty in in-drift conditions by providing higher seepage rates (SNL 2007 [DIRS 181244], Section 6.5.1.7).

Drift-Wall Condensation ACMs—Two ACMs for drift-wall condensation were considered: (1) a thermal conductivity/heat transfer ACM and (2) a computational fluid dynamics simulation for drift condensation processes ACM.

In the Thermal Conductivity/Heat Transfer ACM, the air phase is treated as a solid material. To account for the higher heat transfer between surfaces due to convection, the effective thermal conductivity of the solid (air) can be increased so that the same amount of heat can transfer from one surface to another for the same temperature difference. This ACM is essentially accounted for in the MSTHM Abstraction. This ACM is not considered further because it is implemented in the MSTHM Abstraction (SNL 2007 [DIRS 181648], Sections 6.1.4 and 6.4).

Another ACM simulates the drift with a computational fluid dynamics code and the surrounding rock with a porous media code. The computational fluid dynamics code FLUENT

(Fluent, Inc. 2003 [DIRS 164315]) contains limited porous media capabilities that only consider single-phase flow. To more rigorously simulate physical processes of the rock, the software would need to be able to simulate partially saturated flow as well as phase change in the porous media. Conduction-only heat transfer in the surrounding rock and the invert is acceptable, and this ACM is not considered further (SNL 2007 [DIRS 181648], Section 6.1.4).

No ACMs were recommended for inclusion in the TSPA-LA Model.

Table 6.3.3-1. Spatial Variability and Uncertainty Distributions for $1/\alpha$ for Method A as Defined in the Abstraction of Drift Seepage

$1/\alpha$ (Lithophysal Units)		$1/\alpha$ (Nonlithophysal Units)	
Spatial Variability Distribution	Uncertainty Distribution	Spatial Variability Distribution	Uncertainty Distribution
Uniform Distribution with Mean 591 Pa	Triangular Distribution with Mean 0	Uniform Distribution with Mean 591 Pa	Triangular Distribution with Mean 0
Lower Bound is 402 Pa. Upper Bound is 780 Pa.	Lower Bound is – 105 Pa. Upper Bound is + 105 Pa.	Lower Bound is 402 Pa. Upper Bound is 780 Pa.	Lower Bound is – 105 Pa. Upper Bound is + 105 Pa.

Sources: SNL 2007 [DIRS 181244], Section 6.3[a] and DTN: LB0407AMRU0120.001_R0 [DIRS 173280].

NOTE: Only one method, Method A, is used in the TSPA-LA model (SNL 2007 [DIRS 181244], Section 6.3[a]).

Table 6.3.3-2. Spatial Variability and Uncertainty Distributions for Fracture Permeability ($\log(k [m^2])$)

Fracture $\log(k [m^2])$ (Lithophysal Units)		Fracture $\log(k [m^2])$ (Nonlithophysal Units)	
Spatial Variability Distribution	Uncertainty Distribution	Spatial Variability Distribution	Uncertainty Distribution
Log Normal Distribution with Mean – 11.5	Triangular Distribution with Mean 0	Log Normal Distribution with Mean – 12.2	Triangular Distribution with Mean 0
Standard Deviation 0.47	Lower Bound is – 0.92. Upper Bound is + 0.92.	Standard Deviation 0.34	Lower Bound is – 0.68. Upper Bound is + 0.68.

Sources: SNL 2007 [DIRS 181244], Section 6.6.3, Figures 6.6-7 and 6.6-8 and DTN: LB0407AMRU0120.001_R0 [DIRS 173280].

Table 6.3.3-3. Inputs Passed by the TSPA-LA Model to the Seepage Dynamically Linked Library

Input #	Input Parameter Name	Description	Value	Source
1	Infiltration_Scenario_a	Provides the infiltration scenario for the current realization to the seepage DLL.	1= 10th percentile 2= 30th percentile 3= 50th percentile 4= 90th percentile	NA, not data
2	Random_Seed_1	The first of two random number seeds provided to the Seepage DLL for its internal random number generator. This allows the sampling sequence in the Seepage DLL to be repeated, consistent with the Latin hypercube sampling on uncertain parameters in the GoldSim model file.	Uniform (1, 2 ³¹ -1)	NA, not data
3	Random_Seed_2	The second of two random number seeds provided to the Seepage DLL for its internal random number generator (see above).	Uniform (1, 2 ³¹ -1)	NA, not data
4	Alpha_Uncert_Lith_a	Sampled value from uncertainty distribution for capillary strength parameter. The distribution minimum, most likely, and maximum are defined by which method is chosen.	Triangular; see Table 6.3.3-1.	^a Section 6.7.1.1
5	Alpha_Uncert_NonLith_a	Sampled value from uncertainty distribution for capillary strength parameter. The distribution minimum, most likely, and maximum are defined by which method is chosen.	Triangular; see Table 6.3.3-1.	^a Section 6.7.1.1
6	LogK_Uncert_NonLith_a	Sampled value from Log(k) uncertainty for the nonlithophysal rock units.	Triangular (-0.68, 0, 0.68)	^a Section 6.7.1.1
7	LogK_Uncert_Lith_a	Sampled value from Log(k) uncertainty for the lithophysal rock units.	Triangular (-0.92, 0, 0.92)	^a Section 6.7.1.1
8	Density_H2O	Density of seeping water.	960 kg/m ³	^b This is an assumed input parameter.
9	Drift_Diameter	Drift diameter.	5.5 m	^a Section 6.7.1.2
10	WP_Length_Seepage	WP length.	5.1 m	^a Section 6.7.1
11	Seepage_Multiplier	A seepage multiplier for noncollapsed conditions that accounts for additional uncertainty due to drift degradation.	1.2	^a Section 6.7.1.2
12	LogK_SV_Mean_NonLith	The mean of the log of permeability [log(k)] spatial variability for nonlithophysal rock units.	-12.2	^a Section 6.7.1.1
13	LogK_SV_SD_NonLith	The standard deviation of the log of permeability [log(k)] spatial variability for nonlithophysal rock units.	0.34	^a Section 6.7.1.1
14	LogK_SV_Mean_Lith	The mean of the log of permeability [log(k)] spatial variability for lithophysal rock units.	-11.5	^a Section 6.7.1.1
15	LogK_SV_SD_Lith	The standard deviation of the log of permeability [log(k)] spatial variability for lithophysal rock units.	0.47	^a Section 6.7.1.1

Table 6.3.3-3. The Inputs Passed by the TSPA-LA Model to the Seepage Dynamically Linked Library (Continued)

Input #	Input Parameter Name	Description	Value	Source
16	Alpha_SV_LB_Lith	The lower bound for the $1/\alpha$ spatial variability distributions for lithophysal rock. The value is selected based on which of the four ACMs (i.e., methods) is selected during a particular realization for the distribution.	Table 6.3.3-1.	^a Section 6.7.1.1
17	Alpha_SV_UB_Lith	The upper bound for the $1/\alpha$ spatial variability distributions for lithophysal rock. The value is selected based on which of the four ACMs (i.e., methods) is selected during a particular realization for the distribution.	See Table 6.3.3-1	^a Section 6.7.1.1
18	Alpha_SV_LB_NonLith	The lower bound for the $1/\alpha$ spatial variability distributions for nonlithophysal rock. The value is selected based on which of the four ACMs (i.e., methods) is selected during a particular realization for the distribution.	See Table 6.3.3-1	^a Section 6.7.1.1
19	Alpha_SV_UB_NonLith	The upper bound for the $1/\alpha$ spatial variability distributions for nonlithophysal rock. The value is selected based on which of the four ACMs (i.e., methods) is selected during a particular realization for the distribution.	See Table 6.3.3-1	^a Section 6.7.1.1
20	DE_Event_Time	Selects the appropriate disruptive event time (igneous or seismic) based on the scenario class for the simulation.	0 yr for both igneous and seismic, 20,000 yr or 1,000,000 yr if nominal case	NA, not data
21	Scenario_Flag_Feed_Seep	Determines which scenario class (e.g., nominal, igneous, or seismic) is being simulated.	1 = nominal 2 = igneous 3 = seismic	NA, not data
22	Seismic_Event_Freq_Seep_Feed	Annual exceedance frequency of the seismic event.	0.5 yr^{-1}	Section 6.3.3.1.3
23	Seismic_Thresh_Lith	Seismic event frequency at or below which collapse occurs for lithophysal rock.	1 yr^{-1} = collapsed condition 0 yr^{-1} = noncollapsed condition	Section 6.3.3.1.3
24	Seismic_Thresh_NonLith	Seismic event frequency at or below which collapse occurs for nonlithophysal rock.	1 yr^{-1} = collapsed condition 0 yr^{-1} = noncollapsed condition	Section 6.3.3.1.3
25	Rock_Str_Reduction_Lith	Placeholder for Lithophysal Rock Strength Reduction Function.	0	NA, not data

Table 6.3.3-3. The Inputs Passed by the TSPA-LA Model to the Seepage Dynamically Linked Library (Continued)

Input #	Input Parameter Name	Description	Value	Source
26	Rock_Str_Reduction_NonLith	Placeholder for Nonlithophysal Rock Strength Reduction Function.	0	NA, not data
27	DE_Seepage_Model	Selects appropriate disruptive event seepage model flag based on the scenario class for the simulation.	Igneous or Seismic	NA, not data
28	Rock_Str_Thresh_Lith	Loss of rock strength, which will result in drift collapse in lithophysal rock units.	40%	^a Section 6.4.2.4.1
29	Rock_Str_Thresh_NonLith	Loss of rock strength, which will result in drift collapse in nonlithophysal rock units.	40%	^a Section 6.4.2.4.1
30	Print_Flag	Controls the amount of information that is written to output files (e.g., none, seepage output only, all possible output, debug information only).	NA	NA, not data
31	Thermal_Seep_Temp_Limit	Drift crown temperature above which seepage will not occur.	96°C	^a Section 6.3.2
32	Flow_Focusing_Flag	Specifies whether to use the flow-focusing factor built into the Seepage DLL or to use a value of 1.0 for flow focusing.	0 = use abstraction, 1 = use 1.0	NA, not data
33	End_Time	Specifies the time to which the Seepage DLL runs (TSPA-LA Model simulation time) and returns seepage time histories.	20,000 yr or 1,000,000 yr	NA, not data
34	Seepage_Uncertainty	Provides a value that is used to sample the seepage distribution in the Seepage DLL.	Uniform (0,1)	^a Section 6.7.1.1
35	Climate4_FF_Index	Index for post 10-k climate state. Used to allow for flexibility in choosing percolation fluxed for the post 10-k climate state.	1	NA, not presently used

NOTE: ^a SNL 2007 [DIRS 181244].

^b A low density (960 kg/m³, associated with water at 100°C) is used to maximize the volumetric flow.

Table 6.3.3-4. Drift-Wall Condensation: 1,000 Years; High Dispersion Coefficient, Low Invert Transport Properties, Well-Ventilated Drip Shield

	Slope (c)	Y-intercept (d)
Rate (CW)	-1.33E+00	1.08E+02
Standard Error	1.42E+00	1.45E+02
Rate R-Squared	4.67E-01	—
	Slope (a)	Y-intercept (b)
Probability (P _w)	-2.59E-02	5.71E-02
Standard Error	9.35E-03	2.93E-02
Probability R-Squared	2.87E-01	—

Source: DTN: MO0702PALOVERT.000_R2 [DIRS 180377]

NOTE: An example of 1 of the 4 tables that provide values of regression slopes, intercepts, and statistical parameters for \hat{P}_w and CW.

Table 6.3.3-5. Parameter Distributions for Drift Wall Condensation Abstraction

Parameter Name in TSPA-LA Model	Description	Distribution
DWC_Dispersivity_Cond_a	A random variable specifying whether the high dispersivity or low dispersivity modeling case is used (0 = low; 1 = high).	Discrete (p, v) [(0.5, 0), (0.5, 1)]
DWC_Invert_Properties_Cond_a	A random variable specifying whether the high invert transport or low invert transport modeling case is used (0 = low; 1 = high). Note that for TSPA-LA, the high invert transport case was determined to be an unrealistic upper bound (DTN: MO0706SPAFEPLA.001_R0 [DIRS 181613], FEP 2.1.08.14.0A). Only the value of zero is used.	Discrete (p, v) [(1.0, 0), (0.0, 1)]
DWC_Ventilated_Cond_a	A random variable specifying whether the ventilated or unventilated drip shield modeling case is used (0 = unventilated; 1 = ventilated).	Discrete (p, v) [(0.5, 0), (0.5, 1)]
Seepage_Condensation_Prob_a ^a	Random variable U[0,1] to determine the seepage/condensation regime for the first failed waste package in a seepage environment.	Uniform (0,1)
DWC_Std_Error_a_a	An uncertainty multiplier for the standard deviation on the slope coefficient for determining probability of condensation from the percolation rate.	Normal: mean = 0, standard deviation = 1
DWC_Std_Error_b_a	An uncertainty multiplier for the standard deviation on the y-intercept coefficient for determining probability of condensation from the percolation rate.	Normal: mean = 0, standard deviation = 1
DWC_Std_Error_c_a	An uncertainty multiplier for the standard deviation on the slope coefficient for determining condensation rate from the percolation rate.	Normal: mean = 0, standard deviation = 1
DWC_Std_Error_d_a	An uncertainty multiplier for the standard deviation on the y-intercept coefficient for determining condensation rate from the percolation rate.	Normal: mean = 0, standard deviation = 1

Source: SNL 2007 [DIRS 181648], Table A-3.

^a Seepage_Condensation_Prob_a is a TSPA parameter developed in this report.

Table 6.3.3-6. Alternative Conceptual Models Considered for the Drift Seepage and Drift-Wall Condensation Submodels

Alternative Conceptual Models	Key Assumptions	Screening Assessment and Basis
Drift Seepage: Flow through discrete fractures	ACM that simulates flow through discrete fractures rather than through a stochastic continuum.	Screened out. It was concluded that conceptual model uncertainty is small compared to other sources of uncertainty that are explicitly accounted for by the base case conceptual model, its numerical implementation, and the associated uncertainty estimates that are propagated through the TSPA-LA Model.
Drift Seepage: Episodic-Preferential Flow in Superheated Rock	The effectiveness of the vaporization barrier was examined with an ACM representing water flow into a superheated rock environment (SNL 2007 [DIRS 181244], Section 6.4.3.2). In this ACM, the thermally perturbed downward flux from the condensation zone toward the superheated rock zone is conceptualized to form episodic preferential-flow patterns.	Screened out. It was concluded that results of the ACM are reasonably consistent with the thermal seepage process-model results used for this abstraction (SNL 2007 [DIRS 181244], Section 6.4.3).
Drift Seepage: Flow-focusing factor based on a coarser resolution of scale	The ACM flow-focusing factor was based on a coarser resolution of scale at which the flow-focusing factors were averaged over 5-meter long sections along the bottom of the model (SNL 2007 [DIRS 181244], Section 6.6.5.2.2).	Screened out. It was concluded that the flow focusing model based on the finer grid resolution gave more conservative results and therefore the appropriate model to use (SNL 2007 [DIRS 181244], Section 6.6.5.2.3).
Drift Seepage: Igneous seepage model that considers a capillary barrier and flow diversion	The two ACMs for evaluating drift seepage after an igneous event are based on a conceptual model where thermal contraction gives rise to numerous fractures and joints in the cooling process filling the drift with fractured magma of relatively high permeability and low capillary strength (SNL 2007 [DIRS 181244], Section 6.5.1.7). This conceptualization gives rise to a capillary barrier and flow diversion. The two ACMs are based on whether the non-collapsed seepage lookup table or the collapsed seepage lookup table is used.	Screened out. The model for igneous seepage used in the TSPA-LA model was chosen on the basis that it would be conservative to use percolation flux as the seepage flux.
Drift-Wall Condensation: Thermal Conductivity/Heat Transfer	In the Thermal Conductivity/Heat Transfer ACM, the air phase is treated as a solid material (SNL 2007 DIRS [181648], Section 6.1.4).	Screened out. This ACM is essentially accounted for in the MSTHM Abstraction (SNL 2007 [DIRS 181648], Sections 6.1.4 and 6.4).
Drift-Wall Condensation: CFD simulation for drift condensation processes	ACM simulates the drift with a CFD code and the surrounding rock with porous media code. The CFD code FLUENT (Fluent, Inc. [DIRS 164315]) contains limited porous media capabilities that only consider single-phase flow (SNL 2007 DIRS [181648], Section 6.1.4).	Screened out. The CFD code was determined to have insufficient advantages over the selected model (SNL 2007 [DIRS 181648], Section 6.1.4).

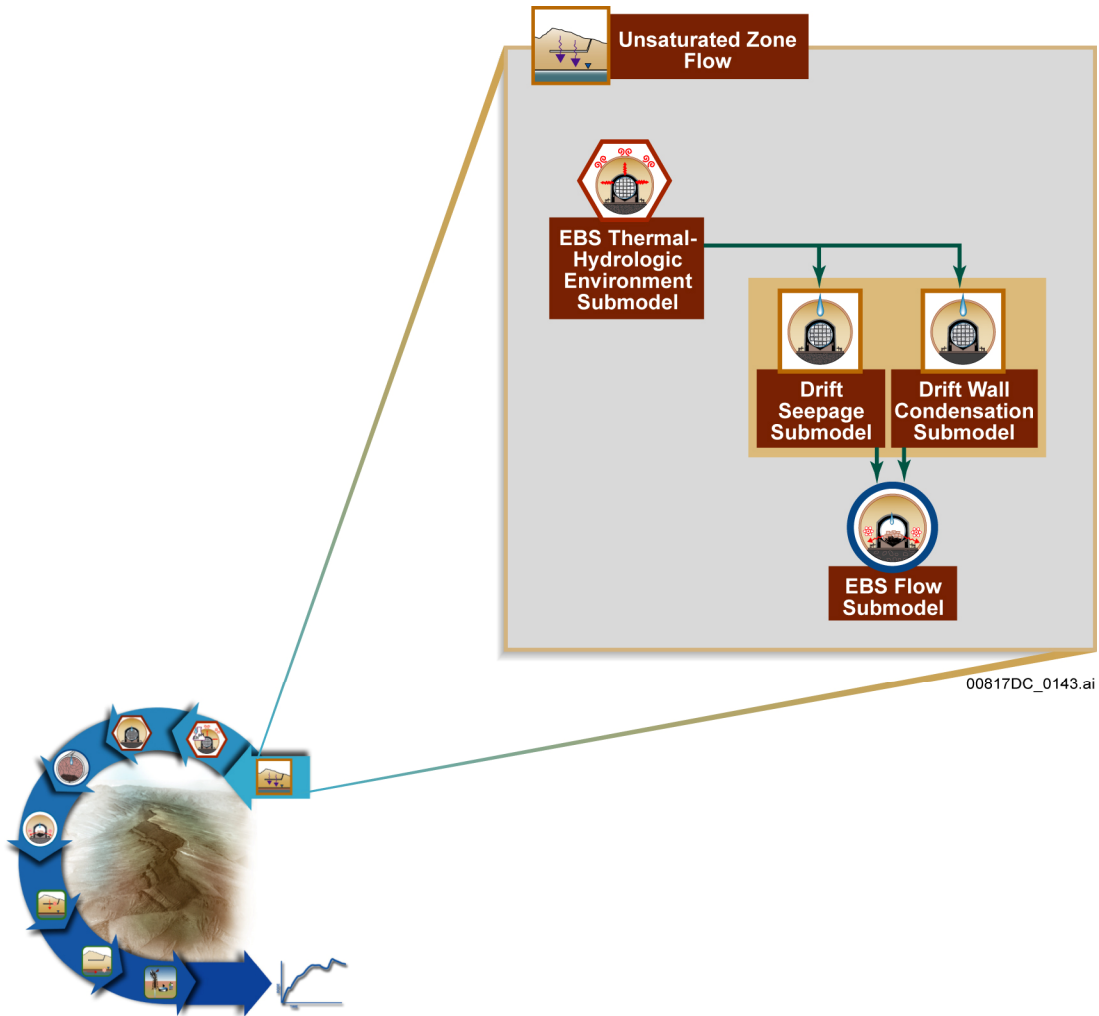


Figure 6.3.3-1. Information Flow Diagram for the Drift Seepage and Drift Wall Condensation Submodels

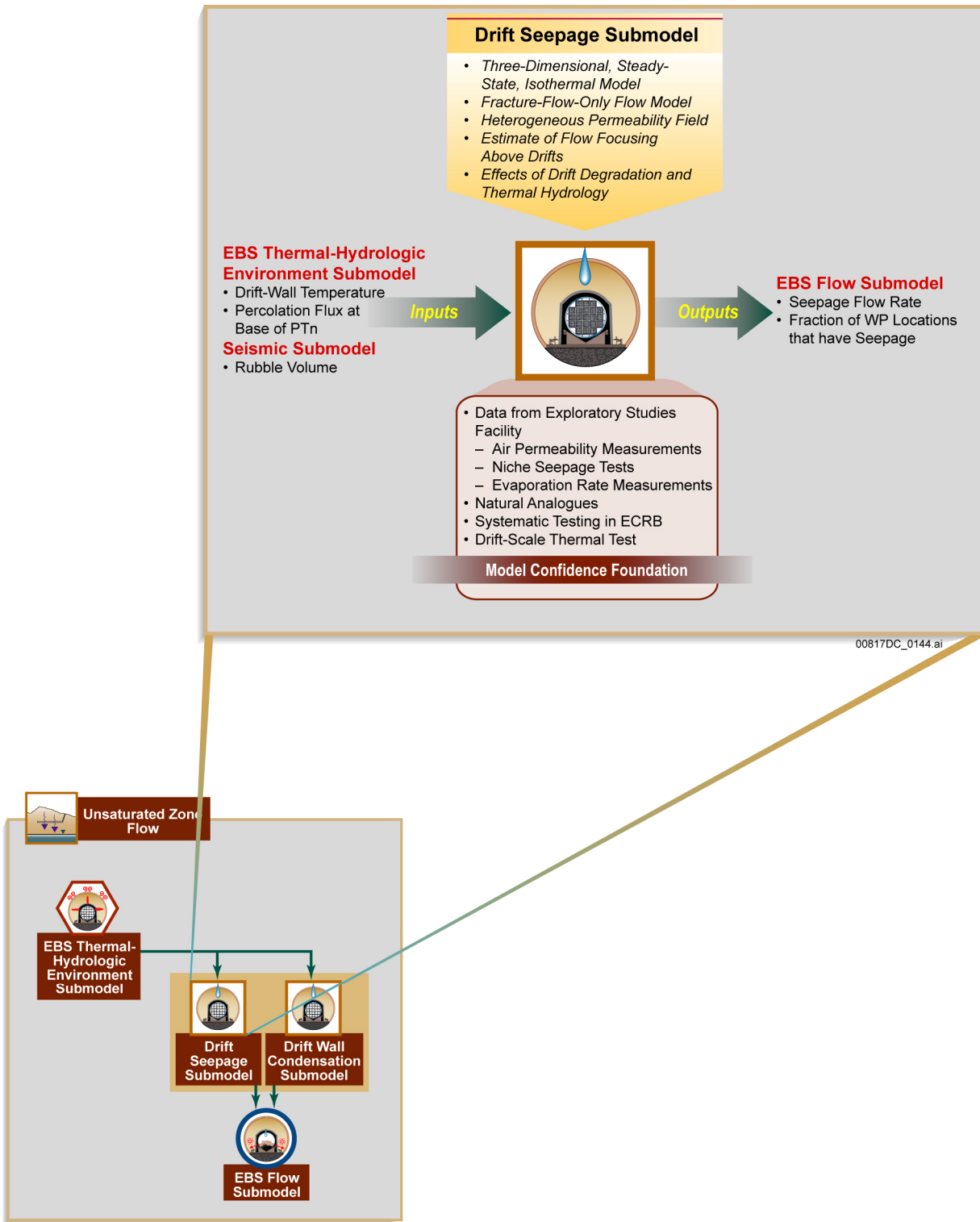
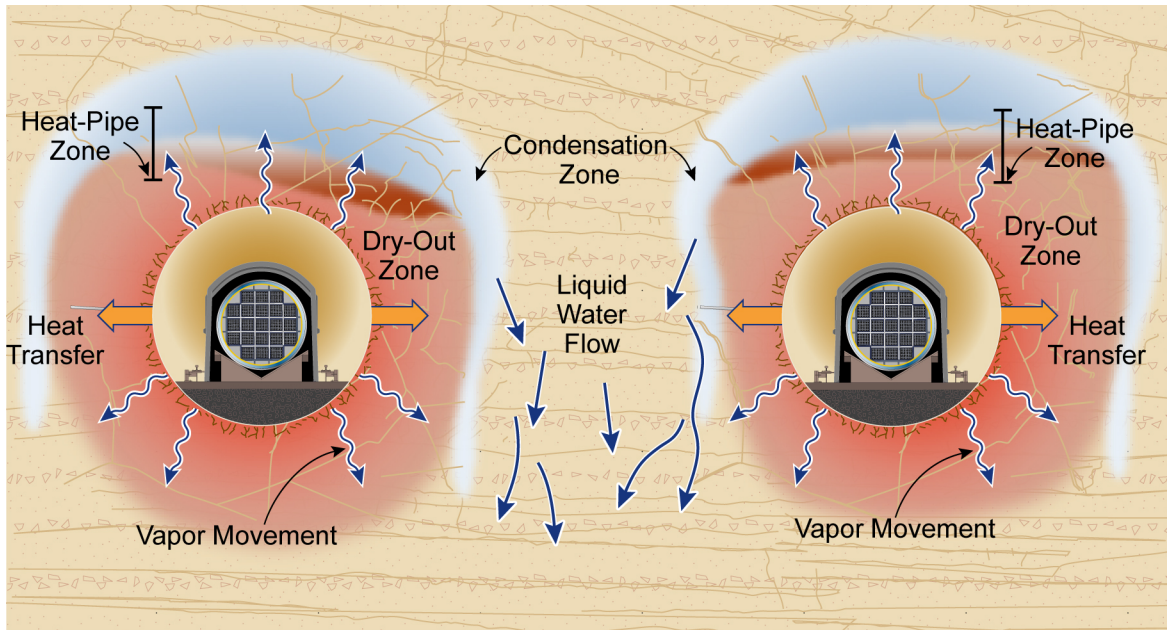


Figure 6.3.3-2. Inputs, Outputs, and Basis for Model Confidence for the Drift Seepage Submodel



00817DC_0145.ai

Source: Modified from BSC 2004 [DIRS 169734], Figure 5-81.

Figure 6.3.3-3. Schematic Illustration (not to scale) of Thermal-Hydrologic Processes in the Vicinity of the Emplacement Drifts Due to Repository Heating

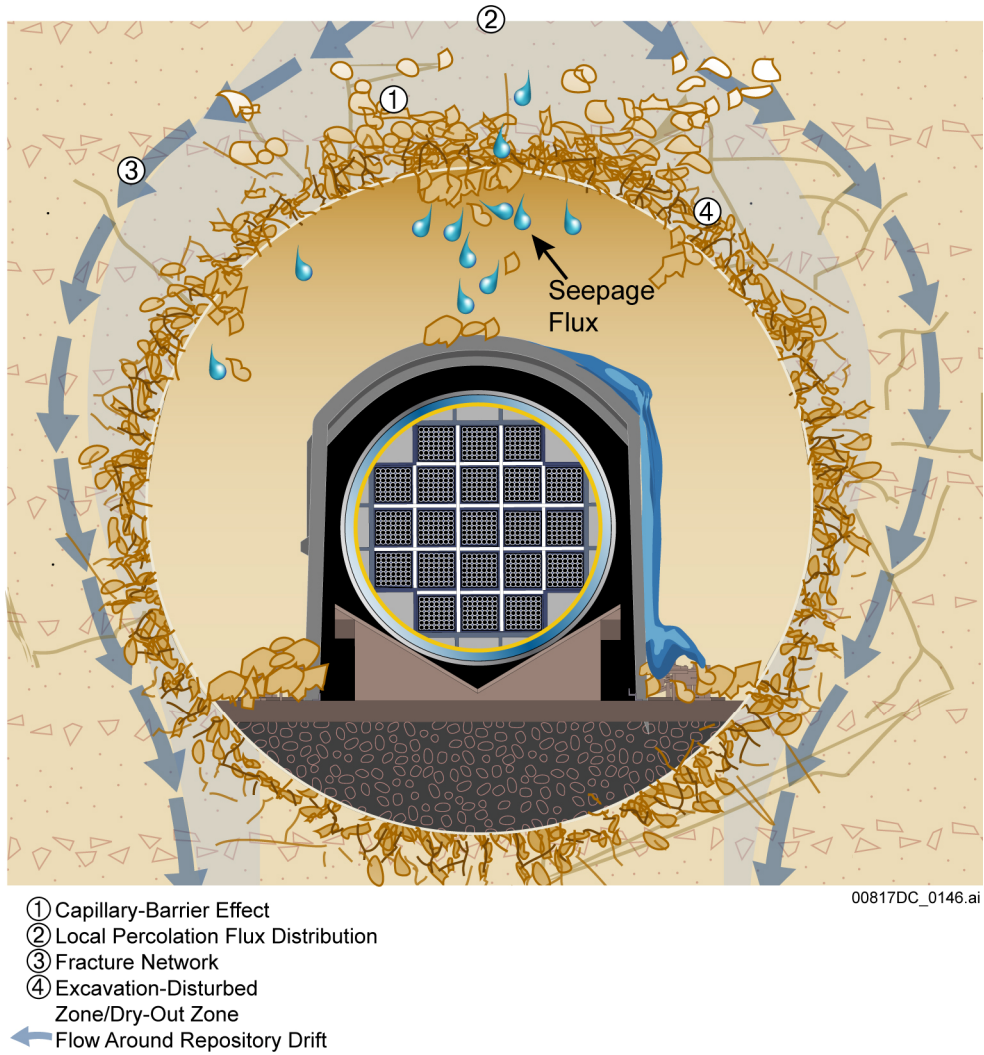
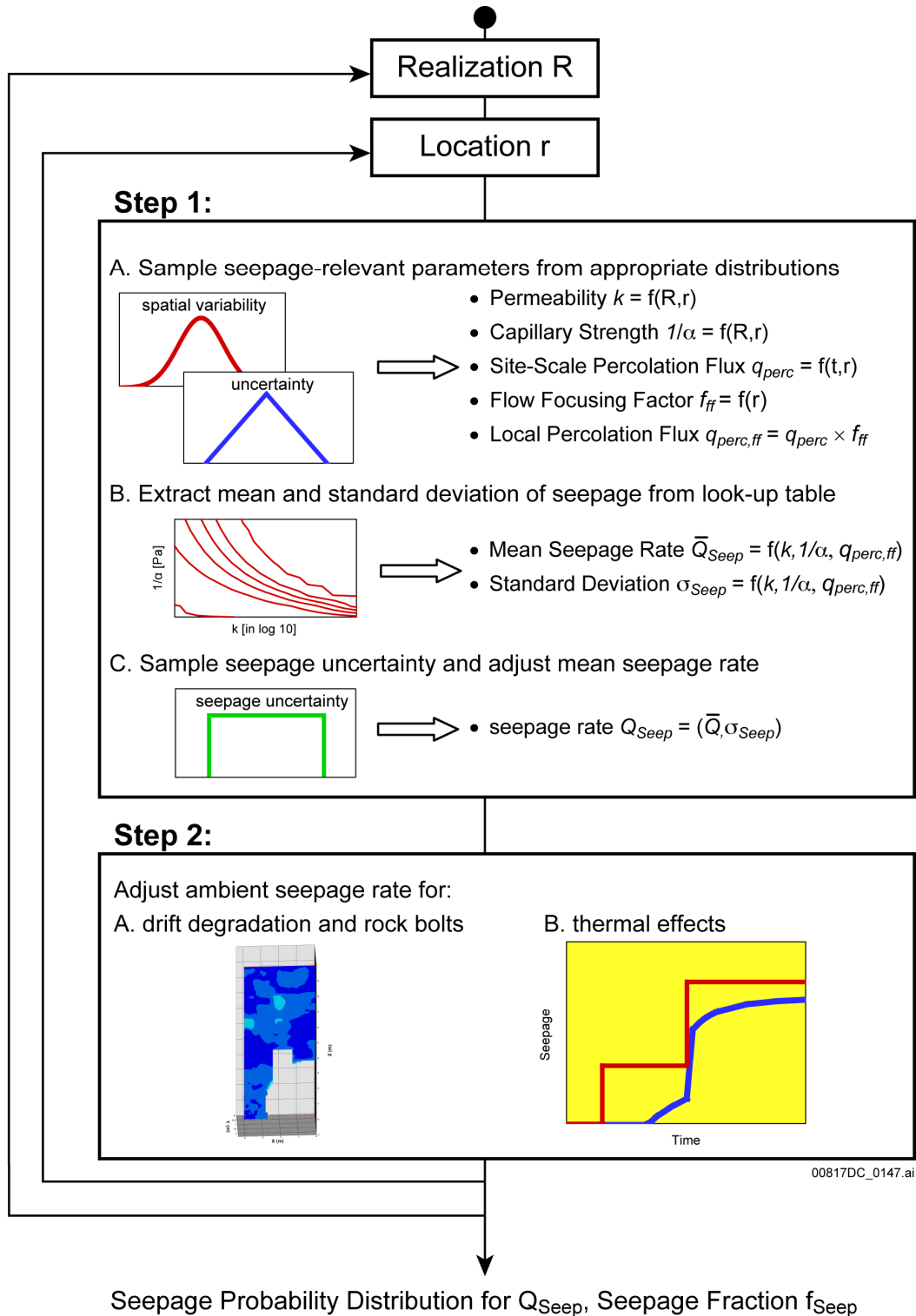


Figure 6.3.3-4. Schematic Illustration of the Processes Affecting Ambient Drift Seepage



Source: SNL 2007 [DIRS 181244], Figure 6-1[a].

Figure 6.3.3-5. Procedure for Probabilistic Calculation of Seepage at Selected Timesteps in the TSPA-LA Model

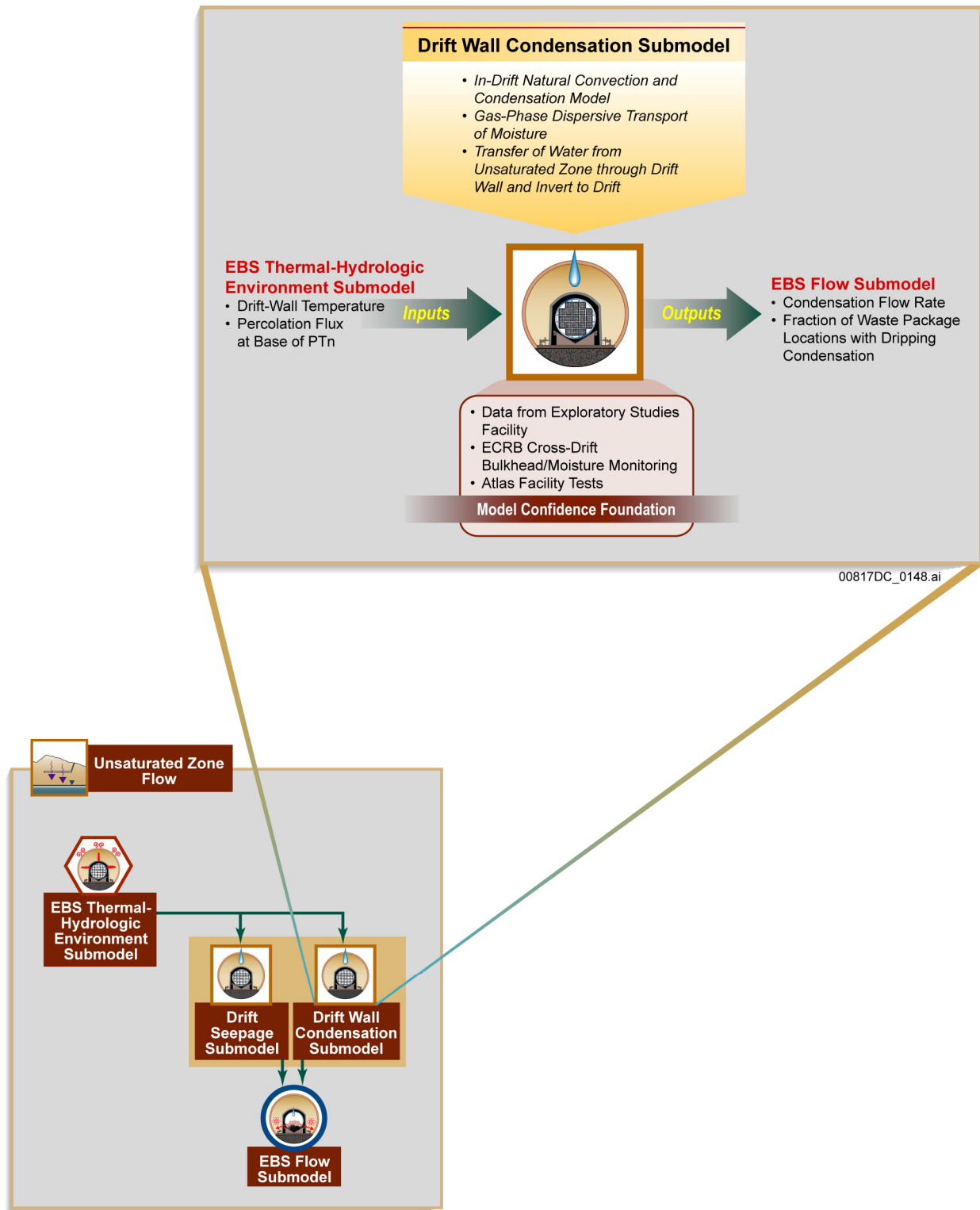


Figure 6.3.3-6. Inputs, Outputs, and Basis for Model Confidence for the Drift Wall Condensation Submodel

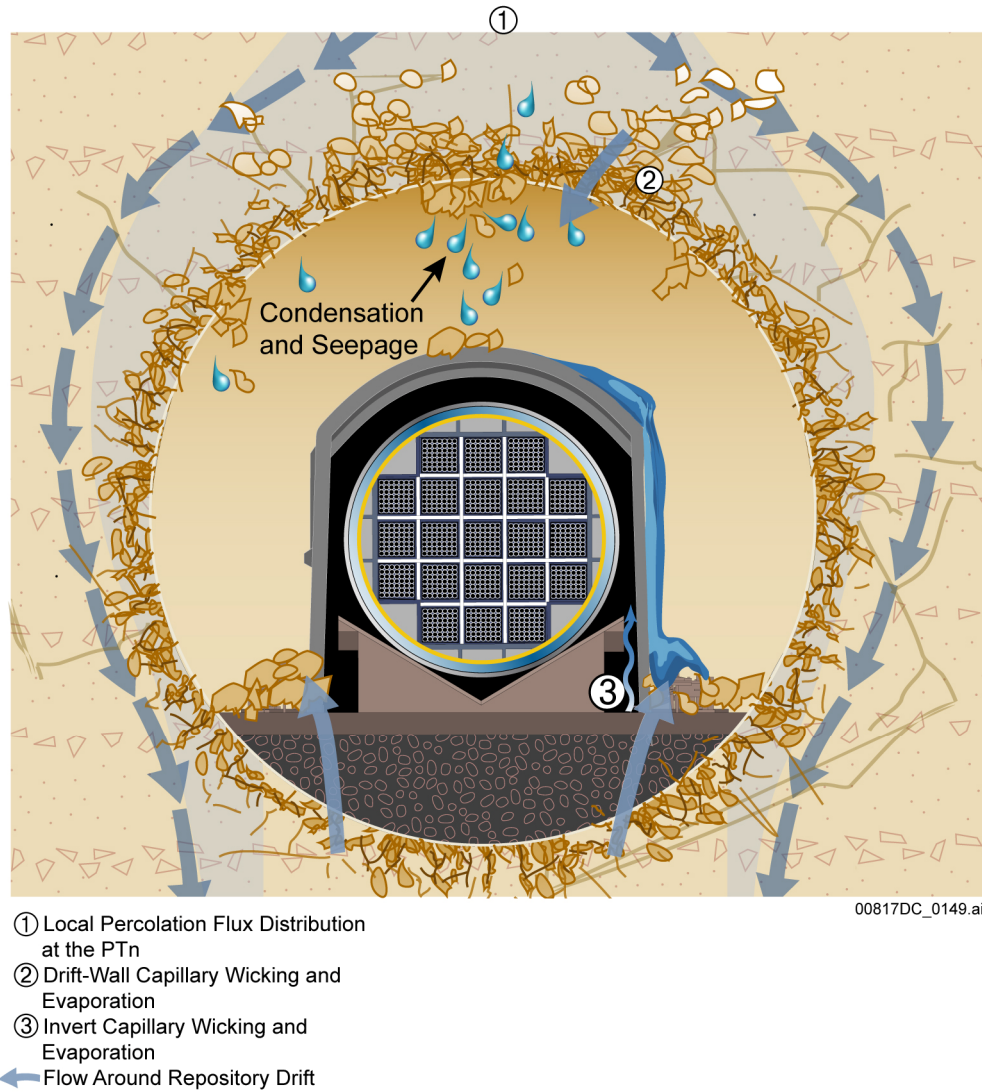
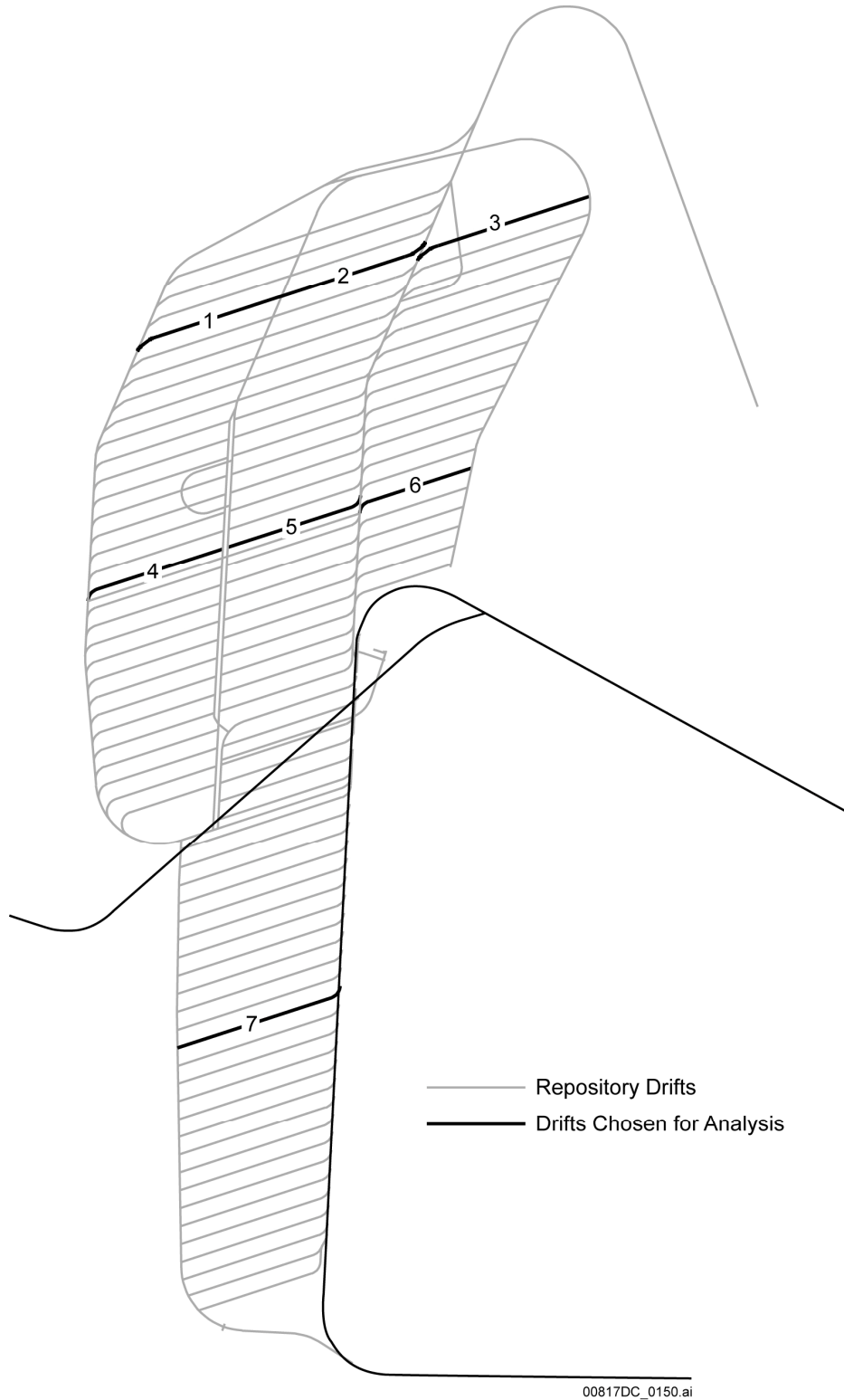


Figure 6.3.3-7. Schematic Illustration of the Processes Affecting Drift-Wall Condensation



Source: Modified from SNL 2007 [DIRS 181648], Figures 6-1[a] and 6-2[a].

Figure 6.3.3-8. Schematic Depicting Approximate Locations of Disposal Drifts Chosen for Condensation Analysis

6.3.4 Engineered Barrier System Chemical Environment

Engineered Barrier System: Physical and Chemical Environment (EBS P&CE) (SNL 2007 [DIRS 177412]) suite of models is implemented in both the TSPA-LA Model and for calculations external to the TSPA-LA Model. The EBS P&CE Abstractions are implemented by the EBS Chemical Environment Submodel. This submodel consists of an algorithm to calculate the time-dependent partial pressure of CO₂ (P_{CO_2}) and look-up tables to determine the values of the time-dependent parameters pH, ionic strength, aqueous chloride concentration [Cl⁻], and aqueous nitrate concentration [NO₃⁻]. These chemical-environment variables determine whether localized corrosion of the WP outer barrier occurs in the TSPA-LA Localized Corrosion Initiation Analysis, and they determine radionuclide mobility in the invert (i.e., radionuclide solubility and colloid stability) in the TSPA-LA Model. Within the TSPA-LA Model, outputs of the EBS Chemical Environment Submodel primarily serve as inputs used to calculate radionuclide solubility (Section 6.3.7.5.3) and colloid stability (Section 6.3.7.6.3) in the invert. Other than the P_{CO_2} in the drift, the EBS Chemical Environment Submodel does not provide input to in-package chemistry because *In-Package Chemistry Abstraction* (SNL 2007 [DIRS 180506], Section 6.6.2[a]), shows that the chemistry inside a failed WP is insensitive to incoming water composition.

The EBS Chemical Environment Submodel, as implemented in both the TSPA-LA Model and the Localized Corrosion Initiation Analysis, simulates the temporal changes of P_{CO_2} , pH, ionic strength, [Cl⁻], and [NO₃⁻] by using models developed in *EBS P&CE* (SNL 2007 [DIRS 177412], Section 6.15). The algorithm for P_{CO_2} calculates the P_{CO_2} as a function of time and incoming seepage water composition. The response surfaces for pH, ionic strength, [Cl⁻], and [NO₃⁻] are calculated as functions of incoming seepage water composition, water-rock interaction parameter (WRIP), temperature, and P_{CO_2} . The relative humidity is the independent variable in using the response surfaces. The P_{CO_2} is used as an input to the Dissolved Concentration Limits Submodel (Section 6.3.7.5) and the In-Package Chemistry Submodel (Section 6.3.7.2), as applied to the interior of a failed WP. In addition, P_{CO_2} , pH, and ionic strength are used as inputs to the Dissolved Concentration Limits Submodel (Section 6.3.7.5) and the EBS Colloids Submodel (Section 6.3.7.6), as applied in the invert. The pH, [Cl⁻], and [NO₃⁻] are used to assess the potential to initiate localized corrosion on the WP outer barrier (Section 6.3.5.2). The EBS TH Environment Submodel described in Section 6.3.2 provides the comprehensive time histories of temperature and relative humidity to the EBS Chemical Environment Submodel crown seepage chemistry calculations and provides the representative time histories to the EBS Chemical Environment Submodel invert chemistry calculations. Information flow and connections between the EBS Chemical Environment Submodel and other TSPA-LA Model components and submodels are shown on Figure 6.3.4-1. Figure 6.3.4-2 presents an overview of the important in-drift processes that impact the results, inputs, outputs, and level of confidence in the EBS Chemical Environment Submodel. Figure 6.3.4-3 illustrates the locations of in-drift EBS structures and materials, including WPs, DSs, and the invert.

6.3.4.1 Conceptual Model

The EBS Chemical Environment Submodel quantifies P_{CO_2} in the drift and invert; pH and ionic strength in the invert water; and pH, $[Cl^-]$, and $[NO_3^-]$ in the crown seepage water. The *EBS P&CE* (SNL 2007 [DIRS 177412]) applies the same P_{CO_2} to the drift, the invert, and the inside of the WP. Various physical and chemical processes in the WPs and geochemical processes in the invert depend on the output from the EBS Chemical Environment Submodel. The P_{CO_2} inside the WPs influences the degradation of the waste forms and the solubility of the radionuclides inside failed WPs. The P_{CO_2} in the invert influences the solubility of the radionuclides in the invert. Brines that form by evaporative concentration from seepage which enters the invert by dripping, can influence radionuclide mobility (i.e., radionuclide solubility and colloid stability) in the invert. Acidic or alkaline water in the invert could enhance the solubility of radionuclides. The ionic strength of water in the invert will control the stability of colloidal material transporting sorbed radionuclides and could also influence the solubility of radionuclides in the invert. The pH, $[Cl^-]$, and $[NO_3^-]$ of the crown seepage water dripping onto a WP are parameters used to assess the initiation of localized corrosion of the WP outer barrier.

The *EBS P&CE* (SNL 2007 [DIRS 177412]) performed an analysis of the evolution of the physical and chemical environment in the EBS, including an evaluation of likely changes to the compositions of gas, water, and solids within the emplacement drifts under repository conditions. The following influences were evaluated for their potential to cause compositional changes in water in the EBS:

- The compositions of water and gas that enter the drifts from the host rock
- Changing thermal conditions in the drifts
- The interactions of seepage water and gas with introduced engineered materials
- The compositions of evaporating or condensing waters within the drifts.

The overall conceptual model is as follows. As infiltrating water moves downward toward the repository, it moves up a thermal gradient. The thermal gradient extends from the land surface to the repository level and is assumed to vary linearly with depth. The water interacts with minerals in the rock, maintaining equilibrium with calcite and amorphous silica, present in excess, and dissolving alkali feldspar, while precipitating out one or more secondary phases. The degree of feldspar dissolution is a function of the temperature at any location along the percolation path, and is calculated using a temperature-dependent dissolution rate. The dissolution rate was estimated for ambient conditions from the degree of alteration that the tuff has undergone since it erupted, 12.8 million years ago, and adjusted for temperature using literature data for the activation energy for feldspar dissolution (SNL 2007 [DIRS 177412], Section 6.3.2.1). Little evaporation or degassing occurs as the water moves up the thermal gradient, until it reaches a lower-saturation zone around which steam and gas can readily escape into the drift, where steam is transported axially to cooler zones and condenses. The low saturation zone is the drift and areas in the surrounding rock, including fractures connecting to the drift, which are readily accessed by the in-drift atmosphere. Evaporation occurs at the boundary between the higher saturation area surrounding the drift and the lower saturation area, which will, hereafter, be referred to as the evaporation front. During the boiling period, this boundary corresponds to the boiling zone around the drift. At later times, it corresponds to the drift wall and fractures extending outward from the drift, close enough to be in gas-phase

equilibrium with the drift wall. The P_{CO_2} in the drift is controlled by equilibrium with the water at the evaporation front, with dilution by water vapor, generated by evaporation at the front.

As seepage waters enter drifts their chemical compositions may change due to evaporation, mineral precipitation, or both. Throughout the thermal period (depending on the relative humidity in the drifts), evaporative concentration of seepage can occur in the EBS. Evaporation increases aqueous species concentrations, mineral precipitation, and the concentration of the most soluble components in brines. In accordance with the geochemical divide theory, the composition of the seepage water changes according to the sequence of minerals that precipitate from that solution as a function of initial water composition, thermal conditions, relative humidity, and gas composition where the evaporation occurs (SNL 2007 [DIRS 177412], Section 6.3.3.1).

Figure 6.3.4-4 depicts several representative locations along a vertical flow path from the crown of the drifts to the base of the invert. The chemical compositions of the water and the gas at each of these representative locations could directly affect the degradation rates of the EBS, the quantities and species of mobilized radionuclides, and/or the transport rates of radionuclides and fluids flowing through the drifts into the UZ.

The following describes conditions shown on Figure 6.3.4-4, Locations 1 through 5 (adapted from (SNL 2007 [DIRS 177407], Figure 6.6-4) and SNL 2007 [DIRS 177412], Section 6.5).

Location 1 (Drift Wall and Air Gap)—Possible seepage water and gas chemistries at Location 1 could be modified by interactions with engineered materials, such as rock bolts and stainless steel sheets and their corrosion products, or directly drip into the drifts and onto surfaces of the DSs (Location 2). Generally, potential seepage water interactions with engineered materials and their corrosion products will not alter the major ion composition in water entering the drifts (SNL 2007 [DIRS 177412], Section 6.8 and Tables 6.8-3 through 6.8-6). Given the limited longevity of the low-alloy steels that comprise some of the ground support and all of the invert materials such as gantry rails, support beams, and other engineered materials, this effect would be on the order of hundreds of years for most materials placed within the drifts (SNL 2007 [DIRS 177412], Section 6.5.2). A sensitivity analysis investigating the potential impacts on water chemistry revealed the impacts are negligible (SNL 2007 [DIRS 177412], Section 6.8). For the longer-lasting materials, such as the 316L stainless steel that comprises the wire mesh ground support component, sensitivity analyses also show that corrosion processes have a negligible effect on the composition of seepage waters (SNL 2007 [DIRS 177412], Section 6.8). Any potential impact of emplaced materials is indirectly considered in the TSPA-LA Model through the output of the EBS P&CE suite of models.

Location 2 (Surface of the DS)—Some portion of the water from Location 1 may be diverted directly to the invert (Location 5) by the DSs, or may undergo evaporative processes, and/or react with debris sitting on the DSs. If the DSs are breached, these fluids could flow onto the surface of the WPs (Location 3) but could only flow into the WPs (Location 4) through an available pathway. Corrosion products associated with the DSs are not expected to adversely affect the compositions of any waters flowing off or through DSs, due to the very slow corrosion rates for titanium and the insoluble nature of titanium oxides (SNL 2007 [DIRS 177412], Section 6.5.1.1). For the same reasons, the removal or addition of trace elements by sorption or

dissolution processes associated with active corrosion of the DSs' titanium alloy is not considered.

Location 3 (Outer Surface of WPs)—Alloy 22, the alloy of the WP outer barrier, like the titanium used for DSs, is also highly corrosion resistant (SNL 2007 [DIRS 177412], Section 6.5.1.2). The processes occurring at Location 2 also apply to Location 3. The potential for localized corrosion on the WP outer barrier depends on whether or not seepage-derived water contacting the WPs is capable of initiating localized corrosion.

Location 4 (Inside the WP)—This portion of the conceptual process is reported in other modeling reports, such as *In-Package Chemistry Abstraction* (SNL 2007 [DIRS 180506]) and in Section 6.3.7.2 of this report.

Location 5 (Invert)—The chemical environment in the invert affects radionuclide solubility and colloid stability. Both radionuclide solubility and colloid stability could affect the radionuclide mobilization from the source term for transport from the EBS to the UZ. Implementation of the P&CE integrated invert chemistry abstraction model is discussed in *EBS P&CE* (SNL 2007 [DIRS 177412], Section 6.13.4, Section 6.15.2, and Table 6.15-1).

6.3.4.2 TSPA Abstraction

Within the TSPA-LA Model, the EBS Chemical Environment Submodel calculates time-dependent P_{CO_2} in the gas phase in the drift above the invert and pH and ionic strength conditions in the invert. Within the Localized Corrosion Initiation Analysis (Section 6.3.5.2), the EBS Chemical Environment Submodel calculates time-dependent P_{CO_2} in the gas phase in the drift above the invert and the pH, $[Cl^-]$, and $[NO_3^-]$ in the crown seepage water. The same time-dependent P_{CO_2} in the gas phase in the drift above the invert is used for the drift P_{CO_2} , the in-package P_{CO_2} , and the invert P_{CO_2} .

The EBS Chemical Environment Submodel is based on the Near Field Chemistry model developed in *Engineered Barrier System: Physical and Chemical Environment* (SNL 2007 [DIRS 177412]). The Near Field Chemistry model provides potential seepage water compositions at the drift wall, the water-rock interaction parameter, and the range of in-drift P_{CO_2} . The evolution of pH, ionic strength, $[Cl^-]$, and $[NO_3^-]$ are also modeled using response surfaces in the form of look-up tables. Each look-up table is a function of initial water type, water-rock interaction parameter, temperature, and P_{CO_2} with relative humidity as the independent variable. The interaction between seepage water and engineered materials is not included in the analysis because the EBS P&CE Abstraction determined that this interaction has a negligible impact on the composition of seepage water and in-drift gas phases (SNL 2007 [DIRS 177412], Sections 6.5, 6.7, and 6.8). The following processes, represented by the EBS Chemical Environment Submodel, are abstracted below:

- Temporal evolution of incoming seepage water composition, where seepage includes dripping from the drift crown
- Changing P_{CO_2} in the drifts and the invert

- Evaporative evolution of seepage water composition from the drift crown and in the invert.

Evolution of Incoming Seepage Composition—The Near Field Chemistry model defines four starting waters as representative of the potential range of the Topopah Spring Tuff pore water compositions (SNL 2007 [DIRS 177412], Sections 6.3.2 and 6.6). As pore water percolates downward, it interacts with minerals in the rock. The water-rock interactions modify the water composition. During the thermal pulse, the degree of modification due to water-rock interactions is increased, relative to ambient conditions, as the water percolates down through the heated rock above the repository. Ultimately, this thermally altered water is what enters the drift and controls the chemical conditions in the drift.

The degree of alteration is determined by the amount of water-rock interaction, quantified by the parameter called the water-rock interaction parameter. The water-rock interaction parameter is affected by the percolation rate through the rock and the thermal field through which the water passes. Ambient conditions are characterized as having zero water-rock interaction. Large water-rock interactions can be caused by high temperatures and slow percolation fluxes through the TSw. Lower temperatures and/or faster water movement will cause less water-rock interaction. The model follows a packet of water from the surface as it passes through the time-dependent thermal field to the repository taking into account the climate changes that change the velocity of the infiltrating water.

The EBS physical and chemical environment defines water-rock interaction parameter as a time-dependent function of the glacial transition percolation flux and the thermal measure. The thermal measure is defined as the sum of peak WP temperature (in degrees C) and the duration of boiling (in years). Obviously, this parameter is not really physical because it is in mixed dimensional units. However, the summed value captures the effects of variations in the thermal history of a given WP due to the location in the repository, assumed rock properties (i.e., thermal conductivity), and WP specific heat generation rate. Therefore, it provides a useful metric for discriminating between thermal histories at different repository locations. The percolation rate also can influence the thermal measure of the WP because high percolation tends to cool the repository more quickly. The water-rock interaction parameter is parametrically evaluated at each location (i.e., thermal measure) using twenty different sets of four percolation fluxes representing the three climate states and the post-10,000 year percolation state. The glacial transition flux is used to represent each of the twenty sets of flux values. Thermal measures and glacial-transition percolation fluxes have been extracted from the MSTHM results for the representative WPs used in TSPA-LA. Once the thermal measure and glacial transition flux is specified, the time-dependent value of water-rock interaction parameter can be found from the water-rock interaction parameter look-up table.

Multiscale Thermohydrologic Model (SNL 2007 [DIRS 181383], Section 6.3.15[a]) provides the data for calculating the thermal measure. These MSTHM files contain the thermal histories for each representative package. The maximum temperature and the duration of boiling are manually extracted from the files and then added together. Note that the duration of boiling is defined as the time from WP emplacement until the WP cools below 96° C. These calculated thermal measures are then used to create two look-up tables in the TSPA-LA Model, one for CSNF WPs and one for CDSP WPs.

Uncertainty in input parameters for calculating the water-rock interaction parameter values is propagated through the Near Field Chemistry model as described in *EBS P&CE* (SNL 2007 [DIRS 177412], Section 6.12.2.5). These water-rock interaction parameter values are passed to TSPA as a beta distribution, the mean value of which is extracted from the water-rock interaction parameter look-up table. The maximum value of the beta distribution is specified to be 2.838 times the mean, the minimum is 0.2039 times the mean, and the standard deviation is 0.4251 times the mean. This uncertainty is primarily due to uncertainty in the feldspar dissolution rate (SNL 2007 [DIRS 177412], Section 6.12.2.5). In each realization, the TSPA-LA Model extracts the water-rock interaction parameter value from the look-up table and generates a new distribution at each timestep. The TSPA-LA Model correlates the water-rock interaction parameter beta distribution to a stochastic parameter, WRIP_beta_rand_a, which is uniform stochastic between 0 and 1. This correlation insures that even though the shape of the beta distribution changes at each timestep, the distribution is sampled at the same probability level at each timestep for the entire realization (SNL 2007 [DIRS 177412], Section 6.15.1).

The water-rock interaction parameter and the WP temperature form the basis for calculating the P_{CO_2} in the drift. Relevant CO_2 concentrations in the gas phase within the rock are difficult to determine (SNL 2007 [DIRS 177412], Section 6.3.2.5). As water percolates downward through the thermal field and heats up, CO_2 is partitioned into the gas phase. This is offset by the effects of feldspar dissolution, which raises the alkalinity and reduces the degree of partitioning into the gas phase. The relative rates of these two processes are important because the degree to which the gas phase acts as an open system—the amount of CO_2 that would be lost or gained by gas phase advection and mixing—is unknown. Given that matrix saturations are high and fracture porosity is low, it is assumed for the Near Field Chemistry model that gas phase transport is limited, except for the area immediately around the drift, where loss into the drift can occur; therefore, the gas phase composition at any location in the rock column is determined by assuming equilibrium with the aqueous composition, rather than being controlled by gas phase advection and mixing.

P_{CO_2} as a Function of Time—Calculating the P_{CO_2} in the drift is difficult because it is the result of competing processes such as evaporation, degassing, precipitation, diffusion, and advection of gas in the fractures, and scavenging of CO_2 by condensation in the cooler drift ends. Two bounding cases are considered (SNL 2007 [DIRS 177412], Section 6.3.2.8):

- *Minimum CO_2 concentration in the drift.* In this bounding case, gas movement into and out of the drift, and through the mountain, is assumed to occur readily through fractures. The CO_2 concentration in the air fraction entering the drift is equal to the ambient CO_2 concentration in the mountain at the repository level (10^{-3} bars). The contribution of this to the total CO_2 in the drift atmosphere is equal to this concentration times the mole fraction of air in the drift. Added to this is the CO_2 that is released by evaporating water at the dryout front. This yields a minimum concentration for CO_2 in the drift.
- *Maximum CO_2 concentration in the drift.* Behind the evaporation front, the gas phase is assumed to be in equilibrium with the aqueous phase at the temperature of the evaporation interface, assuming that the water moved up the temperature gradient to the interface without degassing. Treating the drift as a closed system, the in-drift P_{CO_2} would equal this value, which can be taken as a maximum for the in-drift atmosphere. If

the model predicts large amounts of feldspar dissolution, but relatively low temperatures (e.g., for extremely slow percolation flux rates, water percolated through hot rocks, but did not reach the drift wall until it had cooled), then it is possible for the predicted maximum P_{CO_2} to actually be below 10^{-3} bars. This is because the alkalinity increases as feldspar dissolves, increasing the amount of CO_2 dissolved into the water. If this occurs, it is assumed that the maximum P_{CO_2} value is 10^{-3} bars.

Thus, combining the lower and upper bounds for the in-drift P_{CO_2} yields the possible range of CO_2 concentrations in the drift and also in the invert.

Evaporative Evolution of Seepage at the Drift Crown and in the Invert—Equilibrium compositions of aqueous solutions and mineral precipitates that may form from seepage water within the emplacement drifts were calculated using the model developed in Section 6 and summarized in Section 8 of *In-Drift Precipitates/Salts Model (IDPS)* (SNL 2007 [DIRS 177411]), hereafter referred to as the IDPS Process Model. Calculations of water compositions at chemical equilibrium were performed using the geochemical equilibrium code, EQ3/6 Version 8.0 (*Software Code: EQ3/6. V8.0* (BSC 2003 [DIRS 162228])), and a Pitzer thermodynamic database developed specifically for that purpose (SNL 2007 [DIRS 177412], Table 4.1-1 and Section 6.2.6). The IDPS Process Model simulates the evolution of water in the drifts as it evaporates from its initial composition into concentrated brine. The *EBS P&CE* applies the IDPS Process Model to each of the four starting waters (SNL 2007 [DIRS 177412] Section 6.6) to produce chemical composition look-up tables (SNL 2007 [DIRS 177412] Sections 6.15 and 8.2). Within the TSPA-LA Model, the EBS Chemical Environment Submodel evaluates the EBS P&CE Abstraction to determine the chemistry of two drift waters. One type of water is seepage water dripping from the drift crown and the second type of water is the invert water that originated as water dripping from the drift crown. Seepage water dripping from the drift crown may flow onto the DS and, in the event of a failed DS, may subsequently contact the WP surface. Invert water that originated as water dripping from the drift crown may flow directly into the invert or may contact the DS and/or WP before it reaches the invert.

The implementation instructions for evaluating the EBS P&CE, with uncertainties, are given in the *EBS P&CE* (SNL 2007 [DIRS 177412], Sections 6.12 and 6.15). The look-up tables for pH, ionic strength, $[Cl^-]$, and $[NO_3^-]$ are calculated as functions of incoming seepage water composition, water-rock interaction parameter (WRIP), temperature, and P_{CO_2} . The relative humidity is the independent variable in using the look-up tables. These chemical composition look-up tables will be referred to as IDPS look-up tables, because they are generated with the IDPS Process Model, and to distinguish them from other look-up tables (such as water-rock interaction parameter look-up tables illustrated in Table 6.3.4-1) that are generated by the EBS P&CE suite of models (SNL 2007 [DIRS 177412], Section 6.15).

As described below, there are 396 IDPS look-up tables for seepage and invert water composition spanning combinations of P_{CO_2} and temperature for each of the four starting water types, 11 water-rock interaction parameter levels, and nine combinations of three P_{CO_2} values and three temperatures. Each table lists values for chemical composition, including pH, ionic strength, $[Cl^-]$, and $[NO_3^-]$ with relative humidity as the independent variable. Each IDPS look-up table is defined for a specific starting water type, temperature, and P_{CO_2} . The tables are defined for P_{CO_2} values of 10^{-2} , 10^{-3} , and 10^{-4} bar; and temperature values of 30°C, 70°C, and 100°C. There are

99 tables for all possible combinations for each of the four starting waters. The IDPS tables for the TSPA-LA are part of DTN: SN0701PAEBSPCE.001_R1 [DIRS 180523] and guidance for using these inputs is provided in *EBS P&CE* (SNL 2007 [DIRS 177412], Sections 6.12 and 6.15).

An example of an IDPS look-up table is shown in Table 6.3.4-2.

Model Uncertainties, Variabilities, and Discretization Errors—Model confidence for incoming seepage water, P_{CO_2} , pH, ionic strength, $[Cl^-]$, and $[NO_3^-]$ is discussed in the following paragraphs.

Incoming Seepage Water—The Near Field Chemistry process model (SNL 2007 [DIRS 177412]) provides potential seepage water compositions and the water-rock interaction parameter values for use in the P&CE abstraction models. Uncertainties in the inputs are treated as follows. The four input waters (Groups 1 through 4) were chosen statistically to represent the variability in 34 TSw waters upon evaporation. The uncertainty in the starting water composition is represented by randomly selecting one of the four water types for each realization. Because representative waters are used, it is also necessary to sample the range of Cl:N in the 34 TSw waters from a discrete CDF to capture the uncertainty associated with these key chemical parameters. Output seepage water compositions are presumed to span the natural variability of the pore water compositions in the repository units (SNL 2007 [DIRS 177412], Section 6.12.3).

Partial Pressure of Carbon Dioxide Gas—The range of uncertainty and variability is included in the abstractions of P_{CO_2} by using minimum and maximum P_{CO_2} bounding cases and then scaling between ambient and the bounding values. These two bounding cases provide the range of P_{CO_2} . The TSPA-LA Model uses a uniform stochastic variable, PCE_Delta_pCO2_a, between -1 and 1, to choose which of the bounding cases to use in each realization (SNL 2007 [DIRS 177412], Section 6.15.1). A negative value of the variable implies using the minimum P_{CO_2} case and a positive value implies the maximum P_{CO_2} case. The actual P_{CO_2} in the drift is calculated by linearly scaling between ambient (0.001 bars) and the minimum or maximum, using the absolute value of PCE_Delta_pCO2_a as the scaling factor. This scaling accounts for the uncertainty in the in-drift P_{CO_2} .

pH, Ionic Strength, $[Cl^-]$, and $[NO_3^-]$ —IDPS uncertainty factors for the $[Cl^-]$, $[NO_3^-]$, $[Cl^-]/[NO_3^-]$, and ionic strength of in-drift water are used directly by the P&CE abstraction models. The uncertainty associated with $[Cl^-] + [NO_3^-]$ is calculated assuming linear combinations of the individual uncertainties for $[Cl^-]$ and $[NO_3^-]$ provided by the IDPS Model (SNL 2007 [DIRS 177412], Table 6.12-1). These uncertainties apply between 20°C and 140°C and are defined as triangular distributions with the most likely uncertainty equal to 0.0 and the maximum and minimum uncertainties shown in Table 6.3.4-3 (SNL 2007 [DIRS 177412], Table 6.12-1).

The IDPS uncertainty for pH was developed by comparison of modeled data with pH values measured in several evaporation and mineral solubility experiments, and the process of measuring pH has significant error. The pH uncertainty value is taken directly from the look-up tables and is adjusted by the uncertainties reported in Table 6.3.4-3 (SNL 2007 [DIRS 177412],

Table 6.12-2), using a triangular distribution for relative humidity values below 75 percent. Between 100 percent and 75 percent relative humidity, pH uncertainties are sampled from a discrete CDF archived in DTN: SN0703PAEBSPCE.007_R2 [DIRS 184141] (see SNL 2007 [DIRS 177412], Section 6.12.3.1 for a discussion of how and why the pH uncertainty was reduced in the *EBS P&CE*).

No uncertainty is associated with the ionic strength below 85 percent relative humidity from the look-up tables because the ionic strength is not used by the TSPA-LA Model at these concentrations. Between 85 percent and 100 percent relative humidity, the ionic strength is adjusted for uncertainty by applying a triangular distribution and the value in Table 6.12-1 of *EBS P&CE* (SNL 2007 [DIRS 177412]). The guidance for applying these uncertainty distributions is provided in *EBS P&CE* (SNL 2007 [DIRS 177412], Section 6.12.3) and the input distributions are captured in DTN: SN0703PAEBSPCE.007_R2 [DIRS 184141].

6.3.4.3 TSPA-LA Model Implementation

The EBS Chemical Environment Submodel is implemented in the TSPA-LA Model to calculate the chemistry (pH and ionic strength) of the water in the invert (discussed in Section 6.3.4.3.1). The EBS Chemical Environment Submodel is also implemented in the Localized Corrosion Initiation Analysis (Section 6.3.5.2) to calculate the chemistry (pH, $[Cl^-]$, and $[NO_3^-]$) of the seepage water from the crown of the drift (discussed in Section 6.3.4.3.2). Although performed in two separate GoldSim files for three different applications, the submodel implementations are similar.

6.3.4.3.1 Invert Chemistry

The EBS Chemical Environment Submodel calculations for the invert are performed in two main levels of the TSPA-LA Model: global and local. Global calculations can be applied to all WPs and local calculations pertain only to those WPs in the local percolation subregion or percolation subregion environment. To reduce redundancy, the EBS Chemical Environment Submodel calculations that can be applied equally to all percolation subregions and both WP types are performed at a higher (global) level. For example, the selection of one of the four starting water compositions is performed at the global level. In the TSPA-LA Model, the selection of one of these four initial water compositions is randomly sampled with equal probability. The probability of selecting any one of the four source waters is 25 percent (SNL 2007 [DIRS 177412], Section 6.15.1). Once selected, the initial water composition determines which total carbon tables and maximum P_{CO_2} tables are used to calculate the P_{CO_2} . P_{CO_2} in the drift and in the invert must also match the selected starting water. Therefore, P_{CO_2} in the drift and P_{CO_2} in the invert are determined at the global level and the resulting P_{CO_2} values are applied to the entire repository. The EBS Chemical Environment Submodel calculations for the pH and ionic strength of the invert water require invert temperature and invert relative humidity, which are percolation subregion specific feeds from the EBS TH Environment Submodel (Section 6.3.2), and must be performed separately (locally) within each percolation subregion.

Inputs—Sections 6.9.3 and 6.15 of *EBS P&CE* (SNL 2007 [DIRS 177412]) provide the guidance for applying the 396 IDPS look-up tables for seepage composition captured in SN0701PAEBSPCE.001 [DIRS180523]. The IDPS look-up tables are used to determine the pH

and ionic strength in the invert as a function of starting water type, water-rock interaction parameter, temperature and P_{CO_2} . In the TSPA-LA Model implementation, the independent variable in each of the IDPS look-up tables is the applicable relative humidity. For the dependent variables, column 1 contains the pH, column 2 contains the ionic strength, column 3 contains $[Cl^-]$, and column 4 contains $[NO_3^-]$. Only the pH and ionic strength values are used in the invert chemistry calculations. The $[Cl^-]$ and $[NO_3^-]$ values are only used in the crown seepage chemistry calculations (Section 6.3.4.3.2). Each set of look-up tables was developed for each temperature combination of 30°C, 70°C, and 100°C; and P_{CO_2} values of 10^{-2} , 10^{-3} , and 10^{-4} bar; and 11 water-rock interaction parameter levels for a total of 99 look-up tables for each of the 4 starting water types. The PCE_Chemistry_Tables container in the TSPA-LA Model's GoldSim model file provides more information regarding these look-up tables and their applications. The methodology for applying uncertainty to the calculated pH and ionic strength is described in Section 6.12.3 of EBS P&CE (SNL 2007 [DIRS 177412]), and the applied uncertainty values are captured in DTN: SN0703PAEBSPCE.007_R2 [DIRS 184141], Estimated IDPS Uncertainties.xls. Additional calculation details are provided below and in the TSPA-LA Model GoldSim file.

The following describes the determination of the seepage water composition, invert temperature, invert relative humidity, and P_{CO_2} and their use in selecting the appropriate IDPS look-up tables for chemical composition for the interpolation of the appropriate pH and ionic strength values.

Global Calculations—Global level calculations begin with selecting one of the four initial starting waters, the representative WP and its thermal measure, and then calculating the water-rock interaction parameter for each TSPA percolation subregion (SNL 2007 [DIRS 177412], Section 6.15). Each TSPA-LA Model realization randomly selects one of the four starting percolating water compositions used for all percolation subregions. All the starting percolating water compositions are equally probable and, therefore, the probability of any given water being selected is 25 percent.

The water-rock interaction parameter is the one time-dependent independent parameter in the EBS Chemical Environment Submodel calculated at the global level. The water-rock interaction parameter describes the evolution of the water and specifies, along with the temperature and P_{CO_2} , which of the IDPS look-up tables (0-L) to use for pH, ionic strength, $[Cl^-]$, and $[NO_3^-]$. As described earlier, the water-rock interaction parameter requires sampling from a beta distribution at every timestep. This resampling, as well as the separation of aleatory and epistemic uncertainty, requires that the water-rock interaction parameter for every percolation subregion and WP type be calculated as a time-series at the global level before the main calculation. Then the water-rock interaction parameter is passed to the local level calculations for use along with the temperature and P_{CO_2} in selecting the appropriate IDPS look-up table for pH, ionic strength, $[Cl^-]$, and $[NO_3^-]$.

Local Calculations—After the starting water is selected and the water-rock interaction parameter is calculated at the global level, the appropriate P_{CO_2} for the drift and the invert can be calculated. P_{CO_2} values are determined at each timestep. The drift P_{CO_2} is used to calculate radionuclide solubilities in the WPs (Section 6.3.7.5) and total carbonate concentration in the failed WPs (Section 6.3.7.2). The same P_{CO_2} applies in the invert and is used to calculate

radionuclide solubilities in the invert (Section 6.3.7.5) and the pH and ionic strength of the invert water.

The P_{CO_2} values in the invert are determined at each simulation timestep. The TSPA-LA Model then uses the invert P_{CO_2} value, the selected starting water composition, and water-rock interaction parameter value (0-L), along with the invert temperature and relative humidity feeds from the EBS TH Environment Submodel (Section 6.3.2), to determine pH and ionic strength in the invert water using the IDPS look-up tables. The EBS TH Environment Submodel (Section 6.3.2) feeds for the representative invert temperature and relative humidity are percolation subregion-specific values, so the remaining calculations in the EBS Chemical Environment Submodel are performed locally (i.e., separately for each percolation subregion or percolation subregion environment).

WPs occupying representative emplacement drift locations, shown on Figure 6.1.4-2, are characterized by representative time histories of TH (temperature and relative humidity) and average drift-seepage rates that are provided by the EBS TH Environment Submodel (Section 6.3.2) and the Drift Seepage Submodel (Section 6.3.3.1), respectively. The EBS Chemical Environment Submodel uses these conditions and P_{CO_2} to calculate time-dependent pH and ionic strength conditions in the invert for the representative WP location in each percolation subregion.

The determination of pH and ionic strength in the invert water is performed locally within each percolation subregion in the TSPA-LA Model. The actual chemistry used in the invert is determined by the scenario class, the dripping or non-dripping environment, whether the WP and/or DS is intact, whether drift wall condensation occurs, and the seepage flux, as specified in Table 6.3.4-4. The EBS TH Environment Submodel (Section 6.3.2) provides the EBS Chemical Environment Submodel the representative temperature and relative humidity for each percolation subregion at each timestep.

The discussion presented below describes how the IDPS look-up tables are applied in the TSPA-LA Model to determine the chemical parameters in the invert. Although presented as the calculation of invert chemistry in the TSPA-LA Model, the following discussion is meant to be a robust discussion of the EBS Chemical Environment Submodel covering the submodel applications in both the TSPA-LA Model and the Localized Corrosion Initiation Analysis (Section 6.3.5.2). In evaluating the EBS Chemical Environment Submodel for crown seepage chemistry in the Localized Corrosion Initiation Analysis (Section 6.3.5.2), the tables are still applicable and a discussion of these tables is still warranted.

At each timestep, the EBS Chemical Environment Submodel accesses eight of the 396 IDPS look-up tables (see example in Table 6.3.4-2) and uses the current starting water, water-rock interaction parameter value, P_{CO_2} , temperature, and relative humidity to determine the corresponding pH and ionic strength in the invert. The eight most appropriate IDPS look-up tables for the local environment calculations in the invert are determined by eliminating tables that are not appropriate for current invert conditions, as described below. The starting water (1, 2, 3, or 4) reduces the applicability of the 396 IDPS look-up tables to 99. The applicability of the 99 IDPS look-up tables are reduced at each timestep to 18 by choosing only those tables that are associated with the water-rock interaction parameter value at the timestep. The actual

chemical conditions are determined by interpolation of values between eight of the 18 IDPS tables. The water-rock interaction parameter value is a decimal number between 0 and 10 that determines which of 11 sets of nine IDPS look-up table to use. These 11 sets of nine IDPS tables can be thought of as arranged in layers. The floor function can be used to calculate the integer below the water-rock interaction parameter value of interest and the ceil function can give the integer above the water-rock interaction parameter value. Thus, the actual water-rock interaction parameter value is somewhere between two layers of IDPS look-up tables. These 18 tables in two layers are further reduced to eight by selecting those tables that represent the eight nearest neighbors to the desired temperature and P_{CO_2} . For example, if the invert temperature is below 70°C, the IDPS look-up tables corresponding to 30°C and 70°C will be used and the 100°C tables can be excluded. Otherwise, the IDPS look-up tables corresponding to 70°C and 100°C will be used and the 30°C tables can be excluded. Similarly, if the invert P_{CO_2} is below 10^{-3} bar, the IDPS look-up tables corresponding to 10^{-2} bar can be excluded, and if the invert P_{CO_2} is above 10^{-3} bar, the IDPS look-up tables corresponding to 10^{-4} bar can be excluded. The eight remaining IDPS look-up tables, four in each water-rock interaction parameter value layer, are the resulting look-up tables consistent with the current value of the water-rock interaction parameter, invert temperature, and invert P_{CO_2} .

To select the pH and ionic strength corresponding to the specific invert relative humidity desired from each of the eight IDPS look-up tables, the EBS Chemical Environment Submodel applies linear interpolation in three directions between the eight tables. When selecting pH and ionic strength values for temperature and P_{CO_2} values that fall between the pre-defined values of the IDPS look-up tables, the parameters are estimated from the eight look-up table results using linear interpolation for temperature and water-rock interaction parameter layer, and log-linear interpolation for P_{CO_2} . Chemistry values are extrapolated for pH and ionic strength if P_{CO_2} is outside the range of 10^{-4} to 10^{-2} bar. Extrapolation of P_{CO_2} is valid over the range 10^{-5} to 2×10^{-2} bar (SNL 2007 [DIRS 177412], Section 7.2.2). For temperatures greater than 100°C and less than 30°C, values are taken from the 100°C or 30°C IDPS look-up tables, respectively (SNL 2007 [DIRS 177412], Section 6.15.1). If the relative humidity is greater than the highest relative humidity value in the IDPS look-up tables, the TSPA-LA Model uses those pH and ionic strength values that are associated with the highest relative humidity in the applicable IDPS look-up table. If relative humidity is lower than the lowest relative humidity value in the IDPS look-up tables, the TSPA-LA Model uses the pH and ionic strength that are associated with the lowest relative humidity in the applicable look-up table (SNL 2007 [DIRS 177412], Section 6.15.1).

After the pH and ionic strength parameters are calculated, these quantities are adjusted for epistemic uncertainty and discretization error in accordance with the specific instructions provided in Section 6.12.3 of *EBS P&CE* (SNL 2007 [DIRS 177412]). The uncertainty for pH, ionic strength, $[Cl^-]$, $[NO_3^-]$, and $[Cl^-]/[NO_3^-]$ is specified as a function of the relative humidity. Except for the pH in the highest relative humidity range, the distributions are triangular distributions (DTN: SN0703PAEBSPCE.007_R2 [DIRS 184141]). The IDPS uncertainty for pH was developed by comparison of modeled data with pH values measured in several evaporation and mineral solubility experiments, and the process of measuring pH has significant error. In the *EBS P&CE* (SNL 2007 [DIRS 177412], Section 6.12.3.1), the uncertainty in pH, for the range from 100 percent to 75 percent relative humidity is determined indirectly, by

comparison of measured and predicted concentrations of pH-sensitive aqueous species. For this relative humidity range, the pH uncertainties are sampled from a discrete distribution archived in DTN: SN0703PAEBSPCE.007_R2 [DIRS 184141]. At relative humidities below 75 percent, the IDPS pH uncertainty value is used.

Additional detail on the application of uncertainty to the calculated pH and ionic strength in the invert is provided in the PEFs associated with the uncertain parameters. Additional details on the EBS Chemical Environment Submodel calculations, including the application of uncertainty, are provided in the TSPA-LA Model's GoldSim model file.

The EBS Chemical Environment Submodel provides the following outputs for each percolation subregion and each representative WP and early-failed WP group in dripping and non-dripping environments:

- Time-dependent P_{CO_2} in the invert
- Time-dependent pH in the invert
- Time-dependent ionic strength in the invert.

6.3.4.3.2 Crown Seepage Chemistry

The EBS Chemical Environment Submodel is also used to calculate the time-dependent $[Cl^-]$, $[NO_3^-]$, $[Cl^-]/[NO_3^-]$, and pH of the seepage water contacting the WP surface in the event that a DS fails to divert flow around a WP. These chemical-environment variables are used to calculate localized corrosion on the WP outer surface. These determinations are made outside of the main TSPA-LA Model in an analysis developed exclusively for determining the potential for localized corrosion occurrence (identified as the Localized Corrosion Initiation Analysis (Section 6.3.5.2)).

The EBS Chemical Environment Submodel is used to calculate pH, $[Cl^-]$, and $[NO_3^-]$ in the crown seepage water in the Localized Corrosion Initiation Analysis. The inputs and calculations discussed in Section 6.3.4.3.1 for the invert chemistry calculations are equally suitable for determinations of the crown seepage chemistry used in the Localized Corrosion Initiation Analysis. However, the feeds for P_{CO_2} , relative humidity, and temperature differ from the invert application. The crown seepage water application of the EBS Chemical Environment Submodel performs the same submodel calculations as the invert calculations using the same 396 IDPS look-up tables, but it includes different feeds for the applicable P_{CO_2} , temperature, and relative humidity. In the invert application of the EBS Chemical Environment Submodel, the applicable temperature and relative humidity is the representative invert temperature and invert relative humidity from the EBS TH Environment Submodel (Section 6.3.2). The representative data set is defined in Section 6.3.2.2.1 as the TH response histories for each of the five repository subregions based on a single, representative WP for each fuel type. The Localized Corrosion Initiation Analysis (Section 6.3.5.2) uses the WP surface temperature and relative humidity along with the drift P_{CO_2} to evaluate conditions on the WP surface from the 396 IDPS look-up tables. Similar to the seepage model, the Localized Corrosion Initiation Analysis evaluates WPs at each of the 3,264 subdomain locations from the MSTHM Process Model (SNL 2007 [DIRS 181383], Section 6.2.12[a]) as opposed to using representative packages for each subregion. When the IDPS look-up tables are used, instead of accessing columns 1 and 2 for pH and ionic strength,

the crown seepage calculations use the same look-up tables but they extract chemical information from column 1 for pH, column 3 for $[Cl^-]$, and column 4 for $[NO_3^-]$.

Global Calculations—The global calculations for the evaluation of crown seepage chemistry using the EBS Chemical Environment Submodel determine the applicable starting water and the water-rock interaction parameter time history. The implementation is identical to the previous discussion regarding invert calculations and is not being repeated.

Local Calculations—The local calculations of the EBS Chemical Environment Submodel determine the P_{CO_2} pH, $[Cl^-]$, and $[NO_3^-]$ of the crown seepage water. The extraction of chemical parameters from the 396 IDPS look-up tables is similar to that described for the invert water pH and ionic strength; however, WP surface values for temperature, P_{CO_2} , and relative humidity are fed into the look-up table selections and subsequent calculations.

Section 6.12.3 in *EBS P&CE* (SNL 2007 [DIRS 177412]) discusses the addition of uncertainty to the EBS Chemical Environment Submodel calculations. The application of uncertainty for pH is analogous to the invert implementation. The treatment of $[Cl^-]$ and $[NO_3^-]$ uncertainty is significantly different from that previously discussed and requires further discussion.

The following steps should be taken to calculate the $[Cl^-]$, $[NO_3^-]$, $[Cl^-+NO_3^-]$ concentrations and $[Cl^-]/[NO_3^-]$ ratios. The EBS P&CE abstraction models (SNL 2007 [DIRS 177412], Section 6.12.3) use the molal concentrations of Cl and N to represent $[Cl^-]$ and $[NO_3^-]$ concentrations.

1. TSPA chooses a P&CE potential seepage water chemistry look-up table from among the 396 look-up tables using a randomly selected group water type (1 through 4); a water-rock interaction parameter value (0, 1, 2,...10); a P_{CO_2} value of either 10^{-2} , 10^{-3} , 10^{-4} , bar; and a $T_{wp} = 30^\circ C$, $70^\circ C$, or $100^\circ C$. The T_{wp} , and the independent variable, RH_{wp} , are provided by the MSTHM (SNL 2007 [DIRS 181383], Appendix VIII[a]). The data used to make the look-up table selection are archived in DTNs: SN0701PAEBSPCE.001_R1 [DIRS 180523]; SN0701PAEBSPCE.002_R0 [DIRS 179425]; and SN0703PAEBSPCE.006_R2 [DIRS 181571].
2. TSPA evaluates potential salt separation by comparing the relative humidity from the look-up table selected in Step 1 with the salt separation relative humidity found in the group water salt separation tables (e.g., Gp1_Salt_separation_table.xls) in DTN: SN0703PAEBSPCE.006_R2 [DIRS 181571]. The relative humidity of salt separation is used directly from the salt separation look-up tables for all group waters.
 - 2.A. In the event of no salt separation:
 - a. Use the $[Cl+N]$ concentrations from the look-up tables archived in DTN: SN0701PAEBSPCE.001_R1 [DIRS 180523].
 - b. Sample uncertainty in $[Cl+N]$ by using the appropriate relative humidity range from IDPS uncertainty table and archived in DTN: SN0703PAEBSPCE.007_R2 [DIRS 184141] by applying a triangular distribution.

- c. Calculate $([C+N] + \text{uncertainty}) (= x)$ obtained in Steps 2a and 2b.
 - d. Sample $([Cl^-]/[NO_3^-]) (= y)$ from discrete CDFs in DTN: SN0703PAEBSPCE.007_R2 [DIRS 184141]. Uncertainty due to the use of a single pore water to represent a group of waters (e.g., the effect of binning potential starting pore waters chemically) is incorporated into the model by sampling the $[Cl^-]/[NO_3^-]$ ratio (represented by Cl:N) for each starting water group from a discrete CDF for the starting water values.
 - e. Using $x = ([Cl+N] + \text{uncertainty})$ and $y = (Cl:N)$ sampled from the CDFs to solve for $[Cl^-]$ and $[NO_3^-]$, the calculated values will include uncertainty.
- 2.B. In the event of salt separation:
- a. Once salt has separated, the Cl:N CDFs no longer apply and $[Cl^-]$, $[NO_3^-]$, $[Cl^-]/[NO_3^-]$, and pH are taken directly from the look-up tables selected in Step 1 above. These values are valid at any relative humidity below that for salt separation.
 - b. The model assumes that $[Cl^-]$ is proportional to $[Cl:N]$, and thus the uncertainties will also be correlated. Once TSPA samples the uncertainty on $[Cl^-]$ using a triangular distribution with the end-points as shown in the IDPS uncertainty table, an offset of the same sign (either positive or negative) is applied to the $[Cl:N]$.
 - c. The look-up tables remain valid until the relative humidity in the drift exceeds the salt separation threshold. At that point, the look-up tables no longer apply and TSPA is instructed to assume that a Cl-rich brine can form. Because the process of salt-brine separation cannot be explicitly modeled, the P&CE report (SNL 2007 [DIRS 177412], Section 6.12.3) abstraction models do not attempt to provide the chemistry for the Cl-rich brines.

The crown seepage water pH, $[Cl^-]$, and $[NO_3^-]$ are used to assess the potential for localized corrosion on the WP outer barrier in the Localized Corrosion Initiation Analysis (Section 6.3.5.2).

6.3.4.4 Model Component Consistency and Conservatism in Assumptions and Parameters

To enhance understanding of the complex interactions within the TSPA-LA Model, a discussion of consistency among model components and submodels, and identification of conservative assumptions in abstractions, process models, and parameter sets supporting the EBS Chemical Environment Submodel is provided below.

6.3.4.4.1 Consistency of Assumptions

Seepage Water Compositions—The In-Package Chemistry Abstraction does not use the EBS Chemical Environment crown seepage (EBS P&CE suite of models) as its starting waters (Section 6.3.7.2.1). In the In-Package Chemistry Abstraction, a liquid influx (dripping case or seepage dripping) model where water from the drift, simulated as typical groundwater, enters a

WP at a rate determined by the seepage flow through the openings in the breached WP (SNL 2007 [DIRS 180506], Section 6.3).

Effect on the TSPA-LA Model—Using a typical groundwater as the starting water for the in-package chemistry model will have little effect on the TSPA-LA results. As discussed in the *In-Package Chemistry Abstraction* (SNL 2007 [DIRS 180506], Section 6.6.2[a]), the composition of the liquid influx has little effect on the in-package chemistry because the degradation reactions and the secondary minerals that precipitate have a large influence on the water composition inside the WP.

Partial Pressure of CO₂—The In-Package Chemistry Abstraction uses the in-drift EBS Chemical Environment Submodel (Section 6.3.7.2.1) for P_{CO_2} in the WP rather than calculating the P_{CO_2} inside the WP. The Near Field Chemistry process model developed in *EBS P&CE* (SNL 2007 [DIRS 177412]) provides potential seepage water compositions, which are then used to generate look-up tables for P_{CO_2} maximum and for total dissolved carbon used to calculate P_{CO_2} minimum.

Effect on the TSPA-LA Model—Using a single P_{CO_2} for the drift, invert, and WP conditions is the best way to have a consistent gas phase composition throughout the drift and is actually a good approximation because gas transport in and out the waste package is relatively fast. In addition, while in-package pH does depend on P_{CO_2} , in-package ionic strength does not depend on the value of P_{CO_2} (SNL 2007 [DIRS 180506], Section 6.6.3[a]).

6.3.4.4.2 Identification of Conservatism in Submodels and Abstractions

Mixing In the Invert—Water passing through a breached WP (i.e., reacting with the waste form and corrosion products) would be expected to enter the invert and mix with water that had been diverted around the DS and WP, as well as with waters already present in the invert that have equilibrated with the relative humidity in the drift. The TSPA-LA Model uses the in-package chemistry in the WP and the invert for a WP that exhibits advective releases. Mixing of waters would change buffer capacities of the EBS Chemical Environment.

pH buffering—The In-Package Chemistry Abstraction (Section 6.3.7.2.1) conceptual model is a batch reactor model that consists of water, oxygen, carbon dioxide, waste forms, and metal alloys. The In-Package Chemistry Abstraction considers the potential for mineral precipitation and WP internal materials to act as pH buffers (SNL 2007 [DIRS 180506], Section 6.3). However, neither the In-Package Chemistry Abstraction nor the P&CE model consider the potential for surface complexation reactions to buffer pH, despite the presence of abundant EBS components in the drift.

6.3.4.5 Alternative Conceptual Model(s) for Engineered Barrier System Chemical Environment

Section 6.2 outlines the general consideration and treatment of ACMs used to support the TSPA-LA Model. A brief description of ACMs for the EBS Physical and Chemical Environment is presented below and summarized in Table 6.3.4-5.

PTn Pore Water ACM—The EBS Physical and Chemical Environment Model uses pore water compositions from the TSw to represent ambient conditions for the four starting waters (SNL 2007 [DIRS 177412], Section 6.6). The ACM selects ambient pore water from the overlying formation, the PTn, and then allows this water to seep up the geothermal gradient (from 23 to 96°C) which is downward, through the TSw to the repository horizon (SNL 2007 [DIRS 177412], Section 6.11).

This ACM was not selected for use in the TSPA-LA Model because an analysis showed that using the TSw pore water adequately captures the chemistry of representative PTn pore waters. The use of PTn starting compositions does not significantly impact the key chemical components (pH, P_{CO_2} , Ca, K, Si) of seepage (SNL 2007 [DIRS 177412], Section 6.11).

Treatment of Alkali Feldspar by the Near Field Chemistry Model: Kinetics versus Equilibrium—Within the EBS Physical and Chemical Environment Model, the mixed feldspar phase adopted to represent the volcanic feldspar observed in the Topopah Spring Tuff, is treated kinetically, i.e., this phase is always undersaturated with respect to clays, zeolites, and its own end-members (SNL 2007 [DIRS 177412], Section 6.11.2). An alternate approach would be to assume that the volcanic feldspar has reached equilibrium or near equilibrium, and thus thermodynamic controls of feldspar dissolution (e.g. saturation indices) must be considered when calculating seepage water compositions.

This equilibrium ACM was not chosen because at or near ambient temperatures, the volcanic waters are usually undersaturated with respect to feldspars and the kinetic treatment of the alkali feldspar is the appropriate approach (SNL 2007 [DIRS 177412], Section 6.11.2).

Closed System Model with Respect to CO₂—The IDPS Model (SNL 2007 [DIRS 177411], Section 6.5), which is a process model implemented by the EBS P&CE suite of models (SNL 2007 [DIRS 177412]), describes an ACM that assumes a closed drift system with respect to CO₂. In a closed system, there is little or no exchange of CO₂ between the solution and the atmosphere; that is, the solution is modeled as essentially isolated from the atmosphere and H₂CO₃ is treated as a non-volatile acid. What little exchange might occur in a natural system approximating a closed system would alter the fugacity of CO₂ in the atmosphere. A closed system model might be appropriate for a wetter climate; however, relative humidity would be approximately 100 percent and little or no evaporation would occur.

A closed system with respect to CO₂ is not implemented in the TSPA-LA because the expected volume ratio of air to water in the drift is so large that CO₂ degassing from, or dissolving into, seepage water in the drift will negligibly affect CO₂ fugacity compared to the uncertainty in the input value for CO₂ fugacity. However, the EBS P&CE Model incorporates the uncertainty of an open or closed system by using the maximum and minimum P_{CO_2} values in the abstraction for the TSPA-LA (SNL 2007 [DIRS 177412], Section 6.3.2.8 and Section 6.15.1). The minimum value assumes a completely open system and the maximum value assumes a closed system. The actual system behaves in a manner between these two end-member assumptions.

INTENTIONALLY LEFT BLANK

Table 6.3.4-1. Illustration of the Form of the Mean Water-Rock Interaction Parameter Table

Thermal Measure	Year	Percolation Flux (mm/yr)	Percolation Flux (mm/yr)
		0.05231146	0.495274154
37.7552	50.1	3.77E-09	3.77E-09
37.7552	51	3.77E-08	3.77E-08
37.7552	52	7.55E-08	7.55E-08
37.7552	55	1.89E-07	1.89E-07
37.7552	60	3.79E-07	3.79E-07
37.7552	65	5.71E-07	5.71E-07
37.7552	70	7.64E-07	7.64E-07
37.7552	75	9.61E-07	9.61E-07
37.7552	80	1.16E-06	1.16E-06
37.7552	90	1.58E-06	1.58E-06
37.7552	100	2.01E-06	2.01E-06
37.7552	120	2.96E-06	2.96E-06
37.7552	140	3.98E-06	3.98E-06
37.7552	160	5.09E-06	5.09E-06
37.7552	180	6.27E-06	6.26E-06
37.7552	200	7.51E-06	7.50E-06
37.7552	220	8.80E-06	8.79E-06
37.7552	240	1.01E-05	1.01E-05
37.7552	260	1.15E-05	1.15E-05
37.7552	280	1.29E-05	1.29E-05
37.7552	300	1.44E-05	1.44E-05
37.7552	320	1.59E-05	1.59E-05
37.7552	340	1.74E-05	1.74E-05
37.7552	360	1.89E-05	1.89E-05
37.7552	380	2.05E-05	2.05E-05
37.7552	400	2.21E-05	2.21E-05
37.7552	420	2.37E-05	2.37E-05
37.7552	440	2.54E-05	2.54E-05
37.7552	460	2.70E-05	2.70E-05
37.7552	480	2.87E-05	2.87E-05
37.7552	500	3.04E-05	3.04E-05
37.7552	520	3.21E-05	3.21E-05

Source: DTN: SN0703PAEBSPCE.006_R2 [DIRS 181571],
WRIP_Lookup_Table.xls.

Table 6.3.4-2. Illustration of the Form of an In-Drift Precipitated Salts Look-up Table for Each Unique Set of Values of Carbon Dioxide Partial Pressure, P_{CO_2} , and Temperature

Relative Humidity	pH	Ionic Strength	[Cl ⁻]	[NO ₃ ⁻]
	$-\log([H^+])$	molality	molality	molality
0.999995	6.45	6.45	0.000041	0.000006
0.999994	6.64	6.64	0.000065	0.000010
0.999992	6.84	6.84	0.000102	0.000016
0.999989	7.04	7.04	0.000162	0.000026
0.999984	7.23	7.23	0.000256	0.000041
0.999977	7.42	7.42	0.000406	0.000065
0.999966	7.61	7.61	0.000643	0.000103
0.999948	7.79	7.79	0.001017	0.000163
0.999921	7.97	7.97	0.001607	0.000258
0.999898	8.06	8.06	0.002108	0.000340
0.999881	8.09	8.09	0.002368	0.000409
0.999822	8.18	8.18	0.003312	0.000649
0.99982	8.18	8.18	0.003361	0.000661
0.999816	8.18	8.18	0.003412	0.000673
0.999814	8.19	8.19	0.003455	0.000683
0.999813	8.19	8.19	0.003464	0.000686
0.9998111	8.19	8.19	0.003505	0.000696
0.999811	8.19	8.19	0.003515	0.000699
0.999809	8.20	8.20	0.003568	0.000713
0.999807	8.20	8.20	0.003622	0.000727
0.999805	8.21	8.21	0.003680	0.000742
0.999803	8.21	8.21	0.003740	0.000758
0.999801	8.22	8.22	0.003802	0.000774
0.999799	8.23	8.23	0.003868	0.000791
0.999796	8.23	8.23	0.003938	0.000809
0.999794	8.24	8.24	0.004011	0.000828
0.999792	8.25	8.25	0.004087	0.000847
0.999789	8.25	8.25	0.004168	0.000868
0.999786	8.26	8.26	0.004253	0.000889
0.999784	8.27	8.27	0.004329	0.000908
0.99978	8.28	0.004439	0.000935	0.000937
0.999777	8.29	0.004540	0.000960	0.000962
0.999773	8.29	0.004647	0.000986	0.000987
0.99977	8.30	0.004760	0.001014	0.001012
0.999766	8.31	0.004881	0.001044	0.001041

Table 6.3.4-2. Illustration of the Form of an In-Drift Precipitated Salts Look-up Table for Each Unique Set of Values of Carbon Dioxide Partial Pressure, P_{CO_2} , and Temperature (Continued)

Relative Humidity	pH	Ionic Strength	[Cl ⁻]	[NO ₃ ⁻]
	$-\log([H^+])$	molality	molality	molality
0.999762	8.32	0.005010	0.001075	0.000427
0.999757	8.33	0.005147	0.001108	0.000441
0.999753	8.34	0.005294	0.001143	0.000455
0.999748	8.35	0.005451	0.001180	0.000469
0.999742	8.37	0.005620	0.001220	0.000485
0.999737	8.38	0.005801	0.001263	0.000502
0.999731	8.39	0.005997	0.001309	0.000521
0.999724	8.40	0.006208	0.001358	0.000540
0.999717	8.42	0.006437	0.001412	0.000562
0.999709	8.43	0.006685	0.001469	0.000584
0.999701	8.45	0.006956	0.001532	0.000609
0.999692	8.46	0.007252	0.001600	0.000636
0.999682	8.48	0.007577	0.001674	0.000666
0.999671	8.50	0.007935	0.001756	0.000698
0.999659	8.52	0.008332	0.001846	0.000734
0.999646	8.53	0.008772	0.001946	0.000774
0.999631	8.56	0.009265	0.002057	0.000818
0.999614	8.58	0.009820	0.002181	0.000868
0.999595	8.60	0.010449	0.002322	0.000924
0.999574	8.63	0.011166	0.002482	0.000987
0.99955	8.65	0.011993	0.002666	0.001060
0.999522	8.68	0.012956	0.002879	0.001145

Source: This table is an example modified from DTN: SN0701PAEBSPCE.001_R1 [DIRS 180523].

NOTE: The table entries for relative humidity, [Cl⁻], [NO₃⁻], pH, and ionic strength have been rounded for display purposes and are based upon the seepage evaporation look-up table for Starting Water 1, $P_{CO_2} = 0.01$ bar, and $T = 70^\circ\text{C}$.

For TSPA-LA Model use, the tabulated values displayed here are not used; the values are taken directly from DTN: SN0701PAEBSPCE.001_R1 [DIRS 180523]. Also, the table in the DTN has more lines than shown here, ending at an RH value of 0.500002.

Table 6.3.4-3. Illustration of Estimated Model Uncertainty Ranges for In-Drift Precipitated Salts Submodel Outputs of pH and Ionic Strength

Parameter	Units	Relative Humidity				
		Range 100% - 85%	Range 85% - 65%	Range 65% - 40%	Range 40% - 20%	Range 20% - 0%
I	log molal	+/- 0.1	0	0	0	0
Cl	log molal	0.0	+/- 0.1	+/- 0.4	+/- 0.5	+/- 0.7
N	log molal	0.0	+/- 0.2	+/- 0.4	+/- 0.5	+/- 0.9
Cl:NO ₃	log mole ratio (unit less)	0.0	+/- 0.2	+/- 0.5	+/- 0.5	+/- 1.4
Cl+N	log molal	0.0	+/- 0.22	+/- 0.57	NA	NA
		Range 100% - 75%	Range 75% - 65%	Range 65% - 0%		
pH	pH units	^a See table	+/- 1	+/-2		

Sources: Modified from DTN: SN0703PAEBSPCE.007_R2 [DIRS 184141],
PCE_IDPS-Uncertainties.xls.

Ionic strength uncertainty below 85 percent relative humidity is zero (SNL 2007 [DIRS 177412], Table 6.12-1).

NOTE: These uncertainties are defined as triangular distributions.

^aTable in the pH row refers to a table of pH uncertainty values contained within the source DTN.

Table 6.3.4-4. Summary of Chemistry for Seepage and Condensation in the TSPA-LA Model

	Seepage		No Seepage	
	Drift-Wall Condensation	No Drift-Wall Condensation	Drift-Wall Condensation	No Drift-Wall Condensation
Seismic/Nominal				
WP Outer Barrier; DS Intact	Dry air or humidity environment only.	Dry air or humidity environment only.	Dry air or humidity environment only.	Dry air or humidity environment only.
WP Outer Barrier; DS Failed	Use seepage composition equilibrated to T, RH, P_{CO_2} of WP outer barrier.	Use seepage composition equilibrated to T, RH, P_{CO_2} of WP outer barrier.	Use seepage composition equilibrated to T, RH, P_{CO_2} of WP outer barrier.	Dry air or humidity environment only.
IPC; DS Intact (WP Failed)	[F]=0; use chemistry for non-dripping case.	[F]=0; use chemistry for non-dripping case.	[F]=0; use chemistry for non-dripping case.	[F]=0; use chemistry for non-dripping case.
IPC; DS Failed (WP Failed)	[F]≤Fmax; use chemistry for seepage case if $Q_4 \geq 0.1$ L/yr; otherwise non-dripping chemistry.	[F]≤Fmax; use chemistry for seepage case if $Q_4 \geq 0.1$ L/yr; otherwise non-dripping chemistry.	[F]=0; use chemistry for seepage case if $Q_4 \geq 0.1$ L/yr; otherwise non-dripping chemistry.	[F]=0; use chemistry for non-dripping case.
Invert; DS Intact (WP Failed)	Use seepage composition equilibrated to T, RH, P_{CO_2} of invert.	Use seepage composition equilibrated to T, RH, P_{CO_2} of invert.	Use seepage composition equilibrated to T, RH, P_{CO_2} of invert.	Use seepage composition equilibrated to T, RH, P_{CO_2} of invert.
Invert; DS Failed (WP Failed)	Use in-package chemistry (seepage-based) to represent advective transport.	Use in-package chemistry (seepage-based) to represent advective transport.	Use in-package chemistry (seepage-based) to represent advective transport.	Use seepage composition equilibrated to T, RH, P_{CO_2} of invert.
Igneous Intrusion				
IPC; DS Failed (WP Failed)		Use basalt water without modification for environment; choose from alternatives in in-package chemistry documentation.		
Invert; DS Failed (WP Failed)		Use in-package chemistry selected above.		

Source: SNL 2007 [DIRS 177412], Table 6.15-1.

Table 6.3.4-5. Alternative Conceptual Models Considered for EBS Physical and Chemical Environment

Alternative Conceptual Models	Key Assumptions	Assessment and Basis
PTn Pore Water ACM	PTn pore water is used for the starting composition for the water that travels up the geothermal gradient downward through the TSw to the repository horizon (SNL 2007 [DIRS 177412], Section 6.11).	Not recommended for TSPA. Using PTn starting water compositions does not significantly impact the key chemical components (pH, P_{CO_2} , Ca, K, Si) of seepage (SNL 2007 [DIRS 177412], Section 6.11). Using TSw starting waters adequately captures the behavior and uncertainty of the PTn pore water.
Treatment of Alkali Feldspar by the Near Field Chemistry Model: Kinetics versus Equilibrium	Volcanic feldspar has reached equilibrium or near equilibrium, and thus thermodynamic controls of feldspar dissolution (e.g. saturation indices) must be considered when calculating seepage water compositions (SNL 2007 [DIRS 177412], Section 6.11.2).	Not recommended for TSPA. At or near ambient temperatures, the volcanic waters are usually undersaturated with respect to feldspars and the kinetic treatment of the alkali feldspar is the appropriate approach (SNL 2007 [DIRS 177412], Section 6.11.2).
Closed System Model with Respect to CO_2	Carbonate exchange with the gas phase via CO_2 degassing or dissolution results in a corresponding increase or decrease of CO_2 in the gas phase (SNL 2007 [DIRS 177411], Section 6.5).	Not recommended for TSPA. A closed system with respect to CO_2 is not implemented in the IDPS model because the expected volume ratio of air to water in the drift is so large that CO_2 degassing from, or dissolving into, seepage water in the drift will negligibly affect the CO_2 fugacity compared to the uncertainty in the input value for CO_2 fugacity. A closed system might be appropriate in a wetter climate; however, RH would be ~100% and little or no evaporation would occur. To address this issue further, the IDPS model is used to quantify the output uncertainty resulting from the uncertainty in CO_2 fugacity in the P&CE Model (SNL 2007 [DIRS 177412], Section 6.3.2.8 and Section 6.15.1).

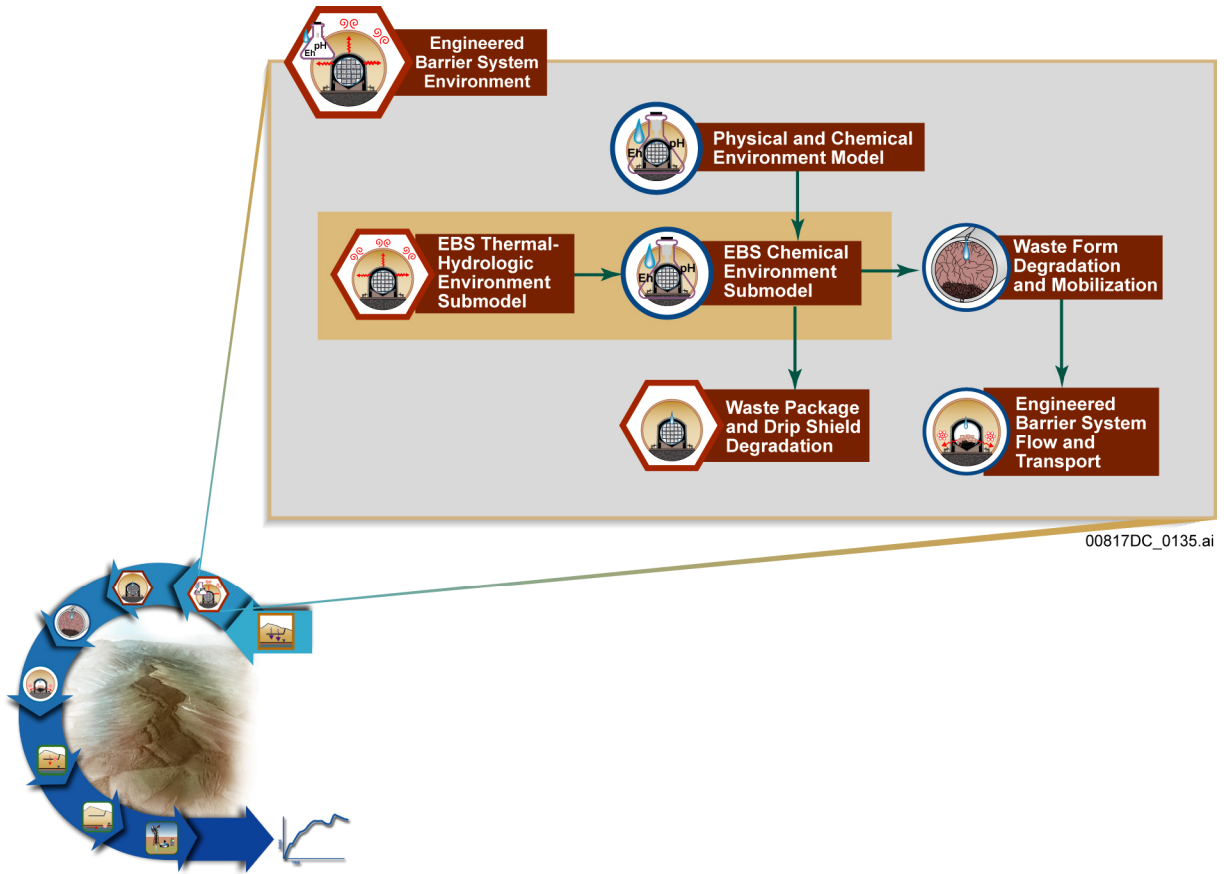


Figure 6.3.4-1. Information Flow Diagram for the EBS Chemical Environment Submodel

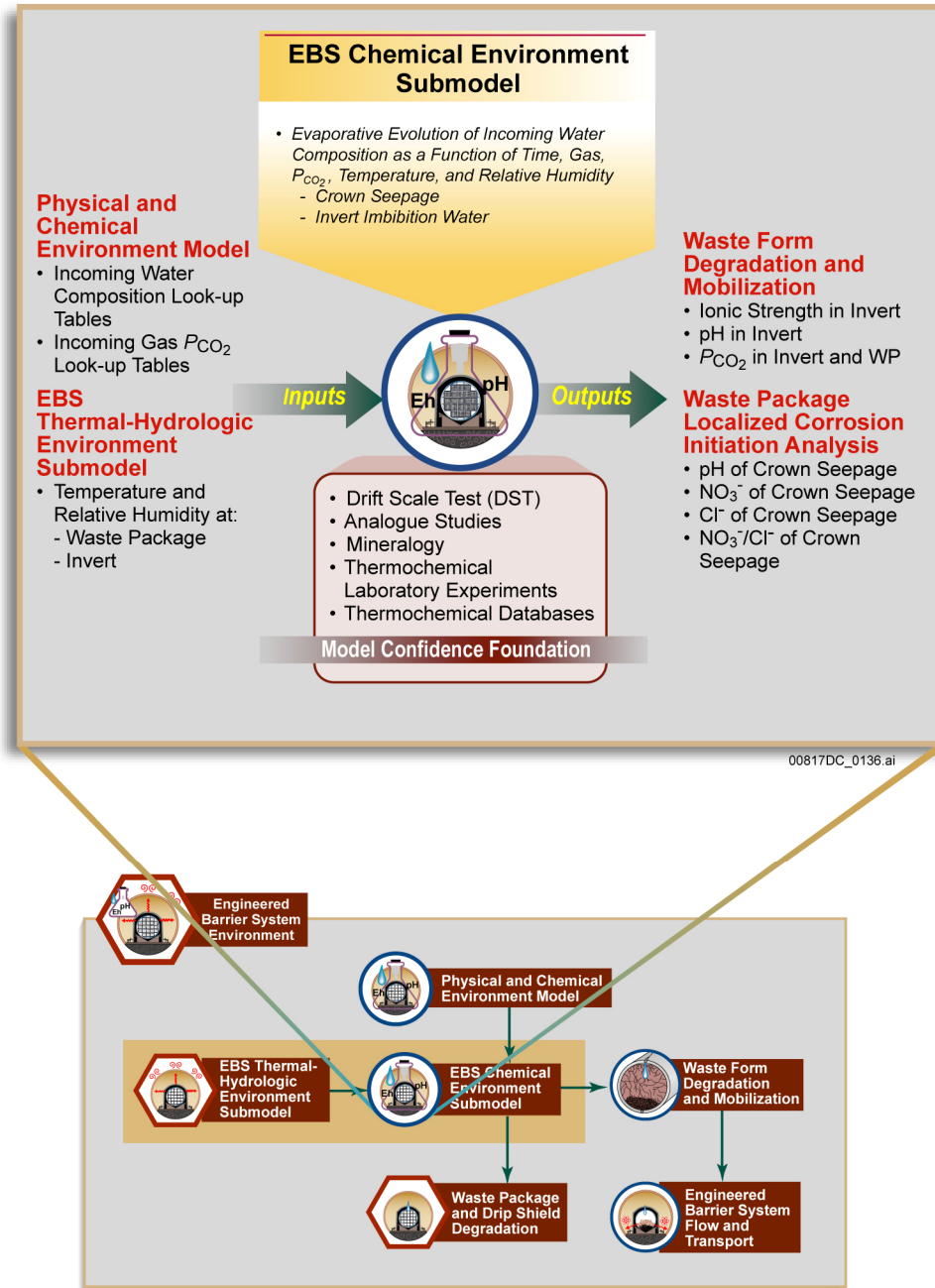


Figure 6.3.4-2. Inputs, Outputs, and Basis for Model Confidence for the EBS Chemical Environment Submodel

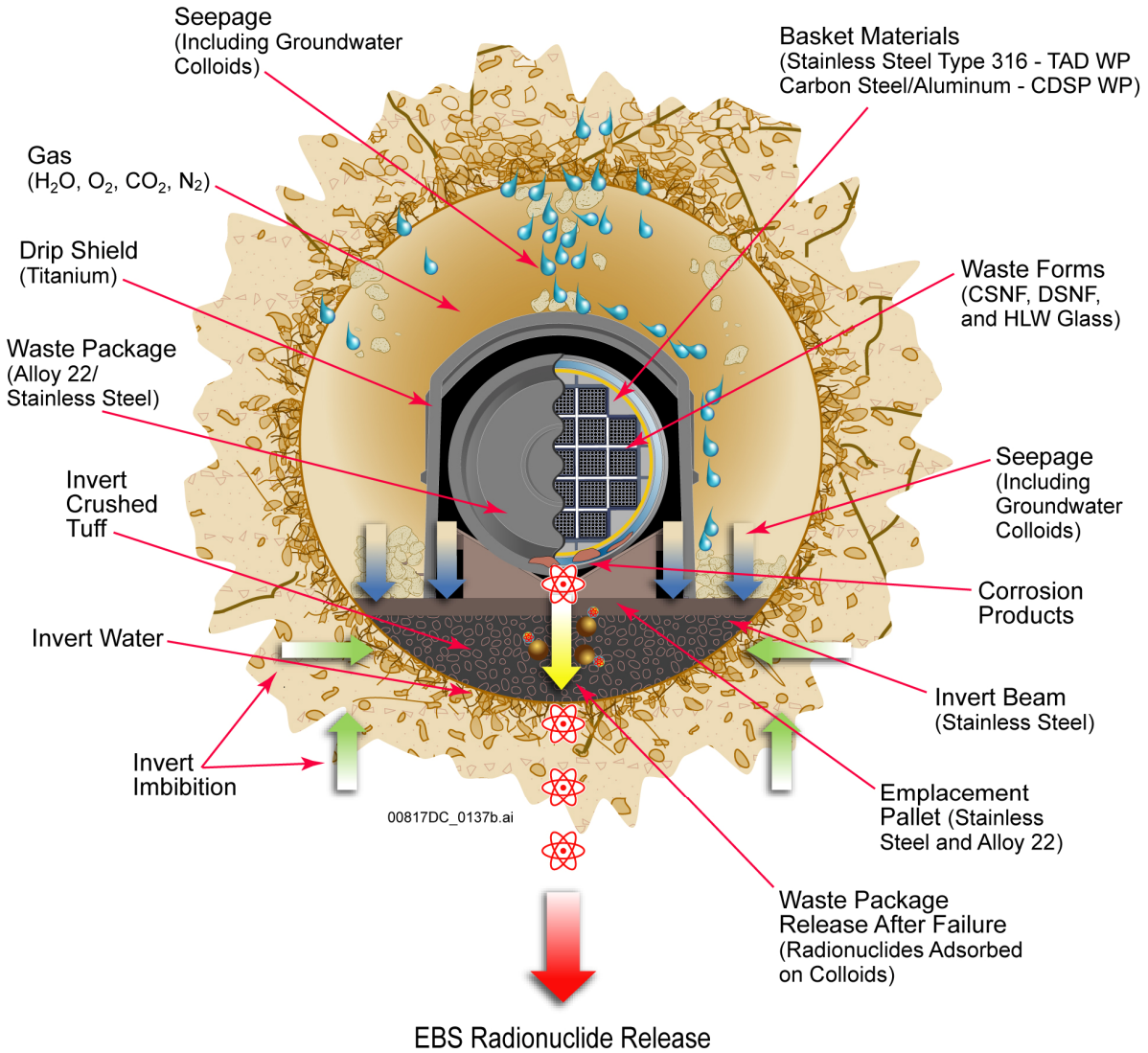


Figure 6.3.4-3. General EBS Design Features and Materials, Water Movement, and Drift Degradation

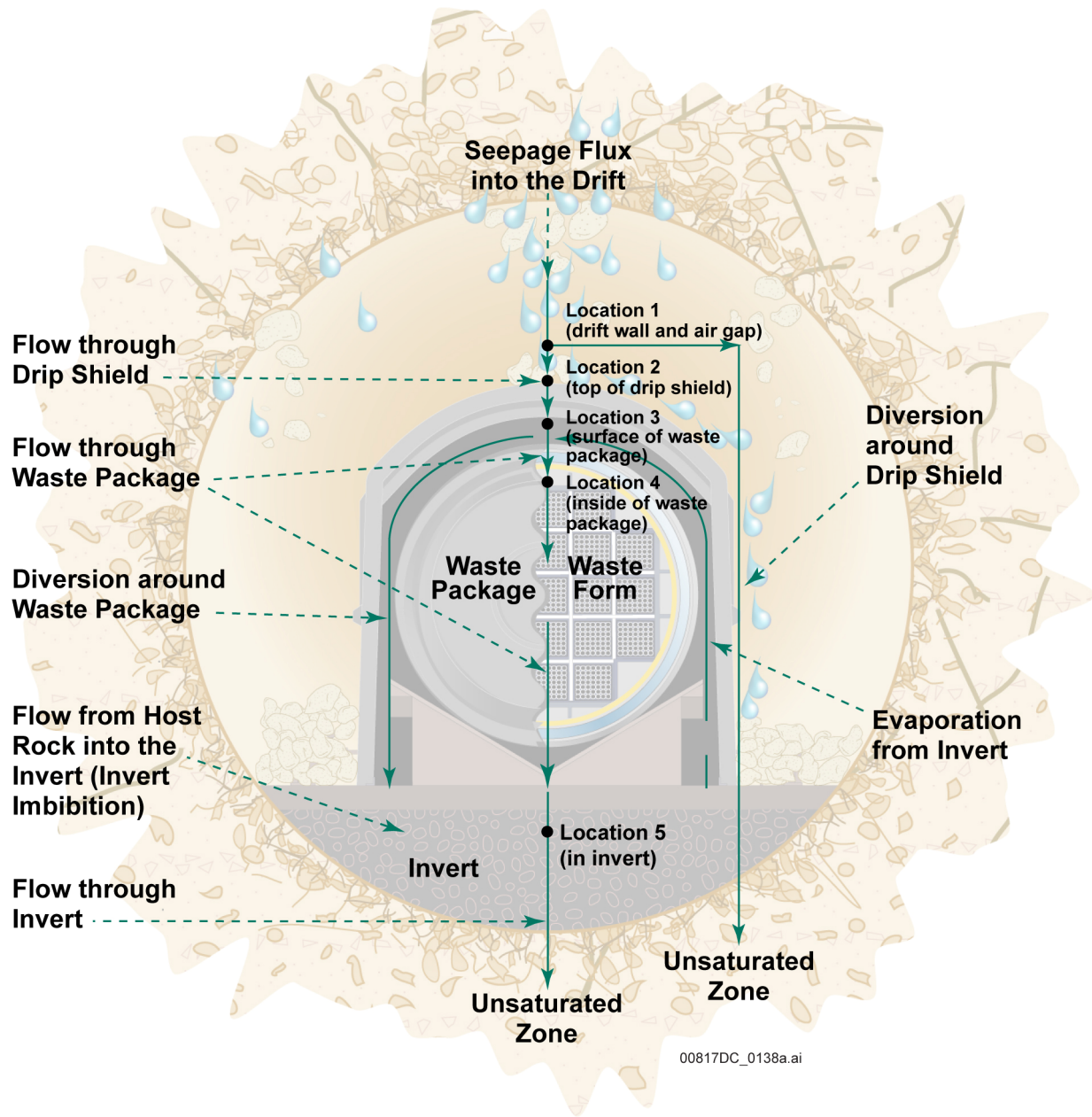


Figure 6.3.4-4. Schematic Diagram of EBS Flow Pathways (arrows) and Critical Locations (labels)

6.3.5 Waste Package and Drip Shield Degradation

The WPs and DSs are important components of the EBS. Figure 6.3.5-1 is a schematic illustration of the design features of the WPs and DSs. The two primary design functions of the DSs are to prevent seepage water from dripping directly on the WPs and to provide protection from rockfall damage to the WPs. The primary design functions of the WPs are to isolate the waste from the repository environment until the WPs fail and, after WP failure, to limit and delay the release of radionuclides to the EBS. The TSPA-LA Model for WP degradation includes five degradation mechanisms: general corrosion, microbially influenced corrosion (MIC), stress corrosion cracking (SCC), localized corrosion, and early failure of WPs. The TSPA-LA Model for DS degradation includes two degradation mechanisms: general corrosion and early failure of DSs. The DS and WP degradation mechanisms and their disposition for implementation in the TSPA-LA Model are documented in Table 6.3.5-1. The degradation mechanisms and their abstraction models are described in *General Corrosion and Localized Corrosion of the Drip Shield* (SNL 2007 [DIRS 180778], Section 6.1[a]); *General Corrosion and Localized Corrosion of Waste Package Outer Barrier* (SNL 2007 [DIRS 178519], Sections 6.4.3, 6.4.4, and 6.4.5); *Stress Corrosion Cracking of Waste Package Outer Barrier and Drip Shield Materials* (SNL 2007 [DIRS 181953], Section 6); and *Analysis of Mechanisms for Early Waste Package/Drip Shield Failure* (SNL 2007 [DIRS 178765], Section 6). The early failure of WPs and DSs is documented in two places. WP early failure resulting from weld flaws is documented in Section 6.3.5. All other WP and DS early failure degradation modes are documented in Section 6.4. The implementation of the localized corrosion degradation mechanism for the outer surface of WPs is summarized in the next paragraph. The relationships between the WP and DS Degradation Model Component and other TSPA-LA Model components and submodels are illustrated on Figure 6.3.5-2. The primary submodel supplying input to the WP and DS Degradation Model Component is the EBS TH Environment Submodel (Section 6.3.2), which provides exposure conditions (i.e., temperature and relative humidity) on WP outer surfaces. Output from the WP and DS Degradation Model Component is provided to the Waste Form Degradation and Mobilization Model Component and the EBS Flow and EBS Transport Submodels in the form of time-dependent tabulations of the fraction of WPs and DSs failed and the average breached area per failed WP and DS. Figure 6.3.5-3 summarizes the issues considered in the formulation of the WP and DS Degradation Model Component and its inputs and outputs.

The TSPA-LA Model implementation of localized corrosion of the outer surfaces of WPs is accomplished by exercising several interfaced TSPA-LA Model components and submodels in combination with the Localized Corrosion Initiation Abstraction in a probabilistic framework external to the TSPA-LA Model. A stand-alone analysis is used to compute time-dependent brine chemical composition and corrosion potential on WP outer surfaces. Outputs of the stand-alone analysis are time-dependent tabulations that specify the fraction of WPs that fail due to localized corrosion as a function of time. These WP fractional failure histories are imported into the TSPA-LA Model and used in the determination of WP degradation. The TSPA-LA implementation of localized corrosion is described in detail in Section 6.3.5.2.3.

The remainder of Section 6.3.5 is summarized as follows: Section 6.3.5.1 describes the WP and DS degradation conceptual models. The inclusion or exclusion of potentially important degradation mechanisms is outlined in Section 6.3.5.1.1. These include general corrosion, MIC,

and SCC. Manufacturing and material defects that result in WP early failures are also included. Section 6.3.5.1.2 contains the abstraction models corresponding to these conceptual models. Section 6.3.5.1.3 describes their implementation in the TSPA-LA Model. Section 6.3.5.2 focuses on the localized corrosion abstraction for the WP outer surface. This section describes how localized corrosion initiation is evaluated on the WP outer surface and how the results of this analysis are incorporated into the TSPA-LA Model. Section 6.3.5.3 discusses differences in assumptions and parameter sets that have arisen in the development of the supporting information for the TSPA-LA Model. Section 6.3.5.4 and Table 6.3.5-2 outline ACMs used to build confidence in the base-case model and ensure that the base-case model adequately captures the range of conceptual model uncertainty.

6.3.5.1 Waste Package and Drip Shield Degradation

DSs will be installed over the WPs just prior to repository closure. DSs will be made of Titanium Grade 7 plates with Titanium Grade 29 stiffeners and support beams to provide both corrosion resistance and structural strength. The DS plates will be at least 15 mm thick (SNL 2007 [DIRS179354], Table 4-2). As long as they remain substantially intact, the DSs will divert water that seeps into the drift away from the WPs and preclude damage to WPs resulting from rockfall. Because titanium is highly corrosion resistant, initial breaches of the DSs will not occur under nominal conditions until approximately 230,000 years postclosure (Section 6.3.5.1.3). The probability of DS plate failure before 10,000 years due to seismic ground motion and the resulting rockfall is estimated to be less than 3.4×10^{-4} (Section 7.3.2.6.1.3.2). WPs will prevent contact between water and waste as long as they are not breached and will limit water flow and radionuclide migration even after the WPs are breached. The WPs have a dual-metal design consisting of an inner vessel and a WP outer barrier. The inner vessel is composed of a 50-mm-thick layer of modified Stainless Steel Type 316. The WP outer barrier is a 25-mm-thick layer of Alloy 22, a corrosion-resistant nickel-based alloy (SNL 2007 [DIRS179394], Table 4-1). Alloy 22 protects the modified 316 stainless steel inner vessel from corrosion, and the modified 316 stainless steel inner vessel provides additional structural support for the thinner Alloy 22 WP outer barrier. The potential corrosion performance of the modified 316 stainless steel inner vessel is far less than that of the more corrosion-resistant Alloy 22 WP outer barrier. For this reason, the corrosion performance of the WP inner vessel is conservatively not included in this analysis. The WP outer barrier has a single Alloy 22 closure lid. The WP closure lid is welded to the WP outer barrier after the waste form (SNF or HLW glass, or both) is loaded.

6.3.5.1.1 Conceptual Model

The DSs and WPs are expected to be subject to many potential degradation mechanisms during the first 10,000 years after repository closure. Several of these degradation mechanisms were determined as ineffective under repository-relevant exposure conditions. The inclusion or exclusion of potentially important degradation mechanisms in the TSPA-LA Model is summarized in Table 6.3.5-1 and described as follows:

- General corrosion is a relatively uniform thinning of materials that occurs at all times. This degradation process is included in the TSPA-LA Model as a degradation mechanism for both the DSs and WPs (DTN: MO0706SPA FEPLA.001_R0)

[DIRS 181613], FEP Numbers 2.1.03.01.0B and 2.1.03.01.0A). The conceptual models and abstractions are discussed in *General Corrosion and Localized Corrosion of the Drip Shield* (SNL 2007 [DIRS 180778], Section 6.1[a]) and *General Corrosion and Localized Corrosion of Waste Package Outer Barrier* (SNL 2007 [DIRS 178519], Section 6.4.3).

- Localized corrosion (pitting, crevice corrosion) is a phenomenon in which corrosion progresses at discrete sites or in a non-uniform manner.
 - Localized corrosion is excluded from the TSPA-LA Model as a DS degradation mechanism (DTN: MO0706SPAFEPLA.001_R0 [DIRS 181613], FEP Number 2.1.03.03.0B).
 - Localized corrosion is included as a WP degradation mechanism (DTN: MO0706SPAFEPLA.001_R0 [DIRS 181613], FEP Number 2.1.03.03.0A). Crevice corrosion is used to represent localized corrosion for the WP under the exposure conditions expected in the repository environment. This is a conservative and bounding assumption, as the initiation threshold for crevice corrosion in terms of exposure conditions is lower than for pitting corrosion (SNL 2007 [DIRS 178519], Section 6.4.4).
- SCC is a crack propagation process caused by the combined interaction of mechanical stress and corrosion reactions acting on a susceptible material. Possible sources of mechanical stress include weld-induced-residual stresses, plasticity-induced-residual stresses caused by seismic events, residual stresses produced by rockfall, and sustained rock rubble loading.
 - SCC is excluded in the TSPA-LA Model as a DS degradation mechanism (DTN: MO0706SPAFEPLA.001_R0 [DIRS 181613], FEP Number 2.1.03.02.0B).
 - SCC is included as a WP degradation mechanism (DTN: MO0706SPAFEPLA.001_R0 [DIRS 181613], FEP Number 2.1.03.02.0A). Because the waste container is fully annealed prior to being loaded with the waste form, the majority of the WP will not have appreciable residual tensile stresses upon emplacement. The outer barrier closure lid weld region cannot be fully annealed and is stress mitigated (by low plasticity burnishing) to produce a layer of compressive stress (SNL 2007 [DIRS 179394], Section 4.1.2.3; and SNL 2007 [DIRS 179567], Section 4.1.1.3) that prevents SCC initiation until general corrosion removes this layer (SNL 2007 [DIRS 181953], Section 8.4.2.1). Because fully annealed WPs will not contain tensile stresses, they will not be subject to SCC from nominal degradation processes. The WP outer surface is protected from rockfall by the presence of the DSs. Therefore, in the Nominal Scenario Class, SCC is considered only for the closure-lid welds. The number and size of weld flaws due to manufacturing defects is calculated in *Analysis of Mechanisms for Early Waste Package/Drip Shield Failure* (SNL 2007 [DIRS 178765], Section 6.3.1). Distributions for weld flaw number and size are incorporated into the WP SCC Abstraction. Weld flaws are not part of the Waste Package EF Modeling Case discussed in Section 6.4. *Stress Corrosion*

Cracking of Waste Package Outer Barrier and Drip Shield Materials discusses the modeling approach used to assess the degradation of the WP outer barrier due to SCC (SNL 2007 [DIRS 181953], Sections 6.4 and 6.5). SCC of the WP outer surface due to seismic degradation processes is discussed in Section 6.6.

- MIC is caused by the activity of microorganisms. Microorganisms can affect the corrosion of an alloy either by acting directly on the metal or through their metabolic products. MIC is documented in *General Corrosion and Localized Corrosion of the Drip Shield* (SNL 2007 [DIRS 180778], Sections 6.7.2 and 6.4[a]) and in *General Corrosion and Localized Corrosion of Waste Package Outer Barrier* (SNL 2007 [DIRS 178519], Section 8.2).
 - MIC is excluded from the TSPA-LA Model as a DS degradation mechanism (DTN: MO0706SPAFEPLA.001_R0 [DIRS 181613], FEP Number 2.1.03.05.0B).
 - MIC is included as a WP degradation mechanism as a multiplier to the general corrosion rate (DTN: MO0706SPAFEPLA.001_R0 [DIRS 181613], FEP Number 2.1.03.05.0A).
- Thermal aging and phase instability caused by prolonged exposure to elevated temperature environments can lead to microstructural changes of WP and DS materials, which could change their corrosion behavior. This process is excluded from the TSPA-LA Model as a DS degradation mechanism and as a WP degradation mechanism (DTN: MO0706SPAFEPLA.001_R0 [DIRS 181613], FEP Numbers 2.1.11.06.0B and 2.1.11.06.0A).
- Hydrogen-induced cracking is caused by the migration of atomic hydrogen into the metal and subsequent formation of metal hydrides. This process can cause metals to be more brittle and susceptible to cracking. This process is excluded from the TSPA-LA Model as a DS degradation mechanism and as a WP degradation mechanism (DTN: MO0706SPAFEPLA.001_R0 [DIRS 181613], FEP Numbers 2.1.03.04.0B and 2.1.03.04.0A).
- Mechanical damage due to dynamic loading conditions can damage WPs and DSs.
 - Mechanical damage is excluded as either a DS or WP degradation mechanism in the Nominal Scenario Class (DTN: MO0706SPAFEPLA.001_R0 [DIRS 181613], FEP Numbers 2.1.03.07.0B, 2.1.03.07.0A, and 2.1.06.07.0B).
 - Seismic-induced rockfall is included as a degradation mechanism for both DSs and WPs in the Seismic Scenario Class (DTN: MO0706SPAFEPLA.001_R0 [DIRS 181613], FEP Numbers 1.2.03.02.0C and 1.2.03.02.0B). The Seismic Scenario Class conceptual model and TSPA-LA Model implementation are discussed in Section 6.6.
- Radiolysis can result in the generation of hydrogen peroxide and changes in chemical conditions leading to enhanced corrosion. This process is excluded as a degradation

mechanism for both DSs and WPs (DTN: MO0706SPAFEPLA.001_R0 [DIRS 181613], FEP Number 2.1.13.01.0A).

Igneous-induced DS and WP degradation is discussed in *Number of Waste Packages Hit by Igneous Events* (SNL 2007 [DIRS 177432], Section 6.3). The impact of igneous events on DS and WP performance is summarized in Section 6.5 of this report.

Seismic-induced DS and WP degradation is described in *Seismic Consequence Abstraction* (SNL 2007 [DIRS 176828]) and summarized in Section 6.6 of this report.

6.3.5.1.2 Abstraction of Waste Package and Drip Shield Degradation

The WP and DS degradation processes included in the TSPA-LA Model are incorporated into the WP and DS Degradation Model Submodel, as documented in this section. The direct output from the WP and DS Degradation Submodel is a set of histories for WP and DS failure and the subsequent number of breaches in failed WPs and DSs, as a function of time. The WP and DS Degradation Submodel includes the DS General Corrosion Abstraction for DS degradation, the WP General Corrosion Abstraction, the WP MIC Abstraction, and the WP SCC Abstraction for WP degradation. The WP and DS Degradation Submodel also includes the abstraction for closure-lid weld flaws due to manufacturing defects. The primary submodel supplying input to the WP and DS Degradation Model Component is the EBS TH Environment Submodel (Section 6.3.2). The EBS TH Environment Submodel provides temperature and relative humidity histories. The WP degradation mechanisms modeled by the WP and DS Degradation Submodel (general corrosion, SCC, and MIC) are not chemistry-dependent. The DS general corrosion is chemistry dependent, and the development of two different abstractions for the outer and inner DS surfaces reflects this dependence. The WP general corrosion rate is a function of the temperature on the WP surface, while DS corrosion rates are independent of temperature.

DS Performance—General corrosion is the only DS degradation mechanism modeled in the WP and DS Degradation Submodel. This process is modeled as being independent of temperature and relative humidity and is initiated at the time of repository closure. General corrosion is modeled separately for the outer and inner surfaces of the DSs, each with a different general corrosion rate. The major difference between the inner and outer surfaces of the DSs is that the outer surfaces may be exposed to a more complex chemical environment because dust and/or seepage may reside on or contact the outer surfaces of the DSs. The inner surfaces are not expected to be exposed to seepage water.

The general corrosion models for the topside and underside surfaces of the DSs were developed based on corrosion rates determined from the weight-loss measurements of the Titanium Grade 7 coupons after a 2.5-year exposure to at the Long-Term Corrosion Testing Facility at Lawrence Livermore National Laboratory. The resulting weight-loss data set was divided into three groups with distinctively different rate distributions; namely, Aggressive Condition, Intermediate Condition, and Benign Condition. These groups span the range of expected conditions in the repository environment. The data subsets for two bounding conditions (Aggressive Condition and Benign Condition) were used for the model development and analysis (SNL 2007 [DIRS 180778], Section 6.1[a]). The data points termed aggressive were obtained from solutions

of simulated concentrated water considered to be representative of the evolution of groundwater compositions relevant to the repository environment.

The topsides of DSs in seeping environments in the repository are considered to be subject to the potentially aggressive conditions represented by the simulated concentrated water data. Because of the small number of data points available, the corrosion model for aggressive conditions is considered uncertain. The Student's t-distribution was used to characterize the uncertainty in the mean of the aggressive condition data (SNL 2007 [DIRS 180778], Section 6.1.6.2[a]). The undersides of all DSs are considered to be subject to benign conditions at all times. The uncertainty of the general corrosion model for benign conditions was developed by assuming the mean of the probability model is uncertain and the variance constant. A normal probability distribution was developed to characterize this uncertainty (SNL 2007 [DIRS 180778], Section 6.1.7.1[a]).

Although there is acknowledged variability in the DS general corrosion processes (SNL 2007 [DIRS 180778], Sections 6.1.6.1[a] and 6.1.7.2[a]), it is not considered in the TSPA-LA Model implementation. For TSPA-LA Model purposes, only the global aspect of DS degradation (DS thinning) is considered to be important. For the Seismic GM Modeling Case calculations the structural response is based on a discrete set of DS thicknesses (Section 6.6.1.2.2.1). Therefore, the uncertain Student's t-distribution for aggressive conditions and the uncertain normal distribution for benign conditions are used to model general corrosion on the topsides and undersides, respectively, of the DSs.

The general corrosion abstraction for the Titanium 29 DS framework in repository environments was developed in terms of the comparative behavior of Titanium Grade 29 versus Titanium Grade 7 (SNL 2007 [DIRS 180778], Section 6.2[a]). A cumulative distribution function (CDF) for the general corrosion rate ratio of Titanium Grade 29 to Titanium Grade 7 was developed. This CDF is to be sampled independently for every realization of the TSPA-LA Model. This parameter is used in the abstraction for DS damage in the Seismic Scenario Class (Section 6.6).

WP Performance—WP performance is modeled in the TSPA-LA Model by the WP and DS Degradation Model Component using two submodels. The first submodel, the WP and DS Degradation Submodel, includes general corrosion, MIC, and SCC. The second submodel, the WP Localized Corrosion Initiation Submodel, models the initiation and propagation of localized corrosion.

Two WP configurations are analyzed in the TSPA-LA Model file. The first WP configuration is referred to as the CSNF WP configuration for which the TAD canister configuration parameters are used. The second WP configuration analyzed is the CDSP WP configuration for which the 5 HLW/1 DOE SNF Long WP configuration parameters are used.

The WP surfaces are analyzed as being composed of sub-areas referred to as patches in order to represent spatial variation in degradation processes across the WP surfaces. The general corrosion, MIC, and SCC degradation mechanisms are modeled at the patch level on WPs, as shown on Figure 6.3.5-4, with each patch having, in general, a different general corrosion rate or SCC response. Figure 6.3.5-5 illustrates general corrosion processes for both dripping and non-dripping environments and degradation on the surfaces of both the DSs and the WPs. The

patches located in the last annulus shown on the WP on Figure 6.3.5-4 represent the closure-lid weld region, and SCC is modeled only on these closure-lid patches for nominal degradation processes. In contrast, SCC is modeled on the whole WP surface for seismic degradation processes (Section 6.6).

The general corrosion model used for the WP is based on weight-loss measurements for samples exposed in the Long-Term Corrosion Testing Facility (SNL 2007 [DIRS 178519], Section 6.4.3). For the WP outer barrier, samples with the crevice geometry were used to generate the general corrosion rate distribution (applied at 60°C). The crevice geometry samples have nominal dimensions of 2 in. × 2 in. × 1/8 in. and a 0.312-in. diameter hole in the center for sample mounting (SNL 2007 [DIRS 178519], Section 6.4.3). Therefore, the exposed surface area, A , for a crevice geometry sample is calculated as follows:

$$A = 2ab + 2bc + 2ac - \left(\frac{\pi d^2}{2} \right) + \pi dc \quad (\text{Eq. 6.3.5-1})$$

where a is the length of the specimen, b is the width of the specimen, c is the thickness of the specimen, and d is the diameter of hole. Using the dimensions above, the exposed surface area for a crevice sample (converted to mm²) is 5,787 mm². The general corrosion analysis performed by the WAPDEG 4.07 software (STN: 10000-4.07-00 [DIRS 181774]; and STN: 10000-4.07-01 [DIRS 181064]) is limited to a maximum of 1,500 patches. Therefore, the TSPA-LA Model analysis uses a patch size of about four times that of the crevice coupon area of 23,150 mm² (output DTN: MO0707WPDRIPSD.000 [DIRS 183005]).

The surface areas of the CSNF and CDSP WPs are taken to be the values used in the EBS Radionuclide Transport Abstraction for the maximum diffusive area of corrosion products for the path through the outer barrier. These are defined in the file *SN0703PAEBSRTA.001-RTA.Input.Tables.doc* (DTN: SN0703PAEBSRTA.001_R3 [DIRS 183217], Table 8.2-6, parameters Diff_Area_CSNF_2_Max and Diff_Area_CDSP_2_Max). The number of patches used for calculation purposes can be derived by dividing the CSNF and CDSP surface areas by the patch area giving 1,430 patches for CSNF WPs and 1,408 patches for CDSP WP. The general corrosion rate distribution applied to the WP outer barrier is modified to reflect this change in scale between the smaller crevice geometry sample size and the patch size. This calculation is documented in output DTN: MO0707WPDRIPSD.000 [DIRS 183005].

For modeling purposes, the WP outer barrier is composed of two different regions; the closure-lid weld region and the shell region. The closure-lid weld region is represented as an annulus, one-patch side wide and with the same radius as the WP (Figure 6.3.5-1). Making the reasonable analysis assumption that the patches are square, the length of one side of a patch is then about 152 mm. The fraction of area represented by the closure-lid weld region for CSNF WPs is given by:

$$\frac{\text{Closure-Lid Weld Region Area}}{\text{WP Surface Area}} = \frac{\pi(\text{diameter})(152)\text{mm}^2}{\pi(\text{diameter})(5691)\text{mm}^2} \approx 0.0267 \quad (\text{Eq. 6.3.5-2})$$

or about 38 patches. For CDSP WPs, the fraction of area represented by the closure weld region is:

$$\frac{\text{Closure-Lid Weld Region Area}}{\text{WP Surface Area}} = \frac{\pi(\text{diameter})(152)\text{mm}^2}{\pi(\text{diameter})(5145)\text{mm}^2} \approx 0.0295 \quad (\text{Eq. 6.3.5-3})$$

or about 42 patches.

The CSNF and CDSP WP lengths are 5,691 mm and 5,145 mm, respectively. These are defined in the file *SN0703PAEBSRTA.00-RTA Input Tables.doc* (DTN: SN0703PAEBSRTA.001_R3, [DIRS 183217], Table 8.2-6).

Note that the surface area of the closure lids themselves was not considered to be part of the WP surface area. Because the WP surface area is used primarily to determine the fraction of WP surface area subjected to SCC, it is conservative and appropriate to ignore the closure lid surface area in determining the total WP surface area.

Analyses presented in *Stress Corrosion Cracking of Waste Package Outer Barrier and Drip Shield Materials* (SNL 2007 [DIRS 181953], Section 6.6.1) indicate that the distance between two neighboring cracks must be greater than the plate thickness for the stress (and stress intensity factor) profile to be of sufficient magnitude to propagate a crack through-wall. Therefore, for the WP outer barrier outer closure-lid (which is 25 mm thick) and again making the analysis assumption that the patches are square (side length about 152 mm), about six cracks per patch are able to propagate through-wall.

Modeling degradation mechanisms at the patch level permits a representation of spatial variability in the degradation on the WP surfaces. Every WP patch is assigned a different corrosion rate and every WP is assigned different exposure conditions (WP temperature and relative humidity) and will, therefore, corrode at a different rate and fail at a different time. This variation represents WP-to-WP variability.

The WP and DS Degradation Submodel also considers general corrosion degradation of the WP inner surfaces, or inside-out corrosion. Inside-out general corrosion can only begin after WP failure. Note that inside-out SCC is not modeled because it would be of negligible consequence to WP performance, either because the WP would have already been breached by the much larger patch penetrations due to general corrosion or because the patches susceptible to SCC would have already been breached by SCC, thus reducing or eliminating the state of stress.

General Corrosion and MIC—The WP General Corrosion Abstraction for the outer surface of the WP is documented in *General Corrosion and Localized Corrosion of Waste Package Outer Barrier* (SNL 2007 [DIRS 178519], Section 8.2). The Alloy 22 general corrosion rate is considered to be a function of exposure temperature. The temperature-dependent general corrosion rate follows an Arrhenius relationship (SNL 2007 [DIRS 178519], Equation 6-28):

$$\begin{aligned}
 R &= R_o \exp \left[C_1 \left(\frac{1}{333.15 \text{ K}} - \frac{1}{T} \right) \right] \\
 &= \exp \left[\ln(R_o) + C_1 \left(\frac{1}{333.15 \text{ K}} - \frac{1}{T} \right) \right]
 \end{aligned}
 \tag{Eq. 6.3.5-4}$$

where

T = temperature in Kelvin.

C_1 = a slope term (in Kelvin) determined from short-term polarization resistance measurements for Alloy 22 specimens, tested for a range of sample configurations, metallurgical conditions, and exposure conditions. It is given by a truncated (-3 SD and +2 SD) normal distribution with a mean of 4,905 K and a SD of 1,413 K. The variation in C_1 is due entirely to epistemic uncertainty.

R_o = a rate (in mm/yr) sampled from one of three distributions for the corrosion rate of the WP outer surface at 60°C (333.15 K), developed from weight-loss data obtained from the five-year crevice geometry samples exposed in the Long-Term Corrosion Testing Facility.

For R_o , three Weibull distributions were developed from the five-year corrosion rate results for low, medium, and high uncertainty levels in the general corrosion rate (R_o) (SNL 2007 [DIRS 178519], Section 8.2). The distributions are randomly selected in such a way that the low and high general corrosion rate distributions are each used for 5 percent of epistemic realizations and the medium general corrosion rate distribution is used for the remaining 90 percent of epistemic realizations.

As noted above, the patch area used to analyze the WPs is four times the area of the crevice geometry sample size used to determine the three R_o distributions. Therefore, the general corrosion rates derived from the data analysis are adjusted to account for the effects of this change of scale (Aziz 1956 [DIRS 159379]; Shibata 1996 [DIRS 119589]). The method employed to accomplish this change in scale corresponds to using the highest of four sampled corrosion rates (from the two-parameter Weibull distribution) to analyze general corrosion of the WP patch. The approach is conservative because it is probable that not all four samples from the Weibull distribution will have the highest rate. A more realistic representation of the overall general corrosion rate would be the average of the four sampled corrosion rates. However, this approach would not account for the fact that one fourth of the patch has the maximum of the four sampled corrosion rates. On this basis, the proposed approach is conservative and appropriate for this application. Scaling the corrosion rates shifts the median general corrosion rate to higher values and decreases the probability of sampling lower general corrosion rates. This effect is shown on Figure 6.3.5-6 where the original distributions for R_o are plotted, along with the distributions resulting from a change of scale (or size factor) of four. The analysis for the change of scale is developed in the MathCad sheet, *WDlnRGC-ESC-hml.xmcd*, documented in TSPA output DTN: MO0707WPDRIPSD.000 [DIRS 183005].

The WP outer barrier is assumed to be subject to MIC when the relative humidity at the WP outer barrier surface is above a relative humidity threshold, which is uniformly distributed between 75 and 90 percent (SNL 2007 [DIRS 178519], Section 8.2). The entire variance of this

distribution is due to uncertainty. The effect of MIC on general corrosion of the WP outer barrier is represented by a multiplication factor (or MIC factor) to the general corrosion rate in the absence of MIC, such that:

$$CR_{MIC} = CR_{st} \times f_{MIC} \quad (\text{Eq. 6.3.5-5})$$

where CR_{st} is the general corrosion rate in the absence of MIC, f_{MIC} is the MIC enhancement factor, and CR_{MIC} is the general corrosion rate in the presence of MIC. The MIC enhancement factor is assumed to be uniformly distributed between 1 and 2, and the entire variance of the distribution is due to patch-to-patch variability (SNL 2007 [DIRS 178519], Section 8.2).

SCC—All regions of the WPs, except the outer-closure-lid weld region, are solution annealed before the WPs are loaded with waste. Thus, in the absence of seismic activity, they do not develop residual stress or stress-intensity factors high enough for SCC to occur from nominal degradation processes (SNL 2007 [DIRS 181953], Section 6.5.3). The outer barrier closure-lid is 25 mm thick, as shown on Figure 6.3.5-7. The outer barrier closure lid weld region cannot be fully annealed and is stress mitigated (by low plasticity burnishing) to produce a layer of compressive stress (SNL 2007 [DIRS 179394], Section 4.1.2.3; SNL 2007 [DIRS 179567], Section 4.1.1.3) that prevents SCC initiation until general corrosion removes this layer (SNL 2007 [DIRS 181953], Section 8.4.2.1). SCC can be initiated on a smooth surface (incipient cracks) or at an existing weld flaw (due to manufacturing defects).

The analysis in *Stress Corrosion Cracking of Waste Package Outer Barrier and Drip Shield Materials* (SNL 2007 [DIRS 181953], Section 8) summarizes the abstractions for the SCC initiation and propagation process, the stress and stress intensity thresholds, and the crack growth model based on the slip dissolution film rupture (SDFR) theory.

In *Stress Corrosion Cracking of Waste Package Outer Barrier and Drip Shield Materials* (SNL 2007 [DIRS 181953], Section 8.4.2.2), it is noted that the hoop stress, which promotes radially oriented crack growth, is the dominant component of stress in the WP outer barrier closure-lid weld regions. On this basis, only the hoop stress profiles are considered in the TSPA-LA Model SCC implementation. The hoop stress (σ in MPa) as a function of depth (x in mm) in the closure weld regions of the Alloy 22 WP outer barrier is given by a third order polynomial equation (SNL 2007 [DIRS 181953], Equation 64):

$$\sigma(x, 0) = A_0 + A_1 \times x + A_2 \times x^2 + A_3 \times x^3. \quad (\text{Eq. 6.3.5-6})$$

The second argument in the stress function is used to represent angular variation ($\theta = 0$ arbitrarily chosen) around the circumference of the Alloy 22 WP outer closure-lid weld region. The angular variation is included using the following functional form (SNL 2007 [DIRS 181953], Equation 65):

$$\sigma(x, \theta, z) = (\sigma(x, 0) - \nabla \sigma \times (1 - \cos \theta)) \left(\frac{\sigma(th, \theta) + z}{\sigma(th, \theta)} \right) \quad (\text{Eq. 6.3.5-7})$$

where x is the distance from the weld surface, θ is the angle in degrees from the reference location $\theta=0$, $\sigma(x, 0)$ is the calculated weld residual stress profile at an angle $\theta=0$, and distance x from the weld surface, th is the lid thickness, $\nabla\sigma$ is the angular variation of the mean stress, and z is the uncertain scaling factor discussed below. Because stress intensity factor (K_I) is a linear function of stress, the variability in stress intensity factor around the circumference can be calculated as (SNL 2007 [DIRS 181953], Equation 66):

$$K_I(x, \theta, z) = K_I(x) \times \left(\frac{\sigma(th, \theta) + z}{\sigma(th, 0)} \right) \quad (\text{Eq. 6.3.5-8})$$

where th is the thickness of the closure-lid weld, z is the uncertain scaling factor discussed below, and $K_I(x)$ is the stress intensity factor at the zero position. The variation of the stress and stress intensity factor profiles with angle is due to variability.

The uncertainty in the stress and stress intensity factor profiles is introduced through a scaling factor, z . The scaling factor, z , which is sampled from a truncated normal distribution with a mean of zero and an SD of 5 percent of the yield strength, YS, has an upper-bound of 15 percent of the yield strength and a lower-bound of -15 percent of the yield strength (SNL 2007 [DIRS 181953], Section 6.5.6.2).

Flaws in the closure-lid welds are possible sites for SCC initiation. Weld flaws are generally larger than other surface defects and are conservatively considered to maintain their depth relative to the advancing general corrosion front (i.e., they are not removed by general corrosion processes). As discussed above, only radially oriented weld flaws are potential sites for SCC initiation. Weld flaws are a result of manufacturing defects (flaws not detected by the inspection processes). The analysis of the nondetection of weld flaws is documented in Section 6.3.1 of *Analysis of Mechanisms for Early Waste Package/Drip Shield Failure* (SNL 2007 [DIRS 178765]). The analysis was performed using the results from the welding of Alloy 22 specimen rings that duplicate closely the outer lid weld of a WP. Sixteen specimen rings were welded, employing procedures, processes, and equipment similar to that expected to be used for the closure of the WP. Nondestructive examinations were performed to accumulate significant information on the weld flaws and included ultrasonic and radiographic testing, which was followed by metallographic examination. This information consisted of weld flaw location, size, and shape. Based on this information, distributions were developed to characterize the size of the flaws in the through-wall extent of the weld, their density (mean number of flaws per volume of weld), and their depth (distance between the outer surface of the weld and the onset of the flaw).

The probability of nondetection, P_{ND} , of weld flaws of length x using an ultrasonic testing inspection technique is given by (SNL 2007 [DIRS 178765], Equation 17):

$$P_{ND}(x) = \varepsilon + \frac{1}{2}(1 - \varepsilon) \operatorname{erfc} \left(\nu \times \ln \left(\frac{x}{b} \right) \right) \quad (\text{Eq. 6.3.5-9})$$

where

- x = size of the flaw (in mm)
- ε = lower limit of P_{ND}
- ν = shape factor
- b = characteristic flaw size, in mm, which is the flaw size at the median of the P_{ND} distribution
- erfc = complementary error function.

Weld flaw sizes follow an exponential distribution of parameter λ_s normalized to the weld thickness (th) (SNL 2007 [DIRS 178765], Equation 8). The flaw size probability density function is:

$$f_s(x) = \frac{\lambda_s \exp(-\lambda_s \cdot x)}{1 - \exp(-\lambda_s th)} \quad (\text{Eq. 6.3.5-10})$$

The flaw size distribution parameter (representing uncertainty), λ_s , is gamma distributed with shape parameter n_f (the number of weld flaws), and scale parameter, $1/S_f$ (where S_f is the cumulative size of test weld flaws).

The fraction of nondetected defects remaining in the weld (of thickness th) after inspection is given by the convolution of the probability of nondetection and the flaw size probability density (SNL 2007 [DIRS 178765], Equation 19):

$$F_{nr}(th) = \int_0^{th} P_{ND}(u) f_s(u) du . \quad (\text{Eq. 6.3.5-11})$$

The distribution for the number of defects before any inspection or repair is characterized by a flaw count distribution parameter λ_c (SNL 2007 [DIRS 178765], Equation 11). The flaw count distribution parameter (representing epistemic uncertainty), λ_c , is gamma distributed with shape parameter, $(n_f + 1/2)$, and scale parameter, $1/V_f$, where V_f is the cumulative weld volume in the test welds (SNL 2007 [DIRS 178765], Section 6.3.1.3).

The distribution for the number of defects that remain after inspection can be defined in terms of the quantities derived above. It is Poisson distributed with parameter λ (count per closure weld). For a weld of volume V and thickness th , λ is given by the product (SNL 2007 [DIRS 178765], Equations 23 and 24):

$$\lambda = F_\theta \times F_\psi \times F_{nr}(th) \times (V \times \lambda_c) \quad (\text{Eq. 6.3.5-12})$$

where

F_{θ} = fraction of weld flaws that are radially oriented (SNL 2007 [DIRS 178765], Equation 16) (equal to 0.008)

F_{ψ} = fraction of embedded weld flaws able to propagate (SNL 2007 [DIRS 181953], Section 6.3.4.2) (equal to 0.25)

$F_{nr(th)}$ = fraction of nondetected flaws.

Note that Equation 6.3.5-12 includes two factors that are not explicitly discussed in Section 6.3.1.8 of *Analysis of Mechanisms for Early Waste Package/Drip Shield Failure* (SNL 2007 [DIRS 178765]). The first, F_{θ} , accounts for the fact that not all weld flaws will be radially oriented, and the second, F_{ψ} , for the fact that not all embedded weld flaws will propagate.

The detection and repair analysis uses coefficients such that there is a 50 percent probability of detection and repair of a 1/16 inch weld flaw (SNL 2007 [DIRS 178765], Appendix A.5). This treatment is conservative because design uses a repair criterion to repair all flaws 1/16 in. or greater (SNL 2007 [DIRS 179394], Table 4-1).

The slip dissolution-film rupture model describes the propagation of cracks after the stress and stress intensity thresholds are met. The slip dissolution-film rupture model relates SCC initiation and subsequent crack advance to the metal oxidation that occurs when the protective film at the crack tip is ruptured. The slip dissolution model can be applied to assess the breach of the WP due to crack propagation for either manufacturing defects (weld flaws) or inherent defects such as grain boundary junctions, surface asperities, or roughnesses (incipient cracks), or both. Inputs to the slip dissolution mechanism include threshold stress, threshold stress-intensity factor, an incipient crack size, and crack-growth-rate parameters.

The threshold stress is defined as the minimum stress at which cracks initiate on a smooth surface. This analysis refers to these as incipient cracks (to distinguish them from weld flaws) and typically form at local surface defects such as grain boundary junctions and surface roughness. Incipient cracks are considered to be 0.05 mm in length at the time of their nucleation (SNL 2007 [DIRS 181953], Section 8.4.2.1). The threshold stress is defined as a uniform distribution between 90 and 105 percent of the yield strength (SNL 2007 [DIRS 181953], Section 8.4.2.1). Incipient cracks nucleate when general corrosion has penetrated to the depth at which the stress profile (Section 8.4.2.2) exceeds the threshold stress. Weld flaws are already nucleated and, thus, do not require a stress threshold to nucleate. However, most weld flaws are embedded within the material and, therefore, are not exposed to the environment. As general corrosion proceeds, some initially embedded weld flaws will be exposed to the environment. The distribution for the number of weld flaws capable of propagation by the slip dissolution mechanism was derived in Equation 6.3.5-12.

Stress corrosion crack growth can occur when the stress intensity factor at the tip of the incipient crack or weld flaw exceeds or is equal to a threshold stress intensity factor. The depth of the tip is the sum of the general corrosion depth and the crack or weld flaw depth. The stress intensity

factor at this depth is determined from the stress intensity factor profile (Equation 6.3.5-8). The threshold stress intensity factor, K_{ISCC} , is given as a function of the repassivation slope, n , and the mean general corrosion rate, V_{GC} :

$$K_{ISCC} = \left(\frac{V_{GC}}{\bar{A}} \right)^{1/4n} \quad (\text{Eq. 6.3.5-13})$$

where \bar{A} is a function of n (repassivation slope) and V_{GC} is 7.23E-6 mm/yr (SNL 2007 [DIRS 181953], Section 8.4.2.3).

Once crack growth initiates, the crack(s) grows at a velocity given by (SNL 2007 [DIRS 181953], Section 8.4.2.3):

$$V_i = \bar{A} (K_i(x, \theta))^{4n} . \quad (\text{Eq. 6.3.5-14})$$

The repassivation slope n should be sampled from a truncated (at ± 2 SD) normal distribution with a mean of 1.165 and upper and lower bounds of 1.395 and 0.935, respectively. The variation in the repassivation slope, n , is entirely due to uncertainty.

Figure 6.3.5-8 provides a summary and illustration of the information flow between the DS and WP General Corrosion and SCC Abstractions.

Treatment of Uncertainty—The TSPA-LA modeling of WP degradation accounts for variability by simulating the performance of several hundred WPs. The effects of spatial and temporal variations in the exposure conditions across the repository are included by explicitly incorporating the relevant exposure condition histories into the TSPA-LA Model. The exposure condition parameters that are considered to vary over the repository are temperature and relative humidity on the WP outer surfaces. In addition, the TSPA-LA Model considers spatial variability in corrosion processes on a single WP due to variability in corrosion rates. This variability is represented by dividing the WP outer surface area into sub-areas called patches and stochastically sampling the degradation model parameter values for each patch. The use of patches explicitly represents the variability in degradation processes on a single WP at a given time. Every WP in a given simulation is assigned different exposure conditions, thus addressing WP-to-WP variability.

In the TSPA-LA Model, epistemic uncertainty in WP and DS degradation is analyzed with multiple realizations of the TSPA-LA Model. For each realization, values are sampled for the uncertain degradation parameters shown in Table 6.3.5-3, and these values are passed to the WP and DS Degradation Submodel. Each TSPA-LA Model realization includes a complete model simulation of WP and DS degradation, using explicit values of the uncertain degradation parameters, as described in the following paragraphs.

General corrosion rates for the inner and outer surfaces of the DSs are represented by two distributions, one for aggressive environmental conditions and one for benign environmental conditions. These distributions represent epistemic uncertainty in DS general corrosion rates. For each realization, two general corrosion rates are sampled and applied to all DSs. All DSs in

a given realization fail at the same time. The Titanium Grade 29 to Titanium Grade 7 general corrosion rate multiplier, used to model general corrosion of the DS framework components in the Seismic GM Modeling Case, represents epistemic uncertainty and is sampled once for each realization of the TSPA-LA Model.

The general corrosion rate of the WP outer surface is temperature-dependent and includes epistemic uncertainty and spatial variability components. Epistemic uncertainty in the general corrosion rate is contained in its temperature-dependent slope term, C_I (Equation 6.3.5-4). For each realization, a single general corrosion rate slope term is sampled and applied to all WPs, to represent epistemic uncertainty in the general corrosion rate with exposure temperature. The Alloy 22 general corrosion rate (R_o), which is represented by one of three CDFs determined from the five-year crevice geometry samples (Equation 6.3.5-4), has both variability and uncertainty components. Each individual CDF represents variability; the choice of which CDF to use for a particular realization represents the epistemic uncertainty in the fitting process. For every realization, each patch of each WP will have a different sampled value of R_o . In addition, spatial and temporal variability of the exposure temperature in the repository lead to spatial and temporal variability in the general corrosion rates used to model general corrosion of Alloy 22, due to the dependence of the general corrosion rate on temperature. A different exposure history file is assigned to each WP, resulting in a different WP surface temperature at each timestep. The net result is that every patch on each WP will have a different general corrosion rate, determined by the temperature read from the thermal history files at each timestep.

MIC is represented by an enhancement factor applied to the general corrosion rate of the WP outer surface, when the relative humidity threshold is exceeded. The value for the threshold relative humidity above which MIC takes place sampled from a uniform distribution, which represents epistemic uncertainty in the threshold. This distribution is sampled once per realization. The enhancement factor is also sampled from a uniform distribution, which represents spatial variability of the corrosion rate among various areas or patches on the WP outer surface. The MIC enhancement factor is sampled for each WP patch and applied if the threshold relative humidity is exceeded. The MIC enhancement factor has an additional WP-to-WP variability component due to the imposition of the relative humidity threshold, since the relative humidity on the WP surface varies from package to package.

The evaluation of weld flaw sizes and numbers of weld flaws includes epistemic uncertainty and variability. The variation in weld flaw sizes is expressed as variability at the WP level, given by a probability density function dependent on an uncertain flaw size parameter that is sampled for each realization (Equation 6.3.5-10). The variation in the number of weld defects is expressed as variability at the WP level given by a Poisson distribution with an uncertain parameter (count per closure weld) (Equation 6.3.5-12). This parameter is a function of the flaw size and count parameters that are sampled as uncertain for each realization (SNL 2007 [DIRS 178765], Table 7-1). The number and size of the weld flaws are randomly distributed to WP patches subject to SCC degradation. Thus, each SCC patch on every WP will have different initial values for the number and size of the weld flaws.

The evaluation of SCC initiation and propagation for the outer closure lid includes epistemic uncertainty and variability. Variability is represented by the variation of the stress and stress-intensity factor profiles with angle and depth. The epistemic uncertainty in the stress and

stress-intensity factor profiles is introduced through a scaling factor, z . The variations in the threshold stress and stress-intensity factor distributions are entirely due to epistemic uncertainty. The thresholds are sampled once per realization. The sampled threshold values are applied to all WP patches. The epistemic uncertainty in crack growth rate is a function of the repassivation slope. The variation in the repassivation slope is entirely due to epistemic uncertainty. The repassivation slope is sampled once per realization. The sampled repassivation slope value applies to all WP patches.

6.3.5.1.3 Implementation in the TSPA-LA Model

Overview—The TSPA-LA WP and DS Degradation Submodel makes use of several related software packages. The WAPDEG V4.07 software is a DLL that is responsible for simulating the spatial variability in WP degradation. The GoldSim V9.60.100 software (STN: 10344-9.60-01 [DIRS 181903]) is used to pass values to the WAPDEG V4.07 software and is responsible for treating the epistemic uncertainty in the WAPDEG V4.07 inputs. The GoldSim V9.60.100 software also calls several other DLLs that are used to incorporate uncertainty and variability in the inputs to the WAPDEG V4.07 software. These include the SCCD V2.01 software (STN: 10343-2.01-00 [DIRS 181157]; STN: 10343-2.01-01 [DIRS 181054]) for the treatment of variability in stress and stress-intensity factor profiles, and the CWD V2.0 software (STN: 10363-2.0-00 [DIRS 162809]; STN: 10363-2.0-01 [DIRS 181037]) for the treatment of uncertainty in the number and size of closure-lid weld manufacturing defects. The MkTable_LA V1.0 software (STN: 11217-1.0-00 [DIRS 181047]; STN: 11217-1.0-01 [DIRS 181048]) is used to randomly select a specified number of environment-history tables from the total set of environment-history tables. Each WP within a percolation subregion is assigned a different environment-history table. The environment-history tables are an output of the PREWAP_LA V1.0 software (STN: 10939-1.1-00 [DIRS 181053]), which processes the results from the comprehensive MSTHM Abstraction (Section 6.3.2.3). The PREWAP_LA V1.0 software reads these input files and writes corresponding environment-history output files, containing a subset of the data read from the MSTHM Abstraction files. These output files are created in a format that is compatible with the input files required by the WAPDEG V4.07 software program.

In the TSPA-LA Model, some of the parameters for the DS and WP degradation modes are sampled at the global level but the calculations, which use these parameters, are done at the second level of discretization (Section 6.1.5.3) in the percolation subregions associated with each WP type (CSNF WP or CDSP WP). The number of WPs to be emplaced in the repository is 11,629 (Table 6.3.7-1). The repository is divided into five spatially defined percolation subregions or bins (Section 6.3.2.2.1). Each percolation subregion contains a different number of WPs and is subject to different environmental conditions.

WP and DS Degradation Submodel—GoldSim Interface—The TSPA-LA Model file will typically call the WAPDEG V4.07 software program several times per GoldSim realization. The exact number of calls will depend on the modeling case being run. In the Nominal Modeling Case, 10 WAPDEG simulations are required: one for each CDSP WP and CSNF WP in each of the five repository percolation subregions. The main input to the WAPDEG V4.07 software program is a vector data element of real numbers. The values in the vector data element specify degradation models and degradation model parameters. The WAPDEG V4.07 software program

also requires distributions and tables stored in text files that cannot be passed by GoldSim. GoldSim instead passes line numbers that point to entries in a text file (WD4DLL.WAP) containing a list of the file names required by the WAPDEG V4.07 software. The vector data element and the contents of the files identified in the text file are the only inputs to the WAPDEG V4.07 software. The development of the WAPDEG input vector and associated files is documented in detail in TSPA output DTN: MO0707WPDRIPSD.000 [DIRS 183005].

Global Parameters and Calculations—The general corrosion of DSs has been specified with epistemic uncertainty in Section 8.1[a] of *General Corrosion and Localized Corrosion of the Drip Shield* (SNL 2007 [DIRS 180778]). Two uncertain mean corrosion rates are sampled independently per realization and are used for the general corrosion calculations for the DS. For this purpose, TSPA uses the parameters WDDSAggrGC_Mean_a and WDDSBenignGC_Mean_a (Table 6.3.5-3) for the Titanium Grade 7 corrosion rates. In addition, the DS general corrosion rate for aggressive conditions is used on the top side of all DSs, whether or not they encounter seeping conditions. The use of the aggressive rate for DSs that are not seeped on has no impact on dose calculations in the Nominal Modeling Case. The impact of the use of the aggressive rate for the top sides of DSs that are not seeped on in the Seismic GM Modeling Case is discussed in Appendix C (Section C6.3.1).

The earliest possible DS failure time can be calculated by combining the most severe degradation rates from the aggressive and benign distributions. Using the distributions given in the first two rows of Table 6.3.5-3 and using values at the 0.9999 probability level gives an aggressive rate of 5.75×10^{-5} mm/year and a benign rate of 0.824×10^{-5} mm/year. Combining these gives a rate of 6.57×10^{-5} mm/year, which corresponds to a DS failure time of about 230,000 years.

Some of the parameters defining the general corrosion rate for the WP are sampled globally, but the actual calculation of the WP general corrosion rate is done at the percolation subregion level, because the WP general corrosion rate is a function of exposure temperature. The first input to the calculation of the WP general corrosion rate is the slope term for the general corrosion rate, given by a truncated (-3 SD and +2 SD) normal distribution with a mean of 4,905 K and an SD of 1,413 K (DTN: MO0703PAGENCOR.001_R4 [DIRS 182029]). This parameter represents epistemic uncertainty and is sampled once per realization. The second parameter is a rate distribution (in mm/yr) for the WP outer surface at 60°C. One of three rate distributions is chosen randomly in such a way that the low and high general corrosion rate distributions are each used for 5 percent of realizations and the medium general corrosion rate distribution is used for the remaining 90 percent of realizations (DTN: MO0703PAGENCOR.001_R4 [DIRS 182029]). This distribution is sampled by the WAPDEG V4.07 software for every patch on each WP. Because the temperature of the WP surface is different for every WP simulated in a given percolation subregion, the result is a different general corrosion rate for every patch on every WP. General corrosion of Alloy 22 is implemented in WAPDEG using the general linear functional form (BSC 2002 [DIRS 162606], Section 4.2.6.5). The WP thickness is taken to be 25 mm, the minimum value specified for design purposes (SNL 2007 [DIRS 179394], Table 4-1).

The relative humidity threshold for MIC is an epistemically uncertain parameter, sampled once per realization. The relative humidity threshold is uniformly distributed between 75 percent and 95 percent. The MIC factor is uniformly distributed between one and two

(DTN: MO0703PAGENCOR.001_R4 [DIRS 182029]). However, the calculation is done at the percolation subregion level because the initiation of MIC occurs when a threshold relative humidity is exceeded. A unique relative humidity is read, as a function of time, from the environment-history tables generated by the MkTable_LA V1.0 software for each WP surface. The CWD V2.0 software implements the abstraction for the number and size of weld flaws documented above (Equations 6.3.5-9 to 6.3.5-12). The CWD V2.0 software is executed two times per realization: once for the outer-closure lid of the CSNF WPs and once for the outer-closure lid of the CDSP WPs. The CWD V2.0 software computes the cumulative probability of a manufacturing defect based on the probability for the nondetection of weld defects. The inputs to this calculation are weld thickness, weld volume (weld length \times weld cross-section), the defect fraction considered, a detection threshold, a characteristic defect size, a shape factor, a defect count parameter, and a defect-size parameter. All of these inputs are taken from DTN: MO0701PASHIELD.000_R2 [DIRS 180508], except the weld length, which is calculated as the product of π and the outside diameter of the WP outer corrosion barrier (SNL 2007 [DIRS 179567], Table 4-8). The output of each invocation of the CWD V2.0 software consists of two tables and the probability of occurrence of at least one defect per WP. These output tables contain distributions for the density and size of defect flaws on the outer-closure lid. The CWD outputs are direct inputs to the WAPDEG V4.07 software.

The SCCD V2.01 software implements the abstraction for the stress and stress intensity factor profiles documented above (Equations 6.3.5-6 to 6.3.5-8). The SCCD V2.01 software is executed once per realization for the outer-closure lid. The SCC calculation is the same for both CDSP WPs and CSNF WPs. The SCCD V2.01 software calculates the variation in stress and stress intensity factor versus depth and angle. The inputs to this calculation are four regression coefficients from the model abstraction for stress as a function of depth, the sine of the fracture angle, the number of angles to be calculated, the expected yield strength, the yield-strength scaling factor, the angular amplitude of the stress variation, the uncertainty model, and an uncertain deviation from median yield-strength range. All of these inputs are taken from DTN: MO0702PASTRESS.002_R2 [DIRS 180514], except the sine of the fracture angle (SNL 2007 [DIRS 181953], Section 6.5.3.3.1 and Figure 6-18) and the uncertainty model (output DTN: MO0707WPDRIPSD.000_R0 [DIRS 183005], AB-TSPA-DOC (PEF 93)). Also required is the stress intensity factor versus depth profile for the zero reference angle. The outputs of the SCCD V2.01 software are stress and stress intensity factor tables, as a function of depth, calculated at a number of angles (equally spaced and in the range 0 to π radians, inclusive) (DTN: MO0702PASTRESS.002_R2 [DIRS 180514]). The SCCD V2.01 software outputs are direct inputs to the WAPDEG V4.07 software.

Percolation Subregion Parameters and Calculations—The total number of WPs modeled is 11,629 (8,213 CSNF WPs and 3,416 CDSP WPs) (DTN: MO0702PASTREAM.001_R0 [DIRS 179925], Item 4 of worksheet UNIT CELL in spreadsheet *DTN-Inventory-Rev00.xls*). These WPs are partitioned among the five percolation subregions according to the percolation-flux distributions. The resulting partitioning is described in Section 6.3.2.2.1 and shown in Table 6.3.2-2. In the Nominal Modeling Case, the WAPDEG V4.07 software runs twice for each of the five percolation subregions: once for the CSNF WPs in that subregion and once for CDSP WPs. A sensitivity analysis (documented in output DTN: MO0709TSPA WPDS.000 [DIRS 183170]) was executed with 250, 500, 1,000, 1,500, and 3,000 DS and WP pairs. Comparison of the mean and 95th percentile WP first failure curves

showed that the analysis results were not very sensitive to the number of DS and WP pairs simulated over the range investigated. Therefore, in the TSPA-LA Model, if the percolation subregion contains fewer than 500 DS/WP pairs, the number of CSNF and CDSP DS and WP pairs simulated by the WAPDEG V4.07 software is equal to the number of pairs in the subregion. If the subregion contains more than 500 DS/WP pairs, then only 500 CSNF and 500 CDSP DS/WP pairs are simulated by the WAPDEG V4.07 software.

The primary submodel supplying input to the WP and DS Degradation Model Component is the EBS TH Environment Submodel (Section 6.3.2). The EBS TH Environment Submodel provides temperature and relative humidity histories for eight DS/WP pairs, composed of six CSNF WPs and two CDSP WPs at each of the 3,264 repository subdomain locations (Section 6.3.2.2). These 3,264 repository subdomain locations are partitioned among the five percolation subregions according to the percolation-flux distributions (Section 6.3.2.2.1). The resulting partitioning is shown in Table 6.3.2-2.

Each WAPDEG simulation requires a unique exposure history for each of the DS/WP pairs being simulated. The MkTable_LA V1.0 software samples these exposure histories from those available for the percolation subregion. The set of exposure histories that is available for sampling is determined by the WP type (CSNF WP or CDSP WP), the percolation subregion, the infiltration scenario, and the thermal conductivity. An external text file, *WDHist.inp*, contains a list of file names corresponding to exposure histories. The external file, *WDHist.inp*, is a generic file pointing to one of twelve possible files. These files correspond to combinations of the four possible infiltration scenarios (corresponding to the four climate states) and high, medium, and low thermal conductivity. The choice of which three files to use is controlled by the MFCP_LA V1.0 software (STN: 11071-1.0-00 [DIRS 167884], STN: 11071-1.0-01 [DIRS 181045]) on the basis of the sampled values for infiltration scenario and thermal-conductivity uncertainty.

WAPDEG V4.07 Software Overview—The WAPDEG V4.07 software simulates corrosion degradation of WPs by three penetration modes: patch penetration (due to general corrosion), crack penetration (due to crack tip growth or SCC), and pit penetration (due to pitting corrosion or crevice corrosion) (BSC 2002 [DIRS 162606], Section 3.3). Only the first two of these modes are invoked in the TSPA-LA Model. The WAPDEG V4.07 software structure specifies corrosion-affecting events that affect specific degradation processes. Each event is identified by a unique integer in the WAPDEG input vector. Each event has both event-specific data and generic data. The event-specific data triggers effects that are unique to that event. The data that describes the generic event effects has the same input structure for each event and is read at the end of the event-specific data. There are four possible generic effects of any event. These are to immediately fail the patches affected by the event, and/or to initiate localized corrosion modes, and/or to accelerate a corrosion mode or modes, and/or to reduce thresholds (BSC 2002 [DIRS 162606], Section 3).

General corrosion of Alloy 22 is implemented in the WAPDEG V4.07 software using the general linear functional form (BSC 2002 [DIRS 162606], Section 4.2.6.5). The form used for the TSPA-LA implementation of the Alloy 22 corrosion rate is:

$$D = \exp\left(\ln(R_o) + \frac{C_1}{333.15} + \varepsilon\right) \exp\left(-\frac{C_1}{T}\right) t^n \quad (\text{Eq. 6.3.5-15})$$

where D is corrosion depth (mm), t is time (yr), and T is exposure temperature (K). The parameter ε is not used in the TSPA-LA implementation. It is set to zero. The time exponent, n , has the value 1.0. The effect of MIC on the general corrosion of the WP is analyzed by the use of a MIC event (BSC 2002 [DIRS 162606], Section 4.2.7.10).

In the WAPDEG V4.07 software, the weld flaws are defined by a manufacturing defects event (BSC 2002 [DIRS 162606], Sections 3.3.2.1 and 4.2.7.2). The manufacturing defects event has only one specific effect, to introduce manufacturing defects onto patches. SCC is implemented in WAPDEG by the use of a slip dissolution event (BSC 2002 [DIRS 162606], Sections 3.3.2.1.1 and 4.2.7.5). Incipient cracks are automatically included in the event, but weld flaws must be specifically included via a manufacturing defects event. The slip dissolution event models the rate of crack growth and defines the time of crack penetration. The slip dissolution event implements the abstraction for crack growth presented in Equations 6.3.5-13 and 6.3.5-14.

The development of the WAPDEG input vector and associated files is documented in output DTN: MO0707WPDRIPSD.000 [DIRS 183005].

WP and DS Degradation Submodel Output—There is a one-dimensional table and a two-dimensional table output for each implementation of the WAPDEG V4.07 software. The one-dimensional table contains WP first-failure times versus the fraction of WPs failed. The WP first-failure time is defined as the first penetration by any mechanism (general corrosion or SCC) of the WP. The format of both of these tables is as follows; the first column contains the WP first-failure times in years (sorted in increasing order) and the second column contains the cumulative fraction WPs failed. The two-dimensional table contains 12 columns. The number of rows is controlled by the parameter NumBin (output DTN: MO0707WPDRIPSD.000 [DIRS 183005]) defined in the TSPA-LA Model and passed to the WAPDEG V4.07 software. The column contents are explained in *User's Manual for WAPDEG 4.07* (BSC 2003 [DIRS 162606], Table 19).

The outputs generated by the WP and DS Model Component and used by the EBS Flow and Transport Model Component (Sections 6.3.6 and 6.3.8) for each percolation subregion and each fuel type (CSNF and CDSP WPs) are:

- The average fraction of WP surface failed by general corrosion (patches), per failed WP, and the average fraction of WP surface failed by cracks, per failed WP, as a function of time
- The fraction of all the WPs and DSs in the subregion that were breached, as a function of time.

Note that the average fraction of WP surfaces failed by general corrosion or by cracks are values that apply to all WPs and DSs in a given percolation subregion and for a given fuel type. These values are calculated by the WAPDEG V4.07 software as an average over failed WPs.

6.3.5.2 Localized Corrosion on the Waste Package Outer Surface

The WP Localized Corrosion Initiation Submodel for the WP outer surface is based on the Localized Corrosion Initiation Abstraction developed in *General Corrosion and Localized Corrosion of Waste Package Outer Barrier* (SNL 2007 [DIRS 178519], Section 8.3.1). The temperature, pH, chloride-ion concentration, and nitrate-ion concentrations in aqueous solutions on the WP outer surface are the primary factors that determine the potential for initiating localized corrosion. These are obtained from the EBS TH Environment Submodel and the EBS Chemical Environment Submodel. Localized corrosion requires the presence of a liquid water film on the WP surface. Two types of aqueous solutions may lead to environmental conditions conducive to localized corrosion initiation on the WP outer surface: (1) dripping crown seepage water that contacts the WP outer surface, and (2) salt deliquescence in dust particles that may reside on the WP outer surface. Localized corrosion resulting from salt deliquescence in dust particles was screened out (SNL 2007 [DIRS 181267]). Also discussed in this section is the localized corrosion growth model, which applies to the WP during the time period when localized corrosion is indicated by the Localized Corrosion Initiation Abstraction. Appendix N discusses the details of the implementation of localized corrosion in the TSPA-LA Model.

6.3.5.2.1 Conceptual Model

Initiation of Localized Corrosion (Crevice Corrosion)—The Localized Corrosion Initiation Abstraction stipulates that localized corrosion of the WP outer surface occurs when the open-circuit potential, or corrosion potential (E_{corr}), is equal to or greater than the critical threshold potential ($E_{critical}$); that is, $\Delta E = E_{critical} - E_{corr} \leq 0$ (SNL 2007 [DIRS 178519], Section 8.3.1).

The open-circuit corrosion potential is the potential measured across a metal sample when it is immersed in a liquid. The corrosion potential can change with time, eventually approaching a steady state. Therefore, the long-term steady-state corrosion potential was used for the corrosion potential model of Alloy 22 (SNL 2007 [DIRS 178519], Section 4.1.1.5).

The long-term corrosion potential abstraction for the WP outer surface was developed using a regression model fit to the long-term corrosion potential data as a function of the major exposure-environment variables: temperature, pH, chloride ion concentration, and nitrate ion concentration. Only data with an immersion time of 250 days or higher were used (SNL 2007 [DIRS 178519], Section 6.4.4.5). The WP outer surface is potentially susceptible to crevice corrosion if an acidic chloride-containing solution with relatively lower concentrations of inhibitive ions contacts the WP outer surface while it is at elevated temperature.

The crevice repassivation potential from cyclic potentiodynamic polarization tests was selected as a conservative measure of $E_{critical}$, as described in *General Corrosion and Localized Corrosion of Waste Package Outer Barrier* (SNL 2007 [DIRS 178519], Section 6.4.4.1). The crevice repassivation potential (E_{rrev}) is the potential at which the reverse scan of a cyclic potentiodynamic polarization curve using a creviced sample crosses the forward scan.

Corrosion Penetration Rate—Because of the relatively high corrosion resistance of Alloy 22, there are limited experimental results regarding localized corrosion under the conditions expected in the repository. The Localized Corrosion Penetration Rate Abstraction for the WP

outer surface was based on results that bound the extreme penetration rates found in the literature for Alloy 22. This distribution is considered to be a highly conservative representation of the localized corrosion rates of Alloy 22 for the exposure conditions anticipated in the repository environment (SNL 2007 [DIRS 178519], Section 8.3.2).

The Localized Corrosion Initiation Submodel uses a constant (time-independent) penetration rate after localized corrosion is initiated (SNL 2007 [DIRS 178519], Assumption 5.4). This constant penetration rate is sampled from the epistemic uncertainty distribution for the localized corrosion rate and differs from realization to realization. Although the localized corrosion rate is modeled as time invariant, the crevice corrosion propagation rate would be expected to decrease with increasing depth of the crevices and time under realistic conditions. The use of constant penetration rate versus time is a highly conservative assumption because localized corrosion rates generally decrease with time and this decrease is even more likely under the thin water film environment that is expected to form on the WP outer surface in the postclosure repository period, as described in *General Corrosion and Localized Corrosion of Waste Package Outer Barrier* (SNL 2007 [DIRS 178519], Section 8.3.2) and *Waste Package Degradation Expert Elicitation Project* (CRWMS M&O 1998 [DIRS 100349], Table 3-2).

In the absence of specific information regarding local environments on the WP, the area of the Alloy 22 WP outer barrier that is contacted by seepage is considered to be potentially subject to localized corrosion (SNL 2007 [DIRS 178519], Section 8.3.1).

6.3.5.2.2 Model Abstraction

For the TSPA-LA Model, the Localized Corrosion Initiation Abstraction uses the crevice repassivation potential (E_{rcrev}) as the critical potential. The crevice repassivation potential for crevice corrosion on the WP outer surface is defined in terms of WP surface temperature and chemical conditions as follows:

$$E_{rcrev} = a_o + a_1 T + a_2 \ln[Cl^-] + a_3 \left[\frac{[NO_3^-]}{[Cl^-]} \right] + a_4 T [Cl^-] + \epsilon_{rcrev} \quad (\text{Eq. 6.3.5-16})$$

where a_o , a_1 , a_2 , a_3 , and a_4 are regression constants, T is the WP outer surface temperature ($^{\circ}C$), pH is the negative log of the hydrogen ion activity, $[NO_3^-]$ is the nitrate ion molality (moles/kg water), and $[Cl^-]$ is the chloride ion molality (moles/kg water), as presented in DTN: MO0703PAGENCOR.001_R4 ([DIRS 182029], file: *LC_Initiation.pdf*). The coefficient values and their epistemic uncertainty (± 1 SD) are $a_o = 190.242 \pm 18.373$, $a_1 = -3.008 \pm 0.225$, $a_2 = -46.800 \pm 3.126$, $a_3 = 535.625 \pm 26.140$, and $a_4 = 0.061 \pm 0.010$. The error term, ϵ_{rcrev} , is a term representing data variance not explained by the fitting procedure and has a normal distribution with a mean of zero mV versus the saturated silver chloride electrode and an SD of 45.055 mV versus saturated silver chloride. The units of the coefficients should be consistent with E_{rcrev} having units of mV. The covariation of the coefficients (due entirely to epistemic uncertainty) was represented through the use of a covariance matrix derived in *General Corrosion and Localized Corrosion of Waste Package Outer Barrier* (SNL 2007 [DIRS 178519], Section 8.3.1; DTN: MO0703PAGENCOR.001_R4 [DIRS 182029]). The Localized Corrosion Initiation Abstraction stipulates that the calculated value of E_{rcrev} be

compared to the ± 2 SD prediction intervals of the unconstrained model and be truncated at these values. These coefficients are sampled in the TSPA-LA Model using a Cholesky factorization method to induce correlation (output DTN: MO0707WPDRIPSD.000 [DIRS 183005]).

The long-term steady-state corrosion potential, E_{corr} , for the WP outer surface is expressed as:

$$E_{corr} = c_0 + c_1 T + c_2 pH + c_3 \frac{[NO_3^-]}{[Cl^-]} + c_4 T \frac{[NO_3^-]}{[Cl^-]} + c_5 pH \frac{[NO_3^-]}{[Cl^-]} + c_6 pH \ln[Cl^-] + \varepsilon_{corr}$$

(Eq. 6.3.5-17)

where c_0 , c_1 , c_2 , c_3 , c_4 , c_5 , and c_6 are coefficients of the parameters, and the other parameters are as previously defined. The regression coefficients and their epistemic uncertainty (± 1 SD) are: $c_0 = 1,051.219 \pm 119.774$, $c_1 = -3.024 \pm 0.977$, $c_2 = -155.976 \pm 11.495$, $c_3 = -1,352.040 \pm 252.224$, $c_4 = 10.875 \pm 1.890$, $c_5 = 137.856 \pm 23.158$, and $c_6 = -8.498 \pm 0.801$ (DTN: MO0703PAGENCOR.001_R4 [DIRS 182029], file: *LC_Initiation.pdf*). The error term, ε_{corr} , is a term representing data variance not explained by the fitting procedure and has a normal distribution with a mean of zero mV versus SSC and an SD of 85.265 mV versus SSC. The units of the coefficients should be consistent with E_{corr} having units of mV.

The covariation of the coefficients (due entirely to epistemic uncertainty) was represented through the use of a covariance matrix derived in DTN: MO0703PAGENCOR.001_R4 [DIRS 182029]. As with the crevice repassivation potential, E_{rcrev} , the uncertainty of the parameter coefficients of the corrosion potential, E_{corr} , should be limited to ± 2 SDs. These coefficients are sampled in the TSPA-LA Model using a Cholesky factorization method to induce correlation (output DTN: MO0707WPDRIPSD.000 [DIRS 183005]).

The WP Localized Corrosion Penetration Rate Abstraction propagates corrosion in the WP outer surface at a constant rate (SNL 2007 [DIRS 178519], Assumption 5.4). The extreme penetration rates found in the literature were used to bound localized corrosion rates for Alloy 22 under expected repository conditions. Based on these published rates, the localized corrosion propagation rates for the WP outer surface were estimated to be log uniformly distributed with a range from 12.7 to 1,270 $\mu\text{m}/\text{year}$ (DTN: MO0703PAGENCOR.001_R4 [DIRS 182029]).

Localized corrosion initiation requires the presence of liquid brine on the WP outer surface. This brine may be formed by aqueous solutions dripping onto the WP surface. For intact or moderately degraded drifts, there is no seepage water contacting the WP surface if the drift-wall exposure temperature is greater than 100°C (SNL 2007 [DIRS 181244], Section 6.5.3) or if the WP surface temperature is greater than 120°C. The 120°C limit is inferred from examination of peak drift-wall and WP temperatures for the seven modeled uncertainty cases presented in *Multiscale Thermohydrologic Model* (SNL 2000 [DIRS 181383], Table 6.3-49[a]). For collapsed drifts, boiling conditions persist later into the repository lifetime (SNL 2007 [DIRS 181383], Figure 6.3-79[a]). Therefore, the thermal seepage limit for intact or moderately degraded drifts can be considered bounding. Thus, the only relevant chemistries to consider for localized corrosion initiation, for WP surface temperatures greater than 120°C, are those that result from dust deliquescence. However, localized corrosion resulting from salt deliquescence

in dust particles was screened out of the TSPA-LA Model, based on geochemical analyses (DTN: MO0706SPAFEPLA.001_R0 [DIRS 181613], FEP Number 2.1.09.28.0A). Therefore, localized corrosion initiation at WP temperatures greater than 120°C need not be considered.

The limits of applicability and the procedures for the implementation of the Localized Corrosion Initiation Abstraction in the TSPA-LA Model are defined in *General Corrosion and Localized Corrosion of Waste Package Outer Barrier* (SNL 2007 [DIRS 178519], Section 8.3.1). The following initiation criteria apply:

1. Crown seepage localized corrosion does not occur if the drift-wall temperature is greater than 100°C (WP surface temperature greater than 120°C).
2. If it has been determined that localized corrosion can occur and the WP exposure temperature is at least 20°C but does not exceed 120°C, then the empirical correlations for the long-term corrosion potential (E_{corr}) and crevice repassivation potential (E_{rcrev}) are evaluated with the following implementation rules:
 - a. If the nitrate-to-chloride ion ratio in the environment exceeds one then evaluate E_{rcrev} and E_{corr} at a nitrate-to-chloride ion ratio of one. If the molality of chloride ion is less than 0.0005 molal, evaluate the nitrate-to-chloride ion ratio with a chloride ion concentration of 0.0005 molal.
 - b. If the molality of the chloride ion in the environment exceeds 20 molal, then evaluate E_{rcrev} and E_{corr} at a chloride ion molality of 20 molal. If the chloride ion molality is less than 0.0005 molal, then evaluate E_{rcrev} and E_{corr} at a chloride ion molality of 0.0005 molal.c.
 - c. If the pH in the environment exceeds 10, then evaluate E_{rcrev} and E_{corr} at a pH of 10. If the pH in the environment is less than 1.9, then initiate localized corrosion.
3. If the WP relative humidity is below the threshold at which halite precipitates and the WP is below a failed DS, then when re-wetting occurs the in-package chemistry lookup tables no longer apply and TSPA is instructed to assume that Cl-rich brine can form (SNL 2007 [DIRS 177412], Sections 6.12.3 and 6.15.1.3). The relative humidity of salt separation for all modeled waters is archived in DTN: SN0703PAEBSPCE.006_R2, files: *Gp1_Salt_Separation_table.xls*, *Gp2_Salt_Separation_table.xls*, *Gp3_Salt_Separation_table.xls*, *Gp4_Salt_Separation_table.xls* [DIRS 181571]. Because the process of salt-brine separation cannot be explicitly modeled, the P&CE report (SNL 2007 [DIRS 177412]) abstraction models do not attempt to provide the chemistry for the Cl-rich brines. In this situation it is conservatively assumed that localized corrosion initiates when re-wetting occurs.
4. If crown seepage localized corrosion is determined to initiate, then allow localized corrosion to continue to occur at the sampled propagation rate, regardless of changes in the chemical environment.

5. The area of the Alloy 22 WP outer barrier that is contacted by seepage is potentially subject to localized corrosion (SNL 2007 [DIRS 178519], Section 8.3.1).

6.3.5.2.3 Implementation in the TSPA-LA Model

The Localized Corrosion Initiation Abstraction, described in Sections 6.3.5.2.1 and 6.3.5.2.2, provides input to the localized corrosion implementation in the TSPA-LA Model file by determining if environmental conditions on the WP outer surface will initiate localized corrosion and lead to WP failure. The Localized Corrosion Initiation Submodel is implemented in a modified version of the TSPA-LA Model, referred to as the Localized Corrosion Stand-Alone Model (output DTN: MO0709TSPALOCO [DIRS 182994]). Only the TSPA-LA submodels that are required to produce feeds to the Localized Corrosion Initiation Submodel are retained. The implementation of the thermal histories and the implementation of the seepage abstraction in the Localized Corrosion Stand-Alone Model differ from the corresponding implementations in the TSPA-LA Model. These differences are discussed below.

Implementation of the Localized Corrosion Initiation Submodel

Localized Corrosion Initiation Submodel calculations result from the interfacing of several TSPA-LA Model submodels and abstractions, as illustrated on Figure 6.3.5-9, to determine whether or not environmental conditions on the WP outer surface will initiate localized corrosion and lead to failure. These submodels include:

- EBS Chemical Environment Submodel look-up tables for P_{CO_2} in the emplacement drifts and abstraction bin history maps for incoming seepage composition history (Section 6.3.4.2). These abstractions are used to define P_{CO_2} in the emplacement drift as a function of time, and to define the chemical composition of seepage water entering the drifts as a function of time. P_{CO_2} is an input to the chemical evolution of crown seepage water.
- EBS Chemical Environment Submodel look-up tables for the chemical evolution of crown seepage water on the WP outer surface (Section 6.3.4.3.2) and distributions for the nitrate to chloride ratio (sampled once per realization). The EBS P&CE Abstraction is used to calculate the chloride concentration, nitrate concentration, and pH in crown seepage water as functions of relative humidity. These quantities are then used to evaluate localized corrosion initiation.
- Drift Seepage Submodel (Section 6.3.3.1). The calculations outlined in *Abstraction of Drift Seepage* (SNL 2007 [DIRS 181244], Section 6.7.1) and the seepage response surfaces for nondegraded and degraded drifts are used to determine if seepage occurs at each repository subdomain location.
- EBS TH Environment Submodel (Section 6.3.2). The EBS MSTHM Abstraction (Section 6.3.2.3) provides time-dependent values for temperature and relative humidity on WP surfaces and the drift-wall temperature. The EBS MSTHM Abstraction also provides time-dependent adjusted values that are used to correct temperature and relative humidity values for the insulating effect of rubble caused by drift degradation induced

by seismic ground motion in the lithophysal units. Drift-wall temperatures are used to calculate thermal seepage in the nonlithophysal units. WP temperatures, with adjusted values for rubble, are used to calculate thermal seepage in the lithophysal units.

- Localized Corrosion Initiation Abstraction (Section 6.3.5.2.2). The Localized Corrosion Initiation Abstraction derives the criteria for localized corrosion initiation.
- Seismic Ground Motion Damage Submodel (Section 6.6). The volume of rubble accumulated in the lithophysal and nonlithophysal zones are inputs to the Drift Seepage Submodel, as described above. The time of first DS plate failure due to seismic damage is used to determine the time of initiation of localized corrosion.
- WP and DS Degradation Submodel (Section 6.3.5). The time of first DS failure due to general corrosion is used to determine the time of initiation of localized corrosion. The general corrosion rate parameters and the MIC factor are used to determine a general corrosion rate, which is added to the localized corrosion rate to determine the WP failure fraction histories.

Figure 6.3.5-9 also illustrates the WP failure fraction histories that are the primary outputs produced by the Localized Corrosion Initiation Submodel. Figure 6.3.5-10 illustrates the steps taken to implement localized corrosion initiation in the Localized Corrosion Initiation Submodel. The Localized Corrosion Initiation Submodel, includes two computational loops: an outer epistemic uncertainty loop, and an inner spatial and temporal variability loop. In the outer loop, epistemic uncertainties associated with localized corrosion initiation, chemical environment on the WP outer surface, drift seepage, and rubble (natural backfill caused by a strong seismic ground motion event) are sampled using LHS for each localized corrosion realization. These epistemic uncertainties include the following (Table 6.3.5-4).

- Fifteen uncertain parameters from the Localized Corrosion Initiation Abstraction (Section 6.3.5.2.2); 14 coefficients that correspond to the linear regression fitting parameters ($a_0, a_1, a_2, a_3, a_4, \epsilon_{rcrev}, c_0, c_1, c_2, c_3, c_4, c_5, c_6,$ and ϵ_{corr}) associated with the crevice repassivation potential and the long-term steady-state corrosion potential, respectively; one uncertain parameter that represents the epistemic uncertainty in the localized corrosion propagation rate.
- Six parameters that quantify the evolution of the chemical environment on the WP outer surface; one parameter is used to select crown seepage starting water type (Section 6.3.4.3.1); one uncertain parameter represents uncertainty in partial pressure of CO₂; four parameters represent epistemic uncertainty (Table 6.3.4-3, Section 6.3.4.3.2) in calculated chloride concentration, the nitrate-to-chloride ratio, the combined chloride and nitrate concentration, and pH (each of these four is represented by one of several possible distributions, depending on relative humidity). Five parameters that represent uncertainty in drift-seepage, including the seepage uncertainty scale factor and the uncertainty in fracture permeability and capillary strength for both the lithophysal and nonlithophysal units (Tables 6.3.3-1 and 6.3.3-2, and Section 6.3.3.1.2).

- One parameter that represents epistemic uncertainty in thermal conductivity of the rubble deposited on the DSs and WPs due to drift degradation in the lithophysal unit (Section 6.6.1.3).
- Two uncertain parameters used to select exposure histories; one that represents epistemic uncertainty in infiltration scenario; one that represents epistemic uncertainty in thermal conductivity of the host rock.
- Two parameters that represent the uncertainty in the maximum rubble volume for the lithophysal and nonlithophysal units.
- Two uncertain parameters that represent the epistemic uncertainty in the Titanium Grade 7 general corrosion rate for aggressive and benign conditions; one uncertain parameter that represents the epistemic uncertainty in the temperature dependence of the Alloy 22 general corrosion rate; one uncertain parameter that represents the relative humidity threshold for the application of the MIC factor.
- Four parameters that represent uncertainty in the general corrosion rate of Alloy 22.

The MSTHM Abstraction subdivides the repository footprint into 3,264 equal-area subdomains and supplies temperature and relative humidity time histories for six CSNF WPs and two CDSP DS/WP pairs at each subdomain-center location. Time-dependent values for average drift-wall temperature are also supplied at each location. The TH variables and their associated locations are grouped into one of five repository subregions based on percolation flux at the base of the PTn (Section 6.3.2.2.1). Localized corrosion initiation analyses are implemented for each of the 12 cases considered by the MSTHM Abstraction. These 12 cases represent the combinations of epistemic uncertainty in infiltration and host-rock thermal conductivity (Section 6.3.2.2).

The implementation of the thermal histories and the implementation of the seepage abstraction in the Localized Corrosion Stand-Alone Model differ from the corresponding implementation in the TSPA-LA Model. In the TSPA-LA Model, EBS Chemical Environment Submodel calculations for representative temperature and relative humidity histories, are used for all subdomain locations in a particular percolation subregion (Section 6.3.2.3). In the TSPA-LA Model, the implementation of drift seepage is accomplished through the use of an external DLL (STN: 11076-1.3-00 [DIRS 181058]), which implements the same calculations but whose output is the fraction of WPs that experience seepage, averaged over all MSTHM subdomains in a percolation subregion (Section 6.3.3.1.3).

After the epistemic parameters are sampled, the percolation subregion and the TH case from the set of 12 are selected. Next, for each outer-loop realization, an inner loop over the TH locations in the percolation subregion is executed. The inner loop represents spatial and temporal variability in the parameters. It includes:

- Two sets of temperature and relative humidity time histories (associated with one of six CSNF WP time histories or one of two CDSP WP time histories): the first set represents values to be used under conditions of no drift collapse (or minor drift

collapse); the second set is adjusted for the presence of rubble by adding an increment in temperature and relative humidity (Section.3.2).

- Drift-seepage parameters for flow focusing factor, spatial variability of fracture permeability, and capillary strength (Equation 6.3.3-1, Tables 6.3.3-1 and 6.3.3-2, and Section 6.3.3.1.2.).

The following steps are performed at each WP location within this loop for each percolation subregion and at each timestep:

1. The chemical environment on the WP outer surface due to crown seepage is determined. A calculation is first made to determine if seepage into the drift occurs.

This calculation is implemented for each WP location, as described in the Drift Seepage Abstraction (Section 6.3.3.1), using the sampled drift-seepage parameters representing epistemic uncertainty and variability, the percolation flux, and the drift-wall temperature to account for thermal seepage effects. In addition, if seepage occurs and a WP is located in the lithophysal unit, the adjusted (for the presence of rubble) WP temperature history is used to determine whether or not incoming seepage contacts the WP. If seepage does not contact the WP at the current location and time, localized corrosion initiation due to crown seepage is not evaluated. If drift seepage occurs, the following two evaluations are implemented.

2. The chemical environment on the WP outer surface, in terms of nitrate concentration, chloride concentration, nitrate-to-chloride ratio, and pH due to evolution of crown seepage, is calculated through time, as described in Section 6.3.4.3.2, using temperature and relative humidity time histories for the WP. If the WP is located in the lithophysal unit, the WP temperature and relative humidity values are adjusted for the presence of rubble from drift degradation in the Seismic Scenario Class using the thermal adjustment histories.
3. The values of temperature, relative humidity, pH, chloride concentration, and nitrate concentration are checked against the criteria listed in Section 6.3.5.2.2. If these parameters are outside the ranges specified, the appropriate bounding values are used. Otherwise, localized corrosion is initiated if $\Delta E \leq 0$ on a WP.
4. If localized corrosion initiates, the localized corrosion penetration continues at a constant rate through the regulatory period or until the WP is penetrated. The localized corrosion penetration rate is sampled from a uniform distribution from 0.0127 mm/yr to 1.27 mm/yr. A WP is considered failed by localized corrosion if the WP outer surface thickness is fully penetrated by the combined localized corrosion, general corrosion, and MIC penetration depths.

For each repository subregion and WP type, a corresponding fractional failure history is obtained by adding the failed WPs of that type and dividing by the total number of either CSNF WPs or CDSP WPs in the subregion. This evaluation is carried out for each TH timestep until simulation end time.

The evaluation of penetration time includes general corrosion and MIC enhancement of general corrosion. Because general corrosion is much slower than localized corrosion, a simplified general corrosion abstraction is incorporated into the Localized Corrosion Initiation Submodel. This simplified general corrosion abstraction uses the CDF for R_0 , which was developed from the average corrosion rate with a scale factor of four and corresponds to the medium uncertainty level. MIC enhancement of general corrosion is activated only when relative humidity exceeds the MIC threshold.

The primary output from the Localized Corrosion Initiation Submodel is the fraction of CSNF WPs and CDSP WPs that fail by localized corrosion due to crown seepage, as a function of time, in each percolation subregion. These fractions are used to define the number of WPs that fail by localized corrosion during the simulation time and their average breach areas as a function of time.

TSPA-LA Modeling Cases

Localized corrosion is included in the two Seismic Scenario Class modeling cases discussed in Section 6.6, the Seismic GM Modeling Case and Seismic FD Modeling Case; and in the Nominal Modeling Case. In the Igneous Scenario Class, the affected WPs and DSs are immediately destroyed at the time of the intrusion event. Only dripping crown seepage water contacting the WP outer surface is considered, in the TSPA-LA Model, to lead to environmental conditions conducive to localized corrosion on the WP outer surface. The Localized Corrosion Stand-Alone Model was run five times (once for each percolation subregion) for 300 realizations with unified sampling for each of the three modeling cases considered. The model computes time-dependent chemical conditions of brine formation and corrosion potential.

Evaluation of the Localized Corrosion Stand-Alone Model results revealed that conditions for localized corrosion initiation occurred only in the first 12,000 years after closure (Section O1). Beyond this time, the chemistry of the seepage water is benign and localized corrosion no longer initiates. These analyses are documented in output DTN: MO0709TSPALOCO.000 [DIRS 182994]. In addition, localized corrosion can only occur if crown seepage water contacts the WP outer surface (i.e., if the DS is failed).

For the Nominal Modeling Case, the first DS failure occurs at about 230,000 years (Section 6.3.5.1.3), so localized corrosion does not impact this modeling case. In the Seismic GM Modeling Case, there is a low probability (Figure 7.3.2-16) of DS plate failure occurring before 12,000 years. Section 7.3.2.6.1.3.2 discusses the justification for not considering these early DS failures in the context of the Seismic GM (10,000-year) Modeling Case. The same arguments apply to the Seismic GM (1,000,000-year) Modeling Case, when considering localized corrosion, since only the first 12,000 years after closure are relevant. In the Seismic FD Modeling Case, there is a low probability of a fault event (and, therefore, DS failure) in the first 12,000 years after closure. However, localized corrosion does not impact the Seismic FD

Modeling Case even though DSs may be failed during the period of time that seepage water could initiate localized corrosion. The argument for this assertion is based on the observation that, when the DS is failed and the WP damage area is larger than 1/3 of the WP cross-sectional area, the releases cease to change significantly as more damage is applied (Section 7.3.2.7 and Figure 7.3.2-25). Since the dose result is insensitive to the damage area when more than 1/3 of the lid area is damaged, it is not expected that additional localized corrosion damage will affect the dose result.

Since localized corrosion is not expected to impact any of the three TSPA-LA modeling cases where its effects are modeled, the 30 input files (10 for each modeling case) containing the time histories for the fraction of WPs failed by localized corrosion will contain only zero entries. These input files were created using GoldSim v9.60.100 software, as described in output DTN: MO0708TSPAGENT.000 [DIRS 183000].

6.3.5.3 Model Component Consistency and Conservatism in Assumptions and Parameters

To enhance understanding of the complex interactions within the TSPA-LA Model, a discussion of consistency among model components and submodels and identification of conservative assumptions in abstractions, process models, and parameter sets supporting the WP and DS Degradation Model Submodel and the Localized Corrosion Initiation Submodel are discussed below.

6.3.5.3.1 Consistency of Assumptions

Salt Separation on the WP Surface—The current TSPA-LA Model includes a relative humidity threshold switch to account for a potential salt separation process during seepage water evaporation (Section 6.3.5.2.2). In principle, water evaporation on the Alloy 22 WP surface will first cause the precipitation of halite (NaCl) and then the remaining water will flow away from early precipitated salts, leaving the solids behind rich in Cl^- . In this case, the chemistry look-up tables no longer apply from (SNL 2007 [DIRS 177412], Sections 6.12.3 and 6.15.1.3). For implementation purposes, the TSPA-LA Model assumes that localized corrosion always initiates upon re-wetting of the salt film. The implementation for the WP Localized Corrosion Initiation Submodel represents potential differences between several submodels: Drift Seepage, EBS Flow, EBS Chemical Environment, and the localized corrosion aspect of WP degradation. The EBS Chemical Environment Submodel assumes well-mixed equilibrium conditions for chemistry in the drift (Section 5.1.2). Therefore, salt separation is not included in that submodel. In addition, evaporation and flow on a small scale of the possible salt separation phenomenon is overwhelmed by uncertainties at the larger scale of the Drift Seepage Submodel or the EBS Flow Submodel. Evaporation is integral, however, to the equilibrium chemistry response surfaces that are the output of the EBS Chemical Environment Submodel. In order to handle this difference, a conservative assumption is implemented in the TSPA-LA Model, using the NaCl deliquescence relative humidity threshold (Section 6.3.5.2.2; note that concentrated salt solutions are referred to as brines in Section 6.3.5.2.2).

Effect on TSPA—Based on a water volume argument, this separation is unlikely to occur, and if it were to occur, it would be limited in spatial extent. The approach taken in the TSPA-LA results in a greater likelihood that those conditions conducive to localized corrosion might exist

over the entire surface of the WP and is, therefore, conservative. The TSPA-LA Model assumes that there will always be a sufficient volume of brine available for WP degradation regardless of the types of the resulting brines (Section 6.3.5.2.2). In actual repository environments, however, brines formed from evaporation are expected to be limited in volume. For example, obtaining a saturated NaCl brine may require the seepage water to concentrate significantly. That is, 1 L of seepage water would result in only a small volume of NaCl solution. The assumption of sufficient brine volume may lead to a conservative overestimation of the potential for initiating localized corrosion if the brine volumes are too small to cause a continuous water film over the WP surface.

6.3.5.3.2 Identification of Conservatisms in Submodels and Abstractions

Threshold Relative Humidity for General Corrosion Initiation on WPs—There is no threshold relative humidity for the initiation of general corrosion of the WPs. A relative humidity threshold for the initiation of general corrosion clearly exists (ASM International 1987 [DIRS 133378], p. 82). However, there is insufficient information/data to quantify the general corrosion initiation threshold relative humidity for varying water chemistry conditions (SNL 2007 [DIRS 178519], Assumption 5.1). The assumption that no relative humidity threshold for the initiation of corrosion processes exists is conservative because use of a relative humidity threshold would delay the corrosion initiation start time.

Representation of the Critical Threshold Potential—The critical threshold potential ($E_{critical}$) is conservatively represented by the crevice repassivation potential (E_{rcrev}). The crevice repassivation potential (E_{rcrev}) determined from cyclic potentiodynamic polarization tests was selected as a conservative measure for the critical threshold potential ($E_{critical}$). Other less conservative choices for $E_{critical}$ are possible (e.g., the breakdown potential or potentials based on current density thresholds) (SNL 2007 [DIRS 178519], Section 6.4.4.1). The chemical exposure conditions in creviced regions can be more severe than those in noncreviced regions (SNL 2007 [DIRS 178519], Section 1.2). This leads to the measurement of lower repassivation (critical) potentials in creviced versus noncreviced regions.

Stainless Steel Inner Vessel—No corrosion credit is taken for the use of a stainless-steel inner vessel. The 50 mm inner vessel will provide structural support to the thinner outer barrier, and the outer barrier will protect the inner vessel from significant corrosion degradation while it remains intact. The inner vessel could provide some delay of radionuclide release before it fails and also could retard the release rate of radionuclides from the WP (SNL 2007 [DIRS 178519], Section 6.3.3).

General Corrosion Rate of WP Outer Surface—The general corrosion rate of the WP outer surface at a given temperature is time-independent. General corrosion rates of the WP outer surface decrease with time (SNL 2007 [DIRS 178519], Section 6.4.3.5.1). However, there is insufficient information/data to quantify the time dependence. This conservatism is expected to result in the overestimation of WP general corrosion rate (SNL 2007 [DIRS 178519], Figure 7-1).

General Corrosion Rate Distribution for WP Outer Surface—Two coupon (specimen) types are used for general corrosion weight-loss measurements. These are identified as weight-loss

coupons and crevice coupons. The general corrosion rate distribution for the WP outer surface is based on the weight-loss of crevice coupons (specimens). The creviced specimens exhibited generally higher general corrosion rates than the noncreviced specimens. This is attributed to the difference in the surface-polishing treatments between the two groups of specimens (SNL 2007 [DIRS 178519], Section 6.4.3.2). This conservatism is expected to overestimate the general corrosion rates on the WP outer surface. The evaluation of the general corrosion rate using crevice samples was included in the Performance Margin Analysis (PMA) (Appendix C).

General Corrosion Rate Distribution Adjustment for Patch Size—The general corrosion rate distribution is conservatively adjusted for patch size. The patch size used in the TSPA-LA Model is a factor of four larger than the size of the crevice samples in the experiments that generated the data from which the general corrosion rate was derived. The adjustment method is to effectively use the highest of four sampled values for the patch general corrosion rate (Section 6.3.5.1.2). The approach is conservative because it is probable that not all four samples from the Weibull distribution will have the highest rate.

Crevice Corrosion—The dominant form of localized corrosion is assumed to be crevice corrosion as opposed to pitting corrosion, which occurs on boldly exposed surfaces. Additionally, crevice corrosion is applied to the entire WP surface, though it is unlikely that crevice attack would occur over the entire surface area (SNL 2007 [DIRS 178519], Assumption 5.3). The initiation threshold for crevice corrosion, in terms of exposure conditions, is lower than that for pitting corrosion (SNL 2007 [DIRS 178519], Section 6.4.4). This conservatism is expected to result in the overestimation of the number of WPs that experience localized corrosion.

Effects of Inhibitive Anions—No credit is taken in the Localized Corrosion Initiation Abstraction for the effects of inhibitive anions other than nitrate. Nitrate ions inhibit localized corrosion initiation. Carbonate and sulfate ions may also have an inhibitive effect on localized corrosion. However, there is insufficient information and/or data to quantify the effect of other inhibitive anions on localized corrosion initiation (SNL 2007 [DIRS 178519], Section 8.3.1). Results for solutions with significant amounts of other potentially inhibitive ions are conservative (SNL 2007 [DIRS 178519], Section 8.3.1).

Localized Corrosion Rate of WP Outer Surface—The localized corrosion propagation rate for the WP outer surface is assumed to propagate at a (time-independent) constant rate (SNL 2007 [DIRS 178519], Assumption 5.4). The localized corrosion propagation rate is known to decrease with increasing time (SNL 2007 [DIRS 178519], Section 6.4.4.8.2); however, there is insufficient information and/or data to quantify the time dependence. This conservatism is expected to result in the overestimation of the number of WPs that fail due to localized corrosion.

Effect of Changing Chemical Environment on Localized Corrosion Propagation—Once localized corrosion is initiated, it continues to propagate regardless of any changes in the bulk chemical exposure environment. This is a conservative modeling assumption because no detailed chemistry evolution model of the crevice solution is available (SNL 2007 [DIRS 178519], Section 8.3.1). This conservatism is expected to result in the overestimation of the number of WPs that fail due to localized corrosion.

6.3.5.4 Alternative Conceptual Model(s) for Waste Package and Drip Shield Degradation

An important reason for considering ACMs is to help build confidence that plausible changes in modeling assumptions or simplifications will not change conclusions regarding subsystem and total system performance. Section 6.2.1 outlines the general consideration and treatment of ACMs used to support the TSPA-LA Model. Conservatism at the subsystem level was used to select the best ACM to use rather than quantitatively propagate multiple ACMs to the TSPA-LA Model. Generally, additional uncertainty is incorporated into the selected conceptual model if more than one ACM is deemed appropriate for use rather than considering multiple ACMs in the TSPA-LA Model. If an ACM appears to be significant at the subsystem level, then an appropriate abstraction is developed for that ACM for consideration within the TSPA-LA Model. The result of the process is documented within the individual analysis model reports. It is important to note that treatment of ACMs within the individual analysis model reports may differ significantly to be consistent with available data and current scientific understanding. Therefore, a brief description of the WP and DS Degradation Submodel ACMs and the Localized Corrosion Initiation Submodel ACMs are presented below and summarized in Table 6.3.5-2.

Parabolic General Corrosion Rate Law for DS—The parabolic general corrosion rate law for DS degradation (SNL 2007 [DIRS 180778], Section 6.5.6) assumes that the increasing oxide layer thickness on the diffusion of oxidizing species to the underlying metal will have an inhibiting effect on corrosion. This model is less conservative than the primary model and was not recommended for inclusion in the evaluation of DS degradation for the TSPA-LA Model.

Decreasing Rate Law for WP—The corrosion rates of metals and alloys tend to decrease with time (SNL 2007 [DIRS 178519], Section 6.4.3.5.1). The time-dependent general corrosion behavior of the WP was not included in the TSPA-LA because the constant (time-independent) rate model (for a given temperature) is more conservative and bounds the general corrosion behavior of the WP outer surface over the repository time period.

General Corrosion Rate Law Based on Weight-Loss Samples Only—The ACM discussion for a general corrosion rate law for WP degradation based on plain weight-loss samples (rather than crevice samples) and is found in the analysis model report (SNL 2007 [DIRS 178519], Section 6.4.3.5.2). The weight-loss data was fit to a Weibull distribution using maximum likelihood estimators (i.e., using the same methods applied to the crevice sample data). A comparison of the general corrosion rate distribution resulting from fitting the 5-year exposed weight-loss sample to the Weibull distributions based on the crevice sample data shows that this conceptual model is less conservative relative to the base case general corrosion model (SNL 2007 [DIRS 178519], Figures 6-28 and 6-23).

Critical Temperature-Based Localized Corrosion Initiation—The evolution of the WP temperature with time, coupled with the knowledge of the critical temperature for the initiation of localized corrosion (pitting/crevice corrosion), can be used to determine when localized corrosion initiates (SNL 2007 [DIRS 178519], Section 6.4.4.8.1). However, the test conditions at which the required critical temperatures were measured are not directly relevant to the potential environments on the WP surface. In addition, the critical temperature-based model does not account for the effects of electrochemical characteristics of the solution contacting the metal. Therefore, the critical temperature-based model is not considered in the TSPA.

Coupled Environmental Fracture Model—The coupled environment fracture model for stress corrosion crack growth rate was evaluated as an ACM for SCC (SNL 2007 [DIRS 181953], Section 6.4.6). The model, based on charge conservation, incorporates the effects of oxygen concentration, flow rate, and the conductivity of the external environment, as well as accounting for the effect of stress on crack growth. The model underestimated the crack growth rate, as compared to the slip dissolution-film rupture (SDFM) model, when both models were applied to predict the crack growth rate.

Time-Dependent Localized Corrosion Rate—An ACM for localized corrosion penetration is a time-dependent growth law of the form (SNL 2007 [DIRS 178519], Section 6.4.4.8.2):

$$D = k \times t^n \quad (\text{Eq. 6.3.5-18})$$

where D is the depth of penetration, t is time, and k is a growth constant. However, insufficient penetration rate data are available, especially for relatively new materials such as Alloy 22, to determine the values of k and n for the exposure conditions relevant to the repository. This ACM was not recommended for incorporation into the TSPA-LA Model because the data needed to apply the model can only be estimated approximately from open literature. The time-independent constant penetration rate model used in the TSPA-LA Model is more conservative.

Passive Film Breakdown Potential for the Determination of Critical Potential—An alternative technique for the determination of critical potential could be to use the passive film breakdown potential obtained from the forward scan of cyclic potentiodynamic polarization tests (SNL 2007 [DIRS 178519], Section 6.4.4.1). This technique would not account for the (often slow) kinetics of localized corrosion initiation and may not be appropriate for modeling the long time periods involved in repository environments. Furthermore, the breakdown potential is likely to be much higher when the passive film has been formed over long time periods, allowing for a decrease in the film defect density.

WP Surface Area Subjected to Localized Corrosion—No information is available regarding local environments on the WP; therefore, the area affected by localized corrosion due to seepage is based on the fraction of the WP surface exposed to seepage. TSPA has conservatively taken the area affected by localized corrosion to be the area wetted by seepage. Therefore, the entire surface area can potentially undergo localized corrosion. A distribution for the minimum area affected by localized corrosion was developed (minimum of 0.05 percent and maximum of the percent of area wetted by seepage) (SNL 2007 [DIRS 178519], Section 6.4.4.8.3). The ACM has not been implemented in the TSPA-LA Model. Sensitivity analyses have shown that dose results are insensitive to the magnitude of the failed area on the WP once the failed area has reached about 5 percent of the WP surface area (Section 7.3.2.7).

No ACMs were recommended for inclusion in the TSPA-LA Model.

Table 6.3.5-1. Drip Shield and Waste Package Degradation Mechanisms and Their Disposition for Implementation in the TSPA-LA Model

Failure Mechanism	Drip Shield Postclosure Assessment		Waste Package Postclosure Assessment	
	Included in TSPA-LA Model	Screened Out ^a	Included in TSPA-LA Model	Screened Out ^a
General Corrosion	X	—	X	—
Localized Corrosion	—	X	X	—
Stress Corrosion Cracking	—	X	X	—
Microbially Influenced Corrosion	—	X	X	—
Early Failure	X	—	X	—
Aging and Phase Instability	—	X	—	X
Hydrogen Induced Cracking	—	X	—	X
Mechanical Impacts	—	X ^b	—	X ^b
Radiolysis	—	X	—	X

NOTE: ^a Excluded FEPs, as shown in DTN: MO0706SPAFEPLA.001_R0 [DIRS 181613], Table 7.1.

^b Screened out for the Nominal Scenario Class; included for both modeling cases of the Seismic Scenario Class.

Table 6.3.5-2. Alternative Conceptual Models Considered for Drip Shield and Waste Package Degradation

Alternative Conceptual Models	Key Assumptions	Screening Assessment and Basis
Parabolic general corrosion rate law for DS degradation (SNL 2007 [DIRS 180778], Section 6.5.6).	Assumes that the increasing oxide layer thickness on diffusion of oxidizing species to the underlying metal will have an inhibiting effect on corrosion.	Model is less conservative than the primary model.
Decreasing general corrosion rate law for WP degradation (SNL 2007 [DIRS 178519], Section 6.4.3.5.1).	General corrosion rates of metals and alloys tend to decrease with time.	The time-dependent general corrosion behavior of the WP was not included in the TSPA-LA because the constant (time-independent) rate model (for a given temperature) is more conservative and bounds the general corrosion behavior of the WP outer surface over the repository time period.
General Corrosion Rate Based on Weight-Loss Samples Only (SNL 2007 [DIRS 178519], Section 6.4.3.5.2).	A general corrosion rate law for WP degradation based on plain weight-loss samples (rather than crevice samples) was developed. The weight-loss data were fit to a Weibull distribution using maximum likelihood estimators (i.e., using the same methods applied to the crevice sample data).	A comparison of the general corrosion rate distribution resulting from fitting the 5-yr exposed weight-loss samples to the Weibull distribution based on the crevice sample data shows that this conceptual model is less conservative relative to the base case general corrosion model (SNL 2007 [DIRS 178519], Figures 6-28 and 6-23).

Table 6.3.5-2. Alternative Conceptual Models Considered for Drip Shield and Waste Package Degradation (Continued)

Alternative Conceptual Models	Key Assumptions	Screening Assessment and Basis
Critical Temperature-Based Localized Corrosion Initiation Model (SNL 2007 [DIRS 178519], Section 6.4.4.8.1).	The evolution of WP temperature with time, coupled with knowledge of the critical temperature for the initiation of localized corrosion (pitting/crevice corrosion), can be used to determine when localized corrosion initiates.	Test conditions at which the required critical temperatures were measured are not directly relevant to the potential environments on the WP surface. The model does not account for the effects of electrochemical characteristics of the solution contacting the metal. The model is not used in the TSPA-LA.
Coupled environment fracture model for stress corrosion crack growth rate (SNL 2007 [DIRS 181953], Section 6.4.6).	The model, based on charge conservation, incorporates the effects of oxygen concentration, flow rate, and the conductivity of the external environment, as well as accounting for the effect of stress on crack growth.	Model underestimates the crack growth rate, as compared to the slip dissolution/film rupture model, when both models were applied to predict the crack growth rate.
Localized corrosion penetration as a time-dependent growth law (SNL 2007 [DIRS 178519], Sections 6.4.4.8.2 and 7.2.5).	Once initiated, the localized corrosion penetration rate decreases with increasing time.	Data needed to apply the model can only be estimated approximately from open literature. The time-independent constant penetration rate model is more conservative.
Passive film breakdown potential for determination of critical potential (SNL 2007 [DIRS 178519], Section 6.4.4.1).	An alternative technique for the determination of critical potential would be to use the passive film breakdown potential (obtained from the forward scan of the cyclic potentiodynamic polarization tests).	This technique would not account for the (often slow) kinetics of localized corrosion initiation and may not be appropriate for modeling the long time periods involved in repository environments. Furthermore, the breakdown potential is likely to be much higher when the passive film forms over long time periods allowing for a decrease in the film defect density.
No information is available regarding local environments on the WP; therefore, the area affected by localized corrosion due to seepage is based on the fraction of the WP surface exposed to seepage. TSPA has conservatively taken the area affected by localized corrosion to be the area wetted by seepage. Therefore, the entire surface area can potentially undergo localized corrosion.	A distribution for the minimum area affected by localized corrosion was developed (minimum of 0.05 percent and maximum of the percent of area wetted by seepage) (SNL 2007 [DIRS 178519], Section 6.4.4.8.3).	The ACM has not been implemented in the TSPA-LA Model. Sensitivity analyses have shown that dose results are insensitive to the magnitude of the failed area on the WP once the failed area has reached about 5% of the WP surface area (Section 7.3.2.7).

Table 6.3.5-3. Uncertain Inputs to the TSPA-LA Model for Generalized Corrosion of the Drip Shield and Waste Package and Stress Corrosion Cracking of the Waste Package

TSPA_LA Parameter Name	Mathematical Model Symbol	Description	Units	Distribution Specification	Remarks
WDDSBenignGC_Mean_a	None	DS-underside general corrosion rate (epistemic uncertainty)	nm/yr	Normal Mean = 5.15 SD = 0.831	DTN: SN0704PADSGCMT.001_R2, [DIRS 182122], file: TSPA Implementation_DS GC Models.pdf
WDDSAggrGC_Mean_a	None	DS-topside general corrosion rate (epistemic uncertainty)	nm/yr	Student's-t Mean = 46.1 SD = 1.19 Degrees of Freedom: 5	DTN: SN0704PADSGCMT.001_R2, [DIRS 182122], file: TSPA Implementation_DS GC Models.pdf
WDlnR_ESC_L_cdf WDlnR_ESC_M_cdf WDlnR_ESC_H_cdf	$\ln R_o$	Natural logarithm of general corrosion rate: 60°C: WP (spatial variability)	None	Three CDFs corresponding to low, medium, and high levels of epistemic uncertainty in the GC_shape and GC_scale parameters (fourth and fifth rows of this table)	Developed by TSPA from GC_scale and GC_shape parameters Output DTN: MO0707WPDRIPSD.000 [DIRS183005]
GC_shape	None	Shape parameter for Weibull distribution (WP general corrosion)	None	1.380 (low): 5% realizations 1.476 (medium): 90% realizations 1.578 (high): 5% realizations Different values are epistemic uncertainty. Overall distribution is spatial variability.	DTN: MO0703PAGENCOR.001_R4, [DIRS 182029], file: BaseCase GC CDFs.xls
GC_scale	None	Scale parameter for Weibull distribution (WP general corrosion)	None	6.628 (low): 5% realizations 8.134 (medium): 90% realizations 9.774 (high): 5% realizations Different values are epistemic uncertainty. Overall distribution is spatial variability.	DTN: MO0703PAGENCOR.001_R4, [DIRS 182029], file: BaseCase GC CDFs.xls

Table 6.3.5-3. Uncertain Inputs to the TSPA-LA Model for Generalized Corrosion of the Drip Shield and Waste Package and Stress Corrosion Cracking of the Waste Package (Continued)

TSPA_LA Parameter Name	Mathematical Model Symbol	Description	Units	Distribution Specification	Remarks
GC_ULevel_A22_a	None	Distribution for selecting the general corrosion rate CDF, based on a low, medium, or high level of epistemic uncertainty in the Weibull shape and scale parameters (GC_shape and GC_scale)	None	Discrete Distribution [0.05,1][0.9,2][0.05,3]	DTN: MO0703PAGECOR.001_R4, [DIRS 182029], file: BaseCase GC CDFs.xls
C1_GenCorr_A22_a	C1	Temperature dependence-slope term of WP general corrosion rate (epistemic uncertainty)	K	Normal (truncated at +2 SD and -3 SD) Mean = 4,905 SD = 1,413	DTN: MO0703PAGECOR.001_R4, file: BaseCase GC CDFs.xls [DIRS 182029]
Defect_Size_a	λ_s	Flaw size distribution parameter (epistemic uncertainty)	mm ⁻¹	Gamma Mean = n_f / S_f SD = $\sqrt{n_f} / S_f$	DTN: MO0701PASHIELD.000_R2, file: Tables for DTN Readme.doc [DIRS 180508]
Defect_Count_a	λ_c	Flaw count distribution parameter (epistemic uncertainty)	flaws/m m ³	Gamma Mean = $(n_f + 1/2) / V_f$ SD = $\sqrt{n_f + 1/2} / V_f$	DTN: MO0701PASHIELD.000_R2, file: Tables for DTN Readme.doc [DIRS 180508]
Z_OL_a	z	Uncertainty variation in the yield strength of the outer WP closure lid (epistemic uncertainty)	None	Normal (truncated at ± 3 SD) Mean = 0 SD = 1	DTN: MO0702PASTRESS.002_R2, file: Model Output DTN.doc, Table 8-15 [DIRS 180514]
n_SCC_a	n	Stress corrosion cracking growth rate exponent (repassivation rate) (epistemic uncertainty)	None	Normal (truncated at ± 2 SD) Mean = 1.165 SD = 0.115	DTN: MO0702PASTRESS.002_R2, file: Model Output DTN.doc, Table 8-15 [DIRS 180514]

Table 6.3.5-3. Uncertain Inputs to the TSPA-LA Model for Generalized Corrosion of the Drip Shield and Waste Package and Stress Corrosion Cracking of the Waste Package (Continued)

TSPA_LA Parameter Name	Mathematical Model Symbol	Description	Units	Distribution Specification	Remarks
Stress_Thresh_SCC_a	None	Stress threshold for SCC nucleation (epistemic uncertainty)	MPa	Uniform distribution from 315.9 to 368.55.	DTN: MO0702PASTRESS.002_R2, file: Model Output DTN.doc, Table 8-15 [DIRS 180514] This parameter combines the definition for Stress_Thresh_A22 with Yield_Strength_A22 defined in Table 8-15.
MIC_A22_a	f_{MIC}	MIC general corrosion enhancement factor (spatial variability)	None	Uniform Lower bound = 1 Upper bound = 2	DTN: MO0703PAGENCOR.001_R4, file: MIC Summary.pdf [DIRS 182029]
MIC_RHThresh_a	None	Relative humidity threshold for MIC (epistemic uncertainty)	None	Uniform distribution between 75% to 90%	DTN: MO0703PAGENCOR.001_R4, file: MIC Summary.pdf [DIRS 182029]

Table 6.3.5-4. Uncertain Inputs to Localized Corrosion Initiation Stand-Alone Model

TSPA_LA Parameter Name	Model Symbol	Description	Units	Distribution Specification	Remarks
Two_StDev_a0_a	None	Stochastic used to develop the coefficients in crevice repassivation potential functional form (epistemic uncertainty)	None	Normal Distribution Mean = 0 SD = 1	None
Two_StDev_a1_a					
Two_StDev_a2_a					
Two_StDev_a3_a					
Two_StDev_a4_a					
LC_eps_rcrev_a	None	Error term of crevice repassivation potential (epistemic uncertainty)	mV SSC	Normal distribution with a mean of zero and a standard deviation of 45.055	DTN: MO0703PAGENCOR.001_R4, file: Mathcad – Ercrev_Ecorr3.pdf, p. 5 [DIRS 182029]
Two_StDev_c0_a	None	Stochastic used to develop the coefficients in corrosion potential functional form (epistemic uncertainty)	None	Normal Distribution Mean = 0 SD = 1	None
Two_StDev_c1_a					
Two_StDev_c2_a					
Two_StDev_c3_a					
Two_StDev_c4_a					
Two_StDev_c5_a					
Two_StDev_c6_a					
LC_eps_corr_a	None	Error term of long-term corrosion potential model (epistemic uncertainty)	mV SSC	Normal distribution with a mean of zero and a standard deviation of 85.265	DTN: MO0703PAGENCOR.001_R4, file: Mathcad – Ercrev_Ecorr3.pdf, p. 8 [DIRS 182029]
LC_rate_a	None	Localized corrosion penetration rate (epistemic uncertainty)	mm/yr	Log uniform 0 percentile = 0.0127 50th percentile = 0.127 100th percentile = 1.27	DTN: MO0703PAGENCOR.001_R4, file: LC_Propagation.pdf [DIRS 182029]
Seepage_Water_Type_a	None	Seepage water type (epistemic uncertainty)	None	Discrete Uniform [0.25,1][0.25,2][0.25,3] [0.25,4]	SNL 2007 [DIRS 177412], Section 6.15.1

Table 6.3.5-4. Uncertain Inputs to Localized Corrosion Initiation Stand-Alone Model (Continued)

TSPA LA Parameter Name	Model Symbol	Description	Units	Distribution Specification	Remarks
PCE_Delta_PCO2_a	None	Uncertainty in the partial pressure of CO ₂ (epistemic uncertainty)	None	Uniform distribution from -1 to 1.	SNL 2007 [DIRS 177412], Section 6.15.1
PCE_CI_MU_RH_0_20_a	None	Uncertainty in log chloride ion concentration (epistemic uncertainty)	None	Triangular Distribution Minimum: -0.7 Most Likely: 0.0 Maximum: 0.7	DTN: SN0703PAEBSPCE.007_R2, file: PCE_IDPS_uncertainties.xls [DIRS 184141]
PCE_CI_MU_RH_20_40_a	None	Uncertainty in log chloride ion concentration (epistemic uncertainty)	None	Triangular Distribution Minimum: -0.5 Most Likely: 0.0 Maximum: 0.5	DTN: SN0703PAEBSPCE.007_R2, file: PCE_IDPS_uncertainties.xls [DIRS 184141]
PCE_CI_MU_RH_40_65_a	None	Uncertainty in log chloride ion concentration (epistemic uncertainty)	None	Triangular Distribution Minimum: -0.4 Most Likely: 0.0 Maximum: 0.4	DTN: SN0703PAEBSPCE.007_R2, file: PCE_IDPS_uncertainties.xls [DIRS 184141]
PCE_CI_MU_RH_65_85_a	None	Uncertainty in log chloride ion concentration (epistemic uncertainty)	None	Triangular Distribution Minimum: -0.1 Most Likely: 0.0 Maximum: 0.1	DTN: SN0703PAEBSPCE.007_R2, file: PCE_IDPS_uncertainties.xls [DIRS 184141]
PCE_CI_MU_RH_85_100_a	None	Uncertainty in log chloride ion concentration (epistemic uncertainty)	None	Triangular Distribution Minimum: -0.0 Most Likely: 0.0 Maximum: 0.0	DTN: SN0703PAEBSPCE.007_R2, file: PCE_IDPS_uncertainties.xls [DIRS 184141]
PCE_CI_N_MU_RH_40_65_a	None	Uncertainty in log chloride plus nitrate ion concentration (epistemic uncertainty)	None	Triangular Distribution Minimum: -0.57 Most Likely: 0.0 Maximum: 0.57	DTN: SN0703PAEBSPCE.007_R2, file: PCE_IDPS_uncertainties.xls [DIRS 184141]

Table 6.3.5-4. Uncertain Inputs to Localized Corrosion Initiation Stand-Alone Model (Continued)

TSPA_LA Parameter Name	Model Symbol	Description	Units	Distribution Specification	Remarks
PCE_CI_N_MU_RH_65_85_a	None	Uncertainty in log chloride plus nitrate ion concentration (epistemic uncertainty)	None	Triangular Distribution Minimum: -0.22 Most Likely: 0.0 Maximum: 0.22	DTN: SN0703PAEBSPCE.007_R2, file: PCE_IDPS_uncertainties.xls [DIRS 184141]
PCE_CI_N_MU_RH_85_100_a	None	Uncertainty in log chloride plus nitrate ion concentration (epistemic uncertainty)	None	Triangular Distribution Minimum: -0.0 Most Likely: 0.0 Maximum: 0.0	DTN: SN0703PAEBSPCE.007_R2, file: PCE_IDPS_uncertainties.xls [DIRS 184141]
PCE_CI_NO3_MU_RH_0_20_a	None	Uncertainty in log chloride-to-nitrate ion concentration (epistemic uncertainty)	None	Triangular Distribution Minimum: -1.4 Most Likely: 0.0 Maximum: 1.4	DTN: SN0703PAEBSPCE.007_R2, file: PCE_IDPS_uncertainties.xls [DIRS 184141]
PCE_CI_NO3_MU_RH_20_65_a	None	Uncertainty in log chloride-to-nitrate ion concentration (epistemic uncertainty)	None	Triangular Distribution Minimum: -0.5 Most Likely: 0.0 Maximum: 0.5	DTN: SN0703PAEBSPCE.007_R2, file: PCE_IDPS_uncertainties.xls [DIRS 184141]
PCE_CI_NO3_MU_RH_65_85_a	None	Uncertainty in log chloride-to-nitrate ion concentration (epistemic uncertainty)	None	Triangular Distribution Minimum: -0.2 Most Likely: 0.0 Maximum: 0.2	DTN: SN0703PAEBSPCE.007_R2, file: PCE_IDPS_uncertainties.xls [DIRS184141]
PCE_CI_NO3_MU_RH_85_100_a	None	Uncertainty in log chloride-to-nitrate ion concentration (epistemic uncertainty)	None	Triangular Distribution Minimum: -0.0 Most Likely: 0.0 Maximum: 0.0	DTN: SN0703PAEBSPCE.007_R2, file: PCE_IDPS_uncertainties.xls [DIRS184141]
PCE_pH_Uncert_RH_0_65_a	v	Uncertainty in pH (epistemic uncertainty).	None	Triangular Distribution Minimum: -2.0 Most Likely: 0.0 Maximum: 2.0	DTN: SN0703PAEBSPCE.007_R2, file: PCE_IDPS_uncertainties.xls [DIRS 184141]

Table 6.3.5-4. Uncertain Inputs to Localized Corrosion Initiation Stand-Alone Model (Continued)

TSPA_LA Parameter Name	Model Symbol	Description	Units	Distribution Specification	Remarks
PCE_pH_Uncert_RH_65_75_a	None	Uncertainty in pH (epistemic uncertainty)	None	Triangular Distribution Minimum: -1.0 Most Likely: 0.0 Maximum: 1.0	DTN: SN0703PAEBSPCE.007_R2, file: PCE_IDPS_uncertainties.xls [DIRS184141]
PCE_pH_Uncert_RH_75_100_a	None	Uncertainty in pH (epistemic uncertainty)	None	Discrete Distribution	DTN: SN0703PAEBSPCE.007_R2, file: Re-evaluation of pH uncertainty.xls, Tab: CDF of pH uncertainty (5 decimal digits) [DIRS184141]
Seepage_Uncertainty_a	None	Epistemic uncertainty in seepage scale factor	None	Uniform (0,1) Note that the sampled value from the distribution is converted to a uniform distribution between -1.7321 and 1.7321 in the SEEPAGEDLL_LA V1.3 software (STN: 11076-1.3-00 [DIRS 180318]; STN: 11076-1.3-01 [DIRS 181058]).	DTN: LB0407AMRU0120.001_R0, file: Summary_seepage_abstraction.doc [DIRS 173280]
Alpha_Uncert_Lith_a	$1/\alpha$	Epistemic uncertainty in capillary strength in lithophysal units	Pa	Triangular Mode = 0 Min = -105 Max = 105	DTN: LB0407AMRU0120.001_R0, file Summary_seepage_abstraction.doc [DIRS 173280]
Alpha_Uncert_NonLith_a	$1/\alpha$	Epistemic uncertainty in capillary strength in non-lithophysal units	Pa	Triangular Mode = 0 Min. = -105 Max. = 105	DTN: LB0407AMRU0120.001_R0, file: Summary_seepage_abstraction.doc [DIRS 173280]

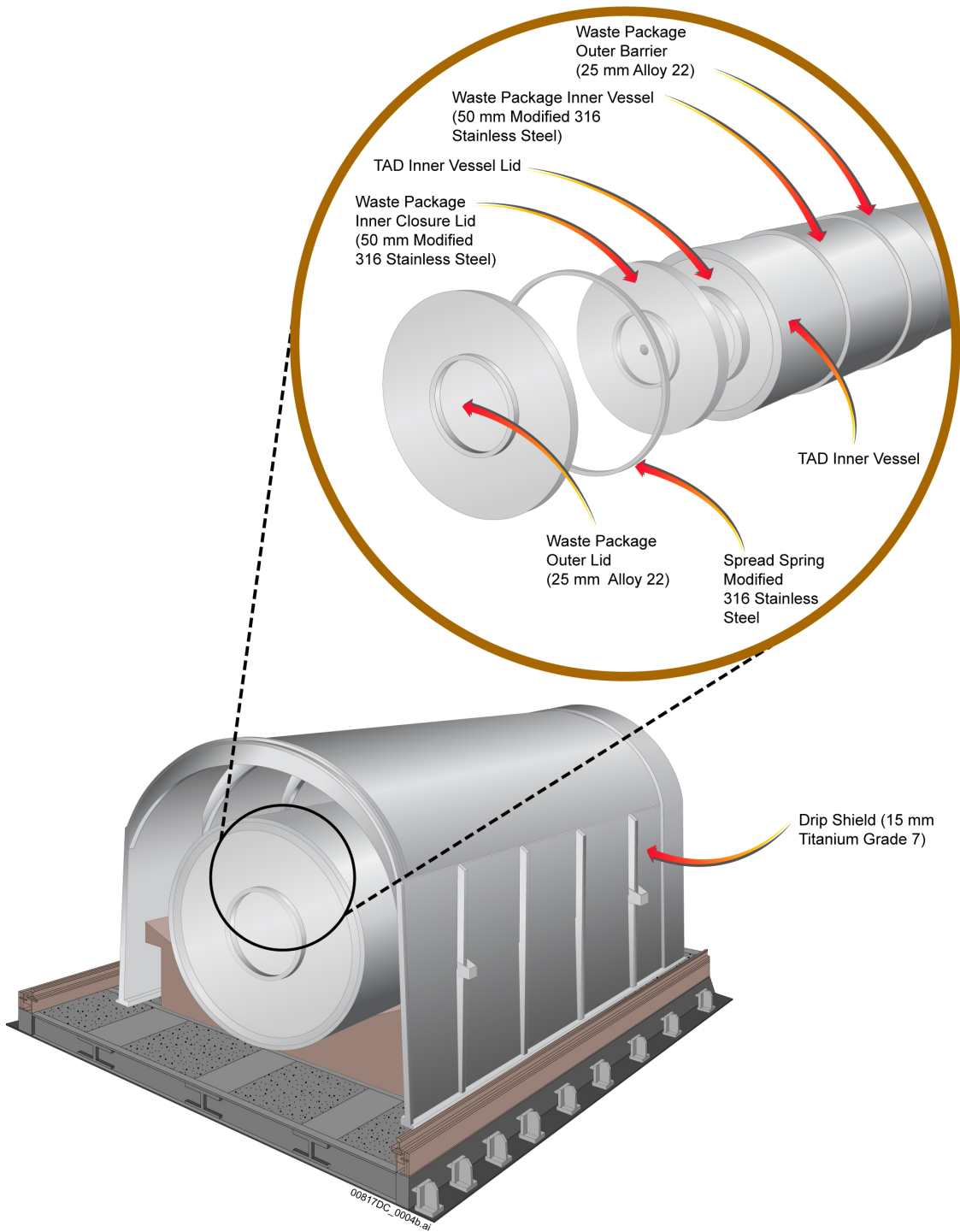
Table 6.3.5-4. Uncertain Inputs to Localized Corrosion Initiation Stand-Alone Model (Continued)

TSPA_LA Parameter Name	Model Symbol	Description	Units	Distribution Specification	Remarks
LogK_Uncert_Lith_a	$\log k$	Epistemic uncertainty in fracture permeability in lithophysal units	log m ²	Triangular Mode = 0 Min. = -0.92 Max. = 0.92	DTN: LB0407AMRU0120.001_R0, file: Summary_seepage_abstraction .doc [DIRS 173280]
LogK_Uncert_NonLith_a	$\log k$	Epistemic uncertainty in fracture permeability in non-lithophysal units	log m ²	Triangular Mode = 0 Min. = -0.68 Max. = 0.68	DTN: LB0407AMRU0120.001_R0, file: Summary_seepage_abstraction .doc [DIRS 173280]
dt_dRh_uncertainty	None	Epistemic uncertainty in the thermal conductivity of the rubble resulting from a seismic event	None	Discrete [0.5,1][0.5, 2]	DTN: MO0505SPAROCKM.000_R0 [DIRS 173893]
Infiltration_Scenario_a	None	Uncertainty in infiltration scenario (10th, 30th, 50th, and 90th percentile) (epistemic uncertainty)	None	Discrete [0.6191,1][0.1568,2][0.1645,3][0.0596,4]	DTN: LB0701PAWFINFM.001_R0, file: factors.doc [DIRS 179283]
Thermal_Conductivity_Uncert_a	None	Uncertainty in thermal conductivity (low, medium, or high) (epistemic uncertainty)	None	Discrete (p. v) [0.29,1], [0.37,2], [0.34,3]	SNL 2007 [DIRS 181383], Table 6.3-47[a]
Vol_Rubble_Max_Lith_a	$V_{rubble_max}^{Lith}$	Volume of lithophysal rock that must fall to fill the drift (epistemic uncertainty)	m ³ /m	Uniform (30,120)	DTN: MO0703PASEISDA.002_R4, Table 1-16 [DIRS 183156]
Vol_Rubble_Max_NonLith_a	$V_{rubble_max}^{NonLith}$	Volume of nonlithophysal rock that must fall to fill the drift (epistemic uncertainty)	m ³ /m	Uniform (30,120)	DTN: MO0703PASEISDA.002_R4, Table 1-16 [DIRS 183156]

Table 6.3.5-4. Uncertain Inputs to Localized Corrosion Initiation Stand-Alone Model (Continued)

TSPA_LA Parameter Name	Model Symbol	Description	Units	Distribution Specification	Remarks
WDDSBenignGC_Mean_a	None	DS-underside general corrosion rate(epistemic uncertainty)	nm/yr	Normal Mean = 5.15 SD = 0.831	DTN: SN0704PADSGCMT.001_R2, file: TSPA Implementation_DS GC Models.pdf [DIRS 182122]
WDDSAggrGC_Mean_a	None	DS-topside general corrosion rate (epistemic uncertainty)	nm/yr	Normal Mean = 46.1 SD = 1.19	DTN: SN0704PADSGCMT.001_R2, file: TSPA Implementation_DS GC Models.pdf [DIRS 182122]
C1_GenCorr_A22_a	C ₁	Temperature dependent-slope term for general corrosion rate (epistemic uncertainty)	K	Normal (truncated at -3 SD and +2 SD) Mean = 4,905 SD = 1,413	DTN: MO0703PAGENCOR.001_R4, file: BaseCase GC CDFs.xls [DIRS 182029]
MIC_A22_a	f_{MIC}	MIC general corrosion enhancement factor (spatial variability)	None	Uniform(1,2)	DTN: MO0703PAGENCOR.001_R4, file: MIC Summary.pdf [DIRS 182029]
MIC_RHThresh_a	None	Relative humidity threshold for MIC (epistemic uncertainty)	None	Uniform(75%,90%)	DTN: MO0703PAGENCOR.001_R4, file: MIC Summary.pdf [DIRS 182029]
lnR0_a	ln R _o	Rate used to calculate the first general corrosion penetration for the calculations in the Localized Corrosion Stand-Alone Model, based on the medium distribution for uncertainty in the Weibull scale and shape parameters (spatial variability)	nm/yr	Weibull scale = 8.134 nm/yr shape = 1.476 Scaled by the average coupon rate with a size factor of 4	Developed by TSPA from GC_scale and GC_Shape parameters in DTN: MO0703PAGENCOR.001_R4 , file: BaseCase GC CDFs.xls [DIRS 182029] Output DTN: MO0707WPDRIPSD.000 [DIRS 183005]

INTENTIONALLY LEFT BLANK



Sources: SNL 2007 [DIRS 179394] and [DIRS 179354].

Figure 6.3.5-1. Schematic Design of the Drip Shield and Waste Package

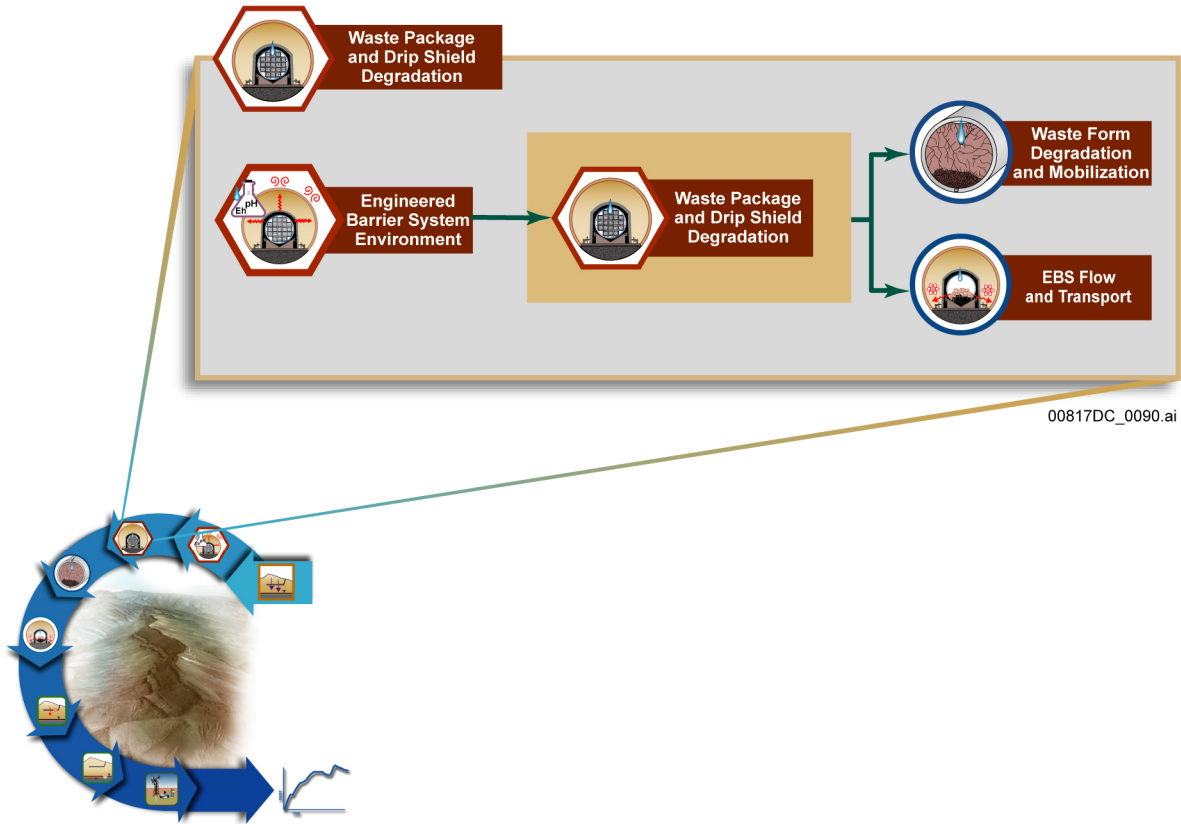


Figure 6.3.5-2. Information Flow Diagram for Waste Package and Drip Shield Degradation

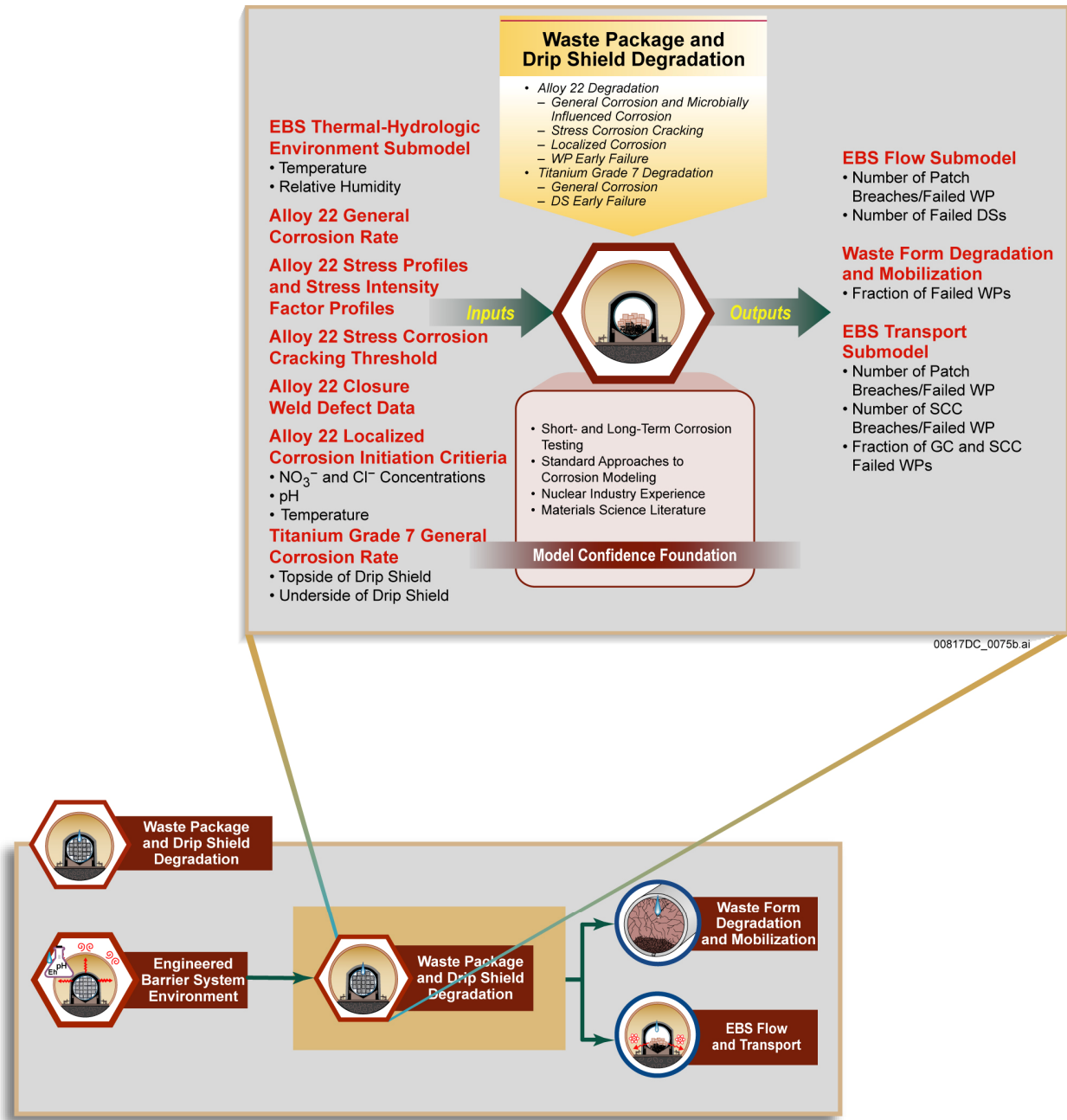
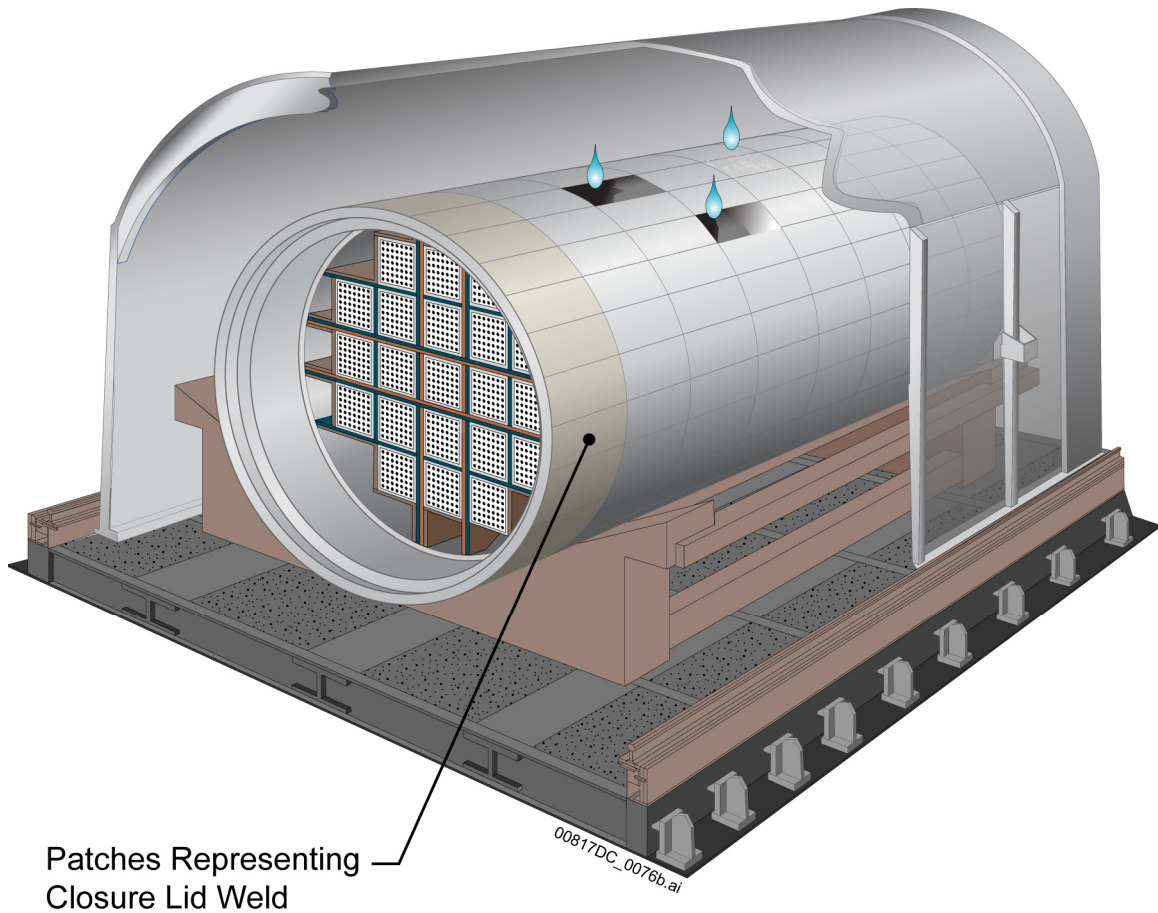


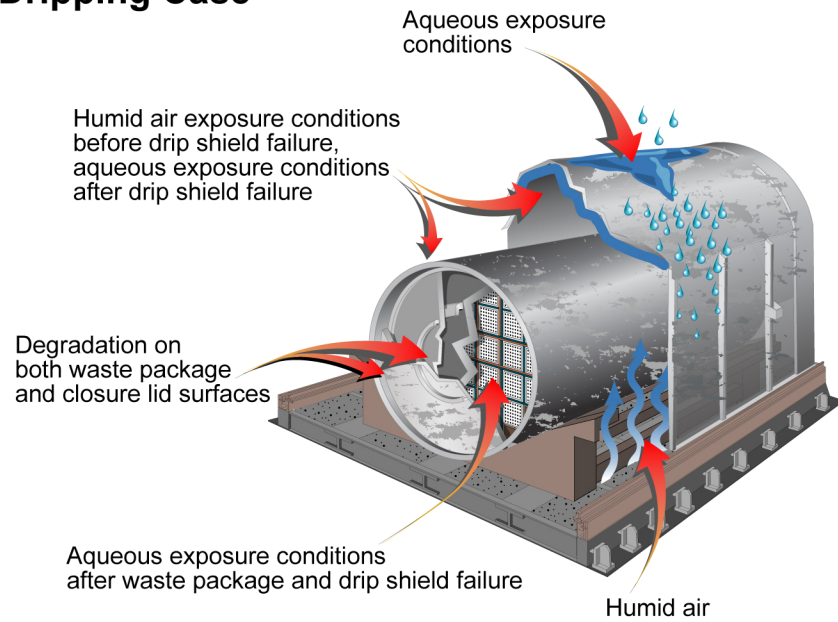
Figure 6.3.5-3. Inputs, Outputs, and Basis for Model Confidence for the Waste Package and Drip Shield Degradation Submodel



NOTE: Figure is for illustration purposes only and is not representative of repository postclosure performance.

Figure 6.3.5-4. Schematic of Waste Package Implementation in the Waste Package Degradation Model Showing a Waste Package in a Dripping Environment After a Drip Shield Failure and Patches Degrading from General Corrosion on the Surface of the Waste Package

Dripping Case



Non-Dripping Case

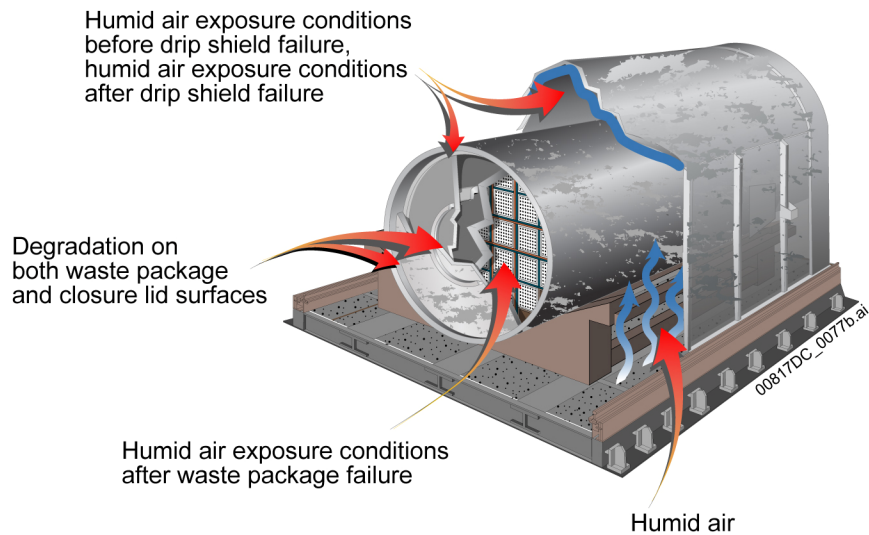
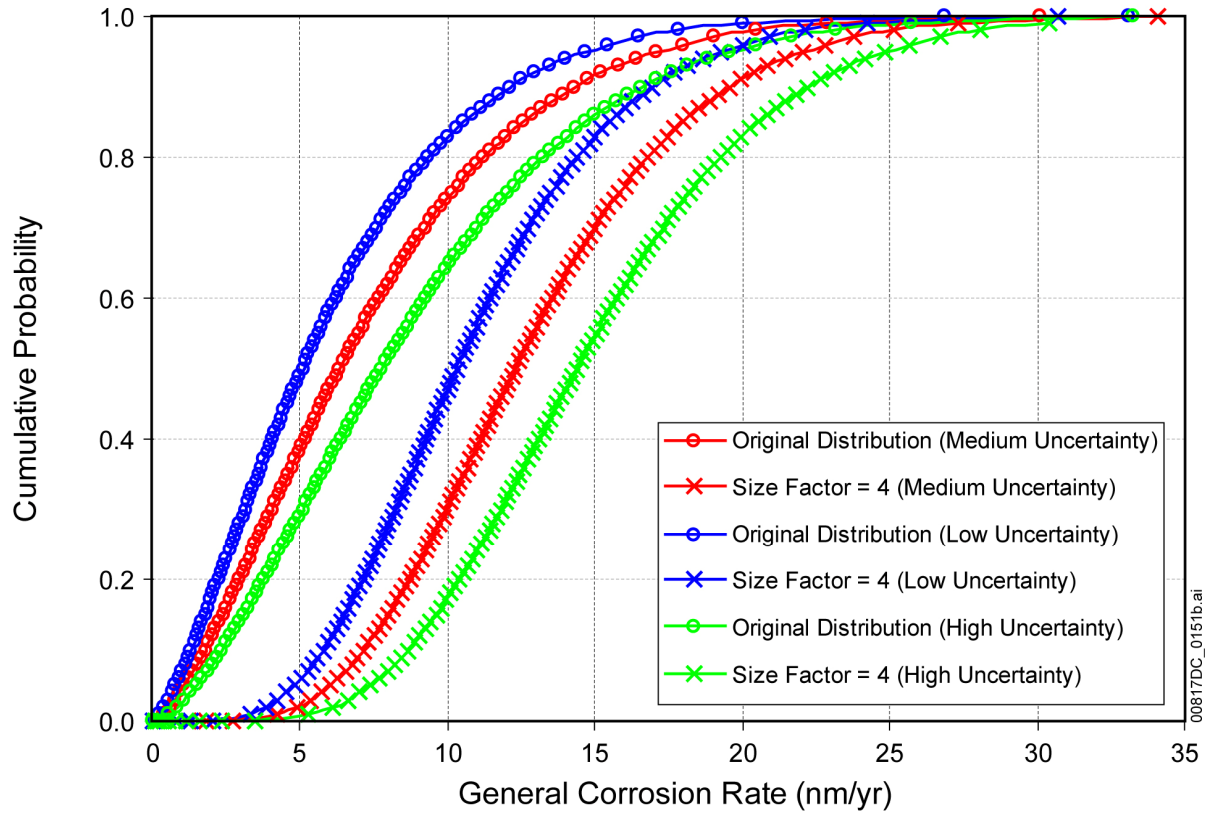


Figure 6.3.5-5. Exposure Conditions and Degradation Processes for the Drip Shield and Waste Package



Source: Output DTN: MO0707WPDRIPSD.000 [DIRS 183005].

Figure 6.3.5-6. Effect of Scaling the General Corrosion Distribution by a Size Factor of Four

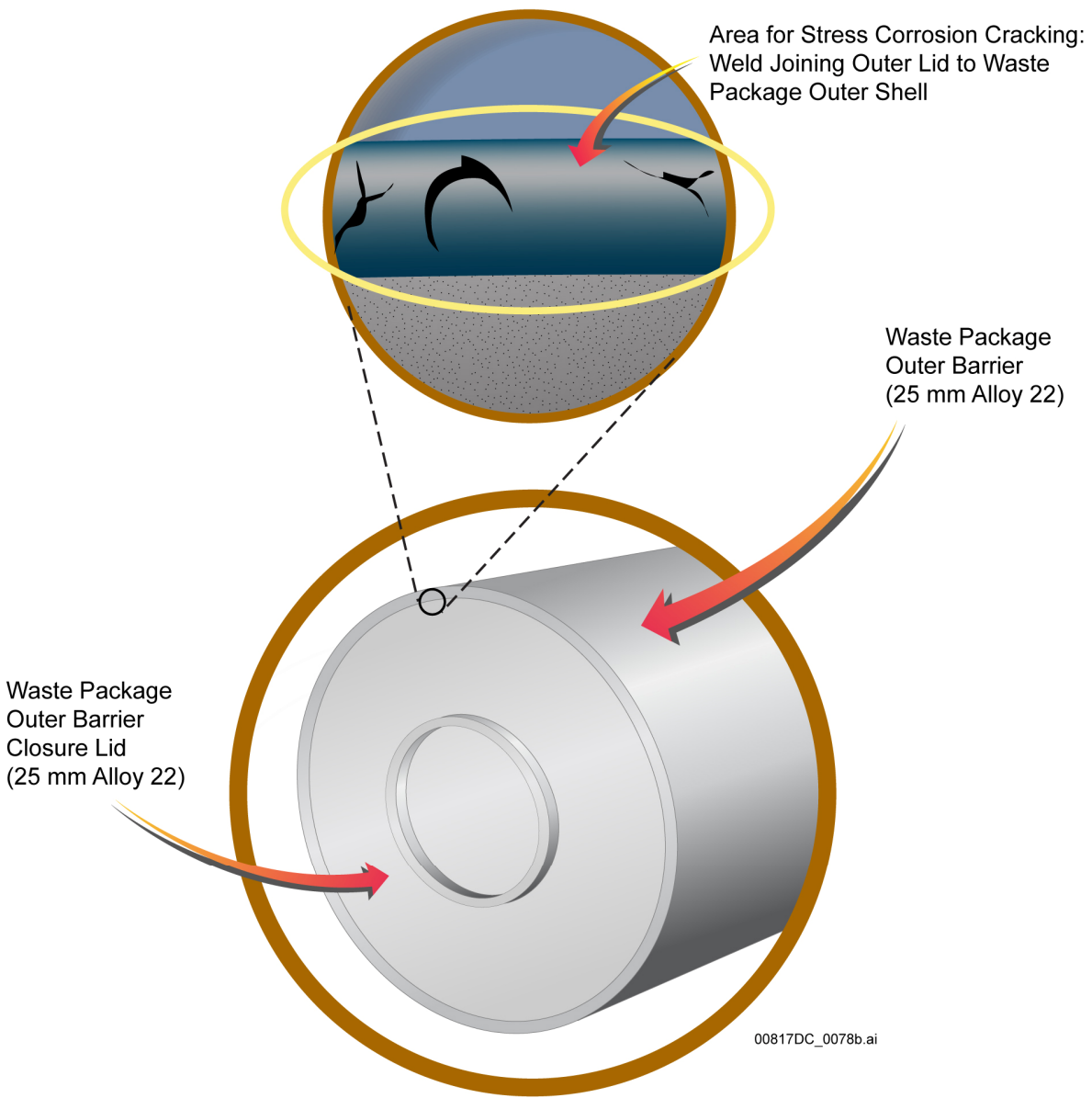


Figure 6.3.5-7. Schematic of Waste Package Closure Lid Design

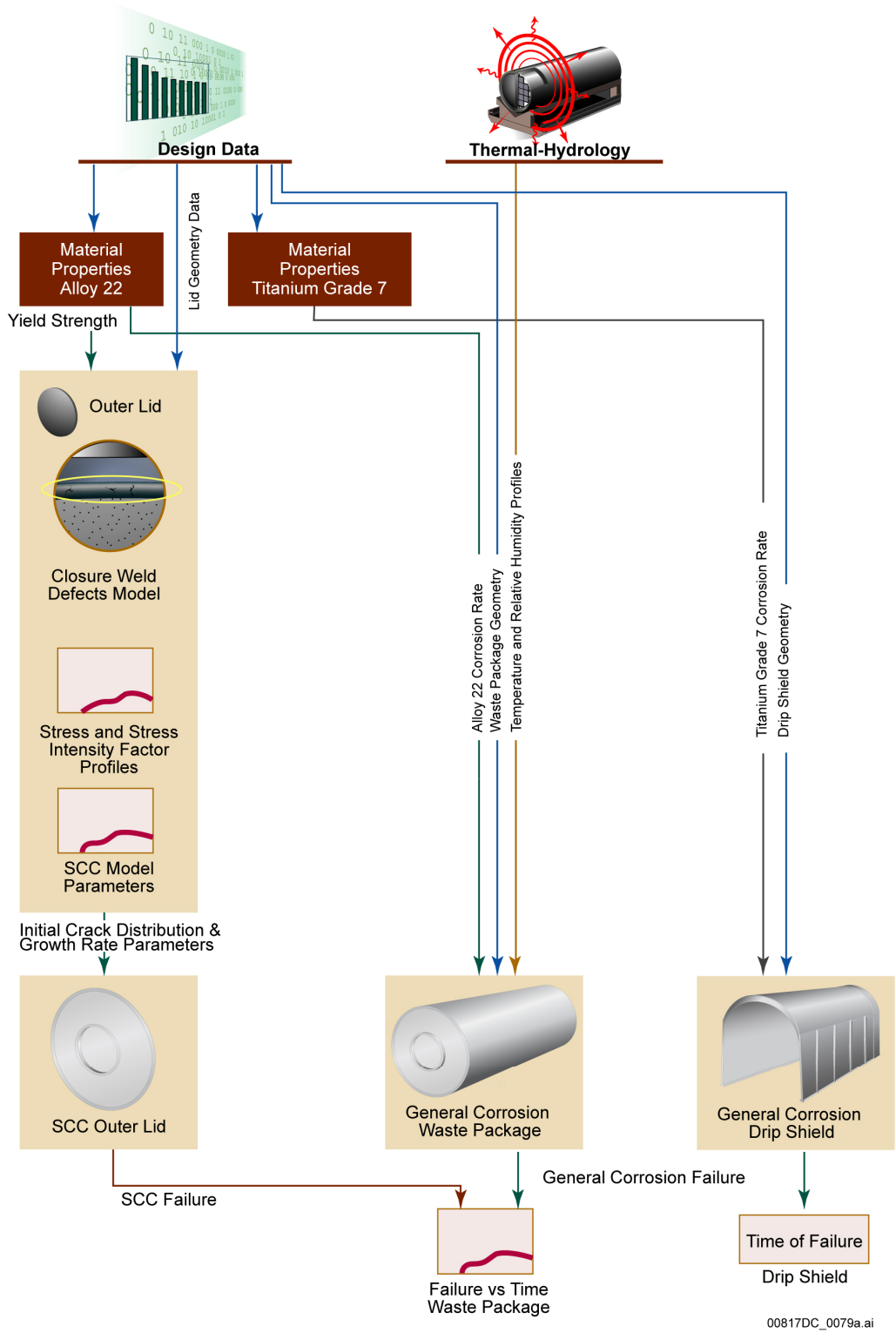
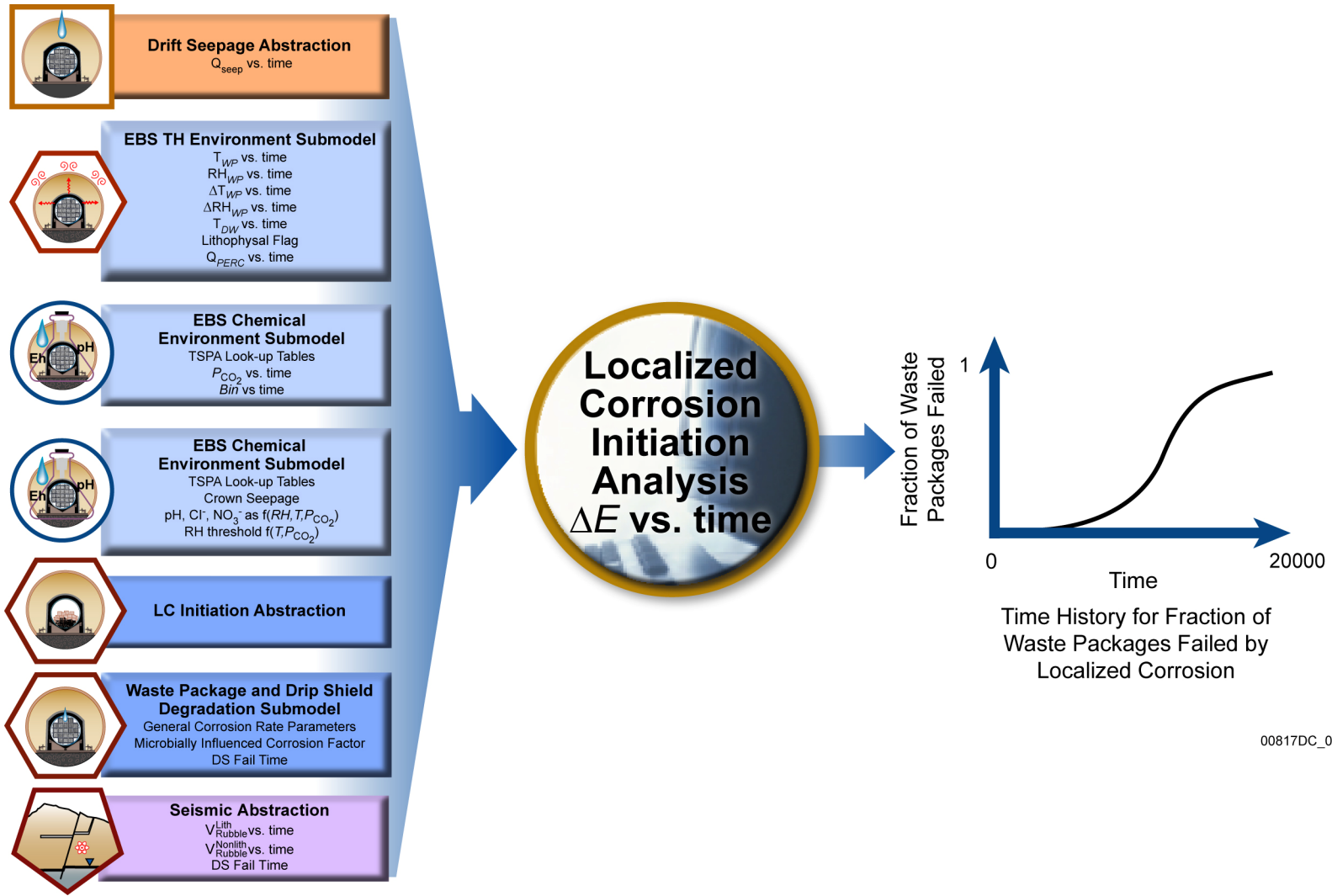


Figure 6.3.5-8. Process and Data Flow for the Waste Package and Drip Shield Degradation Model Component



00817DC_0062.ai

Figure 6.3.5-9. Integration of Submodels for Localized Corrosion Initiation Analysis

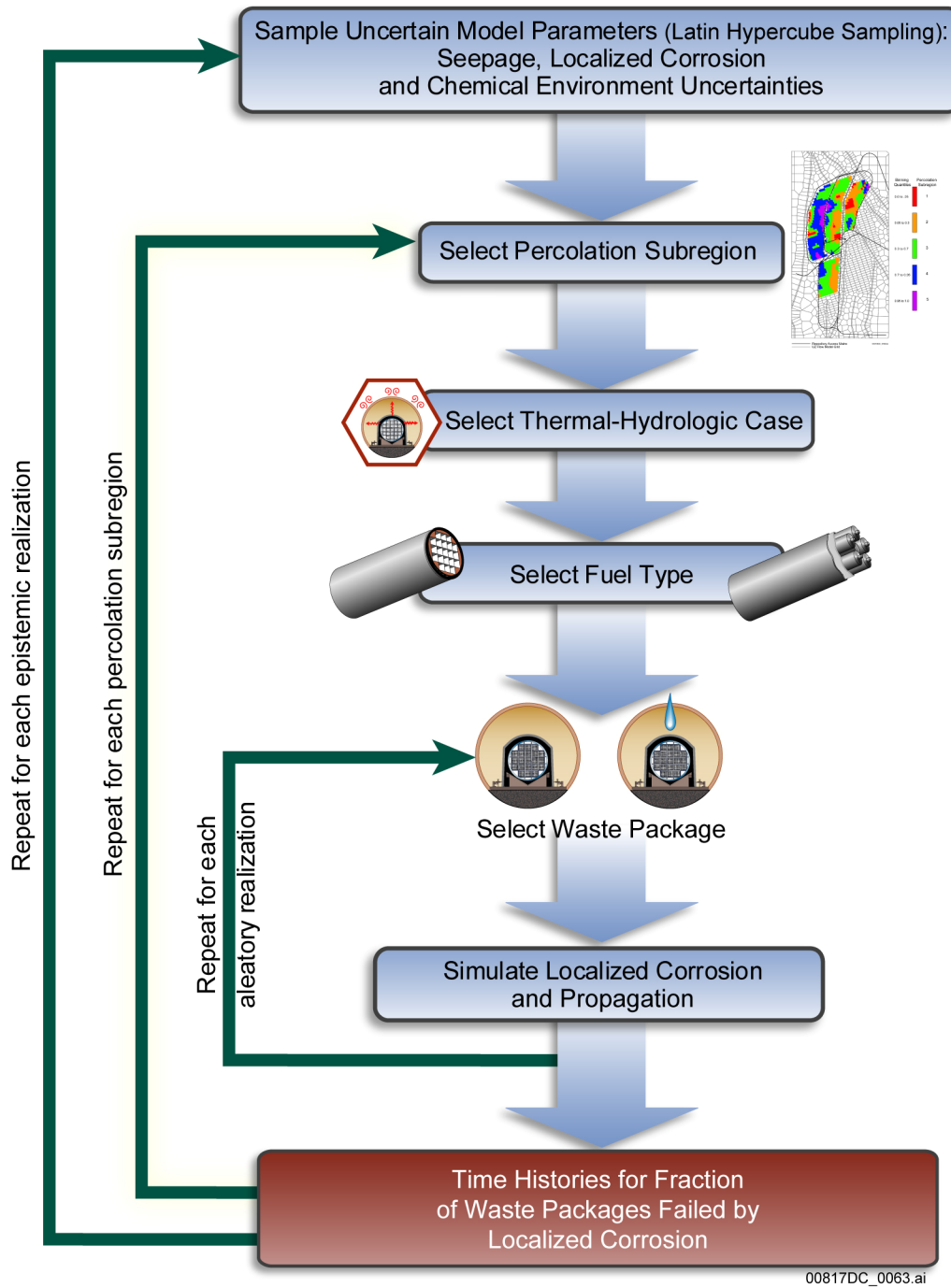


Figure 6.3.5-10. Computational Organization of Localized Corrosion Initiation Analysis for Crown Seepage

6.3.6 Engineered Barrier System Flow

The EBS Flow Submodel implemented in the TSPA-LA Model is described in *EBS Radionuclide Transport Abstraction* (SNL 2007 [DIRS 177407]). The EBS Flow Submodel defines the pathways for water flow in the EBS and specifies how the volumetric flow rate is computed for each pathway. Pathway flow rates are used as inputs to the TSPA-LA EBS Transport Submodel. The primary water inputs are the drift-seepage flow rate (SNL 2007 [DIRS 181244], Section 8.2[a]) and the drift wall condensation flow rate (SNL 2007 [DIRS 181648], Sections 8.1[a] and 8.2[a]). Drift seepage and drift wall condensation are further described in Sections 6.3.3.1 and 6.3.3.2, respectively. These two flow rates are combined in the EBS Flow Submodel to yield a total dripping flow rate. The type, number, and timing of breaches in the WPs and DSs are also inputs to the EBS Flow Submodel and are provided by the WP and DS Degradation Model Component (Section 6.3.5). An additional source of inflow to the EBS is imbibition into the invert crushed tuff from the surrounding UZ rock matrix (SNL 2007 [DIRS 177407], Section 6.3.1.1). The EBS TH Environment Submodel provides this input and calls it the liquid flow in the invert. Information flow between the EBS Flow Submodel and other TSPA-LA Model components and submodels is shown on Figure 6.3.6-1. Figure 6.3.6-2 presents an overview of the inputs, outputs, and foundation for confidence in the EBS Flow Submodel as implemented in the TSPA-LA Model.

6.3.6.1 Conceptual Model

Water is the principal medium for transport of radionuclides through the EBS (SNL 2007 [DIRS 177407], Section 6.1.1). Water, whether present as thin films or bulk stationary or flowing liquid, is necessary for radionuclides to be transported out of the WPs and through the invert to the UZ. Water flow through the EBS will be dependent on a series of processes in the repository. After the WPs are emplaced, radioactive decay of the waste will heat the drifts and locally perturb the normal percolation of water through the mountain. As the drifts cool, some of the water percolating through the mountain may drip into the drifts and subsequently contact some of the DSs. In addition, water that evaporates within the emplacement drifts may condense in cooler regions of the emplacement drifts and drip on DSs in these regions. Over time, the DSs, WPs, and other components of the EBS may degrade, allowing water as dripping or as liquid films to contact the waste forms, resulting in the mobilization and transport of radionuclides through the EBS to the UZ.

The design configuration of the EBS is shown on Figure 6.3.6-3. The drifts will be 5.5 m in diameter (SNL 2007 [DIRS 179354], Section 4.1.1 and Table 4-1). The lower portion of the drifts, commonly referred to as the invert, will be filled with crushed tuff (SNL 2007 [DIRS 179354], Table 4-1). The WPs will be placed on emplacement pallets set on the invert. Titanium DSs will be placed over the WPs and set on the invert.

The primary water input to the EBS will be the total flow rate from two sources: (1) seepage volumetric flow rate into the drifts provided by the Drift Seepage Submodel (Section 6.3.3.1), and (2) condensation volumetric flow rate on the drift walls provided by the Drift Wall Condensation Submodel (Section 6.3.3.2). A secondary source of inflow to the EBS is imbibition into the invert from the surrounding UZ rock matrix. Water from these sources flows

through the EBS along eight pathways, shown on Figure 6.3.6-4 and listed below (SNL 2007 [DIRS 177407], Sections 6.3.2 and 6.3.3).

1. **Seepage and Drift-Wall Condensation**—This is the dripping water flow from the crown (roof) of the drift. Drift seepage and any condensation that may occur on the wall of the drift on the section above the DS are included in the term dripping.
2. **Flow through the DSs**—The flow rate through the DSs is dependent on whether the DS is present. DS failure occurs due to general corrosion (SNL 2007 [DIRS 180778]), which is modeled as occurring uniformly on the DS surface. Stress corrosion cracks may occur, but advection of liquid water through stress corrosion cracks is excluded due to plugging (SNL 2007 [DIRS 181953], Sections 6.8.6 and 8.1.6, and DTN: MO0706SPAFEPLA.001_R0 [DIRS 181613], FEP 2.1.03.10.0B).
3. **Diversion around the DSs**—The dripping flows through the invert that bypasses the WP due to an intact DS.
4. **Flow through the WPs**—Three general types of openings can exist in the WPs due to corrosion: (1) stress corrosion cracks resulting from residual stress or seismic ground motion, (2) breaches resulting from general corrosion, and (3) breaches resulting from localized corrosion. The flow rate through the WPs is based on the presence of breaches due to general corrosion patches and localized corrosion. Localized corrosion is further discussed in Section 6.3.5. Stress corrosion cracks may occur, but advection of liquid water through stress corrosion cracks in the WPs is excluded for the following reasons (DTN: MO0706SPAFEPLA.001_R0 [DIRS 181613], FEP Number 2.1.03.10.0A): (1) capillary behavior allows water to reside indefinitely within the crack without flow, (2) surface tension opposes hydraulic pressure that may be present at the outlet, and (3) stress corrosion cracks are tight, rough, and tortuous, which limits the transient response to dripping water. Flow through the WPs is based on the presence of continuous flow paths through the patches that penetrate the WPs. In addition, vertical flow of dripping into the WPs, through the waste form, and out of the WPs is modeled as not affected by the location of patches on the surface of the WPs. Evaporation from the WP is ignored, as discussed further in Section 6.3.6.4.1.
5. **Diversion around the WPs**—The portion of the dripping water that does not flow into the WPs bypasses the waste forms and flows directly to the invert.
6. **Flow into the Invert**—All water flow from the WPs is modeled as flowing into the invert. All flow from the WPs flows to the invert, independent of breach location on the WPs. In addition, the dripping water that is diverted around the WPs and DSs flows into the invert. The presence of the emplacement pallets is ignored in the abstraction of EBS flow, and the WPs are modeled as being in intimate contact with the invert (SNL 2007 [DIRS 177407], Section 6.3.1.1). Thus, the flow leaving the WPs flows directly into the invert, with no resistance offered by the pallets.

7. **Imbibition Flow to the Invert**—Water can be imbibed from the host-rock matrix into the invert. The EBS TH Environment Submodel provides the rate of water imbibition into the invert from the host rock, which it calls the liquid flow in the invert.
8. **Flow from the Invert to the UZ**—The flow from the invert to the UZ is split so that a portion goes into the UZ fractures and a portion goes into the UZ matrix. The portion of the advective flow from the invert equal to the total dripping flow (F_1) flows directly into the UZ fractures. The portion of the advective flow from the invert equal to the imbibition flow to the invert (F_7) flows into the UZ matrix.

These pathways are time-dependent in the sense that total dripping flow, DS failures, and WP breaches will vary with time and percolation subregions. These pathways are further described in Section 6.3.6.2.

6.3.6.2 Abstraction

Figure 6.3.6-4 and Table 6.3.6-1 show that the flow through the EBS can be described by quantifying the flow rates at various flow pathways within the TSPA-LA Model. The EBS flow calculations are repeated in every percolation subregion for each WP type (CSNF WPs and CDSP WPs). Using F to indicate the flow rate at the numbered points on Figure 6.3.6-4, observe that

- F_1 = seepage from the drift crown and drift-wall condensation dripping onto the DS (i.e., dripping flow)
- F_2 = flow through the DS
- F_3 = dripping flow diverted around the DS to the invert
- F_4 = flow through the WP
- F_5 = dripping flow diverted around the WP to the invert
- F_6 = flow into the invert from flow through the WPs and dripping flow diverted around WP and DS
- F_7 = imbibition flow between the host rock and the invert
- F_8 = flow from the invert to the UZ.

The flow rates within the EBS are calculated based on pseudo steady state flow conditions. The primary input to the EBS Flow Submodel is the total dripping flow, F_1 , and imbibition from host rock to the invert, F_7 . Drift seepage and any condensation that may occur on the wall of the drift are included in this total quantity of dripping water, F_1 . Effects of evaporation are ignored in order to maximize drift seepage, drift wall condensation and, consequently, advective releases of radionuclides. The calculation for various flow pathways in the EBS is described as follows:

The dripping flow diverted around the DS is

$$F_3 = F_1 - F_2 \quad (\text{Eq. 6.3.6-1})$$

The dripping flow diverted around the WP is

$$F_5 = F_2 - F_4 \quad (\text{Eq. 6.3.6-2})$$

The flow entering the invert due to seepage and condensation is

$$F_6 = F_1 = F_3 + F_4 + F_5 \quad (\text{Eq. 6.3.6-3})$$

The flow exiting the invert is

$$F_8 = F_6 + F_7 = F_1 + F_7 \quad (\text{Eq. 6.3.6-4})$$

The result of flow splitting of the dripping flow at the DS, F_2 , and at the WP, F_4 , determines all flow within the EBS. The flow through the DSs is a result of the DS flow splitting logic presented in *EBS Radionuclide Transport Abstraction* (SNL 2007 [DIRS 177407], Section 6.3.2.4) as

$$F_2 = \min \left[F_1 \frac{N_{pDS} l_{DS}}{L_{DS}} f'_{DS}, F_1 \right] \quad (\text{Eq. 6.3.6-5})$$

where

F_1 = seepage + condensation

N_{pDS} = number of DS general corrosion patches (Note that in the TSPA-LA Model, when the DS fails by general corrosion, the entire DS is modeled as having failed at once, and $N_{pDS} = 1$.)

l_{DS} = axial half-length of DS general corrosion patch

L_{DS} = axial length of DS

f'_{DS} = uncertainty factor (Table 6.3.6-2).

Flow through the WPs is a result of the WP flow splitting logic presented in *EBS Radionuclide Transport Abstraction* (SNL 2007 [DIRS 177407], Section 6.3.3.2), and is described as follows:

$$F_4 = \min \left[F_2 \frac{N_{pWP} l_{WP}}{L_{WP}} f'_{WP}, F_2 \right] \quad (\text{Eq. 6.3.6-6})$$

where

F_2 = flow through a DS

N_{pWP} = number of general corrosion patches on failed WP

l_{WP} = axial half-length of general corrosion patch on failed WP

L_{WP} = axial length of WP

f'_{WP} = WP uncertainty factor (Table 6.3.6-2).

The number of general corrosion patches on a failed WP, N_{pWP} , is the time-dependent parameter that controls the fraction of impinging flow that can enter and flow through the WPs. N_{pWP} can vary from zero to the maximum number of patches, depending on the modeling case. N_{pWP} increases with time due to general corrosion in the Seismic GM and Nominal Modeling Cases. N_{pWP} is set to the maximum value in the Igneous Intrusion, Waste Package EF, and Drip Shield EF Modeling Cases. In the Seismic FD Modeling Case, N_{pWP} is based on the number of patches equivalent to the WP damaged area caused by faulting. N_{pWP} is set to a value corresponding to a single drill hole in the Human Intrusion Modeling Case. Because the flow splitting model described by Equation 6.3.6-6 is based on the fractional opening length along the crown of the WP, rather than the fractional opening area over the entire WP, the flow splitting fraction reaches 1 (i.e., all the impinging flow can enter a WP) well before N_{pWP} reaches its maximum. For the mean value of the WP flux uncertainty term, f'_{WP} , equal to 1.2, only about 62 general corrosion patches are required on a CSNF WP to allow 100 percent of the impinging flow to enter a WP. This is about 4 percent of the area of the WP (excluding the lids). The EBS Flow Submodel in the TSPA-LA Model is summarized in Table 6.3.6-1.

Uncertainty in the EBS Flow Submodel—The EBS Flow Submodel uses one uncertain (epistemic) flow splitting parameter to characterize the fraction of flow that enters breaches in the DSs and one uncertain (epistemic) flow splitting parameter to characterize the fraction of flow that enters breaches in the WPs. Each parameter is sampled once per realization and applied to all representative WP locations in a dripping environment. Table 6.3.6-2 provides the distribution type and ranges for these two parameters.

6.3.6.3 TSPA-LA Implementation

The EBS flow calculation consists of two parts in the TSPA-LA Model. The first part of the EBS flow calculation combines the drift seepage and drift-wall condensation flows to determine the total dripping rate onto the DS and into the invert. The second part calculates the flow through the failed WPs and DSs using the flow splitting logic presented in Equation 6.3.6-5 and Equation 6.3.6-6.

Dripping Flow Calculations—The EBS Flow Submodel calculates the dripping flow into the drift. The EBS Flow Submodel receives feeds (inputs) (Figure 6.3.6-2) from the Drift Seepage

Submodel and the Drift Wall Condensation Submodel. The seepage fraction and seepage rate from the Drift Seepage Submodel is passed to the EBS Flow Model. The seepage fraction determines the number of WPs placed in seep and non-seep environments in each percolation subregion. A single element in the model then adds the seepage rate and the drift-wall condensation rate to produce the total dripping rate onto the DS and into the invert for WPs in a seep environment. For a non-seep environment, only the drift-wall condensation rate is used.

Flow Splitting Calculations—The flow splitting calculations determine the volumetric flow rate of water at different locations within the EBS as water moves through breached DSs, breached WPs, and the invert as shown on Figure 6.3.6-4. The volumetric flow rate of water through each breached DS or WP is proportional to the damage fraction on each DS or WP represented by N_{pDS} and N_{pWP} in Equations 6.3.6-5 and 6.3.6-6, respectively. The EBS Flow Submodel introduces two uncertain (epistemic) flow splitting parameters to characterize the fraction of flow that enters breaches on the DSs and WPs. These two parameters are sampled once per realization and applied to all representative DSs and WPs.

Inputs to the EBS Flow Submodel for each WP type and repository subregion include:

- Seepage and condensation rates from the Drift Seepage and Drift Wall Condensation Submodels (Section 6.3.3)
- Damage fraction per failed DS from the WP and DS Degradation Model Component (Section 6.3.5)
- Damage fraction per failed DS from Early DS Failure Abstraction (Drip Shield EF Modeling Case only) (Section 6.4)
- Damage fraction per failed DS from the Seismic Consequences Abstraction (Seismic Scenario Class only) (Section 6.6)
- Damage fraction per failed WP from the WP and DS Degradation Model Component (Nominal Scenario Class only) (Section 6.3.5)
- Damage fraction per failed WP from the Seismic Consequences Abstraction (Seismic Scenario Class only) (Section 6.6).

The EBS Flow Submodel does not use the average number of crack penetrations per failed WP because stress corrosion cracks are too small to allow water flow through these cracks (DTN: MO0706SPAFEPLA.001_R0 [DIRS 181613], FEP Number 2.1.03.10.0A).

The flow splitting model for water flow through a damaged DS is computed by multiplying the dripping flow falling on the DS by the ratio of patch opening length on the DS to the total length of the DS. Similarly, the flow entering each WP is computed by multiplying the flow falling on the WP (i.e., the flow of water through the DS) by the ratio of patch opening length on the WP to the total length of the WP. Both calculations are multiplied by a separate uncertainty factor to account for the variation in location of the patches with respect to the drip location (Table 6.3.6-2). However, the DS corrosion model does not include spatial variation between

DSs or between patches on individual DSs (Section 6.3.5.1.3). Therefore, for the TSPA-LA Model, all the DS patches fail when DS failure occurs. Additionally, when N_{pDS} is equal to the maximum number of DS patches, the DS flow splitting algorithm is not used and $F_2 = F_1$ (Eq. 6.3.6-5).

Outputs from the EBS Flow Submodel are used by: (1) the Waste Form Degradation and Mobilization Model Component (volumetric flow rate through a failed WP) to calculate pH and ionic strength in the WP, and (2) the EBS Transport Submodel (volumetric flow rate through a failed WP and volumetric flow rate through the invert) to calculate advective transport of radionuclides through a failed WP and the invert to the host rock.

6.3.6.4 Consistency and Conservatism in Assumptions and Parameters

To enhance understanding of the complex interactions within the TSPA-LA Model, a discussion of consistency among model components and submodels and identification of conservative assumptions in abstractions, process models, and parameter sets supporting the EBS Flow Submodel is presented below.

6.3.6.4.1 Consistency of Assumptions

Effects of Evaporation on EBS Flow—Less water may be available for transport if evaporation on the DSs or WPs were taken into account. Generally, the heat output from the WPs will cause the DSs to be hotter than the drift wall from which water is dripping. Some water that drips onto the DSs may be evaporated, thereby reducing the flow of water through the DSs. A reduction in the quantity of water flow through the DSs reduces the potential for advective transfer and subsequent release and transport of radionuclides from the WPs (SNL 2007 [DIRS 177407], Section 5.2).

Heat generated by the waste forms also has the potential to evaporate water within the WPs. In this situation, water cannot collect inside the WPs and cannot support the advective transport of radionuclides. However, complexities in the internal geometry of the WPs, particularly the response of any water pooled at the bottom of the WPs and the presence of small conduits for water vapor to escape through stress corrosion cracks, make it difficult to assess evaporation quantitatively. The potential for evaporation in the WPs is ignored in the TSPA-LA Model (SNL 2007 [DIRS 177407], Section 6.3.3.2).

Effect on the TSPA-LA Model—As further discussed in Section 6.3.8, neglecting the evaporation of water on the DSs and WPs means there is more water available for dissolution and advection of radionuclides. Also, neglecting evaporation leads to higher saturation and more diffusion of radionuclides. Evaporation and consumption of water and water vapor entering a WP is evaluated in Appendix C.

6.3.6.4.2 Identification of Conservatism in Submodels and Abstractions

No DS Shadow in the Invert—For dripping locations, water will tend to shed around the DSs and not flow through the region of the invert directly under the DSs. However, because of limited information regarding the flow paths and mixing of waters, this effect is not accounted for (SNL 2007 [DIRS 177407], Section 6.5.2.6). For model scenarios without DS failures, a DS shadow would prevent advective transport for some distance beneath the WP, certainly within the invert and for some distance in the UZ fractures and matrix. However, the TSPA-LA Model assumes advection within the invert in the dripping locations. The effect of this assumption is to increase the release of radionuclides from the invert and increase the diffusive concentration gradient from the waste form to the invert and UZ, thereby conservatively increasing the diffusive mass flux.

All Dripping into Drifts is Assumed to Fall on the DSs—All dripping into drifts is assumed to fall on the DSs, not just dripping above the DSs. The approach taken is to simplify the model since uncertainty in dripping locations is difficult to quantify and seepage into a circular opening is more likely to occur near the crown (SNL 2007 [DIRS 177407], Section 5.1). While all dripping into the drift is assumed to fall on the DSs, the DS flow splitting uncertainty term in Equation 6.3.6-5 is applied. While this uncertainty term may reduce the flow through the DSs to account for the spatial variability of the location of DS patch openings, it does not account for spatial distribution of dripping. The conservative treatment tends to increase the dripping flow contacting the DSs, resulting in an increase in the dripping flow passing through a failed DS and an increase in the dripping flow diverted around the DSs (e.g., passing through the invert) within the dripping locations.

All the Dripping Penetrating a DS Falls on the Crown of the WP—A conservative approach is taken to simplify the modeling approach because uncertainty in dripping locations is difficult to quantify (SNL 2007 [DIRS 177407], Section 5.1). Any increase in the advective flow through the WPs as a result of assuming the entire flow penetrating the DSs falls on the WPs would be negligible with the result of a slight increase in the dripping flow through the breached WPs.

6.3.6.5 Alternative Conceptual Model(s) for Engineered Barrier System Flow

Section 6.2 outlines the general consideration and treatment of ACMs used to support the TSPA-LA Model. Brief descriptions of the EBS Flow Submodel ACMs are summarized in Table 6.3.6-3.

Bathtub Flow Model ACM—This ACM assumes that dripping water collects within the WP before being released to the EBS (SNL 2007 [DIRS 177407], Section 6.6.1). The bathtub effect would be most important during the period when only a few patches or cracks have penetrated the DSs and WPs. In this situation, there may be penetrations through the top of the WP while the bottom surface remains intact, leading to retention of liquid. At later times, the presence of multiple penetrations makes a flow-through geometry the more likely configuration. The response of the bathtub geometry was evaluated for a primary case, with constant boundary conditions and material properties, and for three secondary cases. The three secondary cases considered a step change in inflow rate, such as would occur from a climatic change, a step change in water chemistry, or a step change in flow geometry, as would occur if a patch

suddenly appeared beneath the waterline. All cases included the consideration of two limiting conditions on radionuclide releases: dissolution rate limited and solubility limited.

This ACM was not used for the TSPA-LA EBS Transport Model because analyses indicate that the base-case flow-through model is bounding for use in the TSPA-LA Model with respect to the release of radionuclides (SNL 2007 [DIRS 177407], Section 6.6.1).

Dual-Continuum Invert Model ACM—The dual-continuum invert model is an alternative conceptual EBS transport model in which crushed tuff invert ballast is modeled as a dual-continuum material consisting of intergranular pore space and intragranular pore space (SNL 2007 [DIRS 177407], Sections 6.6.3 and 6.6.4.2). All water dripping into the drift is modeled as flowing through the intergranular pore space and UZ fractures. Imbibition from UZ host rock into the invert is modeled as flowing through the intragranular pore space and into the UZ matrix under gravity. Diffusion of radionuclides also occurs in both the intergranular and intragranular pore spaces, from the WP corrosion products into UZ fractures and matrix, as well as between the two invert continua.

This ACM was not used for the TSPA-LA EBS Transport Model due to insufficient data to validate diffusion coefficients in individual continua and insufficient data to confirm whether this is a bounding approach with respect to chemical behavior in the invert (SNL 2007 [DIRS 177407], Section 6.6.3.5).

INTENTIONALLY LEFT BLANK

Table 6.3.6-1. The EBS Flow Abstraction within the TSPA-LA Model

Flow Pathway	Flow Parameters	Notes
1. Total dripping flow (seepage + wall condensation), F_1	Total dripping flow is a function of seepage flow and drift-wall condensation flow.	Drift Seepage Submodel (Section 6.3.3.1) provides time- and location-dependent values of seepage flow. Drift Wall Condensation Submodel (Section 6.3.3.2) provides time and location-dependent values of drift-wall condensation flow.
2. Flow through the DS, F_2	N_{pDS} is the number of DS general corrosion patches l_{DS} is the axial half-length of patches due to general corrosion of titanium. L_{DS} is the axial length of the DS. f_{DS} is the sampled uncertain parameter, DS_Flux_Uncertainty_a.	WP and DS Degradation Model Component (Section 6.3.5) provides the number of general corrosion patches and stress corrosion cracks on the DS. No flow through stress corrosion cracks due to plugging (SNL 2007 [DIRS 181953], Sections 6.8.6 and 8.1.6, and DTN: MO0706SPAFAEPLA.001_R0 [DIRS 181613], FEP 2.1.03.10.0B).
3. Diversion around DS, F_3	$F_3 = F_1 - F_2$.	Continuity of liquid flow.
4. Flow into the WP, F_4	N_{pWP} is the number of WP general corrosion patches l_{WP} is the axial half-length of all patches due to general corrosion of Alloy 22 (UNS N06022). L_{WP} is the axial length of the WP. f_{WP} is the sampled uncertain parameter, WP_Flux_Uncertainty_a.	WP and DS Degradation Model Component (Section 6.3.5) provides the number of general corrosion patches on the WP. No flow through stress corrosion cracks (DTN: MO0706SPAFAEPLA.001_R0 [DIRS 181613], FEP 2.1.03.10.0A). Pseudo steady state flow through WP (outflow = inflow in steady state; that is bounding for release).
5. Diversion around the WP, F_5	$F_5 = F_2 - F_4$.	Continuity of liquid flow.
6. Flow to the invert, F_6	$F_6 = F_5 + F_4 + F_3$ $= F_1$.	Note that only F_4 can transport radionuclides into the invert.
7. Imbibition flow from the host rock matrix into the invert, F_7	F_7 is an input to the EBS Flow Submodel.	EBS TH Environment Submodel (Section 6.3.2) provides the imbibition flow.
8. Flow from the invert into the UZ, F_8	$F_8 = F_6 + F_7$ $= F_1 + F_7$.	Total dripping flow portion ($F_1 = F_6$) of advective flow from the invert flows into the UZ fractures; imbibition flow (F_7) flows into the UZ matrix.

Source: Developed from SNL 2007 [DIRS 177407], Table 8.1-1.

NOTE: See Figure 6.3.6-4.

Table 6.3.6-2. Drip Shield and Waste Package Flow Splitting Parameters

TSPA-LA Model Name	Mathematical Symbol	Description	Units	Distribution Type	Distribution Specification
DS_Flux_Uncertainty_a	f'_{DS}	DS flow splitting uncertainty factor	None	Uniform	Min = 0 Max = 0.85
WP_Flux_Uncertainty_a	f'_{WP}	WP flow splitting uncertainty factor	None	Uniform	Min = 0 Max = 2.41

Sources: SNL 2007 [DIRS 177407], Table 8.2-4, and DTN: SN0703PAEBSRTA.001_R3 [DIRS 183217].

Table 6.3.6-3. Alternative Conceptual Models Considered for the EBS Flow

Alternative Conceptual Models	Key Assumptions	Assessment and Basis
Dual-continuum invert model	Crushed tuff invert ballast is modeled as a dual-continuum material consisting of intergranular and intragranular pore spaces. All seepage flow into the drift flows through the intergranular pore space and into the UZ fractures. Imbibition from UZ host rock into the invert flows through the intragranular pore space. Diffusion of radionuclides also occurs in both the intergranular and intragranular pore spaces, from the WP corrosion products into UZ fractures and matrix, as well as between the two invert continua (SNL 2007 [DIRS 177407], Section 6.6.4).	Insufficient data to validate diffusion coefficients in individual continua. Insufficient data to confirm whether this is a bounding approach with respect to chemical conditions in the invert for calculating solubility and colloid stability.
Bathtub flow model (alternative to flow-through model)	Seepage water flowing into breached WP accumulates until void volume is filled before water containing dissolved radionuclides flows out. Various cases, such as changing inflow rates and effect of solubility and dissolution rate limits, are evaluated (SNL 2007 [DIRS 177407], Section 6.6.1).	The flow-through model is determined to be conservative with respect to releases of radionuclides for use in the TSPA-LA Model (SNL 2007 [DIRS 177407], Section 6.6.1).

Source: Developed from SNL 2007 [DIRS 177407], Table 6.4-1.

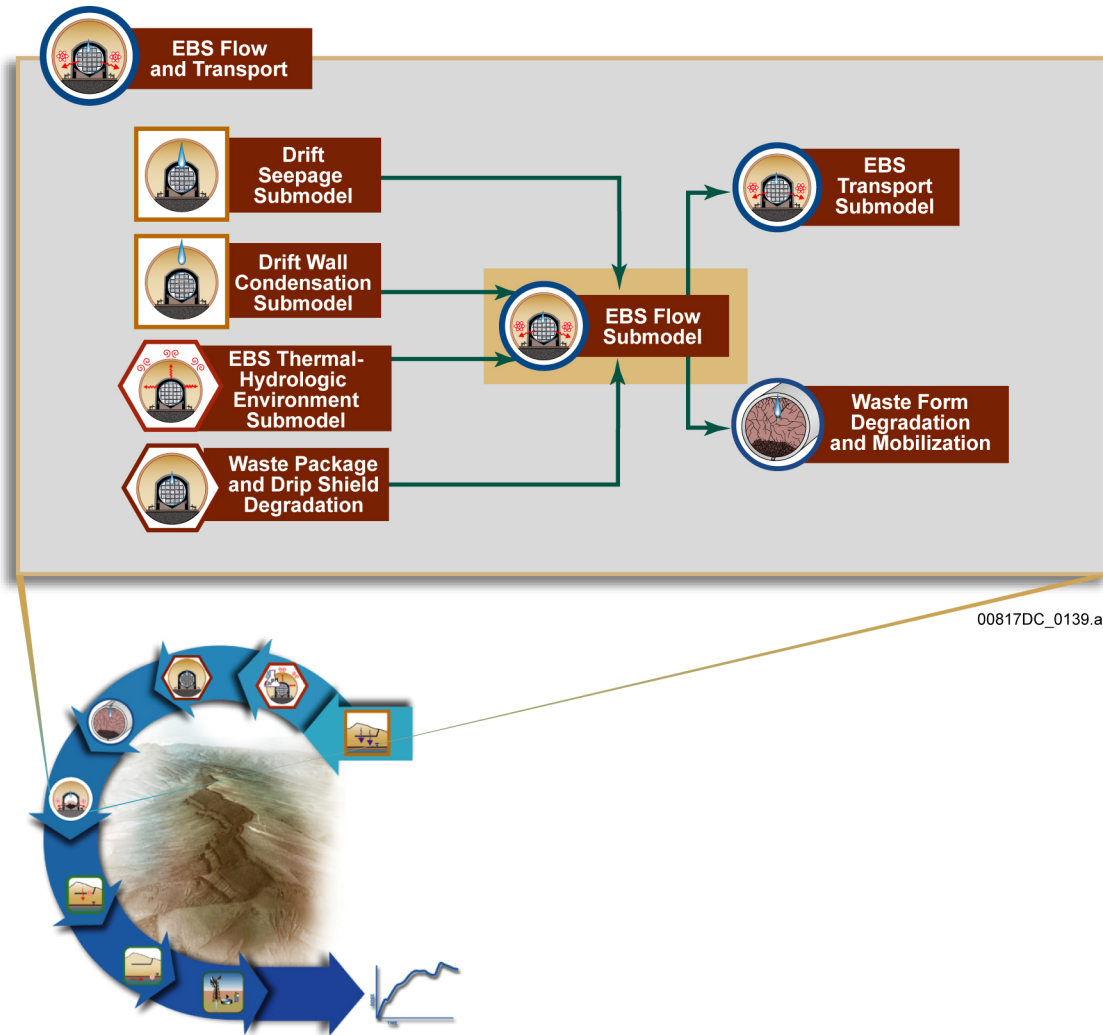


Figure 6.3.6-1. Information Flow Diagram for the EBS Flow Submodel

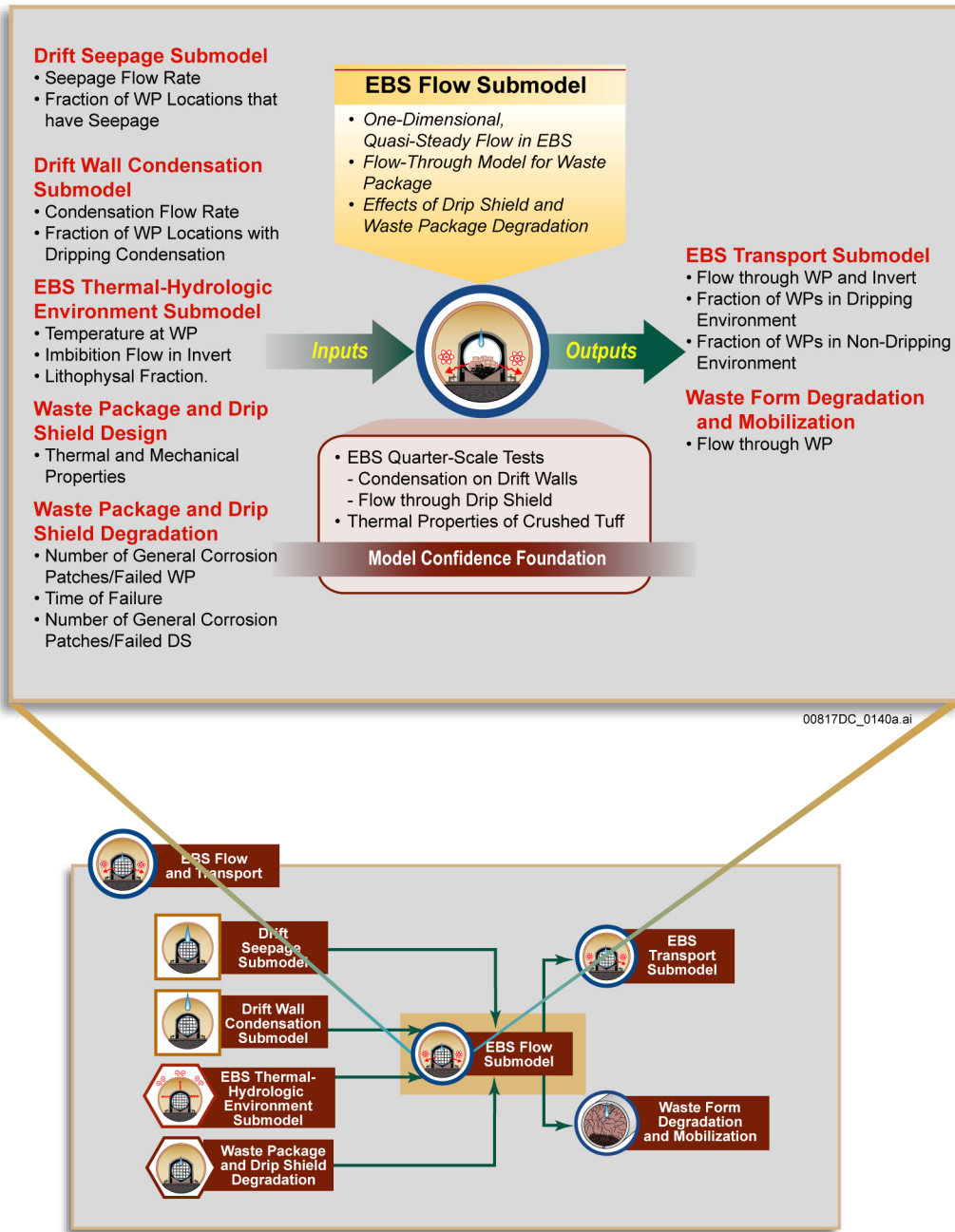


Figure 6.3.6-2. Inputs, Outputs, and Basis for Model Confidence for the EBS Flow Submodel

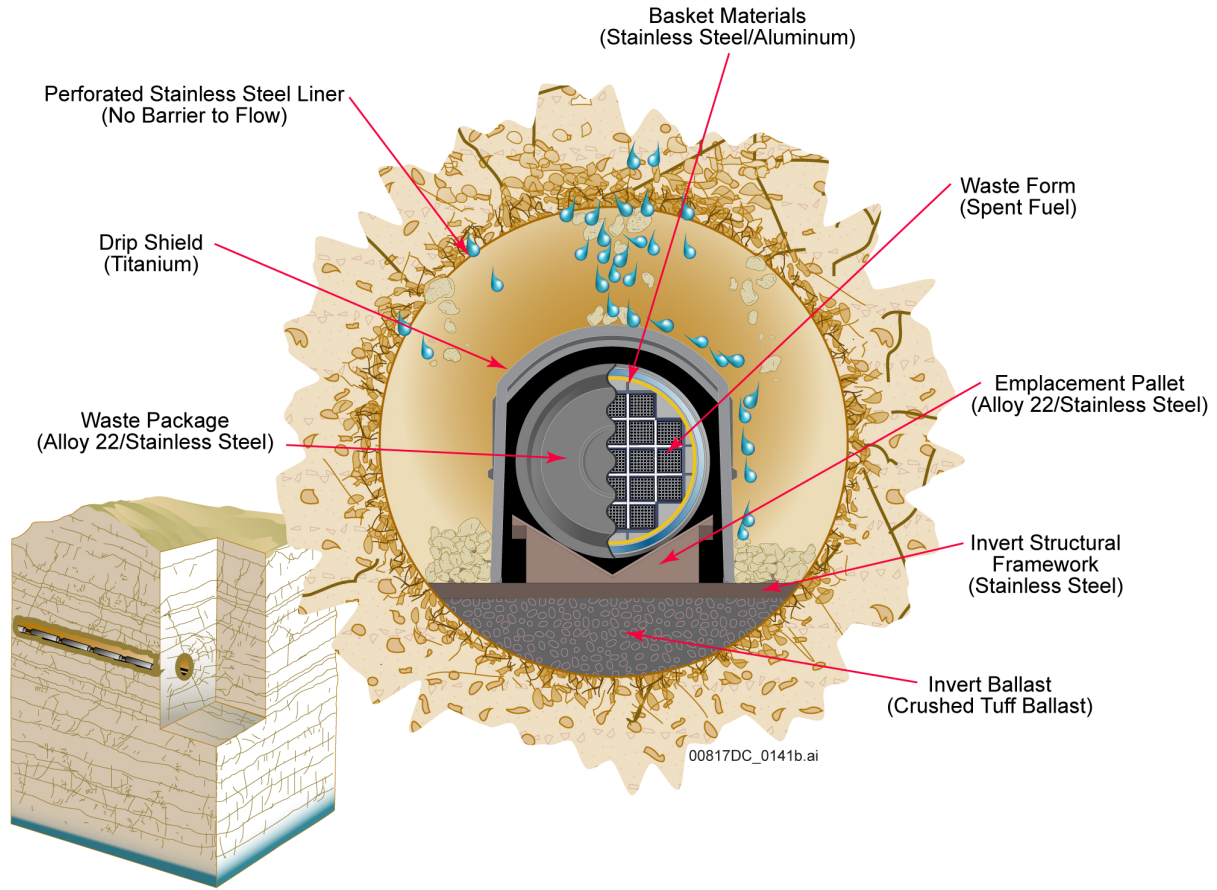


Figure 6.3.6-3. Cross Section of Typical Emplacement Drift

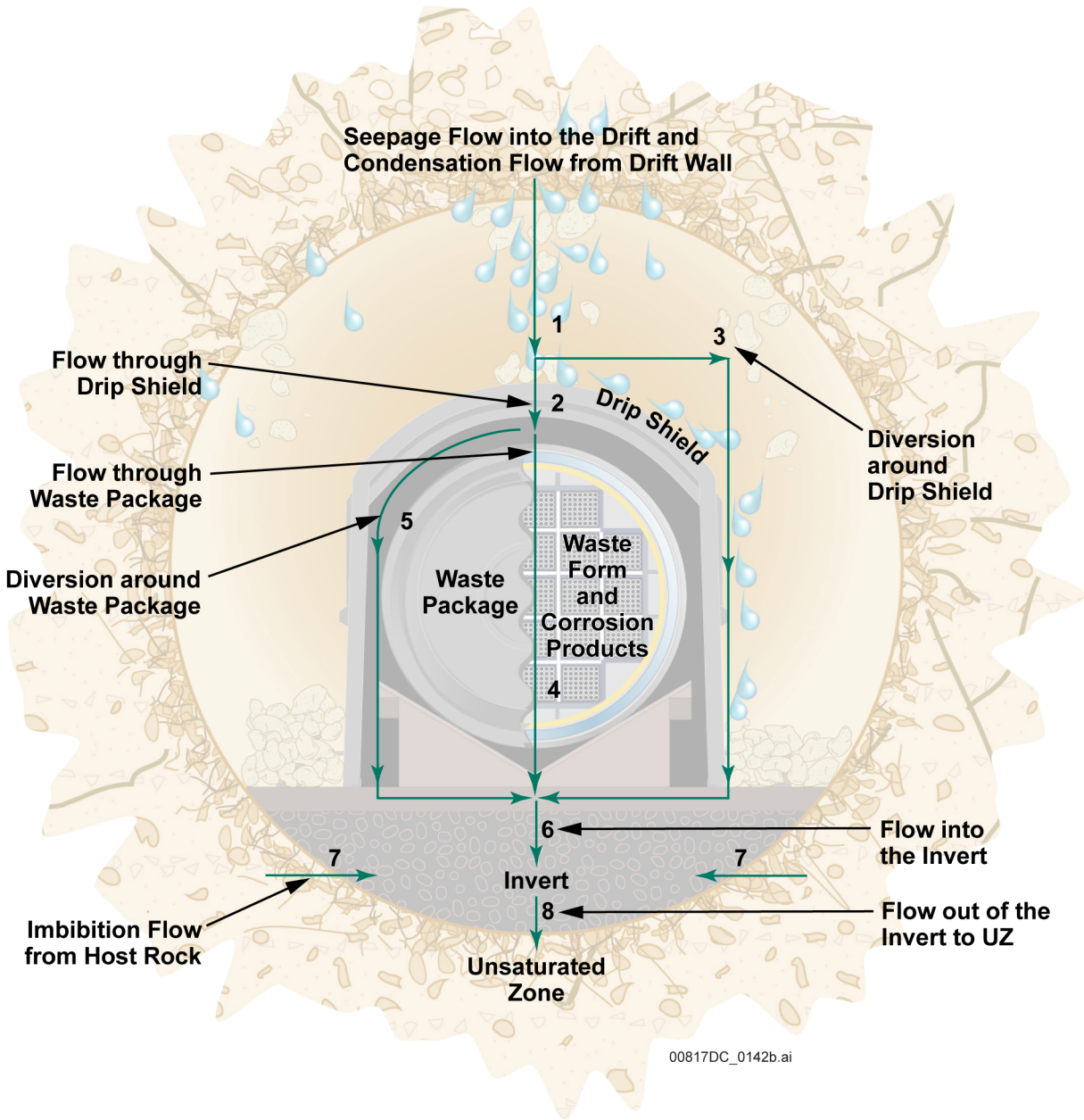


Figure 6.3.6-4. Schematic Diagram of Water Flow Pathways in the EBS

6.3.7 Waste Form Degradation and Mobilization

The Waste Form Degradation and Mobilization Model Component consists of five submodels: (1) Initial Radionuclide Inventory Submodel, which defines the radionuclide inventory and radionuclides of importance for the TSPA-LA; (2) In-Package Chemistry Submodel, which evaluates in-package chemical conditions; (3) Waste Form Degradation Rate Submodel, which calculates the degradation rates of CSNF, DSNF, and HLW waste forms; (4) Solubility (or Dissolved Concentration Limits) Submodel, which calculates solubilities (i.e., dissolved concentration limits) of radioactive elements in a failed WP and in the invert; and (5) EBS Colloids Submodel, which calculates colloidal concentrations of radionuclides in a failed WP and in the invert. Solubilities and colloidal concentration of radionuclides serve as inputs to the EBS Transport Submodel (Section 6.3.8), which calculates radionuclide transport within the WPs from the waste form to the EBS and through the EBS to the UZ below the repository.

The TSPA-LA Waste Form Degradation and Mobilization Model Component receives inputs from the following analyses and/or model reports:

- *Initial Radionuclide Inventories* (SNL 2007 [DIRS 180472]) and *Radionuclide Screening* (SNL 2007 [DIRS 177424])
- *In-Package Chemistry Abstraction* (SNL 2007 [DIRS 180506])
- *CSNF Waste Form Degradation: Summary Abstraction* (BSC 2004 [DIRS 169987]), *DSNF and Other Waste Form Degradation Abstraction* (BSC 2004 [DIRS 172453]), and *Defense HLW Glass Degradation Model* (BSC 2004 [DIRS 169988])
- *Dissolved Concentration Limits of Elements with Radioactive Isotopes* (SNL 2007 [DIRS 177418])
- *Waste Form and In-Drift Colloids-Associated Radionuclide Concentrations: Abstraction and Summary* (SNL 2007 [DIRS 177423]).

The three categories of waste form (CSNF, DSNF, and HLW glass) are contained and disposed in two types of WPs: CSNF WPs and CDSP WPs. The CDSP WPs will contain both DSNF and HLW glass. As was done in the TSPA for the Site Recommendation, WPs containing naval SNF waste forms are conservatively represented as containing CSNF. An evaluation of this conservatism is presented in Section 7.5.

Key inputs to the submodels for the Waste Form Degradation and Mobilization Model Component include: (1) a set of initial materials within the WP and the materials' major elemental compositions and physical and chemical properties; (2) time-dependent water flux into a failed WP provided by the EBS Flow Submodel (Section 6.3.6); (3) temperature and relative humidity in the WP provided by the EBS TH Environment Submodel (Section 6.3.2); and (4) partial pressure of CO₂ in the gas phase (P_{CO_2}) or negative log of partial pressure of CO₂ (pCO_2) provided by the EBS Chemical Environment Submodel (Section 6.3.4).

Many of the abstractions that support the submodels in the Waste Form Degradation and Mobilization Model Component are implemented to describe single representative CSNF and CDSP WPs. The determination of what comprises a representative WP is discussed in Section 6.3.2.2.2. The EBS Transport Submodel is implemented in the TSPA-LA Model at the scale of a single WP (Section 6.3.8). The pertinent EBS Transport Submodel properties (including the Waste Form Degradation and Mobilization Model Component) for a single representative WP are scaled to the total number of WPs that have failed in each percolation subregion. These properties include the mass of available inventory, pore water volumes, mass of solid materials, advective flow rates, and diffusion areas. See the GoldSim user's guide for source-term element details (GoldSim Technology Group 2007 [DIRS 181727]).

The five submodels discussed in this section deal with processes that govern the mobility of radionuclides inside a failed WP. This section presents the principles and submodel implementation for radionuclide availability in a failed WP but does not discuss the specifics regarding transport in the EBS. This discussion is reserved for Section 6.3.8, which explains radionuclide transport as available inventory moves from the waste form into the waste form alteration products, then into the WP corrosion products, then out of the WP opening into the invert.

In general, the radionuclide inventory of each WP may be immediately available for transport upon WP failure or bound in a matrix that must first degrade before the inventory is available for transport inside the WP (Section 6.3.7.1). As discussed in Section 6.3.7.3, no credit is taken for CSNF and DSNF cladding for the TSPA-LA compliance model. After WP failure, the waste form begins to degrade at the calculated rate (Section 6.3.7.4). As the waste form degrades, waste form alteration products are formed (Section 6.3.7.4). The available inventory, from both the degraded waste form and that which was immediately available upon WP failure, is released into the pore water of the alteration product. The available inventory is dissolved in this pore water solution up to its solubility (Section 6.3.7.5). As the waste form degrades, waste form colloids are also formed, and these colloids may facilitate the release of the radionuclides from the breached WPs to the environment. Colloid formation and stability in the EBS are discussed in Section 6.3.7.6. Although the processes described below are closely related to the release of radionuclides from a failed WP into the environment, the topics covered in this section pertain to the availability of the radionuclides for transport. The transport of available radionuclides, by diffusion and advection, is covered in detail in Section 6.3.8.

The chemistry inside a failed WP is calculated by the In-Package Submodel using the abstracted relationships, and then the outputs are fed to other submodels that govern radionuclide availability (Waste Form Degradation Submodel (Section 6.3.7.4), Dissolved Concentration Limits Submodel (Section 6.3.7.5), and EBS Colloids Submodel (Section 6.3.7.6)).

The interaction between the five submodels in the Waste Form Degradation and Mobilization Model Component is common but is limited to the form of the abstractions presented. For example, the waste form degradation rate for a failed CSNF WP was an input to the In-Package Chemistry Process Model. However, the final abstraction, as presented for the TSPA-LA Model, was independent of the waste form degradation rate. This model abstraction is intended to span the range of waste form degradation rates anticipated in the TSPA-LA Model. Therefore, the In-Package Chemistry Submodel (Section 6.3.7.2) does not receive input from the CSNF Waste

Form Degradation Submodel (Section 6.3.7.4.1). The abstracted rate model from the degradation of the CSNF is a function of the pH inside a failed WP. Therefore, in the TSPA-LA Model, the In-Package Chemistry Submodel feeds the pH to the CSNF Waste Form Degradation Submodel (Section 6.3.7.4.1). Other submodel interactions are discussed in greater detail in the subsections below.

The five submodels discussed below are presented sequentially in the sections that follow, but in general, they are evaluated in every timestep of the TSPA-LA Model. Two of the five Waste Form Degradation and Mobilization Model Component Submodels described below may receive feeds from other model components, but they do not receive feeds from the other three submodels in the Waste Form Degradation and Mobilization Model Component. These two submodels are presented first and are the Radionuclide Inventory Submodel (Section 6.3.7.1) and the In-Package Chemistry Submodel (Section 6.3.7.2). The next three submodels discussed are the Waste Form Degradation Submodel (Section 6.3.7.4), the Dissolved Concentration Limits Submodel (Section 6.3.7.5), and the EBS Colloids Submodel (Section 6.3.7.6). These submodels are functions of other submodels of the Waste Form Degradation and Mobilization Model Components, as well as other model components in the TSPA-LA Model. For example, the Waste Form Degradation Submodel, including the calculations of the mass and volume of the alteration products as the waste forms degrade, are functions of the EBS TH Environment Submodel (Section 6.3.2) and the In-Package Chemistry Submodel (Section 6.3.7.2), and receive input feeds directly from these submodels at each TSPA-LA Model timestep. For the purposes of the rate model calculations, the TSPA-LA Model first computes the feed values at each timestep and then evaluates the degradation rate expression for those feed conditions. The simulation software maintains an element hierarchy for evaluating calculations that are dependent on other model calculations at the same simulation time.

Figures 6.3.7-1 and 6.3.7-2 are schematic illustrations showing the submodels of the Waste Form Degradation and Mobilization Model Component, the inputs and outputs of the model component, and the basis for confidence in the model component.

6.3.7.1 Radionuclide Inventory

The *Initial Radionuclide Inventories* analysis (SNL 2007 [DIRS 180472]), hereafter referred to as the Initial Radionuclide Inventory Abstraction for the TSPA-LA, considers four categories of wastes for disposal in the repository: DOE-owned HLW glass (including HLW glass from the Savannah River Site, Idaho National Laboratory, and Hanford, as well as commercial HLW glass from the West Valley Demonstration Project), CSNF, DSNF, and naval SNF. The radionuclides of importance to the TSPA-LA Model dose calculations were assessed in the Initial Radionuclide Inventory Screening Analysis in *Radionuclide Screening* (SNL 2007 [DIRS 177424]). Figure 6.3.7-3 shows how the waste types are to be placed in CSNF and CDSP WPs. The Initial Radionuclide Inventory Abstraction and Initial Radionuclide Inventory Screening Analysis together define the source terms for the CSNF and CDSP WPs in terms of both the quantity of WPs and the radionuclide inventory per WP. These two analyses indicate that 32 radionuclides are used to represent the inventory in the TSPA-LA Model. Note that ^{210}Pb , which is specified to be included in the inventory by the Initial Radionuclide Inventory Screening Analysis, is assumed to be in secular equilibrium with ^{226}Ra and is not explicitly modeled in the TSPA-LA Model. The TSPA-LA Model does account for the dose effects of ^{210}Pb by combining its

biosphere dose conversion factor with its parent, ^{226}Ra . Because the TSPA-LA Model accounts for the degradation and failure of individual WPs, the inventories of these 31 radionuclides are provided on a grams-per-WP basis.

6.3.7.1.1 Conceptual Model

The number of WPs projected to be emplaced in the repository is 11,629 (Table 6.3.7-1). This number of WPs is approximately 4 percent higher than necessary to emplace 70,000 metric tons heavy metal in the repository. This is to completely fill all of the available drifts (DTN: MO0702PASTREAM.001_R0 [DIRS 179925], Assumption 14). Eight WP configurations were designed to accommodate the CSNF, HLW, DSNF, and naval waste forms (Table 6.3.7-1). The CSNF configurations contain the commercial fuel assemblies from PWRs and BWRs. The CDSP WP configurations hold both DSNF and HLW in various-sized canisters within the WP. Naval fuel will be packaged in either short- or long-canister configurations. Even though the naval fuel is not considered a commercial fuel in the TSPA-LA Model, the 417 naval SNF WPs are treated as if they were CSNF WPs (SNL 2007 [DIRS 180472]), Table 7-3[a]). This number of naval SNF WPs is 4 percent higher than the originally specified 400 naval WPs. WPs containing naval SNF waste forms are conservatively represented in the TSPA-LA Model as containing CSNF. This modeling approximation is justified because the fuel degradation characteristics more closely resemble CSNF than DSNF, there is no HLW in a naval fuel WP, and surrogate analyses indicate that the dose due to releases from a CSNF WP bounds the dose due to releases from a naval WP (Section 7.5.3). The mixed oxide fuel (MOX) (Section 6.3.7.1.2.2) inventory is included as CSNF inventory in the TSPA-LA Model for release purposes. In contrast to the naval SNF that is treated as additional packages, the MOX inventory is averaged over the total number of CSNF WPs and then added to the per package CSNF inventory. For release purposes, the lanthanide borosilicate (LaBS) inventory (Section 6.3.7.1.2.2) is included as HLW inventory in the TSPA-LA Model. The LaBS inventory is averaged over the total number of CDSP WPs and then added to the HLW glass per package inventory.

The Initial Radionuclide Inventory Screening Analysis explicitly considered both 10,000-year and 1,000,000-year modeling periods for the repository at Yucca Mountain. Four scenario classes are considered: (1) Nominal Scenario Class, (2) Igneous Scenario Class, (3) Seismic Scenario Class, and (4) Human Intrusion Scenario. The radionuclide screening for each scenario class is based on the premise that the products of activity inventories and screening factors indicate the relative importance of each radionuclide with respect to the radiation dose that a person near the repository might receive (SNL 2007 [DIRS 177424], Section 6.2.1). The Initial Radionuclide Inventory Screening Analysis takes into account such factors as radionuclide decay rates, soil accumulation, uptake by plants, and exposure to contaminated groundwater. This screening analysis also accounts for differences in WPs and waste forms, radionuclide sorption, and radionuclide solubility. Results of the screening analysis are provided in Table 6.3.7-2. This table lists 32 radionuclides that may contribute the majority of the dose for the different scenario classes (Section 6.1.2) implemented in the TSPA-LA Model.

The radionuclide inventory for the CSNF and CDSP WPs, including uncertainty, is provided by the Initial Radionuclide Inventory Abstraction (SNL 2007 [DIRS 180472]) and is a direct input to the TSPA-LA Model. The CSNF, HLW, and DSNF radionuclide inventories are provided on

a grams-per-WP basis. The radionuclide inventories provided by the Initial Radionuclide Inventory Abstraction are calculated at year 2067 for CSNF WPs (DTN: MO0702PASTREAM.001_R0 [DIRS 179925], Assumption 13) and year 2030 for HLW and DSNF (DTN: MO0702PASTREAM.001_R0 [DIRS 179925]). Table 6.3.7-3 shows the expected average inventory in grams per WP for 31 radionuclides at year 2067 for CSNF and year 2030 for DSNF and HLW. For inventory purposes, all waste is assumed to be emplaced in year 2067 and then ventilated for 50 years before closure of the repository. The TSPA-LA Model simulation begins at post-closure and therefore requires an inventory calculated at the time of repository closure, currently estimated to be the year 2117 (DTN: MO0702PASTREAM.001_R0 [DIRS 179925]). Section 6.3.7.1.2.1 describes the radionuclide inventory decay and ingrowth calculations performed for 50 years and 87 years for CSNF and HLW/DSNF, respectively. The additional inventory decay is necessary to account for the preclosure period prior to the start time for the TSPA-LA Model simulations. Table 6.3.7-4a shows the per-package inventories aged to year 2117 and used as input to the TSPA-LA Model. In addition to the initial inventories presented in the Initial Radionuclide Inventory Abstraction discussed above, the TSPA-LA Model also includes MOX SNF and LaBS glass HLW. The contributions of MOX and LaBS glass HLW inventory are discussed in Section 6.3.7.1.2.2. Table 6.3.7-4b shows the per package inventories aged to year 2117 for MOX and LaBS glass HLW. Table 6.3.7-5 shows the specific activity for each radionuclide as well as the curies per package inventories for each WP type in the TSPA-LA Model.

6.3.7.1.2 TSPA-LA Model Abstraction

The Initial Radionuclide Inventory Abstraction specifies the initial quantity (grams/WP) of radionuclides for the CSNF, DSNF, and HLW WPs (Table 6.3.7-3). The initial inventories in each WP are decayed as a function of time. The decay chains and radionuclide half-lives are provided on Figure 6.3.7-4, where the radionuclides used for dose calculations are indicated. The following radionuclides are not members of chains: ^{14}C ($t_{1/2} = 5,720$ yr) and fission products ^{36}Cl ($t_{1/2} = 3.01 \times 10^5$ yr), ^{135}Cs ($t_{1/2} = 2.30 \times 10^6$ yr), ^{137}Cs ($t_{1/2} = 30.1$ yr), ^{129}I ($t_{1/2} = 15.7 \times 10^6$ yr), ^{79}Se ($t_{1/2} = 2.90 \times 10^5$ yr), ^{126}Sn ($t_{1/2} = 2.30 \times 10^5$ yr), ^{90}Sr ($t_{1/2} = 28.8$ yr), and ^{99}Tc ($t_{1/2} = 2.13 \times 10^5$ yr) (DTN: MO0702PASTREAM.001_R0 [DIRS 179925]), and are not produced by decay of other radionuclides in the waste forms, therefore, they are not included on Figure 6.3.7-4.

Table 6.3.7-6 summarizes the treatment of each radionuclide within the EBS Transport Submodel (Section 6.3.8), the UZ Transport Submodel (Section 6.3.9), the SZ Transport Submodel (Section 6.3.10), and the Biosphere Submodel (Section 6.3.11) for the groundwater release modeling cases. Table 6.3.7-2, Column 3, lists the radionuclides transported in the atmosphere for the Volcanic Eruption Modeling Case. Among the 32 important radionuclides listed in Table 6.3.7-6, 27 are tracked and transported by the EBS Transport, the UZ Transport, and the SZ Transport Submodels. The five radionuclides that are not tracked and transported by the EBS, UZ, and SZ Submodels are ^{245}Cm , ^{241}Pu , ^{227}Ac , ^{228}Ra , and ^{210}Pb . In the Biosphere Submodel, doses from ^{227}Ac , ^{228}Ra , and ^{210}Pb are calculated by assuming they are in secular equilibrium with ^{231}Pa , ^{232}Th , and ^{226}Ra , respectively, because their half-lives are short. Doses from ^{245}Cm and ^{241}Pu are not calculated in the Biosphere Submodel because they are only important for their decay effects on the inventory of ^{241}Am and ^{237}Np , as stated in Table 7-1 of the *Radionuclide Screening* (SNL 2007 [DIRS 177424]). The different transport mechanisms for

each radionuclide listed in Table 6.3.7-6 are based upon: (1) the solubility of the radionuclide element within the WP; (2) the subsequent transportability beyond the EBS (based largely on the radionuclide's potential to remain in solution or sorb onto colloids, rather than being sorbed onto the host rock along the transport path from the WP to the biosphere); and (3) the persistence of the radionuclide during the transport period from the WP to the biosphere based on its half-life.

The discussion of uncertainty in the following two paragraphs is taken from information found in DTN: SN0310T0505503.004_R0 [DIRS 168761]. There are a number of sources contributing to the uncertainty in radionuclide inventories. Three sources of uncertainty are common in all waste types. The first is due to the computational method and nuclear characteristics used in predicting future radionuclide inventories (e.g., isotopic neutron cross section or decay half-life). The second source of uncertainty is the completeness of the records that are kept for the CSNF and HLW materials (e.g., burn-up history or HLW batch compositions). The third source, and most difficult to quantify, is the uncertainty about future decisions that will influence the creation, packaging, or shipment of waste. These decisions influence the selection of waste types destined for emplacement into the repository directed by the Nuclear Waste Policy Act of 1982, as amended (42 U.S.C. 10101-10133, 1988 [DIRS 131951]) and implemented under NRC Proposed Rule 10 CFR Part 63 ([DIRS 178394] and [DIRS 180319]). Record keeping is important because, given that the wastes are heterogeneous, the selection process can significantly change the average waste characteristics.

For CSNF, an uncertainty multiplier with a uniform distribution between 0.85 and 1.4 was chosen for the TSPA-LA (SNL 2007 [DIRS 180472], Table 7-2). The sampled multiplier is applied to the nominal CSNF values, provided in Table 6.3.7-3, for all radionuclides except ^{238}U . For DSNF, an uncertainty multiplier is defined to capture the uncertainty for all radionuclides except ^{238}U . The inventory of ^{238}U has much less relative uncertainty than the other radionuclides because it is present in the initial fuel and generally changes little during reactor operation. The DSNF multiplier is defined as a triangular distribution, with a minimum of 0.45, a most likely value of 0.62, and a maximum value of 2.9. This multiplier is applied to the nominal values for DSNF grams per WP in Table 6.3.7-3 for all radionuclides except ^{238}U . For HLW, a triangular distribution is chosen for the HLW uncertainty multiplier, and this multiplier is applied to the nominal HLW inventories shown in Table 6.3.7-3 for all radionuclides, including ^{238}U . The uncertainty multiplier for HLW has a triangular distribution, with a minimum of 0.7, a most likely value of 1, and a maximum value of 1.5. Table 6.3.7-7 summarizes the uncertainty multipliers for each waste type.

6.3.7.1.2.1 Preclosure Radionuclide Decay and Ingrowth

The initial radionuclide inventory is provided as input to the TSPA-LA Model by DTN: MO0702PASTREAM.001_R0 [DIRS 179925]. There are three categories of waste provided in this per-package format: CSNF, HLW glass, and DSNF. Because the sum total of all waste received at the repository in each fuel type category is used to provide the per-package average source term used in the TSPA-LA Model, the inventory has an age associated with the expected year of the last WP emplacement (DTN: MO0702PASTREAM.001_R0 [DIRS 179925]). Based on previous schedules and repository designs, the CSNF inventory was expected to take 24 years to emplace in the repository, with waste emplacement beginning in the year 2010; the year when the last CSNF WP would have gone into the repository was 2033. The

initial radionuclide inventory input to the TSPA-LA Model is provided as it would appear in the year 2033. The HLW and DSNF inventories are each provided to the TSPA-LA Model as they would appear in the year 2030. Table 6.3.7-3 shows the expected average inventory in grams per package for the 31 radionuclides used in the TSPA-LA Model, categorized by waste type, for 2030 and 2033. The current estimate is for emplacement in 2067 (DTN: MO0702PASTREAM.001_R0 [DIRS 179925]). The CSNF waste stream is still being produced; therefore, the inventory abstraction assumes that CSNF waste, similar to what would have been emplaced in the year 2033, will be emplaced in 2067.

Because the TSPA-LA Model begins each simulation at repository closure, currently estimated in the year 2117, there will be 50 (CSNF) or 87 (for HLW and DSNF) years of radionuclide inventory decay and ingrowth before the inventory is first used by the TSPA-LA Model. In order to synchronize the radionuclide inventory age with the starting point of the TSPA-LA Model, an external calculation described below was performed to update the radionuclide inventory before entering them into the TSPA-LA Model.

GoldSim Version 9.60 (SP1) was used to perform the radionuclide aging calculation using the species element and the radionuclide half-lives from the TSPA-LA Model. Figure 6.3.7-4 shows the four radionuclide chains modeled in the TSPA-LA Model (note that ^{14}C and the fission products tracked in the TSPA-LA Model are not shown on this figure). Three inventory elements were created, one for each fuel type category, and the radionuclide inventory provided by the Initial Radionuclide Inventory Abstraction. A GoldSim source element for each fuel type performs the calculation, and a collector cell gathers the aged inventory at the closure year.

The updated CSNF inventory was extracted from a 50-year simulation, and the updated HLW and DSNF inventories were extracted from an 87-year simulation. Table 6.3.7-4a shows the inventories provided by the Initial Radionuclide Inventory Abstraction and the updated inventories, which account for the decay and ingrowth experienced during the preclosure period.

Table 6.3.7-4a shows that the majority of included radionuclides experience little to no decay or ingrowth, with the few exceptions of ^{241}Am , ^{137}Cs , ^{237}Np , ^{238}Pu , ^{241}Pu , ^{90}Sr , and ^{234}U . The fission products ^{137}Cs and ^{90}Sr have half-lives of 30.1 years and 28.8 years, respectively, and have decay but no ingrowth because they do not have parent radionuclides. The inventory changes observed with ^{241}Am , ^{237}Np , and ^{241}Pu are related because they are part of the same decay chain (Figure 6.3.7-4). The half-life of ^{241}Pu is 14.4 years and the half-life of ^{241}Am is 432.7 years. The inventory changes observed with ^{238}Pu and ^{234}U occur because of the relatively short ^{238}Pu half-life of 87.7 years, and the fact that the ^{238}Pu inventory decays into the ^{234}U inventory. The inventory changes observed with ^{227}Ac , more than doubling the initial inventory, occur because of the large initial inventories of ^{235}U and ^{231}Pa , compared to the much smaller initial inventories of ^{227}Ac .

6.3.7.1.2.2 Mixed Oxide Spent Nuclear Fuel and Lanthanide Borosilicate Glass Inclusion

The inclusion of MOX SNF and LaBS glass HLW in the TSPA-LA Model is accomplished by adding radionuclide-specific inventories to the inventories provided by DTN: MO0702PASTREAM.001_R0 [DIRS 179925]. More specifically, the LaBS glass inventory is added to the HLW portion of the initial radionuclide inventory and is then subject to

the same uncertainty sampling applied to the HLW radionuclide inventory. In addition, the MOX SNF is added to the CSNF portion of the initial radionuclide inventory and is also subject to the uncertainty sampling applied to that inventory. The MOX and LaBS inventories are described in the analysis *MOX Spent Nuclear Fuel and LaBS Glass for TSPA-LA* (SNL 2007 [DIRS 177422]).

Because the ages of the MOX and LaBS waste forms are provided at times that are before the closure of the repository, their inventories were decayed, as described in Section 6.3.7.1.2.1, before addition to the TSPA-LA Model. The MOX inventory is provided at the year 2035, so decay and ingrowth are performed for 82 years before entry into the TSPA-LA Model. The LaBS inventory was provided at the year 2003, so decay and ingrowth is performed for 114 years before entry into the TSPA-LA Model. Table 6.3.7-4b shows the additional radionuclide inventories due to MOX and LaBS waste that are used as input to the TSPA-LA Model; only the inventory that was aged to closure (i.e., after 82 and 114 years, respectively) is used in the TSPA-LA Model.

6.3.7.1.3 TSPA-LA Model Implementation

The initial mass of each radionuclide, provided by the Initial Radionuclide Inventory Abstraction in grams per WP and supplemented by the MOX and LaBS glass inventory, is adjusted to reflect the inventory distribution at repository closure and then is used to initialize source terms during each TSPA-LA Model realization (Table 6.3.7-5). The initial masses are then adjusted to account for uncertainty by applying the multipliers shown in Table 6.3.7-7. That is, at the beginning of each realization, the uncertainty multiplier for each waste form is sampled, and the inventories are adjusted by multiplying the uncertainty multiplier by the masses present at repository closure. The inventory is adjusted for radionuclide decay and ingrowth at each timestep by the simulation software using the first order decay rates shown on Figure 6.3.7-4. The CSNF WPs that are modeled in the TSPA-LA Model use the CSNF inventory values only, while the CDSP WPs contain both the DSNF and HLW inventories. The TSPA-LA Model calculates the specific activities for each radionuclide using the half-lives provided by DTN: MO0702PASTREAM.001_R0 [DIRS 179925].

Additional details regarding the placement of CSNF inventories into a GoldSim source element are provided in the discussion of the CSNF Waste Form Degradation Submodel (Section 6.3.7.4.1.3). The CSNF inventory discussion is presented in Section 6.3.7.4.1.3 because the TSPA-LA Model implementation specifically addresses inventory allocation based on the state of the CSNF waste form. Additional details regarding the placement of DSNF and HLW glass inventories into a GoldSim source element are provided in the discussion of the DSNF and HLW glass Waste Form Degradation Submodels (Sections 6.3.7.4.2.3 and 6.3.7.4.3.3). These inventory discussions are presented in Sections 6.3.7.4.2.3 and 6.3.7.4.3.3 because the TSPA-LA Model implementation specifically addresses inventory allocation based on the state of the DSNF waste form and HLW glass waste form.

6.3.7.2 In-Package Chemistry

The abstractions for determining the chemical parameters inside a failed WP are described in *In-Package Chemistry Abstraction* (SNL 2007 [DIRS 180506]), hereafter referred to as the

In-Package Chemistry Abstraction. As to be discussed in Section 6.3.7.2.1, in the TSPA-LA Model, CSNF WPs are discretized into two domains (Cell 1 and Cell 2) and CDSP WPs are discretized into three domains (Cell 1A, Cell 1B, and Cell 2). The In-Package Chemistry Abstraction discussed in this section, deals only with CSNF Cell 1, CDSP Cell 1A, and CDSP Cell 1B (they are collectively called waste form cells, as waste forms are located in those domains). Within the TSPA-LA Model, the In-Package Chemistry Submodel implements the In-Package Chemistry Abstraction to simulate the evolution of the water chemistry inside a failed WP as a function of the relative humidity provided by the EBS TH Environment Submodel (Section 6.3.2), P_{CO_2} provided by the EBS Chemical Environment Submodel (Section 6.3.4), and the water inflow rate provided by the EBS Flow Submodel (Section 6.3.6). Primary outputs from the In-Package Chemistry Submodel that are directly used in the TSPA-LA Model include pH, ionic strength, and total carbonate concentration (ΣCO_3) inside a failed WP.

The water chemistry determined by the In-Package Chemistry Submodel is used by four other Waste Form Degradation and Mobilization submodels. Specifically, the waste form matrix degradation rate for CSNF requires pH and ΣCO_3 ; the waste form matrix degradation rate for HLW requires pH; the dissolved concentration limits of radioactive elements require pH and ionic strength; and the stability of colloids requires pH and ionic strength. It is through the influences on other Waste Form Degradation and Mobilization Submodels that the In-Package Chemistry Submodel affects radionuclide availability for transport. Figure 6.3.7-5 is a schematic illustration of the inputs and outputs to and from the In-Package Chemistry Submodel.

6.3.7.2.1 Conceptual Model

The In-Package Chemistry Abstraction calculates the chemistry of water that has reacted with the WP components, including waste forms and basket materials, inside a failed WP. The In-Package Chemistry Submodel implements the abstraction in the TSPA-LA Model. The In-Package Chemistry Abstraction evaluates two different water ingress conceptual models:

- A vapor influx (non-dripping) model where the condensation of vapor onto the WP internals is simulated as pure water, and the resulting solution is in equilibrium with the relative humidity conditions in the drift (SNL 2007 [DIRS 180506], Section 6.3[a]).
- A liquid influx (dripping case or seepage dripping) model where water from the drift, simulated as typical groundwater or drift wall condensate, enters a WP at a rate determined by the liquid influx rate through the openings in the breached WP (SNL 2007 [DIRS 180506], Section 6.3[a]).

Two types of WPs are considered by the In-Package Chemistry Abstraction: CSNF WPs and the CDSP WPs. Furthermore, CSNF WPs are discretized into two domains:

1. CSNF Cell 1 (CSNF Waste Form Domain). This cell contains all materials within and including the baskets inside the CSNF WP, excluding the guides. This includes the fuel basket assembly of neutron moderator material and thermal shunts, fuel basket tubes, and CSNF assemblies.

2. CSNF Cell 2 (CSNF WP Corrosion Products Domain). This cell contains the TAD canister, and guide assembly.

Similarly, the CDSP WPs are discretized into three domains:

1. CDSP Cell 1A (or 2DHLW Cell). This cell comprises two containers of DHLW glass and their canisters, as designed for the two Multi Canister Overpack 2MCO/2DHLW WP.
2. CDSP Cell 1B (or 2MCO Cell). This cell comprises two containers of N reactor fuel and their canisters, as designed for the 2MCO/2DHLW WP.
3. CDSP Cell 2 (CDSP WP Corrosion Products Domain). This cell contains the divider plate, outer brackets, support tube, and inner vessel.

The In-Package Chemistry Abstraction discussed in this section deals only with CSNF Cell 1, CDSP Cell 1A, and CDSP Cell 1B. The chemistry of Cell 2 of CSNF and CDSP WPs are discussed in Section 6.3.8.

The In-Package Chemistry process model considers the 2MCO/2DHLW WPs, although the most numerous CDSP WPs are the 5DHLW/1DSNF Long. The reasons and justifications for doing that are given in Section 6.6.6[a] of *In-Package Chemistry Abstraction* (SNL 2007 [DIRS 180506]).

The In-Package Chemistry Abstraction conceptual model is discussed in Section 6.3[a] of *In-Package Chemistry Abstraction* (SNL 2007 [DIRS 180506]), and is briefly described in the paragraphs below.

The In-Package Chemistry Abstraction conceptual model is a batch reactor model that consists of water, oxygen, carbon dioxide, waste forms, and metal alloys. The batch reactor system is in equilibrium with atmospheric conditions, and the reactants degrade in the presence of water according to a rate determined by the physical properties and the exposed surface area of each reactant. For each solid reactant, a degradation rate is selected based on experimental measurements, and the surface area available to react is calculated based on the dimensions of the WP internals. During reaction progress, waste forms and metal alloys are consumed, secondary mineral phases and metal (hydr) oxide corrosion products precipitate from solution, and water changes in its composition and mass due to these reactions.

Inputs for the In-Package Chemistry Abstraction models include thermodynamic properties, parameters such as waste form reaction rates and incoming water compositions, gas phase P_{CO_2} , and compositions and degradation rates of WP components (SNL 2007 [DIRS 180506], Sections 6.3[a]).

Physical-chemical processes considered by the In-Package Chemistry Abstraction model include kinetic dissolution of waste forms and WP internal components, equilibrium precipitation and dissolution of secondary minerals and metal corrosion products, equilibrium oxidation and reduction reactions among gases, secondary minerals, and aqueous species, incoming water compositions, and thermal effects on aqueous phase chemistry (SNL 2007 [DIRS 180506], Section 6.3[a]).

Additional sensitivity cases were run to evaluate the system response to changes in the base-case model. These sensitivity cases evaluated different quantities of water inside the failed WP, different seepage compositions, the oxidation state of chromium, different temperatures, P_{CO_2} and P_{O_2} , different water fluxes into the failed WP, different WP and waste form configurations and inventories, different corrosion rates of the WP internals, different predominant iron minerals (goethite versus hematite), and different degradation rates of the waste forms inside the failed WP (SNL 2007 [DIRS 180506], Sections 6.6[a]). These sensitivity studies were used to develop an uncertainty range around the base-case model results.

6.3.7.2.2 Model Abstraction

The In-Package Chemistry Abstractions are derived from the output of the In-Package Chemistry Process Models (SNL 2007 [DIRS 180506]) and provide either parameter distributions or response surfaces for the TSPA-LA Model. Both the vapor influx model and the liquid influx model have separate process and abstraction models, which allow the TSPA-LA Model to implement non-dripping and dripping conditions. In the *In-Package Chemistry Abstraction* (SNL 2007 [DIRS 180506]), the process model output is discussed in Section 6.5[a] and the abstraction model output, combining the base-case results presented in Section 6.5[a] with the sensitivity studies presented in Section 6.6[a], is discussed in Section 6.10[a]. In this section, the in-package ionic strength and pH abstractions are presented for CSNF Cell 1, CDSP Cell 1A, and CDSP Cell 1B under liquid influx and vapor influx conditions. There are total 12 abstractions (six for ionic strength and another 6 for pH) for the three types of cells under two different water influx conditions. The ΣCO_3 abstraction is developed from equilibrium mass action equations and is presented as a single equation for both liquid influx and vapor influx conditions for CSNF Cell 1 only because HLW glass and DSNF degradation rate calculations do not require this parameter.

The geochemical modeling codes, EQ3NR (Software Code: EQ3/6 V7.2b (CRWMS M&O 1999 [DIRS 153964])) and EQ6 (STN: 10075-7.2bLV-02 [DIRS 159731]), were used to simulate the in-package chemical environment (SNL 2007 [DIRS 180506], Section 1[a]). The In-Package Chemistry Abstraction simplifies the outputs into a form compatible with implementation in the TSPA-LA Model, as to be discussed below.

The abstractions of in-package chemistry are applicable for oxidizing conditions ($f_{O_2} = 10^{-0.7}$ bars), a P_{CO_2} range of 10^{-4} to $10^{-1.5}$ bars, a temperature range from 25°C to 100°C, a relative humidity for vapor influx equal or higher than 95 percent, and a water volumetric flux (hereafter referred to as “flux”) for liquid influx equal or higher than 0.1 L/yr (SNL 2007 [DIRS 180506], Section 8.1[a], Table 8-1[a]). Spatially, the applicability of the In-Package Chemistry Abstraction is limited to the waste form cells (i.e., Cell 1 of CSNF WPs, Cell 1a and Cell 1b of CDSP WPs).

The abstraction for the In-Package Chemistry Submodel consists of five parts:

- Part I. Determination of whether In-Package Chemistry needs to be calculated
- Part II. Determination of which abstraction to be used

Part III. Calculation of ionic strength

Part IV. Calculation of pH

Part V. Calculation of the total concentration of aqueous carbonate (for CSNF Cell 1 only).

These parts are discussed in detail below and summarized in Table 6.3.7-8.

Part I. Determine if In-Package Chemistry needs to be calculated—Whenever the water inflow rate is less than 0.1 L/yr and relative humidity is lower than 95 percent, no in-package chemistry calculation is conducted. The reason is, as stated in *In-Package Chemistry Abstraction* (SNL 2007 [DIRS 180506], Section 6.10.9.1[a]), a relative humidity of 95 percent is the minimum threshold value required to predict a meaningful pH and ionic strength from the vapor influx model. “Given the ultimately small volume of water film being considered at these relative humidity conditions (Relative Humidity < 95 percent), virtually all of the waste form materials degraded under these conditions will be precipitated in place and not be available for transport. The small mass of radionuclides that remains dissolved in this minuscule water volume would also not be available for transport because the water film is not expected to be interconnected under these conditions” (SNL 2007 [DIRS 180506], Section 6.10.9.1[a]). In other words, under such conditions, the in-package chemistry becomes undefined, and the in-package chemistry submodel is turned off. The solubilities for all radionuclides, including colloidal species, are set to zero so that no transport is allowed.

However, degradation of waste forms is not considered as ceased below the 95 percent relative humidity threshold because the non-interconnected water film does not prevent waste form from degrading. There are no measurements or methods to calculate waste form degradation rates under vapor flux conditions below 95 percent relative humidity. *In-Package Chemistry Abstraction* (SNL 2007 [DIRS 180506], Section 6.10.9.1[a]) gives the following estimated values for the HLW glass and CSNF waste forms:

1. For HLW glass, its degradation rate under such conditions is assumed to be equal to the degradation rate at pH of 10 under aqueous corrosion conditions, as is done in the TSPA for temperatures greater than 100°C (Assumption 5.5[a]).
2. For CSNF waste form, its degradation rate under such conditions is assumed to be equal to the degradation rate between pH of 6 and 7 under aqueous corrosion conditions. In the TSPA-LA Model, the pH value that is only used to calculate the CSNF degradation rate is uniformly sampled between 6 and 7.

Part II. Determine which abstraction to be used—Whenever the relative humidity is greater than 95 percent or the water inflow rate is greater or equal to 0.1 L/yr, the In-Package Chemistry Submodel is activated, and a decision is to be made to select one of the two abstractions (the vapor influx versus the liquid influx) to generate outputs for ionic strength and pH. The choice depends on the relative humidity, the water flux rate, and the abstraction that predicts lower ionic strength, as shown in Table 6.3.7-8.

As indicated in Table 6.3.7-8, ionic strength is calculated using the vapor influx abstraction whenever the liquid influx rate is less than 0.1 L/yr (and the relative humidity is equal or greater than 95 percent). At or above 0.1 L/yr, ionic strength is calculated using the liquid influx abstraction. There is an exception that if the vapor influx abstraction predicts a lower ionic strength than that predicted by the liquid influx abstraction, then the vapor influx result should be used. In other words, the vapor influx abstraction is used to set a reasonable upper limit for ionic strength. Its justification is provided in *In-Package Chemistry Abstraction* (SNL 2007 [DIRS 180506], Section 6.10.9.1[a]).

Part III. Calculate Ionic Strength—Ionic strength abstractions for the vapor influx case are given as functions of relative humidity with uncertainty added. The mean value is a piecewise linear function of relative humidity:

$$I = a + b * RH \quad (\text{Eq. 6.3.7-1})$$

The intercept (a) and the slope (b) in the above equation have different values under different relative humidities. Table 6.3.7-9 gives those values for CSNF Cell 1, CDSP Cell 1A, and CDSP Cell 1B. The uncertainty range is between the mean value times the lower uncertainty factor (fmin) and the mean value times the upper uncertainty factor (fmax) (i.e., $I \times f_{\min}$, $I \times f_{\max}$). A triangular distribution is assigned for the uncertainty range, with the mean value as the most likely value. The uncertainty factors are also shown in Table 6.3.7-9.

Ionic strength abstractions for the liquid influx case are presented in the logarithm space and are functions of water inflow rate through the breached WPs and time since the representative WP breached. The mean values of logarithm of ionic strength are presented as two-dimensional look-up tables, which are given in Tables 6.3.7-10 through 6.3.7-12 for CSNF Cell 1, CDSP Cell 1A, and CDSP Cell 1B, respectively.

Uncertainties are also included in the logarithm of ionic strength abstractions for the liquid influx case and are presented as a deviation from the mean value. Triangular distributions are assigned to the logarithm of ionic strength for the liquid influx case. That is, the minimum, most likely, and the maximum values are mean-deviation, mean, and mean+deviation, respectively. The deviations are also functions of water inflow rate through the breached WPs and time since breached, presented as two-dimensional look-up tables, which are given in Tables 6.3.7-13 through 6.3.7-15.

Part IV. Calculate pH—When the water influx rate is greater or equal to 0.1 L/yr, the liquid influx pH abstraction will be used to determine in-package pH ranges. The maximum and minimum pHs are functions of $p\text{CO}_2$ (the negative logarithm of P_{CO_2}) and log ionic strength as shown in Tables 6.3.7-16 through 6.3.7-21 for those three different cells under the liquid influx conditions.

When the water influx rate is less than 0.1 L/yr, the vapor influx pH abstraction will be used to determine in-package pH ranges. The maximum and minimum pHs are functions of $p\text{CO}_2$ and log ionic strength, as shown in Tables 6.3.7-22 through 6.3.7-27 for those three different cells under the vapor influx conditions.

For a given $p\text{CO}_2$, the pHs have a uniform distribution between the minimum and maximum pH values defined in the look-up tables in *In-Package Chemistry Abstraction* (SNL 2007 [DIRS 180506], Section 6.10.9.1[a]).

Part V Total Carbonate Concentration Abstraction— ΣCO_3 is used in the degradation rate law for the CSNF waste form. An expression for ΣCO_3 (mol/kg) as a function of temperature, pH, and $P\text{CO}_2$ is based on equilibrium mass action expressions, as discussed in *In-Package Chemistry Abstraction* (SNL 2007 [DIRS 180506], Section 6.10.5). The ΣCO_3 abstraction is captured in *In-Package Chemistry Calculations and Abstractions* (DTN: SN0702PAIPC1CA.001_R2, [DIRS 180451], worksheet *Total Carbonate Validation in Total Carbonate and Eh Abstractions.xls*) as:

$$\Sigma \text{CO}_3 = P\text{CO}_2 \left(10^{K_1} + 10^{pH+K_1+K_2} + 10^{2pH+K_1+K_2+K_3} \right) \quad (\text{Eq. 6.3.7-2})$$

where $P\text{CO}_2$ is the carbon dioxide partial pressure in the gas phase. The in-drift $P\text{CO}_2$ (in units of bars) is provided by the EBS Chemical Environment Submodel (Section 6.3.4).

The K_i values in Equation 6.3.7-2 are temperature dependent. Table 6.3.7-28 provides the temperature-dependent K values. The ΣCO_3 abstraction is valid for temperatures ranging from 0°C to 100°C (SNL 2007 [DIRS 180506], Section 6.10.5).

The In-Package Chemistry Abstraction (SNL 2007 [DIRS 180506], Section 1[a]) lists several other limitations of the model, including: (1) limited availability of data on thin film chemistry; (2) limited availability of long-term metal alloy corrosion information such as the identities of the long-term corrosion products and the evolution of the surface area of the metal WP components as a function of time; (3) simplifications used to define the important processes in the waste form cells; (4) an assumption involving the pH under low water conditions and (5) the approach used to simulate the effects of evaporation.

6.3.7.2.3 TSPA-LA Model Implementation

The abstracted results from the In-Package Chemistry Abstraction are implemented in the TSPA-LA Model to quantify the temporal evolution of values of the aqueous chemistry variables pH, ionic strength, and ΣCO_3 . In the TSPA-LA Model, the In-Package Chemistry Submodel is implemented for four different abstraction conditions representing CSNF and CDSP WPs that have water flow through them and CSNF and CDSP WPs that do not have water flow through them. A WP can have water flow through it only if it is in a dripping environment and its DS has failed and the WP failure is not a crack (e.g., cracks cannot support liquid influx (Section 6.3.6.1)). If WPs in a dripping environment are not dripped upon because the DSs remain intact, or the only failure is a crack, the In-Package Chemistry Submodel for non-dripping conditions (i.e., no water flow through the WPs) is evaluated for the WPs.

For the In-Package Chemistry Submodel, the time reference is to the elapsed time that a WP has been failed. Because the TSPA-LA Model models groups of failed WPs with each member of a group having the same in-package chemical compositions, it is possible that WPs within a group are failed for different periods of time. To account for this, the TSPA-LA Model calculates an average WP failure time for each group of WPs and uses this average time to evaluate the time

dependence for the In-Package Chemistry Submodel. The algorithm for determining the average failed duration in a group of failed WPs is determined by weighting the elapsed duration of failure for the WPs failed in the previous timestep (including the current timestep length) with the new failures in this timestep:

$$\bar{t} = \frac{(N_{WPF_{Failed}}^{New} \times \frac{1}{2} \text{TimeStepLength}) + (N_{WPF_{Failed}}^{Prev} \times (\bar{t}^{prev} + \text{TimeStepLength}))}{N_{WPF_{Failed}}^{New} + N_{WPF_{Failed}}^{Prev}} \quad (\text{Eq. 6.3.7-3})$$

where

- \bar{t} = the average failure time
- $N_{WPF_{Failed}}^{New}$ = the number of new failures in the current timestep
- $N_{WPF_{Failed}}^{Prev}$ = the number of failures in the previous timestep
- \bar{t}^{prev} = the previous value of the average failure time
- TimeStepLength = the timestep length.

Note that this implementation assigns one-half of a timestep length for newly failed WPs (i.e., on average, the new failures occur halfway through the current timestep). In the TSPA-LA Model, for the purposes of evaluating in-package chemistry, the average WP failure time for the current timestep is set to zero years if the WP temperature exceeds the boiling point of water (i.e., dry conditions prevail in the WP).

The In-Package Chemistry Submodel is implemented by accessing abstractions corresponding to the WP type and dripping condition. These abstractions include distributions representing epistemic uncertainties. For pH, uniform distributions are specified for a given pCO₂, and for ionic strength, triangular distributions are specified for a given relative humidity for the vapor influx case or log-triangular distributions are specified for a given time and a given water inflow rate for the liquid influx case. Since pCO₂, relative humidity, and water inflow rate all are time-dependent variables in the TSPA-LA Model, the recommended distributions for pH and ionic strength are also time dependent. In other words, the recommended distributions change with time and depend on the outputs of other submodels. Therefore, the pH and ionic strength values for each realization cannot be predetermined by simple sampling prior to the beginning of the realization. To properly account for this time-dependent nature of the In-Package Chemistry Abstraction, dynamic sampling techniques have been implemented in the TSPA-LA Model.

The dynamic sampling technique samples a distribution representing the CDF percentile defined by the specified distributions (for pH it is uniform, for ionic strength it is either triangular or log triangular) for each realization. This percentile remains constant for each realization for the whole duration of the simulation. The distributions are then determined at each timestep after the values of the time-varying variables become known. After that, this percentile is applied to the distributions to obtain a pH or an ionic strength values for the current timestep.

For example, for realization i , the sampled percentile for pH is 85 percent. At time t , the value of $p\text{CO}_2$ is 2 and ionic strength is 1 for the CSNF Cell 1 of the liquid influx case. According to Tables 6.3.7-16 and 6.3.7-19, the maximum and minimum of pH are 7.19 and 4.99, respectively. Thus, the pH value at the current timestep is $4.99 + 0.85 \times [7.19 - 4.99] = 6.86$. The ionic strength values at each timestep are obtained dynamically by a similar scheme, although it is a little bit more complicated than pH because it has a triangular or a log-triangular distribution.

The ΣCO_3 is calculated at each timestep using Equation 6.3.7-2 and the relationships provided in Table 6.3.7-28. The variables in the calculation include: (1) the calculated pH from the In-Package Chemistry Submodel (discussed above), (2) the WP temperature provided by the EBS TH Environment Submodel (Section 6.3.2), and (3) the P_{CO_2} provided by the EBS Chemical Environment Submodel (Section 6.3.4).

At each timestep, the outputs from the In-Package Chemistry Submodel are provided to four other Waste Form Degradation and Mobilization submodels. The pH and ΣCO_3 are provided to calculate the waste form matrix degradation rate for CSNF and the pH is also provided to calculate the degradation of HLW. The pH and ionic strength are provided to calculate solubility limits of radionuclides and to calculate the stability of colloids.

The outputs from the In-Package Chemistry Submodel are provided for each representative CSNF and CDSP cell (Section 6.1.4.7) in dripping and non-dripping environments in each percolation subregion. These outputs are:

- pH as a function of time
- Ionic strength as a function of time
- ΣCO_3 as a function of time.

6.3.7.3 Cladding Degradation

Most CSNF is encased in zirconium-alloy cladding, and a small percentage is encased in stainless steel cladding. In the TSPA-LA compliance model, no cladding credit is taken for CSNF (SNL 2007 [DIRS 180616], Section 6.2.1.2[a] and Table 7-2[a]). In addition, DSNF cladding has been excluded from consideration in the TSPA-LA Model (DTN: MO0706SPA FEPLA.001_R0 [DIRS 181613], FEP Number 2.1.02.25.0A).

Naval SNF, as discussed in Section 6.3.7.1.1, is conservatively treated as CSNF in the TSPA-LA. Section 7.5.3 demonstrates that the dose resulting from a commercial WP is higher than the dose resulting from a naval WP (Section 7.5.3); thus, representing naval WPs as commercial WPs is conservative. Removing the CSNF cladding credit from the TSPA-LA calculations will not alter that conclusion.

6.3.7.3.1 Conceptual Model

The cladding of all CSNF and DSNF is assumed to be failed upon arrival at the repository (Section 5.1.3).

6.3.7.3.2 TSPA-LA Model Implementation

The TSPA-LA Model contains only two cladding related parameters: a cladding failure parameter and a cladding splitting parameter. In the TSPA-LA compliance model no credit is taken for CSNF cladding, therefore, it is assumed that the initial fraction of failed cladding (Initial_Rod_Failures), and the fraction of fuel available for corrosion (Fuel_Split_Fraction), is one.

6.3.7.4 Waste Form Degradation

The CSNF Waste Form Degradation Abstraction for the TSPA-LA Model is described in *CSNF Waste Form Degradation: Summary Abstraction* (BSC 2004 [DIRS 169987]). The DSNF Waste Form Degradation Abstraction for the TSPA-LA Model is described in *DSNF and Other Waste Form Degradation Abstraction* (BSC 2004 [DIRS 172453]). The HLW Glass Degradation Abstraction for the TSPA-LA Model is described in *Defense HLW Glass Degradation Model* (BSC 2004 [DIRS 169988]). The abstraction models for the waste form matrix estimate the rates at which the CSNF and HLW waste forms degrade as a function of chemical conditions in failed WPs. For DSNF waste forms, an instant degradation rate is implemented, and will be discussed in detail in Section 6.3.7.4.2.

In the TSPA-LA Model, radionuclide inventory added to a GoldSim source element and bound by a matrix (i.e., UO₂ or borosilicate glass) is not available for transport from a failed WP until the binding matrix degrades. The waste form degradation rates, calculated using the submodels discussed below, are applied by GoldSim source elements. Within each source element, the per-package inventory subject to waste form degradation prior to release from the source element is specified by defining an inventory and then specifying that the inventory is “bound in matrix” in the GoldSim source element. The source element requires a fractional degradation rate, and in the TSPA-LA Model, the applicable rate is the output of the Waste Form Degradation submodels, discussed below. Additional details on the use of GoldSim source elements are provided in Section 6.3.8 and in *User’s Guide, GoldSim Probabilistic Simulation Environment Version 9.60* (GoldSim Technology Group 2007 [DIRS 181727]). The source element applies the degradation rate to the bound inventory, releasing the inventory into the cell network where it then becomes available for transport. Transport of available inventory added to the cell network is discussed in Section 6.3.8.2.1.

Section 6.3.7.4.1 discusses the availability of CSNF inventory from the CSNF source elements in the TSPA-LA Model. Section 6.3.7.4.2 discusses the availability of DSNF inventory in the TSPA-LA Model. Section 6.3.7.4.3 discusses the availability of HLW glass inventory in the CDSP WP source elements of the TSPA-LA Model.

6.3.7.4.1 Commercial Spent Nuclear Fuel Waste Form Degradation

In the TSPA-LA Model, the CSNF Waste Form Degradation Submodel implements the CSNF Waste Form Degradation Abstraction described in *CSNF Waste Form Degradation: Summary Abstraction* (BSC 2004 [DIRS 169987]). Internal inputs to the CSNF Waste Form Degradation Submodel include representative WP temperature provided by the EBS TH Environment Submodel (Section 6.3.2) and pH and ΣCO₃ provided by the In-Package Chemistry Submodel

(Section 6.3.7.2). In addition to the temperature, pH, and total carbonate concentration inputs, the CSNF Waste Form Degradation Submodel is also dependent on the partial pressure of oxygen in the failed WP. The output of the CSNF Waste Form Degradation Submodel is the CSNF fractional degradation rate.

6.3.7.4.1.1 Conceptual Model

CSNF pellets and radionuclides in fuel rods with failed cladding will be isolated from the external repository environment until the CSNF WPs are breached. After a CSNF WP is breached, the CSNF may be exposed to dripping water or humid air. Upon exposure to moisture, radionuclides may be released by: (1) instantaneous release of the gap and grain boundary inventories of cesium, iodine, technetium, and strontium; (2) dissolution of the fuel matrix inventory under alkaline and acidic conditions; and (3) instantaneous release of carbon in the WP hardware, external to the cladding. The gap and grain boundary inventory denotes the fission gasses and more mobile radionuclides such as cesium, iodine, and technetium that migrated out of the fuel matrix during reactor operations and accumulated between the fuel pellets and cladding and the fuel matrix grain boundaries. In the TSPA-LA Model, because radionuclides in the gap and grain boundary may be released rapidly, CSNF fuel rods are modeled as two heterogeneous fractions: the matrix inventory and the combined gap and grain boundary inventory. The radionuclide inventory in the fuel matrix is referred to as the bound inventory. The inventory in the gap and grain boundary regions is referred to as the unbound inventory and is modeled as being available for instantaneous release from fuel rods. Additionally, a third CSNF inventory, the carbon inventory in the WP hardware region, is modeled as being available for instantaneous release from the failed WP.

The scope of the CSNF Waste Form Degradation Submodel does not address processes that control the extent to which the radionuclides available for dissolution are mobilized as dissolved and colloidal species. Those features, events, and processes (FEPs) are addressed as follows: Dissolved Concentration Limits Submodel, Section 6.3.7.5; EBS Colloids Submodel, Section 6.3.7.6; and EBS Transport Submodel, Section 6.3.8 illustrates the dependence of CSNF fuel degradation on the In-Package Chemistry Submodel (Section 6.3.7.2) and temperature. Figure 6.3.7-6 provides a schematic drawing of the CSNF fuel rods and CSNF waste form degradation processes.

6.3.7.4.1.2 TSPA-LA Model Abstraction

The CSNF Waste Form Degradation Abstraction developed in *CSNF Waste Form Degradation: Summary Abstraction* (BSC 2004 [DIRS 169987]) provides two abstractions: the instantaneous release fraction of CSNF inventory and the mathematical model for the rate of degradation for the CSNF matrix.

The instantaneous release fraction is computed as the fraction of cesium, iodine, technetium, and strontium in the total inventory in CSNF fuel that is instantly available for release once cladding is degraded, as discussed in Sections 6.3.1 and 6.3.2 of *CSNF Waste Form Degradation: Summary Abstraction* (BSC 2004 [DIRS 169987]). The release fractions implemented in the TSPA-LA Model are captured in *CSNF Radionuclide Release Model* (DTN: MO0404ANLSF001.001_R0 [DIRS 169007]). The fraction of CSNF inventory that

makes up this instantaneous release inventory is specified by four triangular distributions, as defined in Table 6.3.7-29.

CSNF Waste Form Degradation: Summary Abstraction (BSC 2004 [DIRS 169987]) provides the discussion and mathematical forms for alkaline conditions (Section 6.4.1.2), for acidic conditions (Section 6.4.1.3), and for calculating the specific or absolute dissolution rate, subject to a range of pH conditions, temperature conditions, total carbonate concentrations, and oxygen partial pressures (Section 8.2). The mathematical forms, including coefficient values, implemented in the TSPA-LA Model are captured in *CSNF Radionuclide Release Model* (DTN: MO0404ANLSF001.001_R0 [DIRS 169007]). The specific or absolute dissolution rate is a function of four independent variables, which vary spatially in the repository: WP temperature in degrees Kelvin, aqueous pH, ΣCO_3 , and oxygen fugacity according to the rate law:

$$\log_{10}(F) = \log_{10}(A) + a_0 + a_1 \times IT + a_2 \times p\text{CO}_3 + a_3 \times p\text{O}_2 + a_4 \times pH \quad (\text{Eq. 6.3.7-4})$$

where dependent variable

$\log_{10}(F)$ = log base 10 of the fractional dissolution rate of the CSNF in unit of [1/d] (d stands for days)

and independent variables

IT = inverse temperature of the WP [K^{-1}] (i.e., $IT = 1/T$)

$p\text{CO}_3$ = negative base 10 log of ΣCO_3 [molar] (i.e., $p\text{CO}_3 = -\log_{10}([\text{HCO}_3^-] + [\text{CO}_3^{2-}])$)

$p\text{O}_2$ = negative base 10 log of the oxygen partial pressure (atmospheres)

pH = in-package pH

and parameters

$\log(A)$ = log base 10 of the fuel specific surface area (m^2/mg)

a_0, a_1, a_2, a_3, a_4 are regression parameters for the dissolution rate per unit area.

Under dripping conditions, the pH inside a failed WP is a function of the liquid flow rate through the failed WPs (Section 6.3.7.2). The flow rate through the failed WPs depends on the damage state of the WP outer shell and the dripping rate (Section 6.3.6), which may vary in the different percolation subregion environments in the TSPA-LA Model. Therefore, pH and $p\text{CO}_3$ are spatially dependent outputs of the In-Package Chemistry Submodel (Section 6.3.7.2) and in the TSPA-LA Model are calculated within each percolation subregion environment. The partial pressure of O_2 in the WP is a constant value of 0.2 bar and is equated to the partial pressure of O_2 in the drift environment, which is equal to atmospheric O_2 (See Section 5.1.3). The representative temperature of the WPs is a spatially dependent output of the EBS TH Environment Submodel (Section 6.3.2), and in the TSPA-LA Model it is calculated for each percolation subregion.

The dissolution rate is modeled for an alkaline state with a $\text{pH} \geq 6.8$ and an acidic state with a $\text{pH} < 6.8$. The equation used for the alkaline state does not include pH dependence ($a_4 = 0$) and is:

$$\log_{10}(F) = \log_{10}(A) + a_0 + a_1 \times IT + a_2 \times pCO_3 + a_3 \times pO_2 \quad (\text{Eq. 6.3.7-5})$$

The distribution for the log base 10 of the specific surface area and values for the coefficients are presented in Table 6.3.7-30.

The equation used for the acidic state is

$$\log_{10}(F) = \log_{10}(A) + a_0 + a_1 \times IT + a_3 \times pO_2 + a_4 \times pH \quad (\text{Eq. 6.3.7-6})$$

For the acidic state, the dissolution rate does not depend on the ΣCO_3 ($a_2 = 0$). The distribution for the log of specific surface area and the coefficient values is shown in Table 6.3.7-31.

6.3.7.4.1.3 TSPA-LA Model Implementation

After a WP is breached, the entire CSNF is exposed to moisture. Radionuclides are then released by: (1) instantaneous release of the gap fraction inventory and (2) matrix dissolution under alkaline or acidic conditions. Cesium, iodine, technetium, and strontium are in the instantaneous release inventory. The fraction of emplaced inventory that makes up the instantaneous release inventory for cesium, iodine, technetium, and strontium is determined by sampling four triangular distributions representing epistemic uncertainty. These distributions are sampled once per realization. The instantaneous release inventory, the product of the instantaneous release fraction, and the per-package inventory (accounting for decay and ingrowth) are treated as unbound inventory within the inner barrier function of the GoldSim source element (GoldSim Technology Group 2007 [DIRS 181727]).

Similarly, the ^{14}C hardware inventory, the product of the hardware inventory fraction, and the per-package inventory (accounting for decay and ingrowth), are treated as unbound inventory between the inner and outer barrier functions of the GoldSim source element. The hardware inventory fraction originates from neutron activation of stainless-steel hardware outside the fuel rods and is specified to be 18 percent of the ^{14}C inventory in a CSNF WP (SNL 2007 [DIRS 180472], Section 6.7 and Table 7-1[a]).

The TSPA-LA Model considers three CSNF inventories in each CSNF WP of a GoldSim source element (e.g., group of WPs). The first inventory in the CSNF WP is the ^{14}C hardware inventory. At the global level, the hardware inventory is calculated as the fraction of per-package inventory that is associated with the WP hardware and the per-package inventory, discussed in Section 6.3.7.1. This inventory is calculated at the global level but is added to each GoldSim source element within each percolation subregion environment. Within the GoldSim source element, this inventory is immediately released when the WP fails.

The second inventory in the CSNF source term is the instantaneous release inventory. At the global level, the instantaneous release inventory is calculated as the fraction of the per-package inventory that is in the gap and grain boundaries (BSC 2004 [DIRS 169987], Sections 6.3.1

and 6.3.2) and the per-package inventory, discussed in Section 6.3.7.1. The gap and grain boundary inventory fractions are presented in Table 6.3.7-29. If a radionuclide in the CSNF WP is not included in Table 6.3.7-29, the radionuclides' instantaneous release inventory is zero grams per WP. This inventory is calculated at the global level but is added to each GoldSim source element within each percolation subregion environment. Within the GoldSim source element, this inventory is immediately released when the WP fails.

The third inventory in the CSNF source term is the inventory bound in the CSNF matrix. At the global level, the bound inventory is calculated as the total per package inventory minus the other hardware and instantaneous release inventories. This inventory is calculated at the global level but is added to each GoldSim source element within each percolation subregion environment. Within the GoldSim source element, this inventory is bound in a matrix and is only available for transport after the matrix is degraded. In the CSNF WP, the matrix degrades at the calculated degradation rate, discussed in Section 6.3.7.4.1.2. Within an intact CSNF WP, the waste form does not degrade. In a failed CSNF WP, the waste form is allowed to degrade and make radionuclides available for transport.

The fractional degradation rate is calculated using the rate formulas (Equations 6.3.7-5 and 6.3.7-6 described in Section 6.3.7.4.1.2) for conditions with a pH greater than or equal to 6.8 and for conditions with a pH less than 6.8. Degradation rates under both alkaline and acidic conditions are a function of the specific surface areas of exposed fuel, the representative WP temperature provided at each TSPA-LA Model timestep by the EBS TH Environment Submodel (Section 6.3.2), ΣCO_3 provided at each TSPA-LA Model timestep by the In-Package Chemistry Submodel (Section 6.3.7.2), the in-package pH provided by the In-Package Chemistry Submodel (Section 6.3.7.2), and the partial pressure of oxygen inside the failed WP. A triangular distribution is used to represent epistemic uncertainty in a specific surface area of exposed fuel (Tables 6.3.7-30 and 6.3.7-31). This distribution is sampled once per realization and the sampled value is applied in all of the percolation subregion environment degradation rate calculations. The values for the uncertain coefficients in the rate expressions are correlated. The covariance matrix capturing the uncertainties in the rate coefficients was converted to a lower triangular matrix using the Cholesky Factorization method (DTN: MO0404ANLSF001.001_R0 [DIRS 169007]). In the TSPA-LA Model, the uncertainties in the rate model coefficients are sampled with correlation using a Cholesky factorization method to induce correlation using standard normal distributions, as described in Section 6.1.3.

At temperatures greater than 100°C, the In-Package Chemistry Submodel (Section 6.3.7.2) pH and ΣCO_3 are not valid, nor is the CSNF degradation rate equation. Within the TSPA-LA Model, when a breached CSNF WP is exposed to temperatures exceeding 100°C, the calculated CSNF degradation rate is replaced with a rate that instantaneously degrades the exposed waste form, as recommended in the CSNF Waste Form Abstraction (BSC 2004 [DIRS 169987], Section 8.1) and CSNF Radionuclide Release Model (DTN: MO0404ANLSF001.001_R0 [DIRS 169007]). A rate of 1×10^6 per year (i.e., 0.032 per second) is used in the TSPA-LA Model to implement this recommendation because it results in complete CSNF degradation within one year.

The calculated fractional degradation rate is input to the GoldSim source element located in each percolation subregion environment. The GoldSim source element applies the fractional

degradation rate to degrade the CSNF waste form within a failed WP. The fraction of failed WPs is discussed in Section 6.3.5. After the waste form is degraded, the GoldSim source element releases the mass associated with the degraded fuel into the volume occupied by the waste form alteration products, the schoepite rind, and the inventory becomes available for transport. In addition, the GoldSim source element releases the hardware inventory and the instantaneous release inventory into this same volume. For modeling purposes, a default volume is applied before waste form degradation is initiated. Section 6.3.8.2.1 provides the discussion for calculating the volume of rind formed as the CSNF waste form degrades and the subsequent transport of the available inventory to other areas of the failed WP.

A supplemental calculation is provided in the TSPA-LA Model to evaluate the average fraction of the CSNF that is degraded inside each failed WP. This supplemental calculation is provided as an analysis tool for evaluating the performance of the waste form and also provides a desirable result used to determine the volume of rind formed in the waste form (Section 6.3.8.2.1). This calculation is the average fraction of the CSNF waste form that is degraded in the failed CSNF WPs. Equation 6.3.7-7 is the evaluation of F_{cor} in the TSPA-LA Model:

$$F_{cor}(t) = \frac{M_i^{released}(t)}{M_i(t=0)} = 1 - \frac{M_i^{retained}(t)}{M_i(t=0)} \quad (\text{Eq. 6.3.7-7})$$

where

$M_i^{released}$ = the cumulative mass of radionuclide ‘i’ released from the degraded waste form in the failed CSNF WPs

$M_i^{retained}$ = the total mass of radionuclide ‘i’ retained by an undegraded waste form in the failed CSNF WPs

and

$M_i(t=0)$ = the initial inventory (in grams) of radionuclide ‘i’ associated with the failed CSNF WPs.

This calculation uses the knowledge of the internal functions and properties of a GoldSim source element (GoldSim Technology Group 2007 [DIRS 181727]) to evaluate the degradation state of the CSNF matrix inside each failed CSNF WP. The GoldSim source element internally tracks the value of $M_i^{released}$ used in the evaluation of Equation 6.3.7-7. $M_i^{retained}$ can be computed by performing a mass balance on the failed WPs, using the released inventory, $M_i^{released}$, and the initial inventory for the failed WPs, accounting for decay and ingrowth as necessary. As discussed below, the species considered in the TSPA-LA Model calculation of F_{cor} is a non-radioactive species that does not participate in the transport and dose calculations, and is added as supplemental inventory to each CSNF WP specifically to calculate F_{cor} .

The TSPA-LA Model includes 10 grams of an additional species ‘Col’ per CSNF WP. In the TSPA-LA Model ‘Col’ is an unreacting species that is added as a fully bound species in the CSNF waste form. ‘Col’ does not participate in radionuclide decay chains or contribute to the

total dose. As a noncompeting species in the transport calculations ('Col' does not influence the solubility of other elements), 'Col' can be used as a 'tracer' to evaluate the waste form performance. Within each GoldSim source element, the amount of inventory accounting for decay and ingrowth, and number of WPs (both failed and not failed), are internally tracked. In addition, the cumulative amount of each bound and unbound radionuclide, both retained by and released from the waste form, is also tracked. By performing a mass balance on the amount of 'Col' remaining in the waste form, the average fraction of the CSNF waste form that has degraded can be evaluated at each timestep. Within each percolation subregion environment, the total amount of 'Col' associated with the GoldSim source element for that percolation subregion environment is the product of the 'Col' inventory per WP and the number of WPs. The total amount of 'Col' retained by each GoldSim source element is an output of the GoldSim source element and is internally tracked by GoldSim. However, the internally tracked value includes both failed and not failed WPs and is not the value discussed in Equation 6.3.7-7, unless all of the WPs in the source term are failed. The total amount of 'Col' released by the failed WPs associated with each GoldSim source element, $M_i^{released}$ in Equation 6.3.7-7, is also an output of the GoldSim source element and is internally tracked by GoldSim, but it can also be computed by subtracting the amount retained from the total inventory of 'Col.' The total amount of 'Col' released by the GoldSim source element, divided by the number of failed WPs associated with the GoldSim source element, is the average amount of 'Col' released from each of the failed WPs. This result divided by the initial per-package inventory for those failed WPs yields the average fraction of 'Col' released from each failed WP represented by the source element. With the knowledge that the GoldSim source element congruently releases each bound species as the waste form degrades (i.e., if 10 percent of species X is released in one timestep, then 10 percent of all other bound species are also released in that timestep), the average fraction of the waste form degraded in each WP can be equated to the average fraction of 'Col' that is released from each failed WP. This result is used to determine the volume of fuel that is degraded in the CSNF water volume calculations (Sections 6.3.8.2.1) and assess the performance of the CSNF waste form and WP.

6.3.7.4.2 U.S. Department of Energy Spent Nuclear Fuel Waste Form Degradation

The DSNF Waste Form Degradation Abstraction for the TSPA-LA Model is described in *DSNF and Other Waste Form Degradation Abstraction* (BSC 2004 [DIRS 172453]). The DSNF Waste Form Degradation Submodel implements this abstraction and does not require inputs from other TSPA-LA Model submodels. The output of the DSNF Waste Form Degradation Submodel is the instantaneous release of the DSNF inventory from a breached CDSP WP.

6.3.7.4.2.1 Conceptual Model

Several hundred distinct types of DSNF may eventually be emplaced in the Yucca Mountain repository. It is not practical to attempt to determine the impact of each individual fuel type on dose. Instead, the DSNF Waste Form Degradation Abstraction categorized the DSNF in 11 groups (BSC 2004 [DIRS 172453], Sections 1.2, 6.1, and Table 6-2) to represent the entire DSNF inventory for the TSPA-LA Model. These DSNF groups are:

- Group 1 – Naval SNF

- Group 2 – Plutonium/uranium alloy (Fermi 1 SNF)
- Group 3 – Plutonium/uranium carbide (Fast Flux Test Facility -Test Fuel Assembly SNF)
- Group 4 – Mixed oxide and plutonium oxide (Fast Flux Test Facility -Demonstration Fuel Assembly / Fast Flux Test Facility -Test Demonstration Fuel Assembly SNF)
- Group 5 – Thorium/uranium carbide (Fort St. Vrain SNF)
- Group 6 – Thorium/uranium oxide (Shippingport light water breeder reactor SNF)
- Group 7 – Uranium metal (N-Reactor SNF)
- Group 8 – Uranium oxide (Three Mile Island-2 core debris)
- Group 9 – Aluminum-based SNF (Foreign Research Reactor SNF)
- Group 10 – Other (Miscellaneous Fuel)
- Group 11 – Uranium-zirconium hydride (Training Research Isotopes–General Atomics SNF).

For the TSPA-LA Model, an upper-limit degradation model is used for all the DSNF other than naval SNF. In this upper-limit degradation model, the DSNF inventory is immediately available for mobilization, subject to solubility constraints, after the outer surface of the CDSP WP is breached. The release rate of radionuclides from exposed naval SNF is less than that from exposed CSNF. To provide a conservative simplification, the TSPA-LA Model represents naval WPs with an equivalent number of commercial WPs, as discussed in Section 6.3.7.1 and in *Initial Radionuclide Inventories* (SNL 2007 [DIRS 180472], Section 6.2). Thus, naval SNF will not be discussed below as a specific type of DSNF. Figure 6.3.7-7 is a schematic illustration of DSNF waste form degradation within the CDSP WP as part of the model for waste form degradation.

6.3.7.4.2.2 TSPA-LA Model Abstraction

The DSNF Waste Form Degradation Submodel releases the entire per package DSNF inventory for solubilization and mobilization from the CDSP WPs when the WPs are breached. Because of this simplification, the DSNF inventory is treated as unbound inventory in the TSPA-LA Model, and no TSPA parameters are necessary to implement a degradation rate calculation in the TSPA-LA Model.

The volume of water associated with the degraded DSNF is a product of the DSNF rind porosity, rind saturation, and rind volume. Within the representative CDSP WP, the volume occupied by DSNF is 1.0 m³/WP (BSC 2004 [DIRS 172453], Section 8.1, Table 8-1). The porosity of the powdered form of the corrosion product occupying the volume of the DSNF is 0.20 and is fully saturated (SNL 2007 [DIRS 177407], Table 8.2-1).

6.3.7.4.2.3 TSPA-LA Model Implementation

In the TSPA-LA Model, the DSNF degradation rate is based on an instantaneous release of the radionuclide inventory and does not use any input parameters or rate equations. In addition, the DSNF inventory is not placed into a GoldSim source element with the HLW glass inventory. Instead, each time a CDSP WP fails, the DSNF inventory associated with the failed WP (accounting for decay and ingrowth) is placed into the volume of water associated with the volume occupied by the DSNF. Once released, radionuclides are available for transport to the WP corrosion products and through to the EBS, subject to solubility constraints.

In the TSPA-LA Model, the initial DSNF inventory, with the uncertainty described in Section 6.3.7.1 accounted for, changes through time as a result of radionuclide decay. The DSNF inventory for a single package is fed into a GoldSim source element at the global level of the TSPA-LA Model. This source element is used strictly for decay and ingrowth calculations for DSNF inventory and has been specified such that it is not allowed to fail and is, therefore, not a DSNF source for radionuclide releases. This implementation is a calculation to account for radionuclide decay. For each representative inventory (i.e., CSNF, DSNF, or HLW glass), a GoldSim source element internally tracks all of the radionuclide decay calculations for the specified decay chains. By utilizing a source element with the DSNF inventory, the TSPA-LA Model simplifies the implementation of the radionuclide decay and ingrowth calculations for DSNF inventory and is consistent with the decay rates specified for the HLW glass and CSNF inventories. Each time a CDSP WP fails, this DSNF source element is queried for the DSNF inventory, adjusted for decay and ingrowth, and the TSPA-LA Model subsequently adds a discrete amount of mass, equivalent to the current amount of “unexposed” mass in the DSNF source element, into the CDSP WP EBS cell network (Section 6.3.8) for each failed CDSP WP.

The volume of water associated with the fully saturated DSNF corrosion product is a product of the DSNF rind porosity, rind saturation, and DSNF volume.

6.3.7.4.3 High-Level Radioactive Waste Glass Waste Form Degradation

The HLW Glass Waste Form Degradation Submodel for the TSPA-LA Model is described in the HLW Glass Degradation Abstraction (BSC 2004 [DIRS 169988]). Internal inputs to the HLW Glass Degradation Submodel of the TSPA-LA Model include representative WP temperature and relative humidity provided by the EBS TH Environment Submodel (Section 6.3.2), and pH provided by the In-Package Chemistry Submodel (Section 6.3.7.2). The output from the HLW Glass Waste Form Degradation Submodel is the HLW radionuclide fractional degradation rate and the average fraction of the HLW glass that is degraded in each failed WP.

6.3.7.4.3.1 Conceptual Model

The HLW Glass Degradation Abstraction provides a rate equation that describes the degradation rate of HLW glass when the HLW glass is contacted by water or humid air. The radionuclide release rate is calculated as the product of the surface area of HLW glass contacted by water, the degradation rate of the HLW glass, and the mass fractions of the radionuclides in the HLW glass. Degradation of the HLW glass does not occur in the TSPA-LA Model when the relative humidity is less than 44 percent. Mathematical expressions and parameter values for the HLW

glass surface area and degradation rate are described in the following section. The mass fractions of radionuclides in the HLW glass are obtained from the Initial Radionuclide Inventory Abstraction described in Section 6.3.7.1. The HLW Glass Degradation Abstraction also provides functional relationships for the volume of water in the HLW glass degradation products (the rind) and the rind thickness. These parameters are used to model in-package radionuclide transport (Section 6.3.8.2.2) and calculate the diffusive release of radionuclides from the HLW rind. Although the HLW Glass Degradation Abstraction provides the conceptual model for both the glass degradation rate and the subsequent mass and volume of the rind formed from the degradation process, the discussion of the conceptual model for rind formation is deferred to Section 6.3.8.2.2. The rind layer affects the transport of the radionuclides after they become available. The discussions presented in Section 6.3.7, pertain to radionuclide availability, and the discussions presented in Section 6.3.8, pertain to the transport of available radionuclides.

6.3.7.4.3.2 TSPA-LA Model Abstraction

The HLW glass fractional degradation rate is the main quantity calculated in the TSPA-LA Model by the HLW Glass Waste Form Degradation Submodel.

Glass Degradation and Radionuclide Release—The same rate expression is used to calculate the degradation rate of HLW glass exposed to humid air, exposed to dripping water, or immersed in water, as discussed in Section 8.1 of *Defense HLW Glass Degradation Model* (BSC 2004 [DIRS 169988]). The resulting simplified HLW glass dissolution rate expression for the TSPA-LA Model is captured in HLW Glass Degradation Model (DTN: MO0502ANLGAMR1.016_R0 [DIRS 172830]):

$$rate_G = k_E 10^{\eta \cdot pH} \exp(-E_a / RT) \quad (\text{Eq. 6.3.7-8})$$

where

- $rate_G$ = absolute HLW glass dissolution rate (g/m²/d)
- k_E = rate coefficient (g/m²/d)
- η = pH dependence coefficient (dimensionless)
- E_a = effective activation energy (kJ/mol)
- R = universal gas constant (8.14E-03 kJ/mol/K)
- T = temperature (K).

The rate equation requires the specification of three parameter values: k_E , η , and E_a , and the two model variables, temperature and pH. HLW glass degradation does not occur if relative humidity is less than 44 percent (BSC 2004 [DIRS 169988], Section 8.1). If the relative humidity is greater than or equal to 44 percent, the same rate expression is used to calculate the degradation rate when HLW glass is exposed to humid air or dripping water, or is immersed in water. However, separate sets of parameter values are used for degradation in acidic and alkaline solutions. Values for η , E_a , and distributions for k_E for acidic and alkaline solutions are provided in Table 6.3.7-32. In accordance with the guidance provided in Section 8.1 of *Defense*

HLW Glass Degradation Model (BSC 2004 [DIRS 169988]), the degradation rate that is applied in the TSPA-LA Model is the greater of the acidic and alkaline condition degradation rates, regardless of modeled pH. At temperatures greater than 100°C, the In-Package Chemistry Submodel (Section 6.3.7.2) pH calculation is not valid. Therefore, the abstracted rate model, Equation 6.3.7-8, cannot be applied when the representative WP temperature is greater than 100°C. Within the TSPA-LA Model, when a breached CDSP WP is exposed to temperature exceeding 100°C, the abstracted HLW degradation rate model becomes independent of the pH. The developed rate equation is equivalent in form to Equation 6.3.7-8, replacing the pH term with a constant value (= 10) (BSC 2004 [DIRS 169988], Section 8.1). In addition, the alkaline side model coefficients are used to evaluate the modified rate equation. Furthermore, as stated in Section 8.1 of *Defense HLW Glass Degradation Model* (BSC 2004 [DIRS 169988]), glass degradation does not occur when relative humidity is below 44 percent (equivalent to a temperature of 125°C). Under such conditions, the degradation rate of HLW glass is set to zero.

However, if the temperature exceeds the melting point of the glass, as may occur in the Igneous Intrusion Modeling Case, volatile radionuclides may be released. As the glass cools, new crystalline and glass phases may form, which have different radionuclide-retaining properties from the original glass. In order to bound the uncertainty in the release fraction of the volatile radionuclides and in the degradation rates of radionuclide-containing phases, it is assumed that the glass will degrade instantaneously during an igneous intrusion.

The HLW glass mass dissolution rate, presented in *Defense HLW Glass Degradation Model* (BSC 2004 [DIRS 169988], Section 8.1) and captured in HLW Glass Degradation Model (DTN: MO0502ANLGAMR1.016_R0 [DIRS 172830]), is the specific rate, $rate_G$, multiplied by the surface area available for dissolution over a timestep. The surface area that remains as the HLW glass degrades is the product of the specific surface area, the exposure factor, and the mass of HLW glass that remains. The expression used to calculate the HLW glass surface area (m^2) as HLW glass dissolves in a timestep is:

$$S = f_{\text{exposure}} S_{sp} (M_0 - \sum M_t) \quad (\text{Eq. 6.3.7-9})$$

where

S_{sp} = the geometric specific surface area available for reaction (m^2/kg)

f_{exposure} = the exposure factor (accounting for the higher effective surface area of the glass log resulting from cracking of the HLW glass after it is poured into the canister)

M_0 = the initial mass of HLW glass (kg)

$\sum M_t$ = the total mass of HLW glass degraded in all previous timesteps (kg).

The mass of HLW glass degraded in a timestep is calculated as the product of the HLW glass degradation rate for that realization and the duration of the timestep. Table 6.3.7-32 provides the value for the specific surface area. The initial mass of HLW glass is 2,710 kg (DTN: MO0502ANLGAMR1.016_R0 [DIRS 172830]).

The expression used to calculate the surface area for the next timestep is:

$$S = 2.70 \times 10^{-3} f_{\text{exposure}} (2710 - \sum M_t) \quad (\text{Eq. 6.3.7-10})$$

The exposure factor is an uncertain parameter with sampling shown in Table 6.3.7-32. The initial timestep is conducted with $\sum M_t = 0$. The value of $\sum M_t$ is revised after each timestep by adding the mass of HLW glass degraded over the current TSPA-LA Model timestep, as shown below:

$$M_t = \text{rate}_G \times \Delta t \times S \quad (\text{Eq. 6.3.7-11})$$

The release rate of radionuclides due to HLW glass degradation is the product of the HLW glass mass dissolution rate and the mass fraction of a radionuclide in the HLW glass:

$$R_{RN} = S \times \text{rate}_G \times I_{RN} \quad (\text{Eq. 6.3.7-12})$$

where

$$\begin{aligned} R_{RN} &= \text{radionuclide release rate (Ci/d)} \\ I_{RN} &= \text{mass fraction of a radionuclide in the HLW glass (Ci/g)}. \end{aligned}$$

The radionuclide release rate determines the rate of radionuclide release from degraded HLW glass to the volume of water in the rind of altered HLW glass.

6.3.7.4.3.3 TSPA-LA Model Implementation

The HLW glass source term within each percolation subregion environment of the TSPA-LA Model contains two HLW glass inventories: a bound inventory and an unbound inventory. In the TSPA-LA Model, the HLW glass inventory is fully bound in the glass; therefore, the unbound inventory becomes zero grams for each radionuclide in the glass inventory (Section 6.3.7.1). The unbound inventory is included in the TSPA-LA Model to facilitate the development of sensitivity runs. Both inventories are added to each GoldSim source term, but the package inventory is bound in the glass matrix. At the global level, the bound inventory is calculated as the total per-package inventory, including uncertainty, and the unbound inventory is set to zero grams. These inventories are calculated at the global level but are added to each GoldSim source element within each percolation subregion environment. Within the GoldSim source element, the bound inventory is bound in a matrix and is only available for transport after the matrix is degraded. In the CDSP WP, the HLW glass matrix degrades at the calculated degradation rate, discussed in Section 6.3.7.4.3.2. Within an intact CDSP WP, the waste form does not degrade. In a failed CDSP WP, the waste form degrades at the calculated rate, and radionuclides become available for transport.

Degradation of HLW glass starts when the CDSP WPs are breached and if relative humidity is greater than or equal to 44 percent. The rate of degradation used in the TSPA-LA Model is the fractional form of the dissolution rate. This degradation rate is the product of the absolute glass

dissolution rate (Section 6.3.7.4.3.2), the specific surface area of the glass, and the waste form exposure factor. The coefficients in the rate equation are dependent on pH conditions: one set for acidic conditions and one set for alkaline conditions (Table 6.3.7-32). The values for the coefficients are captured in the HLW Glass Degradation Model (DTN: MO0502ANLGAMR1.016_R0 [DIRS 172830]). The rate expression is simultaneously evaluated with both acidic and alkaline condition coefficients with the current inputs, regardless of the applied pH, and the greater of the two calculated rates is applied to degrade the HLW glass. At temperatures greater than 100°C and less than 125°C, the rate expression is evaluated using the alkaline-side coefficients, with the pH term taking on a constant alkaline value (=10). The rate equation is a function of an affinity term, temperature, pH, and HLW glass surface area. The affinity term is treated as an epistemic uncertainty and is represented by two triangular distributions (k_{E_acid} , $k_{E_alkaline}$) used for acidic and alkaline conditions. These distributions are sampled once per realization. The exposure factor, $f_{exposure}$, is treated as an epistemic uncertainty represented by a triangular distribution. This distribution is sampled once per realization, and the same exposure factor is used for alkaline and acidic conditions.

The calculated fractional degradation rate is input to the GoldSim source element located in each percolation subregion environment. The GoldSim source element applies the fractional degradation rate to degrade the HLW glass waste form inside a failed CDSP WP. The fraction of failed WPs is discussed in Section 6.3.5. After the glass degrades, the GoldSim source element releases the mass associated with the degraded waste form into the volume occupied by the waste form alteration products, the rind, and the inventory becomes available for transport. Section 6.3.8.2.2 provides the discussion for calculating the volume of rind formed as the HLW glass waste form degrades and the subsequent transport of the available inventory to other areas of the failed WP.

A supplemental calculation is provided in the TSPA-LA Model to evaluate the average fraction of the HLW glass waste form that is degraded inside each failed WP. This supplemental calculation is provided as an analysis tool for evaluating the performance of the waste form and also provides a desirable result used to determine the volume of rind formed in the waste form (Section 6.3.8.2.2). This calculation is the average fraction of the HLW glass waste form that is degraded in the failed CDSP WPs, and for the purposes of the CDSP rind volume calculation, is called variable F_{cor} to be consistent with the CSNF discussion. Equation 6.3.7-7, and the supplemental discussion provided in Section 6.3.7.4.1.3, is the evaluation of F_{cor} in the TSPA-LA Model and is applicable to both CSNF and CDSP WPs. Within the TSPA-LA Model, the calculation of F_{cor} is the same for both CSNF and CDSP source terms, so the discussion is not repeated.

Although presented in Section 6.3.7.4.3.2, Equations 6.3.7-9 through 6.3.7-12 are not directly incorporated into the TSPA-LA Model. These equations adjust the specific degradation rate to compensate for differences in the amount of glass degraded as a function of time. Using a fractional degradation rate, the type required by GoldSim source elements, the TSPA-LA Model does not need to compensate for depleting the glass as degradation processes occur. Similarly, because the TSPA-LA Model calculates the fraction of the HLW glass that is degraded, F_{cor} for analysis purposes, this result is used to determine the rind volume (Section 6.3.8.2.2) and assess the performance of the HLW glass waste form.

6.3.7.5 Dissolved Concentration Limits

The Dissolved Concentration Limits Abstraction for the TSPA-LA Model is described in *Dissolved Concentration Limits of Elements with Radioactive Isotopes* (SNL 2007 [DIRS 177418]). Within the TSPA-LA Model, the Dissolved Concentrations Limits (i.e., solubility) Submodel implements the Dissolved Concentrations Limits Abstraction to calculate solubilities for 8 elements, including plutonium (Pu), neptunium (Np), uranium (U), thorium (Th), americium (Am), protactinium (Pa), tin (Sn), and radium (Ra). As pointed out in Table 6.3.7-33, for technetium (Tc), carbon (C), iodine (I), cesium (Cs), strontium (Sr), selenium (Se), and chlorine (Cl), no solubility-controlling solids are expected to form under the repository conditions, therefore, their solubilities are not evaluated. As stated in Table 6.3.7-6, actinium (Ac) and curium (Cm) are not transported within the TSPA-LA Model. Thus, their solubilities are not needed and are not evaluated in the solubility abstraction. The output of the Dissolved Concentration Limits Submodel is used in the TSPA-LA Model to constrain the dissolved concentrations of radioactive elements in the WPs and in the invert.

6.3.7.5.1 Conceptual Model

The Dissolved Concentration Limits Abstraction is based on calculations using geochemical modeling tools and thermodynamic databases. Inputs to the Dissolved Concentration Limits Abstraction include solution chemistry, thermodynamic properties, and associated uncertainties of pertinent species (SNL 2007 [DIRS 177418], Table 4-1). Laboratory and field observations and measurements were used in the selection of solubility controlling phases and model validation. The Dissolved Concentration Limits Abstraction details the treatment of solubilities for 8 elements that are included in the TSPA-LA Model. The resulting outputs from the Dissolved Concentration Limits Abstraction are, with exceptions, functions of pH and f_{CO_2} and can be applied for a wide range of environmental conditions in both the WPs and the invert. Figure 6.3.7-8 is a schematic illustration showing the relations of the Dissolved Concentration Limits (Solubility) Submodel with the other submodels of the Waste Form Degradation and Mobilization Model Component.

The selection of solubility controlling phase(s) has a direct impact on the outcome of the Dissolved Concentration Limits Abstraction calculations. Based on the laboratory and field observations, or conservative assumptions, solubility-controlling phases for the 8 elements considered in the TSPA-LA Model were selected, as summarized in Table 6.3.7-33. The justification for using each solid phase is discussed in *Dissolved Concentration Limits of Elements with Radioactive Isotopes* (SNL 2007 [DIRS 177418], Section 6).

The environmental conditions expected in the repository are considered for the solubility calculations. Ligands that can form aqueous complexes with radioactive elements and are common in Yucca Mountain waters, such as OH^- , CO_3^{2-} , F^- , HPO_4^{2-} , Cl^- , SO_4^{2-} , and NO_3^- , are included in solubility calculations in *Dissolved Concentration Limits of Elements with Radioactive Isotopes* (SNL 2007 [DIRS 177418], Section 6). The sensitivity analysis shows that, among the environmental conditions considered by the Dissolved Concentration Limits Abstraction, pH and f_{CO_2} have the primary impact on actinide solubilities. Therefore, those two variables are chosen as the independent variables for solubility calculations. Solubility limits were calculated for a wide range of pH and f_{CO_2} values. Other environmental variables that have

a significant impact on actinide solubilities are accounted for by assigning them as a charge balance species in the Dissolved Concentration Limits Abstraction calculations (e.g., SO_4^{2-}) or through an added uncertainty term to the Dissolved Concentration Limits Submodel (e.g., F^-).

Four types of uncertainties -(1) uncertainties in the K values of solubility controlling solids and aqueous species, (2) uncertainties of activity coefficients, (3) uncertainties in water chemistry, and (4) uncertainties in temperature - have been evaluated in *Dissolved Concentration Limits of Elements with Radioactive Isotopes* (SNL 2007 [DIRS 177418] Section 6.3.3.). In the outputs of the Dissolved Concentration Limits Abstraction, the first two types of uncertainties are combined together by the mean-square-root approach and are collectively called thermodynamic uncertainties. The third type of uncertainty is presented as the uncertainty associated with fluoride concentrations. The last type of uncertainty (i.e., uncertainty in temperature) was treated using a bounding approach. In other words, the solubility calculations are conducted at a temperature of 25°C and are applied for all temperatures greater than 25°C (up to 100°C). The use of solubility values calculated at 25°C for higher temperatures is bounding because there is evidence showing that the solubility of actinides decreases with increased temperature, which is called retrograde solubility in *Dissolved Concentration Limits of Elements with Radioactive Isotopes* (SNL 2007 [DIRS 177418], Section 6.3.3.3).

6.3.7.5.2 TSPA-LA Model Abstraction

Outputs from the Dissolved Concentration Limits Abstraction can be divided into three groups: (1) elements whose solubility is a function of pH and $\log f_{\text{CO}_2}$; (2) radium solubility that is a function of pH only; and (3) elements for which no solubility limits are defined (SNL 2007 [DIRS 177418], Section 8.1).

The first group includes americium, neptunium, plutonium, protactinium, thorium, tin, and uranium. The abstracted solubility models for these elements are in the form of look-up tables with pH and $\log f_{\text{CO}_2}$ as the independent variables. Two uncertainty terms accounting for uncertainties associated with thermodynamic properties and variations in water chemistry are also included for this group of elements. The exception to this treatment is protactinium, where the thermodynamic uncertainty is replaced by uncertainty in the choice of an analogue element. For tin, the uncertainty term associated with variations in fluoride concentrations is not given because the calculated tin solubility is not sensitive to fluoride concentrations (SNL 2007 [DIRS 177418], Section 6.19). For radium, solubility values are given as a step function of pH, uncertainties were not included.

The remaining elements (technetium, carbon, iodine, cesium, chlorine, selenium, and strontium) are considered highly soluble and no solubility-controlling solids are expected to form under repository conditions. Thus, their solubilities are not given. Consequently, their release is controlled by the dissolution rate of the waste form and waste inventories. Each of these three groups is discussed below.

pH and $\log f_{\text{CO}_2}$ Dependent Solubility—The pH and $\log f_{\text{CO}_2}$ dependent solubility for americium, neptunium, plutonium, protactinium, thorium, tin, and uranium can be summarized by the following relationship (SNL 2007 [DIRS 177418], Section 8.1):

$$[\text{Pu, Np, U, Am, Th, and Sn}] = 10^s \cdot 10^{\varepsilon_1} + \varepsilon_2 \cdot N \quad (\text{Eq. 6.3.7-13a})$$

and

$$[\text{Pa}] = 10^s \cdot 10^{\varepsilon_1} + \varepsilon_2 \quad (\text{Eq. 6.3.7-13b})$$

where

- $[E]$ = the logarithm of the predicted solubility for a given element, E
- $S(pH, \log f_{CO_2})$ = the logarithm of the base solubility value from a look-up table for that element, E, which is a function of pH and $\log f_{CO_2}$
- ε_1 = a term accounting for uncertainty in thermodynamic properties for americium, neptunium, plutonium, thorium, and tin (for protactinium, uncertainty is accounted for using the analogue phase Np_2O_5)
- ε_2 = the uncertainty term associated with variations in fluoride concentration. This uncertainty term is perfectly correlated among the Pu, Np, U, Th, Am, and Pa solubility models during sampling. This term has a right-sided triangular distribution with the minimum (indicated by “a”), most probable values (indicated by “b”) equal to one another (i.e., $a = b$) and the maximum value (indicated by “c”) corresponding to the maximum uncertainty.
- $N(pH)$ = multiplication factor used to make the second uncertainty term a function of pH, with the exception of protactinium for which no multiplication factor is used.

While the calculation of uranium solubility uses Equation 6.3.7-13, its implementation is more complex and is discussed separately below. For the other elements listed above, the Dissolved Concentration Limits Abstraction provides a two-dimensional look-up table giving a calculated value of solubility as a function pH and $\log f_{CO_2}$. The look-up tables for americium, neptunium (Np_2O_5 and NpO_2), plutonium, protactinium, thorium, and tin can be found in Tables 6.3.7-34 through 6.3.7-40, respectively. A base solubility value, $S(pH, \log f_{CO_2})$, for each element is obtained for a given pH and $\log f_{CO_2}$ value by linear interpolation of the nearest pH and $\log f_{CO_2}$ values in the table. After the base solubility value is determined, the uncertainty terms are added to it in the manner shown in Equation 6.3.7-13.

In general, two types of uncertainty terms are included to describe the pH and $\log f_{CO_2}$ dependent solubility. The first term, ε_1 , is used to account for uncertainty in the thermodynamic properties used to calculate the solubility look-up tables. These uncertainties are represented by truncated normal distributions with mean values of 0.0 and SDs specific to each element (Tables 6.3.7-41 through 6.3.7-47). The solubility calculations were conducted using the B-dot equation, which is only rigorously applicable up to ionic strength values of 1 molal. In order to extend the applicable range of the solubility model to 3 molal, extra uncertainty is added to the ε_1 uncertainty term (SNL 2007 [DIRS 177418], Section 8.1). For solutions with an ionic strength between 1 molal and 3 molal, a modified SD is used for the ε_1 uncertainty term. This

modification requires that 0.3 be added to the 1 molal SD using the root-mean-square method (SNL 2007 [DIRS 177418], Section 6.3.3.4, Equation 6.3-7). The resulting SDs are also shown in Tables 6.3.7-41 through 6.3.7-47. The ε_1 normal distributions are truncated at the 2σ level for all elements except protactinium (SNL 2007 [DIRS 177418], Section 8.2). The exception to the above discussion of ε_1 is protactinium. For protactinium, ε_1 represents uncertainty in the choice of analogue used to determine the base protactinium solubility, which has a uniform distribution over the range of (-4.42, -0.05) (SNL 2007, [DIRS 177418], Table 6.11-4).

The second uncertainty term, $\varepsilon_2 \bullet N$, is used to account for variations in the base solubility value due to variable fluoride concentration in the fluid. Because the vapor influx mode does not contribute fluoride to the fluid, this uncertainty term is zero for vapor influx mode (SNL 2007 [DIRS 177418], Section 8.1). For the liquid influx mode, this uncertainty term depends on the WP types and ionic strength. Thus, three groups of abstractions for this term were given. Group 1 is for CSNF WPs when ionic strength is less than 0.2 molal, and for CDSP WPs when ionic strength is less than 0.004 molal. Group 2 is for CSNF WPs when ionic strength is greater or equal to 0.2 molal, and for invert under CSNF WPs. Group 3 is for CDSP WPs when ionic strength is greater than or equal to 0.004 molal and for invert under CDSP WPs (SNL 2007 [DIRS 177418], Section 6.19.4.2.2 and Table 6.3-3).

The uncertainty parameters ε_2 are in the form of triangular distributions with minimum and most likely values of zero and maximum values specified for each element (SNL 2007 [DIRS 177418], Section 8.1). These parameters are perfectly correlated with each other during sampling (i.e., with a correlation coefficient of 1.0) (SNL 2007 [DIRS 177418], Section 8.1).

Because the impact of fluoride concentration on the actinide solubilities varies strongly with pH, as described in *Dissolved Concentration Limits of Elements with Radioactive Isotopes* (SNL 2007 [DIRS 177418], Section 6), the second part of the uncertainty term associated with fluoride concentrations, the multiplication factor, N , that is a function of pH, is introduced to present the pH dependency. The multiplication factor, $N(\text{pH})$, is an element-specific parameter that varies from zero to one as a function of pH. It is calculated by normalizing the differences in solubility values between the elevated F^- cases and the base case for each element by the maximum observed difference in solubility values (in *Dissolved Concentration Limits of Elements with Radioactive Isotopes* (SNL 2007 [DIRS 177418], Tables 6.6-4 and 6.6-6). This modification requires that the ε_2 uncertainty terms for each element be fixed at the values sampled for each realization. The sampled value of ε_2 is then multiplied by $N(\text{pH})$ at each timestep to produce a modified ε_2^i . Tables 6.3.7-48 through 6.3.7-52 give the multiplication factors for americium, Np_2O_5 , NpO_2 , plutonium, and thorium. For protactinium, no multiplication factor is used in conjunction with ε_2^i .

Neptunium Solubility—Neptunium solubility is calculated using Equation 6.3.7-13 and the uncertainty terms discussed above. However, two different solubility models are presented for neptunium in *Dissolved Concentration Limits of Elements with Radioactive Isotopes* (SNL 2007 [DIRS 177418], Section 6.6). These two models are based on different solubility-controlling solid phases, Np_2O_5 and NpO_2 . The NpO_2 solubility model is used within WPs when reductants (CSNF fuels or stainless steels) remain. After reductants within WPs are consumed, Np_2O_5 will

be applied. For the invert, the Np_2O_5 solubility model is always applied (SNL 2007 [DIRS 177418], Section 6.6).

Uranium Solubility—There are two methods used to calculate uranium solubility based on different chemistries of in-package fluids (SNL 2007 [DIRS 177418], Section 6.7). In the first method, the amount of silica and alkaline elements in the fluid are far less than the amount of available uranium, which precludes the ubiquitous formation of uranyl silicates (e.g., Na-boltwoodite) and their use as solubility controlling phases. In the second method, the amount of silica and alkaline elements are comparable to the amount of available uranium and uranyl silicates can readily precipitate. These two methods apply as follows:

- Method 1. CSNF WPs that are breached in the Nominal or Seismic Scenario Classes
- Method 2. CDSP WPs breached under all scenario classes, CSNF WPs breached in the course of the igneous intrusion, and for all evaluations in the invert.

Using the first method, uranium solubility is controlled by schoepite under all pH and f_{CO_2} conditions. This method is used because the source of the degrading water in a CSNF WP in the Nominal, Early Failure, or Seismic Scenario Classes is water vapor entering the WPs, which has low or no initial dissolved sodium or silica (SNL 2007 [DIRS 177418], Section 6.7.3). A single look-up table is used for calculating the base solubility value, $S(\text{pH}, \log f_{\text{CO}_2})$ (Table 6.3.7-53). The uncertainty terms are handled using the same method discussed above with a multiplication factor for ϵ_2^i . Values of the uncertainty terms and $N^i(\text{pH})$ for the CSNF WPs (Nominal, Early Failure, and Seismic Scenario Classes) are given in Tables 6.3.7-54 and 6.3.7-55. There are two sets of ϵ_2 and $N(\text{pH})$: one for low ionic strength conditions (< 0.2 molal) and the other for high ionic strength conditions (greater than or equal to 0.2 molal).

Using the second method, uranium solubility is controlled by schoepite, Na-Boltwoodite, or $\text{Na}_4\text{UO}_2(\text{CO}_3)_3$, depending on the pH and f_{CO_2} . In this environment, silica is available to the degrading waste from the CDSP glass, surrounding igneous material, and invert construction material, so Na-boltwoodite is included as a uranium solubility-controlling phase (SNL 2007 [DIRS 177418], Section 6.7.3). As a result, two additional base solubility look-up tables are defined. The solubility limits in Table 6.3.7-56 represent schoepite solubility and extend over lower pH values, where this mineral is the least soluble of the three mineral phases considered. Table 6.3.7-57 represents solubilities of Na-Boltwoodite and $\text{Na}_4\text{UO}_2(\text{CO}_3)_3$ and covers the higher pH ranges. Uncertainties in thermodynamic properties lead to a range of pH and $\log f_{\text{CO}_2}$ values in which either schoepite or Na-Boltwoodite could control the uranium solubility. The shading in Table 6.3.7-56 and the upper shaded area in Table 6.3.7-57 indicate these ranges. For environmental conditions within these ranges, the uranium solubility should be sampled from a uniform distribution with bounds based on the values in Tables 6.3.7-56 and 6.3.7-57. After the base solubility value is determined from one or both of the look-up tables, uncertainties are added as discussed above. Values for the uncertainties are shown in Table 6.3.7-58. The exception is that six sets of ϵ_2 and different $N(\text{pH})$ tables are now defined, as there are two sets for each of the three groups discussed previously, each set is for one solubility look-up table (SNL 2007 [DIRS 177418], Section 6.7.5). Table 6.3.7-59 gives the values of multiplication factors for this solubility model.

Radium Solubility—Radium solubility is based on calculated Ba solubility at 100°C using BaSO₄ as the solubility controlling phase, which is a good analog for modeling radium solubility (SNL 2007 [DIRS 177418], Section 6.12). Since the solubility data of RaSO₄ in the thermodynamic database (data0.ymp.R4) used in the solubility calculations do not have a temperature-dependent relationship, and the solubility data of BaSO₄ indicate that BaSO₄ solubility increases with temperatures up to 100°C, calculated RaSO₄ solubility could be not conservative. To be prudent, radium solubility is based on the conservative analog of RaSO₄ (i.e., BaSO₄ solubility calculated at 100°C (SNL 2007 [DIRS 177418], Section 6.12)).

Radium solubility is presented as a simple step function of pH. For pH values from 3.0 to 7.75, the logarithm of radium solubility is fixed at -1.16 mg/L; and at pH values between 7.75 and 9.75, it is fixed at 1.68 mg/L (log value) (SNL 2007 [DIRS 177418], Table 6.12-1). At pH values greater than 9.75, radium solubility is undefined, and its concentration is controlled by release from the waste form (DTN: MO0702PADISCON.001_R0 [DIRS 179358], Table 10).

Undefined Solubility—Under repository environmental conditions, no solubility-controlling solids are expected to form for carbon, cesium, chlorine, iodine, selenium, and technetium (SNL 2007 [DIRS 177418], Section 8.1); therefore, no solubilities are defined for these elements. Although strontium (Sr) may precipitate in carbonates and sulfates under repository conditions, for the purpose of simplicity, its solubility is also assumed to be undefined. In the TSPA-LA Model, the release of these elements is controlled by the waste inventory and dissolution rates of the waste forms.

Although actinium is not transported in the TSPA-LA Model (Table 6.3.7-60), it is included as a species in the TSPA-LA Model. This is because certain impact analyses consider the transport of actinium in the EBS. For this reason, it is necessary to specify an actinium solubility value in the TSPA-LA Model. However, no thermodynamic data exist for calculating actinium solubility (SNL 2007 [DIRS 177418], Section 6.10). Thus, in the TSPA-LA Model, no solubility is calculated for actinium.

Restrictions on the Dissolved Concentration Limits Abstraction—The solubility models developed for this abstraction are valid for a wide range of environmental conditions and can be applied both inside and outside the WPs. However, these models are subject to the following restrictions (SNL 2007 [DIRS 177418], Table 8-3):

1. The valid temperature range for the solubility models is from 25°C to 100°C.
2. The solubility models are also restricted to pH values between 3.0 and 11.0 and log f_{CO_2} values from -1.5 to -5.0, with f_{CO_2} in the unit of bar.
3. The solubility models are restricted to ionic strength less than or equal to 3 molal.

Treatments of Solubility Model Out-Of-Bounds—Under certain circumstances, the solubility of one or more elements cannot be calculated. This is called Out-of-Bounds solubility model. According to the cause, out-of-bounds can be categorized into three types.

Type I Out-of-Bounds: As shown on Figure 6.3.7-9, Type I out-of-bounds occur when the given pH- f_{CO_2} conditions fall into the gray areas where the solubility look-up table has three valid values (A, B, and C) but with one flagged as invalid (i.e., 500) at D. Since GoldSim two-dimensional look-up tables use rectangular interpolation scheme, a meaningful solubility cannot be calculated using the standard interpolation scheme by the two-dimensional look-up table element. However, in general, solubility can be calculated using EQ3 for these conditions. This type of out-of-bounds is caused by the limited resolutions of solubility look-up tables. A triangular interpolation scheme that produces valid results for the gray shaded areas has been implemented for the uranium solubility models at CSNF Cell 1 to obtain solubility values when this type of out-of-bounds occurs.

Type II Out-of-Bounds: Type II out-of-bounds occurs when the given pH- f_{CO_2} conditions are outside the valid ranges of the solubility look-up table and they cannot be removed by a triangular interpolation scheme. The unshaded area, of the rectangle ABCD on Figure 6.3.7-9 indicates the area where Type II out-of-bounds (in the plutonium solubility model) could occur. However, since the pH- f_{CO_2} conditions given by the In-Package Chemistry Submodel may be narrower than the whole unshaded area, the ranges of pH- f_{CO_2} conditions where Type II out-of-bounds can actually occur can be narrower than as shown on the figure. For the uranium solubility model at CSNF Cell 1, Type II out-of-bounds occurs only for a very narrow range. A base uranium solubility of 1,000 mg/L is assigned for this narrow range (SNL 2007 [DIRS 177418], Table 8-1). This value is justifiable, because the maximum uranium solubility calculated by EQ3 calculations for conditions very close to where Type II out-of-bounds occurs is 500 mg/L. Type II out-of-bounds can also occur for the uranium solubility model at CDSP Cell 1a. Uranium concentrations are capped at 71,400 mg/L (SNL 2007 [DIRS 177418], Table 8-1).

Type III Out-of-Bounds: Type III out-of-bounds occur when ionic strength is greater than 3 molal, and the concentrations of actinides are then capped at the values shown in Tables 6.3.7-60 and 6.3.7-61, for CSNF Cell 1 and CDSP Cell 1b, respectively (SNL 2007 [DIRS 177418], Tables 6.22-2 and 6.22-3).

An empirical approach that addresses Type III out-of-bounds in the plutonium solubility model has been developed and documented below.

The approach relies on the evaluation of the solubility-limited dissolved concentrations model for plutonium (including uncertainties for ionic strength above 1 molal (SNL 2007 [DIRS 177418], Table 6.5-1), against a data set for measured $PuO_2(am)$ solubility at high ionic strengths (Rai et al., 2001 [DIRS 168392]). This evaluation is a direct comparison (Figure 6.3.7-10) of the look-up table model values to the data sets collected in 0.4 and 4 Molar $NaClO_4$ and $NaCl$ solutions (i.e., 0.408 and 4.92 molal $NaClO_4$, respectively), and 0.4 and 4 Molar $NaCl$ solutions (i.e., 0.403 and 4.36 molal $NaCl$, respectively).

Examination of Figure 6.3.7-10 indicates that the measured concentrations of plutonium in perchlorate (an oxyanion) solutions decrease at higher ionic strengths and are closely represented by the solubility-limited dissolved concentrations model for plutonium. The measured concentrations of plutonium in $NaCl$ (salt) solutions increase at higher ionic strength and can be seen to exceed the 2-sigma upper uncertainty band shown on Figure 6.3.7-10 for the model

results. It is noted here that the data shown in the plot (Rai et al., 2001 [DIRS 168392]) are for the longest equilibration times reported by the authors. Because the observed increase for the 4.36 m NaCl solutions is seen for the longer equilibration times, this increase is attributed by Rai et al. (2001 [DIRS 168392]) as probably reflecting alpha radiolysis of the electrolyte to NaOCl with concurrent increase in the solution redox state. However, the measured data for plutonium in the 0.403 m NaCl solutions, show a slight decrease over approximately the same time. In a spectroscopic study of actinide solubilities in highly concentrated chloride solutions (Runde et al., 1997 [DIRS 182190]), it was shown that at increased chloride concentrations, chloride complexes were forming for plutonium (and other actinides), and it was concluded that the higher dissolved actinide concentrations were attributable to this process. Regardless of which of these two possibilities occurred in the experimental work, they are both relevant to potential increased solubility-limited concentrations of plutonium in concentrated chloride solutions above 3 molal, and therefore the data from Rai et al. (2001 [DIRS 168392]) can be used in an empirical approach to define a high ionic strength cap value that is for plutonium in about 4.3 molal chloride solutions. Given the behavior in perchlorate solutions, such a cap value would be bounding for concentrated solutions that are dominated by oxyanions because either mechanism discussed above involved the chloride in the electrolyte directly to account for the increased solubility at higher ionic strength.

Based on the values shown on Figure 6.3.7-10, the solubility cap can be generated to cover the pH range from 4 to 10 and provides an upper bounding value for the dissolved concentration of plutonium that is applicable in concentrated chloride solutions up to ionic strengths of about 4.3 molal. This empirically derived concentration cap is 100 mg/L based on the data set and would be applicable without any further uncertainty treatment because of its bounding nature. For the TSPA-LA Model, this application (TSPA parameter name: Pu_TSPA_DS_Cap) would take place above the 3.0 molal ionic strength limit of the plutonium model. Given the data sets from Rai et al. (2001 [DIRS 168392]), the applicable pH range is from 4 to 10 (the higher end considers the trend of the 4.36 molal NaCl data set, as well as the higher pH behavior of the other data). When pH condition is outside this applicable range, then, the Type III Pu Cap described previously in Tables 6.3.7-60 and 6.3.7-61 is invoked.

As the ionic strength of these solution increases, the equilibrium between the gas phase CO₂ and the aqueous solution will result in a lower solubility of CO₂ due to the “salting-out effect”. The activity coefficient of certain neutral species increases with the increased ionic strength creating a corresponding concentration decrease (Langmuir, 1997 [DIRS 100051], Sec. 4.4). This is particularly true for NaCl solutions where the coefficient in the Setchenow equation is 0.231 for aqueous carbonate (Langmuir, 1997 [DIRS 100051], Section 4.4, page 144, and Table 4.5). This corresponds to lower CO₂ solubility and therefore should result in less effective carbonate complexation of actinides at these higher ionic strengths at any given CO₂ fugacity.

6.3.7.5.3 TSPA-LA Model Implementation

The Dissolved Concentration Limits Abstraction is implemented in the TSPA-LA Model to calculate elemental solubility values for both the in-package (CDSP WP and CSNF WP) and invert environments. The Dissolved Concentration Limits Submodel is implemented at two locations in the TSPA-LA Model. The stochastic elements describing the uncertainty

distributions are defined in the Epistemic_Params submodel. Solubility values are calculated within the EBS_Submodel container, which sits inside the percolation subregion loop.

In the Epistemic_Params Submodel, the stochastic elements describing solubility-related uncertainties are sampled once for each realization. These sampled values are then passed to the EBS_Submodel.

Within the EBS_Submodel, the environmental parameters, pH, $\log f_{\text{CO}_2}$, and ionic strength pertaining to the current percolation subregion are provided to the Dissolved Concentration Limits Submodel by the In-Package Chemistry and EBS Chemical Environment Submodels (Sections 6.3.7.2 and 6.3.4, respectively). These parameter values are then used to obtain a local base solubility value from the look-up tables.

The sampled values of the uncertainty parameters are then added to the local base solubility according to Equation 6.3.7-13 to obtain the final solubility values at each timestep and for each realization. The same value sampled for a given uncertainty parameter is used in all percolation subregions at all times for a particular realization.

The Dissolved Concentration Limits Submodel provides elemental solubilities. The GoldSim software (GoldSim V9.60.100, STN: 10344-9.60-01 [DIRS 181903]), automatically partitions the elemental solubility among the isotopes of an element according to the isotopic ratios (GoldSim Technology Group 2007 [DIRS 181727]) so that the sum of the concentrations of all the element's isotopes will not exceed its solubility.

The GoldSim software requires that all the element's isotopes have the same solubility value. If isotopes of the same element are assigned different solubility values, GoldSim will force all of the isotopes to have the solubility values of the first isotope in the species list. When this is done, a warning message is generated in the GoldSim run log for every timestep and each isotope that had its solubility redefined. In the TSPA-LA Model, solubility values are calculated in units of mg/L. In its internal calculations, GoldSim converts all units to the International System of Units, which for solubility is mol/L. Therefore, each isotope of an element will have a slightly different solubility value after the conversion to the International System of Units. This results in as many as 100,000 warning messages being written to the GoldSim run log. In order to suppress these messages, a slight modification, as described below, is made to the calculated solubility values in the TSPA-LA Model.

The calculated solubility value for an element is converted from mg/L to mol/L by dividing it by the molecular weight of the lightest isotope for that element. For each isotope of an element, this mole-based solubility value is then reconverted to mg/L based on the molecular weight of the isotope in this calculation. As a result, all isotopes of an element will have equivalent solubility values in terms of mol/L but will have slightly differing values in terms of mg/L. This modification introduces a slight discrepancy between calculated solubility values and the estimated concentrations at which the solubility limit is reached in the TSPA-LA Model. Calculated element concentrations can be as much as 0.6 percent higher than the calculated solubility value.

6.3.7.6 Engineered Barrier System Colloids

The Waste Form and In-Drift Colloid Concentration Abstraction for the TSPA-LA Model is described in *Waste Form and In-Drift Colloids-Associated Radionuclide Concentrations: Abstraction and Summary* (SNL 2007 [DIRS 177423]). Within the TSPA-LA Model, the EBS Colloids Submodel implements the Waste Form and In-Drift Colloid Concentration Abstraction to address the formation, stability, and concentration of radionuclide-bearing colloids in the waste form and WP, as well as sorption of dissolved radionuclides. Colloids are fine particles ranging in size from 1 nm to 1 μm in maximum dimension that have the potential to remain in suspension. Colloids are of concern because radionuclides attached to colloids may move faster and farther than dissolved radionuclides; however, colloids may only significantly facilitate radionuclide transport when their suspensions are stable and when they carry significant amounts of radionuclides.

The processes included in the EBS Colloids Submodel are described in this section. Some processes that slow or limit colloid migration were not incorporated into the model, including colloid filtration, colloid sorption at the air-water interface, microbial effects, and the effects of elevated temperature (SNL 2007 [DIRS 177423], Sections 5 and 6.3.1).

6.3.7.6.1 Conceptual Model

Colloids—Three types of colloids were considered in the Waste Form and In-Drift Colloid Concentration Abstraction and are accounted for in the EBS Colloids Submodel implemented in the TSPA-LA Model: (1) Waste form degradation colloids: (a) colloids generated from degradation of the glass waste forms, (b) residue colloids generated from degradation of the CSNF waste forms, and (c) uranium mineral colloids generated from degradation of the SNF waste forms; (2) colloids produced from the steel components of the WPs; and (3) colloids present in natural seepage water entering the EBS.

1. Waste Form Degradation Colloids—(a) Glass Waste Form Colloids—Experimental work at Argonne National Laboratory has shown that quantities of colloids containing plutonium are generated from glass waste during the degradation process. These colloids are a mixture of clays, zeolites, and oxides but are predominantly clays. For further description of these colloids, see *Waste Form and In-Drift Colloids-Associated Radionuclide Concentrations: Abstraction and Summary* (SNL 2007 [DIRS 177423], Section 6.3.3). (b) Residue CSNF Waste Form Colloids—A layer of plutonium and zirconium-rich oxides forms at the reaction front of degrading CSNF waste forms, particles of which may become suspended (SNL 2007 [DIRS 177423], Section 6.3.4). (c) Uranium Mineral SNF Waste Form Colloids—Colloidal-sized particles of uranium minerals such as uranophane have been observed in solutions in contact with degrading CSNF. Degrading uranium metal DSNF has been shown to release colloid-sized particles of UO_2 (SNL 2007 [DIRS 177423], Sections 6.3.5 and 6.3.6).
2. Corrosion Product Colloids—The occurrence of iron oxyhydroxide colloids from the corrosion of the WP materials is included in the Waste Form and In-Drift Colloid Concentration Abstraction described in *Waste Form and In-Drift Colloids-Associated Radionuclide Concentrations: Abstraction and Summary* (SNL 2007 [DIRS 177423], Section 6.3.8). Iron oxyhydroxides derived from the corrosion of steel components in the

repository will occur in two forms: (1) large-sized corrosion products consisting of immobile materials and large particles; and (2) colloid-sized particles that could potentially transport sorbed radionuclides.

3. Seepage Water Colloids—Colloid concentrations in SZ groundwater were used in the Waste Form and In-Drift Colloid Concentration Abstraction to estimate the colloid concentrations in seepage water that could enter a failed WP. There is a wide range in natural groundwater colloid concentrations in the Yucca Mountain vicinity over a relatively narrow range of groundwater ionic strength. The Yucca Mountain colloid concentration data were collected from nine different sources.

Colloid Stability—The stability of a colloidal suspension is controlled by electrostatic and chemical processes at colloid surfaces and by the attractive and repulsive forces between colloids. The attractive force is inversely proportional to both the distance between the colloids and colloid size. That is, the closer the colloids are to each other and the smaller they are, the higher the strength of the attractive force, and the more likely the colloid suspensions are to become unstable and coagulate. Higher ionic strength and higher temperature lead to weaker repulsive forces between colloids, causing colloidal suspensions to become unstable and the colloids to coagulate.

Another factor in colloid stability is pH. Colloids become unstable and flocculate near a pH value (zero point of charge) that is characteristic for a particular colloid mineralogy because of reduced repulsive forces between the colloids. The result is an ionic strength threshold that is dependent on pH, above which, the colloid suspensions are unstable. Examples of the pH dependent ionic strength thresholds are shown on Figure 6.3.7-11 for the idealized minerals that represent the colloid types: montmorillonite for glass degradation and local groundwater clay colloids, ZrO_2 for CSNF degradation colloids with irreversibly attached radionuclides, meta-autunite ($Ca(UO_2)_2(PO_4)_2 \cdot 6-8H_2O$) for SNF degradation colloids with reversibly attached radionuclides, and hematite (Fe_2O_3) for steel degradation colloids (SNL 2007 [DIRS 177423], Section 6.3).

Radionuclide Attachment—Radionuclides may be attached to colloids in many ways. In some cases the attachment and detachment is relatively fast compared to the residence time (in a given transport domain) and can be described as an equilibrium sorption process and modeled via a K_d value. In other cases attachment may be fast but detachment very slow relative to the residence time (in a given transport domain), as in co-precipitation where the radionuclide becomes embedded in the host colloid. This type of attachment is more complex to model and is referred to here as irreversible sorption and modeled via kinetic attachment. Sorption of radionuclides on various types of colloids is approximated as follows:

1. Waste form degradation colloids
 - a. HLW glass degradation colloids – reversible and irreversible
 - b. CSNF degradation rind colloids – irreversible
 - c. SNF uranium mineral colloids – reversible
2. Iron oxyhydroxide colloids – reversible and irreversible

3. Groundwater colloids – reversible.

Nine elements are modeled as reversibly sorbed to waste form and groundwater colloids using a linear isotherm model (K_d): plutonium, americium, cesium, protactinium, thorium, tin, radium, uranium, and neptunium. This list represents the isotopes most likely to exhibit dose-significant colloidal transport (SNL 2007 [DIRS 177423], Section 6.3.12.1). Only plutonium and americium are modeled as irreversibly attached to colloids.

A mechanistic, surface complexation-based competitive sorption model, is developed for sorption of actinides on the steel degradation products that account for the uncertainty in the available sorption sites and for competition among various aqueous complexes for the finite number of sorption sites under a given P_{CO_2} (SNL 2007 [DIRS 177407], Section 6.3.4.2.3 and Section 6.5.2.4). This model is applied for sorption onto both the stationary corrosion products and to the iron oxyhydroxide colloids derived from degradation of steel. Competition among six elements was considered: plutonium, americium, thorium, uranium, neptunium, and nickel. Sorption of thorium, uranium, and neptunium on the iron oxyhydroxide colloids is modeled as reversible (equilibrium) sorption, by computing an effective K_d (based on surface complexation modeling results) while the sorption of plutonium and americium on iron oxyhydroxide colloids is modeled as an irreversible sorption process, by kinetic attachment (with no detachment). Nickel transport is not considered in the TSPA Model however, the effect of nickel is accounted for, in the competitive sorption model.

6.3.7.6.2 TSPA-LA Model Abstraction

The TSPA-LA EBS Colloids Submodel addresses the formation and stability of three types of colloids in the waste forms and WPs and calculates colloid concentrations and reversible sorption of nine radionuclides to colloids. The EBS Colloids Submodel also calculates irreversible attachment of plutonium and americium to HLW and CSNF waste form colloids and iron oxyhydroxide colloids. These features are summarized in Section 6.3.7.6.1 and described in detail in *Waste Form and In-Drift Colloids-Associated Radionuclide Concentrations: Abstraction and Summary* (SNL 2007 [DIRS 177423]).

This section describes the abstraction of these processes for use in the TSPA-LA Model.

Colloid Stability—The following equations and pH bounds describe quantitatively the schematic ionic strength threshold model results on Figure 6.3.7-11. The pH bounds and equation coefficients are provided in Tables 6.3.7-62 through 6.3.7-66.

Groundwater and Glass Degradation Colloids:

$$I_{\text{threshold}} = (-0.008 \times \text{pH}^2) + (0.12 \times \text{pH}) - 0.03 \quad (\text{Eq. 6.3.7-14})$$

If $\text{pH}_{\text{wp,inv}}$ is greater than 9, then the $I_{\text{threshold}}$ value calculated at pH 9 is used, and if $\text{pH}_{\text{wp,inv}}$ is less than 1.5, then colloids are assumed to be unstable (DTN: MO0701PAGROUND.000_R0 [DIRS 179310]).

CSNF Residue (ZrO_2) Colloids:

Between pH 7 and 9.3, the irreversible CSNF colloids are unstable irrespective of the ionic strength.

When the pH is between 4 and 7, the following relationship is used:

$$I_{\text{threshold}} = (0.0089 \times \text{pH}^3) - (0.1466 \times \text{pH}^2) + (0.7462 \times \text{pH}) - 1.092 \quad (\text{Eq. 6.3.7-15})$$

When the pH is greater than 9.3, equation 2-7b is used:

$$I_{\text{threshold}} = (0.087362 \times \text{pH}^3) - (2.4078 \times \text{pH}^2) + (22.126 \times \text{pH}) - 67.791 \quad (\text{Eq. 6.3.7-16})$$

If the pH is less than 4.0, the $I_{\text{threshold}}$ value that was calculated at pH 4.0 is used, and if the pH is greater than 10.6, the $I_{\text{threshold}}$ value calculated at pH 10.6 is used. (DTN: MO0701PACSNFCP.000_R1 [DIRS 180439]).

SNF Uranium Mineral Colloids:

$$I_{\text{threshold}} = -(0.008 \times \text{pH}^2) + (0.14 \times \text{pH}) - 0.4 \quad (\text{Eq. 6.3.7-17})$$

If the pH is less than 4.0, the $I_{\text{threshold}} = 0$; if the pH is greater than 9, the $I_{\text{threshold}}$ value calculated at pH 9 is used (DTN: MO0701PACSNFCP.000_R1 [DIRS 180439]).

Steel Degradation Colloids:

When the pH is between 4.5 and 8.4, the following relationship is used:

$$I_{\text{threshold}} = -0.013 \times \text{pH} + 0.11 \quad (\text{Eq. 6.3.7-18})$$

In contrast, when the pH is between 9.4 and 10.4, the following equation is used:

$$I_{\text{threshold}} = (0.0017 \times \text{pH}^2) - (0.0327 \times \text{pH}) + 0.158 \quad (\text{Eq. 6.3.7-19})$$

If the pH is less than 4.5, the $I_{\text{threshold}}$ value calculated at pH 4.5 is used; and if the pH is greater than 10.4, the $I_{\text{threshold}}$ value calculated at pH 10.4 is used (DTN: MO0701PAIRONCO.000_R1 [DIRS 180440]).

Sorption Capacity—Reversible sorption on waste form and groundwater colloids is modeled by adjusting the sampled K_d value such that the sorption capacity of the colloids is not exceeded (SNL 2007 [DIRS 177423], Section 6.3.12.3). In this approach, the available sorption sites are first partitioned linearly amongst the radionuclides based on their sampled K_d values and their concentrations in solution. From this the theoretical maximum K_d value of the radionuclide is calculated (under given concentrations) and compared to the sampled value. The lower of the two values is then taken. This model is necessarily a recursive model as implemented in GoldSim; i.e., there will be a one timestep delay, as shown below, in the sorption capacity calculation.

By partitioning the total molar density of sorption sites, \bar{c}_{\max_T} , into an allowable molar density of sorption sites for each species, $\bar{c}_{\max_i}^n$, according to the following equation, the model assumes that all sites are available for reversible sorption:

$$\bar{c}_{\max_i}^{n-1} = \bar{c}_{\max_T} \left(\frac{\bar{K}_{d,i} \frac{c_i^{n-1}}{M_{W_i}}}{\sum_j \bar{K}_{d,j} \frac{c_j^{n-1}}{M_{W_j}}} \right) \quad (\text{Eq. 6.3.7-20a})$$

where:

$\bar{K}_{d,i}$ = sampled K_d for the i th species (different for each realization), [=] m^3 solution per kg smectite or uranophane colloids

$\bar{c}_{\max_i}^n$ = molar density of sites for the i th species at the $(n-1)$ th timestep, [=] kg-moles sorbed of i th species per kg colloid mass

\bar{c}_{\max_T} = molar density of sites, [=] kg-moles of sites per kg colloid mass

c_i^{n-1} = aqueous concentration of the i th species at the $(n-1)$ th timestep, [=] kg i th species per m^3 solution

M_{W_i} = molecular weight of i th species, [=] kg of i th species per kg-mole.

Next, each side of Equation 6.3.7-20a is divided by $\frac{c_i^{n-1}}{M_{W_i}}$:

$$\frac{\bar{c}_{\max_i}^{n-1}}{c_i^{n-1}/M_{W_i}} = \bar{c}_{\max_T} \left(\frac{\bar{K}_{d,i}}{\sum_j \bar{K}_{d,j} \frac{c_j^{n-1}}{M_{W_j}}} \right) \quad (\text{Eq. 6.3.7-20b})$$

The left-hand side of the equation is defined to be the maximum allowable partition coefficient, $K_{d,i}^{\max,n}$, for the i th species at the n th timestep:

$$K_{d,i}^{\max,n} \equiv \frac{\bar{c}_{\max,i}^{n-1}}{c_i^{n-1}/M_{w_i}} = \bar{c}_{\max,i} \left(\frac{\bar{K}_{d,i}}{\sum_j \bar{K}_{d,j} \frac{c_j^{n-1}}{M_{w_j}}} \right) \quad (\text{Eq. 6.3.7-20c})$$

At the n th timestep, the partition coefficient, $K_{d,i}^n$, that is used for the i th species is given by the following (i.e., it is the minimum of the competitive K_d computed in Equation 6.3.7-20c and the sampled K_d):

$$K_{d,i}^n = \min(\bar{K}_{d,i}, K_{d,i}^{\max,n}) \quad (\text{Eq. 6.3.7-20d})$$

This sorption capacity model is not needed for sorption calculations on the iron oxyhydroxide colloids, as a mechanistic competitive sorption model has been developed, where the effective K_d is calculated from multiple regression model that accounts for the sorption sites and competition among various elements for the finite number of sorption sites (SNL 2007 [DIRS 177407], Section 6.5.2.4).

Irreversible sorption is modeled for plutonium and americium on iron oxyhydroxide, HLW, and CSNF colloids. This is achieved through the kinetic process by applying only a forward rate constant and zero backward rate constant. The forward rate constant for iron oxyhydroxide colloids is based on experimental values while that for the HLW glass and CSNF colloids is based on matching the predicted concentration of plutonium and americium associated irreversibly with colloids in solution.

6.3.7.6.3 TSPA-LA Model Implementation

All the elements of the EBS Colloids Submodel described in Sections 6.3.7.6.1 and 6.3.7.6.2 are combined in the TSPA-LA Model. The TSPA-LA Model takes the fluid characteristics, pH, and ionic strength and the concentrations of dissolved radionuclides and calculates the mass concentrations of each colloid type.

Reversible sorption of nine elements (plutonium, americium, cesium, protactinium, thorium, tin, radium, uranium, and neptunium) is considered on all colloids, except iron oxyhydroxide colloids, by sampling from an empirically derived K_d range. The sorption capacity is checked at each timestep, and if it is exceeded, the K_d values are adjusted downwards. Irreversible sorption of plutonium and americium is also modeled on HLW glass and CSNF colloids as an 'embedded' mass that is not in equilibrium with the solution. For iron oxyhydroxide colloids, the sorption calculations are based on a mechanistic surface complexation-based competitive sorption model: sorption of thorium, uranium, and neptunium is modeled as reversible by computing an effective K_d while the sorption of plutonium and americium on iron oxyhydroxide

colloids is modeled as an irreversible sorption process by kinetic attachment (with no detachment).

The plutonium concentration associated irreversibly with the HLW glass and CSNF colloids, is sampled from a range first (see range for CPu_Col_WF_Embed_Sampled_a and CPu_Col_CSNF_Sampled_a in Tables 6.3.7-62 and 6.3.7-63) and then based on the ionic strength and pH. The stability of the colloid suspension is determined from the stability field (Figure 6.3.7-11). If found stable then the sampled value is chosen, else the minimum value (CPu_Col_Glass_Embed_Min and CPu_Col_CSNF_Min) is selected. In addition, the concentration range of plutonium associated with a unit colloid concentration is also sampled (see range for CPu_Per_WF_Embed_Col_a and CPu_Per_CSNF_Embed_Col_a in Tables 6.3.7-62 and 6.3.7-63). The ratio of these two values provides the colloid concentration. Based on the mass flux of these colloids (mass of colloids transported in a given timestep), the plutonium mass irreversibly associated with the HLW glass and CSNF colloids is implemented by applying a linear rate constant through solving the mass balance equation (SNL 2007 [DIRS 177407], Section 6.5.2.5). Similar calculation is performed for americium.

Figure 6.3.7-12 provides an overview of the implementation of the EBS Colloids Submodel in the TSPA-LA Model for the WP environment. All uncertain parameters are sampled once for each realization. At each timestep and for each representative WP in each percolation subregion environment in the TSPA-LA Model calculations, the EBS Colloids Submodel uses in-package ionic strength, pH, and dissolved radionuclide concentrations to calculate the formation and stability of colloids and the attachment of radionuclides to stationary corrosion products and to the waste form, iron oxyhydroxide, and seepage water colloids.

The colloid and radionuclide concentration values in the WPs, along with the ionic strength and pH of the solution and dissolved radionuclide concentrations in the solution, serve as source terms for the invert. The EBS Chemical Environment Submodel (Section 6.3.4) calculates the ionic strength and pH of the invert water. Based on the values of ionic strength and pH in the invert, the EBS Colloids Submodel determines colloid stabilities and concentrations for the invert conditions. For all colloid types, the colloid concentration is set to the minimum value when the invert colloid suspensions are unstable. But when the colloid suspensions are stable, the colloid concentrations are calculated differently for the colloid types. For groundwater colloids the sampled value is used, because groundwater colloids may enter the invert directly without going through the WP. For steel degradation colloids and reversible SNF mineral colloids, the concentration of colloids from the upstream corrosion products domain is used because that domain is the source for these colloids in the invert. (Note the steel in the invert is ignored.) For irreversible glass and CSNF residue waste form colloids, the colloid concentration is calculated within GoldSim by the transport of the species "Col" from the waste form domain. The EBS Colloids Submodel redistributes the reversibly sorbed radionuclides and dissolved radionuclides based on the distribution coefficients and the total mass of each type of colloid. For the steel degradation colloids, the distribution coefficients calculated in the corrosion products domain using the competitive sorption model are used in the invert. These colloids and associated radionuclides are then subject to transport through the invert and into the UZ.

The stability of colloids is calculated using the values of ionic strength and pH, with separate relationships for each colloid type. At each timestep and for each representative WP in each

percolation subregion environment, the values of ionic strength and pH of the solutions in the WPs are used as input to determine colloid stability. For all types of colloids, a low, nonzero colloid concentration limit is used under unstable conditions.

6.3.7.7 Model Component Consistency and Conservatism in Assumptions and Parameters

To enhance understanding of the complex interactions within the TSPA-LA Model, a discussion of consistency among model components and submodels and identification of conservative assumptions in abstractions, process models, and parameter sets supporting the Waste Form Degradation and Mobilization Submodel are discussed below.

6.3.7.7.1 Consistency of Assumptions

Waste Form Temperature versus WP Surface Temperature—In the absence of waste form temperatures, the TSPA-LA Model treats waste form temperature as if it were the same as the WP surface temperature. It is expected that waste form temperatures would be higher than WP surface temperatures, and the effect of hotter temperatures is not included in the waste form submodels.

Effect on TSPA—The submodels of the TSPA-LA Model that are directly dependent on the waste form temperature are the In-Package Chemistry Submodel for CSNF WPs (Section 6.3.7.2), the CSNF Waste Form Degradation Rate Submodel (Section 6.3.7.4.1), the HLW Glass Degradation Submodel (Section 6.3.7.4.3), and the EBS Transport Submodel (Section 6.3.8). The influences are discussed below. Both the CSNF Waste Form Degradation Submodel (Section 6.3.7.4.1) and HLW Glass Degradation Submodel (Section 6.3.7.4.3) are direct functions of temperature, with the rate increasing as temperatures increase. The temperature dependence for the In-Package Chemistry Submodel (Section 6.3.7.2) is in the total carbonate abstraction, which only impacts the CSNF Waste Form Degradation Submodel (Section 6.3.7.4.1) calculations. The temperature dependence in the EBS Transport Submodel (Section 6.3.8) pertains to the presence of water inside the waste form. At temperatures greater than 100°C, the TSPA-LA Model assumes that water in the WP evaporates and the system is dry and does not support radionuclide transport.

For all waste forms, the transport of the radionuclides released by any failure mechanism is driven by the amount of water available to entrain and transport the radionuclides past the WP boundary. In the TSPA-LA Model, water will not accumulate in the WP if the temperature is greater than 100°C. Because the waste form temperature is greater than the WP surface temperature, any transport calculations using the lower WP surface temperature would be conservative because water would be accumulating at higher temperatures than physically possible in the waste form.

In-Package Chemistry and the Instantaneous Degradation of CSNF—The In-Package Chemistry Abstraction (SNL 2007 [DIRS 180506]) does not consider the instantaneous degradation of CSNF in the process model and subsequent abstraction. However, within the TSPA-LA Model, the chemistry inside the failed CSNF WP following the instantaneous degradation of the CSNF is determined using the abstractions developed in *In-Package Chemistry Abstraction* (SNL 2007 [DIRS 180506]). Instantaneous degradation of the CSNF

occurs in the Waste Package EF Modeling Case, the Igneous Intrusion Modeling Case, and the Seismic GM and Seismic FD Modeling Cases when CSNF WPs are damaged and the CSNF is exposed to temperatures exceeding 100°C.

Effect on the TSPA—The instantaneous degradation of the CSNF waste form is the recommended waste form treatment when the waste form in a failed CSNF WP is exposed to temperatures exceeding 100°C (Section 6.3.7.4.1.3). The in-package chemistry process models presented in the In-Package Chemistry Abstraction (SNL 2007 [DIRS 180506]) considered very fast degradation rates but did not consider the instantaneous degradation of the CSNF.

Because the in-package pH conditions are controlled by the buffering capacity of the degradation products of CSNF (SNL 2007 [DIRS 180506], Section 6.3.4.1[a]), the instantaneous degradation of CSNF means that the maximum pH buffering capacity will be achieved after the CSNF experiences instantaneous degradation. Thus, the pH conditions within CSNF WPs after instantaneous degradation of CSNF will be well constrained.

Therefore, it is concluded that following the instantaneous degradation of CSNF inside a failed WP, the implemented pH abstraction is sufficient to cover this condition, although the consequence had not explicitly been included in the abstraction process.

The ionic strength abstraction for CSNF WPs under vapor influx conditions is based on Pitzer model calculations for simple salt solutions (SNL 2007 [DIRS 180506], Section 6.10.2.2[a]). Since the Pitzer model calculations are independent of the CSNF degradation rate, assuming instantaneous CSNF degradation would not impact the ionic strength abstraction for CSNF WPs under vapor influx conditions.

A sensitivity analysis has been conducted to evaluate the impact of degradation rates on ionic strength for CSNF WPs under liquid influx conditions (SNL 2007 [DIRS 180506], Section 6.6.5[a]). It reveals that although the CSNF degradation rate does impact the calculated ionic strength in the CSNF simulations, the variation is generally less pronounced than that in the 2DHLW and 2MCO simulations. The variation due to uncertainty in the degradation rates of CSNF and other WP materials has been incorporated in the ionic strength abstraction for CSNF WPs under liquid influx conditions. Moreover, additional uncertainty has been introduced into the ionic strength abstraction by extrapolations (SNL 2007 [DIRS 180506], Section 8.2.2[a]). Thus, the impact of instantaneous degradation of CSNF on the ionic strength for CSNF WPs under liquid influx conditions is captured in the abstraction.

Therefore, it is concluded that following the instantaneous degradation of CSNF inside a failed WP, the implemented ionic strength abstractions for vapor influx and liquid influx modes are sufficient to cover this condition, although the consequence had not explicitly been included in the abstraction process.

Representation of Co-Disposed Fuel—The most numerous CDSP WP in the design for the repository is the 5DHLW/1DSNF Long configuration (Tables 6.3.7-1 and 7.5-3). This WP contains five HLW glass canisters identical to the glass canisters in the 2MCO/2DHLW WP. Although this 5DHLW/1DSNF long WP is the most numerous of the CDSP WPs the total mass of uranium in all of the 2MCO/2DHLW WPs exceeds the total uranium mass in all of the

5DHLW/1DSNF long WPs (Table 7.5-1). That is the reason the In-Package Chemistry Model simulates the 2MCO/2DHLW WP. However, for radionuclide transport calculations (e.g., for mass of degradation products), the TSPA-LA Model simulates the 5DHLW/1DSNF long WP containing Three Mile Island SNF canisters (SNL 2007 [DIRS 177407], Section 6.3.4.6). The major differences between this WP and the 2MCO/2DHLW WP are: (1) the HLW glass waste form domain in the TSPA-LA EBS Transport Submodel contains five HLW glass canisters instead of two, and (2) the DSNF waste-form domain contains UO_2 instead of uranium metal.

Effect on the TSPA-LA Model—The parameters that could potentially be impacted by this difference between the EBS Transport Submodel and the In-Package Chemistry Submodel are pH, ionic strength, and fluoride. The main difference in the conceptual models for the HLW glass waste-form domain would be the total volumes of materials and water, which would be 2.5 times larger in the EBS Transport Submodel (5 canisters instead of 2). This is important only with respect to the turnover rate, which affects ionic strength. For a given liquid influx rate, the turnover rate would be 40 percent (2/5) of the turnover rate of the 2MCO/2DHLW WP. A lower turnover rate increases the effects of degradation rates, which in turn affect ionic strength. However, a reduction of 60 percent in the turnover rate is well within the order-of-magnitude uncertainty of the ionic strength abstraction (SNL 2007 [DIRS 180506], Section 6.10.8.2[a]). The fluoride abstraction, which is only a function of ionic strength (SNL 2007 [DIRS 180506], Section 6.10.3[a]), is therefore, also negligibly affected. The pH abstraction is not affected at all because it is not a function of turnover rate.

In the DSNF waste form domain, the Three Mile Island fuel will quickly degrade to schoepite in the presence of water, similarly to the behavior of both N-Reactor fuel and CSNF. Schoepite will be the dominant alkalinity buffer in the DSNF waste form cell in the EBS Transport Submodel for either co-disposal configuration, 2MCO/2DHLW, or 5DHLW/1 Three Mile Island long. Equilibrium dissolution of schoepite prevents pH from rising much above seven at high carbon dioxide fugacity and much above nine at low carbon dioxide fugacity (SNL 2007 [DIRS 180506], Sections 6.3.4[a] and 6.10.1[a]). On the acid side, degradation of the stainless steel structural materials, which are present regardless of the SNF type, produces oxides that define the pH minimum. Thus, the pH abstractions for N-Reactor fuel (2MCO) can be used for Three Mile Island fuel in the DSNF waste-form domain. Ionic strength and fluoride abstractions of the 5DHLW/1 Three Mile Island long WP can also be approximated by the 2MCO abstractions in the DSNF waste-form domain because the degradation products are similar and because other potential effects are small compared to the order of magnitude uncertainty of the ionic strength abstraction.

Other important DSNF fuel types are mixed-oxide, carbide, and aluminum-based fuels (Table 7.5-3). The justification for using the 2MCO fuel chemistry (pH, ionic strength, and fluoride) to represent them is contained in *In-Package Chemistry Abstraction* (SNL 2007) [DIRS 180506], Section 6.6.6[a].

6.3.7.7.2 Identification of Conservatisms in Submodels and Abstractions

Secondary Phases of Uranium—The TSPA-LA Model does not consider the incorporation of any elements into secondary phases of uranium. Neptunium would likely be incorporated into secondary phases; however, additional quantitative information required to develop a reliable predictive numerical model is not currently available. Using a neptunium-bearing uranyl

compound instead of a pure neptunium phase as the solubility-controlling solid would lead to lower solubilities. The details of this conservatism are discussed in *Dissolved Concentration Limits of Elements with Radioactive Isotopes* (SNL 2007 [DIRS 177418], Section 6.6.4).

Controlling Solid for Radium—Pure RaSO_4 is used as the controlling solid for radium instead of solid solutions. Field studies have shown that radium concentrations in some natural waters are orders of magnitude below levels corresponding to RaSO_4 saturation. Radium concentrations likely correspond to the solubilities of radium in solid solutions in more common sulfate solids such as SrSO_4 or BaSO_4 (SNL 2007 [DIRS 177418], Section 6.12). This results in the overestimation of aqueous radium concentrations.

Solubility versus Temperature—The solubility of radioactive elements at 25°C is used for all temperatures. Actinide solubility values tend to decrease with increasing temperature; however, this conservatism simplifies the model approach (SNL 2007 [DIRS 177418], Sections 6.3.3.3 and 6.4.2.2). This conservatism may result in the overestimation of aqueous radioactive element concentrations.

CSNF Radionuclide Release Rate—In developing the models for the rate of fractional radionuclide release from the CSNF matrix, it is assumed that the fractional degradation rate of the CSNF matrix conservatively bounds the rate of the fractional release of radionuclides located in the fuel matrix. The fission product and actinide elements embedded in the fuel matrix are made available for mobilization and behave (dissolve) as individual elements as the fuel matrix degrades. The fission-product technetium is known to be partly in the form of noble five-metal alloy particles. The properties of the five-metal alloy particles are likely to control the technetium release rate at a level much lower than the CSNF matrix degradation rate. Assuming that technetium release from the CSNF matrix is limited only by the matrix degradation rate, is therefore conservative, as demonstrated in *CSNF Waste Form Degradation* (BSC 2004 [DIRS 169987], Section 5.1).

Specific Surface Area of Corroding CSNF—In assessing the effective specific surface area of corroding CSNF in fuel rods following breaching of the cladding, it is conservatively assumed that the configuration of the fuel is represented by fuel pellet fragments and short fuel rod segments. There is insufficient information to discriminate between the scenarios proposed for the progression of the degradation of fuel rods after the cladding is breached. Thus, the conservative assumption is made that the degradation progresses rapidly, leaving the fuel in the form of fuel pellet fragments or short rod segments (BSC 2004 [DIRS 169987], Sections 5.2 and 6.2.2.1). This is a conservative assumption imposed by the cited source.

All CSNF Cladding Failed at Arrival—The TSPA-LA compliance model assumes all CSNF cladding failed at arrival. The impact of this conservatism is evaluated in the PMA (Appendix C).

Failed Cladding—After cladding failure, no credit is taken for the failed cladding limiting the amount of water or moist air that can contact the fuel pellets. The failed cladding still limits the interaction of the fuel pellets and the environment; however, no credit is taken for this in the TSPA-LA Model. In the TSPA-LA Model, after cladding failure, the fuel pellets corrode as if they were bare fuel pellets (SNL 2007 [DIRS 180616], Section 6.1.4). Credit is taken for the

reduction in the release rate of the radionuclides through the failed cladding. The diffusion of radionuclides across the split opening is modeled in *Cladding Degradation Summary for LA* (SNL 2007 [DIRS 180616], Section 6.2.4).

DSNF Cladding—No credit is taken for DSNF cladding. This simplified modeling approach is used because there is no technical basis for giving credit for DSNF cladding, and the recommended DSNF release model is an upper limit model invoking the complete release of DSNF upon exposure to groundwater (BSC 2004 [DIRS 172453], Section 8.1). Furthermore, a significant fraction of the Uranium Metal SNF (DSNF Group 7), the representative DSNF used in the TSPA-LA Model, is visibly damaged and much of the rest could have small pinholes/cracks in the cladding (BSC 2004 [DIRS 172453], Sections 6.1.7 and 6.1.12).

Note that this conservatism is not applied to naval SNF. Unlike some DSNF, naval SNF is completely characterized, and the degradation of naval SNF was modeled using the same environmental conditions used for the degradation of CSNF.

Degradation Of Metallic Uranium N-Reactor Fuel—A constant degradation rate is used that conservatively bounds degradation of metallic uranium present in N-Reactor fuel; upon WP breach, degradation of DSNF occurs in one timestep of TSPA. Little quality assurance data exists on DSNF fuel, so a conservative approach is used to bound uncertainty in the characteristics of the DSNF fuel (BSC 2004 [DIRS 172453], Section 8.1).

HLW Inventory—The number of canisters of HLW glass is overestimated by about 67 percent because of the assumption to emplace full CDSP WPs in the repository (SNL 2007 [DIRS 180472], Assumption 5.10[a]). The calculation for the number of CDSP WPs (DTN: MO0702PASTREAM.001_R0 [DIRS 179925], Non-commercial, Item 4) indicates that the DSNF waste fills 3,279 WPs with one canister of DSNF per package. However, emplacing HLW canisters in all of the available slots in these packages requires approximately 67 percent more HLW canisters than are actually predicted to be sent to the repository given the HLW allocation of two-thirds of 10 percent of 70,000 metric tons of heavy metal (SNL 2007 [DIRS 180472], Assumption 5.10[a]). This conservatism adds additional HLW glass waste to the inventory in the repository but does not add additional WPs to the repository.

Total Number of Waste Packages—The number of CSNF and CDSP WPs is overestimated by about four percent because TSPA assumes that all of the 108 drifts (including contingency drifts) in the repository design will be filled with WPs (SNL 2007 [DIRS 180472], Assumption 5.14[a]). This additional four percent of both types of WPs is in addition to the 67 percent extra HLW previously discussed. Filling all the drifts with WPs, results in the ‘qualification’ of all 108 drifts for emplacement, but increases the total metric tons of heavy metal in the footprint to 76,223 (including the extra HLW discussed above). The inclusion of more than 70,000 metric tons of heavy metal in the TSPA-LA Model is conservative for dose (SNL 2007 [DIRS 180472], Assumption 5.14[a]).

Degradation of CSNF Waste Greater Than 100°C—If the breached CSNF WP temperature exceeds 100°C, CSNF will undergo ‘dry air oxidation’ (BSC 2004 [DIRS 169987], Section 6.2.2.2). The major effect of dry air oxidation is the very large increase in the specific area of CSNF. As a result, the fractional dissolution rate increases accordingly. Therefore, it is

assumed that the degradation of the CSNF waste form would be instantaneous (BSC 2004 [DIRS 169987], Section 8.1). This treatment is conservative when considering that the estimation for the increase in specific surface area of CSNF undergoing dry air oxidation has a large uncertainty.

6.3.7.8 Alternative Conceptual Model(s) for Waste Form Degradation and Mobilization

Section 6.2 outlines the general consideration and treatment of ACMs used to support the TSPA-LA Model. A brief description of the Waste Form Degradation and Mobilization Submodel ACMs that are summarized in Tables 6.3.7-67 through 6.3.7-71 are presented below.

In-Package Chemistry ACMs—Three ACMs were considered as alternatives to the In-Package Chemistry Abstraction (BSC 2007 [DIRS 180506], Section 6.4). The first ACM was a one-dimensional column composed of n cells, where the reactants in each cell represent the WP components in a vertical cross section of a WP (BSC 2007 [DIRS 180506], Section 6.4.1). This model would eliminate the constraint of the solid-centered flow through mode of a well-mixed batch reactor used in the EQ6 (*Software Code: EQ6. 7.2bLV* (BSC 2002 [DIRS 159731]) calculations in the In-Package Chemistry Abstraction and provide a water stream with a variable composition along its flow path. This ACM was excluded from the In-Package Chemistry Abstraction on the basis that, in comparisons between the vapor influx model and the spatially heterogeneous model, the vapor influx model is much simpler and yielded comparable results (BSC 2007 [DIRS 180506], Section 6.4.1). Inclusion of this ACM in the TSPA-LA Model would not likely have an effect on dose because the implemented abstraction yields comparable results.

The second ACM considered variable-composition seepage entering a failed WP as a function of time, changing with time-varying changes in the physical and chemical environment in the drifts and the EBS (BSC 2007 [DIRS 180506], Section 6.4.2). Section 6.5.2 of *In-Package Chemistry Abstraction* (BSC 2007 [DIRS 180506]) demonstrates that the EQ6 STN: 10075–7.2bLV-02 (BSC 2002 [DIRS 159731]) calculations were largely insensitive to initial seepage water compositions because the WP materials have a stronger influence on the resulting chemistry. Inclusion of this ACM in the TSPA-LA Model would not likely have an effect because the implemented abstraction yields comparable results.

A third ACM considers the alternate methodologies for determining the vapor flux rate through the stress corrosion cracks in a failed WP (BSC 2007 [DIRS 180506], Section 6.4.3). In this ACM, Fick's Law and Stefan Tube Diffusion Calculations are used to develop a relationship between the vapor flux rate through SCC and relative humidity. Calculated results demonstrate that the abstracted relationship presented for the TSPA-LA Model is appropriate, and no change to dose is expected if this ACM were included in the TSPA-LA Model.

The first two ACMs and the associated screening arguments for in-package chemistry are summarized in Table 6.3.7-67. The third ACM was excluded because the abstracted relationship for the vapor flux rate into a stress corrosion cracked-failed WP provided for the TSPA-LA Model is simpler and spans the expected range by this ACM.

CSNF Waste Form Degradation ACMs—Two ACMs for CSNF waste form degradation were considered in the abstraction to TSPA: (1) an electrochemical model based on modeling the rates of redox reactions involved in fuel oxidation and dissolution and (2) a surface complexation model based on a three-step bicarbonate-promoted oxidative dissolution mechanism (BSC 2004 [DIRS 169987], Section 6.4.2).

Using estimates for the unknown parameters in the developed ACMs, an analysis was performed comparing the base-case abstraction with the ACMs. The degradation rates from the electrochemical model were three times greater than the base-case model implemented in the TSPA-LA Model (BSC 2004 [DIRS 169987], Section 7.2). However, it was later concluded that this model was overly conservative because it does not consider slower surface complexation, dissolution, and/or mass transfer limitations. Inclusion of this ACM in the TSPA-LA Model would only have an impact on the TSPA-LA Model dose in the Seismic Scenario when WP failures occur after the WP temperature is less than 100°C. In the Waste Package EF and Igneous Intrusion Modeling Cases, the WP temperature exceeds 100°C after the WP is failed and instantly degrades the CSNF waste form. Using estimates for the unknown parameters, the surface complexation ACM analysis yielded a CSNF degradation rate that was 40 percent lower than the base-case model implemented in the TSPA-LA Model. In the TSPA-LA Model, the inclusion of this ACM would only have a dose impact in the Seismic Scenario when WP failures occur after the WP temperature is less than 100°C. The expected result is a slower degradation rate for the CSNF. Both of these ACMs were screened out of the CSNF Waste Form Degradation Abstraction, and the basis for this assessment is summarized in Table 6.3.7-68.

DSNF Waste Form Degradation ACM—An ACM for DSNF waste form degradation was based on the best-estimates dissolution models presented in *DSNF and Other Waste Form Degradation Abstraction* (BSC 2004 [DIRS 172453], Section 6.3). The application of this ACM would require that the dissolution rate expression be multiplied by the ‘actual’ effective surface area of the SNF. This ACM was screened out of the DSNF Waste Form Degradation Submodel (Section 6.3.7.4.2) because insufficient qualified data on the corrosion rates and the surface areas of the fuel in each group are available. In addition, the upper-limit degradation model that is implemented as a surrogate for all the DSNF, other than naval SNF, is a bounding model with respect to the degradation rate.

HLW Glass Degradation ACM—The HLW Glass Degradation Abstraction (BSC 2004 [DIRS 169988], Section 6.4), screened ACMs to simplify the base-case mechanistic model for HLW glass degradation to a form that could be used in the TSPA-LA Model (Table 6.3.7-69). The screening eliminated parts of the mechanistic model that were deemed unnecessary for describing HLW glass degradation over the range of anticipated physical and chemical conditions in the repository. Most nuclear waste HLW glass degradation models were developed to predict a changing dissolution rate over long times. In contrast, the HLW Glass Degradation Abstraction was developed to provide a constant HLW glass degradation rate under a specific set of exposure conditions that could change for every realization in the simulation because time is not a parameter in the HLW Glass Degradation Abstraction. Instead, the exposure conditions, consisting of the amount of water contacting the HLW glass, the solution pH, and the waste form and in-package temperature, change with time.

ACMs for HLW glass degradation under near-saturation conditions are based on: (1) solid-state diffusion-controlled release; and (2) the composition-independent effective rate constant, which was screened out of the HLW Glass Degradation Abstraction for the TSPA-LA Model analysis. The first ACM was screened out as being unconvincing. Using estimates for unknown fitting parameters, a negligible impact on the calculated rates using this ACM was observed (BSC 2004 [DIRS 169988], Section 6.4.1).

The second ACM considered the effects of different compositions on the intrinsic dissolution rate and affinity term, which in the base-case model implemented in the TSPA-LA Model, have been combined into a single effective rate constant. An analysis of available literature data reveals that combining the two terms into one effective parameter has little effect on the overall reaction rate and that the base-case implementation is more robust for use in the TSPA-LA Model.

The screening arguments are described in detail in *Defense HLW Glass Degradation Model* (BSC 2004 [DIRS 169988], Section 6.4) and are summarized in Table 6.3.7-69. In addition, the *Defense HLW Glass Degradation Model* (BSC 2004 [DIRS 169988], Section 7) indicates that the base-case HLW Glass Degradation Abstraction is validated for HLW borosilicate glass waste forms. Thus, the HLW Glass Degradation Abstraction is applicable to both commercial HLW and DOE-owned HLW glass waste forms.

Dissolved Concentration Limits ACMs—Several ACMs were considered in developing the submodels for the solubility limits of radioactive elements for the TSPA-LA Model (SNL 2007 [DIRS 177418]), and these are summarized in Table 6.3.7-70. Two ACMs are considered for plutonium solubility: (1) the Theoretical fO_2 Model; and (2) the Empirical Eh Model. In the Theoretical fO_2 Model, calculations are carried out with the solution redox condition controlled by theoretical equilibrium between the solution and the atmosphere (with fO_2 equal to 0.2 bars). This ACM is screened out because the results differ significantly from experimental measurements. The Empirical Eh Model uses an empirical (instead of theoretical) equation to set the redox conditions. This ACM is not used because the plutonium solubility results for this model are lower than the experimental values. For the remaining elements (neptunium, thorium, americium, and strontium), the ACMs involved the use of other solubility-controlling solids. These ACMs are screened out because either there is not enough thermodynamic data available to justify their use or a more soluble solid was chosen for conservatism (Table 6.3.7-70).

EBS Colloids ACMs—Three conceptual models were considered as alternatives to the current TSPA-LA EBS Colloids Submodel (SNL 2007 [DIRS 177423], Section 6.4). These ACMs are listed in Table 6.3.7-71, along with the principal bases and screening criteria. The first ACM considers two-site and three-site sorption kinetic models as an alternative to the assumption of irreversible sorption used in the base-case model. The kinetic model represents a useful tool for examining sorption data and examining the evidence for slow reversible sorption of plutonium on colloids. The model clearly demonstrates that the data from Lu et al. (2000 [DIRS 166315]) can be fit with reversible components. The kinetic model has not been adopted because it is immature and the base model is conservative and bounding. A second ACM considers the rate of colloid generation as a function of the waste form degradation rate. In this ACM, the rate of colloid spallation would depend upon the rate of waste degradation. The rate of HLW glass degradation may be defined by the rate of boron release to the alteration fluid, and likewise, the

rate of technetium release could be correlated to the degradation rate of CSNF. However, this ACM is currently not sufficiently developed for application to more generalized conditions. A third ACM considers colloid generation as primarily a function of the rate of advective water flow penetrating the degrading waste forms. This ACM addresses the possibility that colloids can form from both DSNF and CSNF, but their release from the waste weathering rind is governed by the energy of flowing water. The supporting concepts for this ACM were developed in the context of deposition and remobilization of existing colloids under conditions of significant groundwater flow. These conditions likely will not apply to conditions anticipated in the repository.

Table 6.3.7-1. Waste Package Configurations

Waste Package Type	Number of Waste Packages ^a	Spent Nuclear Fuel Unit	Max # of Units per Package	# of Glass Canisters per Package	Glass Unit	Shorthand
CSNF	4,586	PWR assembly	21	0	None	21P-TAD
CSNF	173	PWR assembly	12	0	None	12-Long-TAD
CSNF	3,037	BWR assembly	44	0	None	44B-TAD
CDSP WP	1,940	Short canister	1	5	Short	CDSP-Short
CDSP WP	1,257	Long canister	1	5	Long	CDSP-Long
CDSP WP	219	MCO	2	2	Long	CDSP-MCO
Naval	323	Canister	1	0	None	SNF-Long
Naval	94	Canister	1	0	None	SNF-Short
Total CDSP	3,416					
Total in CSNF+Naval	8,213					
Grand Total	11,629					

Sources: DTN: MO0702PASTREAM.001_R0 [DIRS 179925]; Item 6 of worksheet 'COMMERCIAL,' Item 4 of worksheet 'NON-COMMERCIAL' (waste package configuration), and rows 49 and 59 of worksheet 'UNIT CELL' (numbers of waste packages) in spreadsheet *DTN-Inventory-Rev00.xls*.

NOTE: MCO = multicanister overpack, TAD = transportation, aging, and disposal (canister).

^a These numbers of WPs are 4% higher than would be necessary for 70,000 metric tons heavy metal waste. Assumption 14 in MO0702PASTREAM.001_R0 [DIRS 179925] indicates this is to completely fill all of the available drifts with waste. This assumption implies a total of 417 naval WPs instead of the originally specified 400.

Table 6.3.7-2. Radionuclides Included in TSPA-LA

Radionuclide	Screened-in for Groundwater Modeling Cases: Nominal, Human Intrusion, Igneous Intrusion, and Seismic	Volcanic Eruption Modeling Case
²²⁷ Ac	²²⁷ Ac	²²⁷ Ac
²⁴¹ Am	²⁴¹ Am	²⁴¹ Am
²⁴³ Am	²⁴³ Am	²⁴³ Am
¹⁴ C	¹⁴ C	None
³⁶ Cl	³⁶ Cl	None
²⁴⁵ Cm	Added to ensure that the effect of its decay on the inventory of ²⁴¹ Am are included	
¹³⁵ Cs	¹³⁵ Cs	None
¹³⁷ Cs	¹³⁷ Cs	¹³⁷ Cs
¹²⁹ I	¹²⁹ I	¹²⁹ I
²³⁷ Np	²³⁷ Np	²³⁷ Np
²³¹ Pa	²³¹ Pa	²³¹ Pa
²¹⁰ Pb	Assumed to be in secular equilibrium with ²²⁶ Ra. Not explicitly modeled, but dose effects included with ²²⁶ Ra.	
²³⁸ Pu	²³⁸ Pu	²³⁸ Pu
²³⁹ Pu	²³⁹ Pu	²³⁹ Pu
²⁴⁰ Pu	²⁴⁰ Pu	²⁴⁰ Pu
²⁴¹ Pu	Added to ensure that the effect of its decay on the inventory of ²⁴¹ Am and ²³⁷ Np are included	
²⁴² Pu	²⁴² Pu	²⁴² Pu
²²⁶ Ra	²²⁶ Ra	²²⁶ Ra
²²⁸ Ra	²²⁸ Ra	²²⁸ Ra
⁷⁹ Se	⁷⁹ Se	None
¹²⁶ Sn	¹²⁶ Sn	¹²⁶ Sn
⁹⁰ Sr	⁹⁰ Sr	⁹⁰ Sr
⁹⁹ Tc	⁹⁹ Tc	⁹⁹ Tc
²²⁹ Th	²²⁹ Th	²²⁹ Th
²³⁰ Th	²³⁰ Th	²³⁰ Th
²³² Th	²³² Th	²³² Th
²³² U	²³² U	None
²³³ U	²³³ U	²³³ U
²³⁴ U	²³⁴ U	²³⁴ U
²³⁵ U	²³⁵ U	None
²³⁶ U	²³⁶ U	None
²³⁸ U	²³⁸ U	²³⁸ U
Count	29	22

Sources: Developed from Table 7-1 in *Radionuclide Screening* (SNL 2007 [DIRS 177424]) and DTN: MO0701RLTSCRNA.000_R0 [DIRS 179334].

NOTE: The count in the last row does not include ²⁴⁵Cm, ²¹⁰Pb and ²⁴¹Pu.

Table 6.3.7-3. Nominal Grams of Radionuclides per Waste Package for Each Type of Waste

Year of Projection: CSNF = Year 2067, DSNF = Year 2030, and HLW = Year 2030 Total Number of Waste Packages is 11,629 (8,213 CSNF and 3,416 CDSP WP)			
Radionuclide	Grams per Waste Package		
	CSNF	DSNF	HLW
²²⁷ Ac	2.47E-06	1.22E-03	1.91E-04
²⁴¹ Am	8.18E+03	2.18E+02	3.75E+01
²⁴³ Am	1.24E+03	6.73E+00	5.75E-01
¹⁴ C ^a	1.35E+00	1.81E+00	0.00E+00 ^b
³⁶ Cl	3.23E+00	4.23E+00	0.00E+00 ^b
²⁴⁵ Cm	1.75E+01	9.25E-02	5.43E-02
¹³⁵ Cs	4.36E+03	9.74E+01	1.27E+02
¹³⁷ Cs	5.90E+03	9.72E+01	3.02E+02
¹²⁹ I	1.73E+03	3.56E+01	7.27E+01
²³⁷ Np	4.57E+03	8.14E+01	9.95E+01
²³¹ Pa	9.17E-03	2.14E+00	1.53E+00
²³⁸ Pu	1.52E+03	1.25E+01	3.91E+01
²³⁹ Pu	4.32E+04	2.21E+03	5.58E+02
²⁴⁰ Pu	2.05E+04	4.35E+02	4.61E+01
²⁴¹ Pu	2.66E+03	2.92E+01	1.22E+00
²⁴² Pu	5.28E+03	3.02E+01	3.89E+00
²²⁶ Ra	0.00E+00 ^b	4.57E-05	2.42E-05
²²⁸ Ra	0.00E+00 ^b	1.51E-05	6.00E-06
⁷⁹ Se	4.19E+01	6.82E+00	7.01E+00
¹²⁶ Sn	4.63E+02	9.40E+00	1.70E+01
⁹⁰ Sr	2.49E+03	5.22E+01	1.74E+02
⁹⁹ Tc	7.55E+03	1.58E+02	1.01E+03
²²⁹ Th	0.00E+00 ^b	3.24E-01	3.30E-03
²³⁰ Th	1.52E-01	1.18E-01	8.12E-04
²³² Th	0.00E+00 ^b	2.17E+04	2.98E+04
²³² U	1.02E-02	1.28E+00	4.08E-04
²³³ U	5.76E-02	5.38E+02	1.94E+01
²³⁴ U	1.75E+03	4.73E+02	2.33E+01
²³⁵ U	6.26E+04	2.51E+04	1.41E+03
²³⁶ U	3.84E+04	1.25E+03	5.99E+01
²³⁸ U	7.82E+06	6.84E+05	2.37E+05

Source: DTN: MO0702PASTREAM.001_R0 [DIRS 179925], 'worksheet 'RN INVENTORY' in spreadsheet DTN-Inventory-Rev00.xls.

NOTE: ²¹⁰Pb is not listed in this table because it is considered to be in secular equilibrium with ²²⁶Ra.

^a 18 percent of ¹⁴C for CSNF resides in the hardware outside of the cladding (DTN: SN0310T0505503.004_R0 [DIRS 168761]).

^b Grams listed as 0.00E+00 is the value presented in the data input source.

Table 6.3.7-4a. Radionuclide Inventory Per Waste Package Showing the Amount of Decay and Ingrowth Experienced During the Preclosure Period

Grams Per Waste Package Inventory, g/pkg						
Radionuclide	CSNF at 2067 ^a	CSNF after 50 Years ^b	DSNF at 2030 ^a	DSNF after 87 Years ^b	HLW at 2030 ^a	HLW after 87 Years ^b
²²⁷ Ac	2.47E-06	6.27E-06	1.22E-03	1.39E-03	1.91E-04	9.47E-04
²⁴¹ Am	8.18E+03	9.84E+03	2.18E+02	2.15E+02	3.75E+01	3.37E+01
²⁴³ Am	1.24E+03	1.23E+03	6.73E+00	6.68E+00	5.75E-01	5.70E-01
¹⁴ C	1.35E+00	1.34E+00	1.81E+00	1.79E+00	0.00E+00	0.00E+00
³⁶ Cl	3.23E+00	3.23E+00	4.23E+00	4.23E+00	0.00E+00	0.00E+00
²⁴⁵ Cm	1.75E+01	1.74E+01	9.25E-02	9.18E-02	5.43E-02	5.39E-02
¹³⁵ Cs	4.36E+03	4.36E+03	9.74E+01	9.74E+01	1.27E+02	1.27E+02
¹³⁷ Cs	5.90E+03	1.86E+03	9.72E+01	1.31E+01	3.02E+02	4.07E+01
¹²⁹ I	1.73E+03	1.73E+03	3.56E+01	3.56E+01	7.27E+01	7.27E+01
²³⁷ Np	4.57E+03	5.32E+03	8.14E+01	1.12E+02	9.95E+01	1.04E+02
²³¹ Pa	9.17E-03	1.22E-02	2.14E+00	2.14E+00	1.53E+00	1.53E+00
²³⁸ Pu	1.52E+03	1.02E+03	1.25E+01	6.28E+00	3.91E+01	1.96E+01
²³⁹ Pu	4.32E+04	4.31E+04	2.21E+03	2.20E+03	5.58E+02	5.57E+02
²⁴⁰ Pu	2.05E+04	2.04E+04	4.35E+02	4.31E+02	4.61E+01	4.57E+01
²⁴¹ Pu	2.66E+03	2.40E+02	2.92E+01	4.49E-01	1.22E+00	1.89E-02
²⁴² Pu	5.28E+03	5.28E+03	3.02E+01	3.02E+01	3.89E+00	3.89E+00
²²⁶ Ra	0.00E+00	1.29E-04	4.57E-05	1.80E-04	2.42E-05	2.68E-05
²²⁸ Ra	0.00E+00	1.90E-11	1.51E-05	8.77E-06	6.00E-06	1.20E-05
⁷⁹ Se	4.19E+01	4.19E+01	6.82E+00	6.82E+00	7.01E+00	7.01E+00
¹²⁶ Sn	4.63E+02	4.63E+02	9.40E+00	9.40E+00	1.70E+01	1.70E+01
⁹⁰ Sr	2.49E+03	7.46E+02	5.22E+01	6.43E+00	1.74E+02	2.14E+01
⁹⁹ Tc	7.55E+03	7.55E+03	1.58E+02	1.58E+02	1.01E+03	1.01E+03
²²⁹ Th	0.00E+00	2.07E-05	3.24E-01	5.22E-01	3.30E-03	1.05E-02
²³⁰ Th	1.52E-01	4.32E-01	1.18E-01	2.33E-01	8.12E-04	9.02E-03
²³² Th	0.00E+00	5.63E-02	2.17E+04	2.17E+04	2.98E+04	2.98E+04
²³² U	1.02E-02	6.20E-03	1.28E+00	5.39E-01	4.08E-04	1.72E-04
²³³ U	5.76E-02	1.37E-01	5.38E+02	5.38E+02	1.94E+01	1.94E+01
²³⁴ U	1.75E+03	2.24E+03	4.73E+02	4.79E+02	2.33E+01	4.24E+01
²³⁵ U	6.26E+04	6.27E+04	2.51E+04	2.51E+04	1.41E+03	1.41E+03
²³⁶ U	3.84E+04	3.85E+04	1.25E+03	1.25E+03	5.99E+01	6.03E+01
²³⁸ U	7.82E+06	7.82E+06	6.84E+05	6.84E+05	2.37E+05	2.37E+05

^a DTN: MO0702PASTREAM.001_R0 [DIRS 179925].

^b Output DTN: MO0707EMPDECAY.000 [DIRS 182995].

Table 6.3.7-4b. Supplemental Radionuclide Inventory Per Waste Package due to Mixed Oxide Fuel and Lanthanide Borosilicate Waste Showing the Amount of Decay and Ingrowth Experienced During the Preclosure Period

Grams Per Waste Package MOX and LaBS Specific Additional Inventory, g/pkg				
Radionuclide	MOX at 2035^a	MOX after 82 Years^b	LaBS at 2003^a	LaBS after 114 Years^b
²²⁷ Ac	1.11E-10	4.29E-09	0.00E+00	1.40E-08
²⁴¹ Am	1.90E+01	3.89E+02	2.78E+01	3.40E+01
²⁴³ Am	4.82E+01	4.78E+01	0.00E+00	0.00E+00
¹⁴ C	2.52E-02	2.50E-02	0.00E+00	0.00E+00
³⁶ Cl	2.42E-07	2.42E-07	0.00E+00	0.00E+00
²⁴⁵ Cm	1.36E+00	1.35E+00	0.00E+00	0.00E+00
¹³⁵ Cs	7.00E+01	7.00E+01	0.00E+00	0.00E+00
¹³⁷ Cs	1.64E+02	2.48E+01	0.00E+00	0.00E+00
¹²⁹ I	3.02E+01	3.02E+01	0.00E+00	0.00E+00
²³⁷ Np	1.44E+01	5.55E+01	4.77E-01	6.76E+00
²³¹ Pa	3.99E-06	8.43E-06	0.00E+00	2.94E-05
²³⁸ Pu	1.46E+01	7.63E+00	3.43E+00	1.39E+00
²³⁹ Pu	1.00E+03	9.98E+02	3.48E+03	3.47E+03
²⁴⁰ Pu	7.09E+02	7.03E+02	3.10E+02	3.06E+02
²⁴¹ Pu	4.20E+02	8.21E+00	1.26E+01	5.33E-02
²⁴² Pu	1.79E+02	1.79E+02	6.09E+00	6.09E+00
²²⁶ Ra	8.79E-11	3.03E-07	0.00E+00	8.15E-07
²²⁸ Ra	5.89E-17	2.18E-14	0.00E+00	6.31E-09
⁷⁹ Se	5.30E-01	5.30E-01	0.00E+00	0.00E+00
¹²⁶ Sn	1.13E+01	1.13E+01	0.00E+00	0.00E+00
⁹⁰ Sr	3.57E+01	4.96E+00	0.00E+00	0.00E+00
⁹⁹ Tc	9.75E+01	9.75E+01	0.00E+00	0.00E+00
²²⁹ Th	2.68E-09	1.24E-07	0.00E+00	2.25E-08
²³⁰ Th	4.29E-06	1.07E-03	0.00E+00	1.71E-03
²³² Th	1.15E-06	6.06E-05	1.56E+01	1.56E+01
²³² U	9.85E-06	4.36E-06	0.00E+00	0.00E+00
²³³ U	2.28E-05	8.58E-04	0.00E+00	1.31E-04
²³⁴ U	8.91E-01	7.75E+00	4.24E+00	6.24E+00
²³⁵ U	5.48E+01	5.71E+01	2.61E+02	2.72E+02
²³⁶ U	2.18E+01	2.78E+01	0.00E+00	3.66E+00
²³⁸ U	7.99E+04	7.99E+04	8.58E+02	8.58E+02

^a DTN: MO0702PASTREAM.001_R0 [DIRS 179925].

^b Output DTN: MO0707EMPDECAY.000 [DIRS 182995].

Table 6.3.7-5. Initial Radionuclide Inventories and Initial Radionuclide Activities Per Waste Package Type in the TSPA-LA Model

Per Waste Package Inventory and Activity at Closure, 2117							
Radionuclide	Specific Activity ^a Ci/g	CSNF w/MOX added ^b , g/pkg	CSNF w/MOX added, Ci/pkg	DSNF ^b , g/pkg	DSNF, Ci/pkg	HLW w/LaBS added ^b , g/pkg	HLW w/LaBS added, Ci/pkg
²²⁷ Ac	7.22E+01	6.27E-06	4.53E-04	1.39E-03	1.00E-01	9.47E-04	6.84E-02
²⁴¹ Am	3.43E+00	1.02E+04	3.51E+04	2.15E+02	7.37E+02	6.77E+01	2.32E+02
²⁴³ Am	2.00E-01	1.28E+03	2.56E+02	6.68E+00	1.34E+00	5.70E-01	1.14E-01
¹⁴ C	4.46E+00	1.37E+00	6.09E+00	1.79E+00	7.98E+00	0.00E+00	0.00E+00
³⁶ Cl	3.30E-02	3.23E+00	1.07E-01	4.23E+00	1.40E-01	0.00E+00	0.00E+00
²⁴⁵ Cm	1.72E-01	1.88E+01	3.23E+00	9.18E-02	1.58E-02	5.39E-02	9.27E-03
¹³⁵ Cs	1.15E-03	4.43E+03	5.09E+00	9.74E+01	1.12E-01	1.27E+02	1.46E-01
¹³⁷ Cs	8.67E+01	1.88E+03	1.63E+05	1.31E+01	1.14E+03	4.07E+01	3.53E+03
¹²⁹ I	1.77E-04	1.76E+03	3.12E-01	3.56E+01	6.30E-03	7.27E+01	1.29E-02
²³⁷ Np	7.05E-04	5.38E+03	3.79E+00	1.12E+02	7.90E-02	1.11E+02	7.81E-02
²³¹ Pa	4.72E-02	1.22E-02	5.76E-04	2.14E+00	1.01E-01	1.53E+00	7.22E-02
²³⁸ Pu	1.71E+01	1.03E+03	1.76E+04	6.28E+00	1.07E+02	2.10E+01	3.59E+02
²³⁹ Pu	6.21E-02	4.41E+04	2.74E+03	2.20E+03	1.37E+02	4.03E+03	2.50E+02
²⁴⁰ Pu	2.27E-01	2.11E+04	4.79E+03	4.31E+02	9.78E+01	3.52E+02	7.98E+01
²⁴¹ Pu	1.03E+02	2.48E+02	2.56E+04	4.49E-01	4.62E+01	7.22E-02	7.44E+00
²⁴² Pu	3.94E-03	5.46E+03	2.15E+01	3.02E+01	1.19E-01	9.98E+00	3.93E-02
²²⁶ Ra	9.89E-01	1.29E-04	1.28E-04	1.80E-04	1.78E-04	2.76E-05	2.73E-05
²²⁸ Ra	2.72E+02	1.90E-11	5.17E-09	8.77E-06	2.39E-03	1.20E-05	3.27E-03
⁷⁹ Se	1.53E-02	4.24E+01	6.49E-01	6.82E+00	1.04E-01	7.01E+00	1.07E-01
¹²⁶ Sn	1.13E-02	4.74E+02	5.36E+00	9.40E+00	1.06E-01	1.70E+01	1.92E-01
⁹⁰ Sr	1.38E+02	7.51E+02	1.04E+05	6.43E+00	8.87E+02	2.14E+01	2.95E+03
⁹⁹ Tc	1.70E-02	7.65E+03	1.30E+02	1.58E+02	2.69E+00	1.01E+03	1.72E+01
²²⁹ Th	2.14E-01	2.08E-05	4.46E-06	5.22E-01	1.12E-01	1.05E-02	2.25E-03
²³⁰ Th	2.06E-02	4.33E-01	8.92E-03	2.33E-01	4.80E-03	1.07E-02	2.21E-04
²³² Th	1.10E-07	5.64E-02	6.20E-09	2.17E+04	2.39E-03	2.98E+04	3.28E-03
²³² U	2.21E+01	06.20E-03	1.37E-01	5.39E-01	1.19E+01	1.72E-04	3.80E-03
²³³ U	9.65E-03	01.38E-01	1.33E-03	5.38E+02	5.19E+00	1.94E+01	1.87E-01
²³⁴ U	6.21E-03	2.25E+03	1.40E+01	4.79E+02	2.97E+00	4.86E+01	3.02E-01
²³⁵ U	2.16E-06	6.28E+04	1.36E-01	2.51E+04	5.42E-02	1.68E+03	3.63E-03
²³⁶ U	6.47E-05	3.85E+04	2.49E+00	1.25E+03	8.09E-02	6.40E+01	4.14E-03
²³⁸ U	3.36E-07	7.90E+06	2.65E+00	6.84E+05	2.30E-01	2.38E+05	7.99E-02

^a DTN: MO0702PASTREAM.001_R0 [DIRS 179925].

^b Output DTN: MO0707EMPDECAY.000 [DIRS 182995].

Table 6.3.7-6. Disposition of Radionuclides for Groundwater Release Modeling Cases: Nominal, Igneous Intrusion, and Seismic

Radionuclide (Table 6.3.7-2)	Disposition in WF, EBS, and UZ TSPA-LA Model Components (Section 6.3.7)	Disposition in 3-D UZ FEHM Submodel ^a (Section 6.3.9)	Disposition in SZ Submodels (3-D SZ_Convolute and 1-D Pipe) ^b (Section 6.3.10)	Disposition in Biosphere (Section 6.3.11)
²²⁷ Ac	Not transported	Not transported	Not transported	Dose from 1-D ^g , assuming secular equilibrium with ²³¹ Pa
²⁴¹ Am	Transport embedded colloid ²⁴¹ Am _{emb} (decay to ²³⁷ Np) Transport irreversible FeO colloid ²⁴¹ Am _{FeO} (decay to ²³⁷ Np) Transport reversible colloid and solute (decay to ²³⁷ Np)	Transport slow irreversible colloid ²⁴¹ Am _{irs} (decay to ²³⁷ Np) Transport fast irreversible colloid ²⁴¹ Am _{irf} (decay to ²³⁷ Np) Transport reversible colloid and solute (decay to ²³⁷ Np)	3-D transport of americium/plutonium slow irreversible colloid [SZ BTC 6] 3-D transport of americium/plutonium fast irreversible colloid [SZ BTC 10] 3-D transport of americium/thorium/protactinium reversible colloid [SZ BTC 2]	Dose from 3-D
²⁴³ Am	Transport embedded colloid ²⁴³ Am _{emb} (decay to ²³⁹ Pu _{emb}) Transport irreversible FeO colloid ²⁴³ Am _{FeO} (decay to ²³⁹ Pu _{FeO}) Transport reversible colloid and solute (decay to ²³⁹ Pu)	Transport slow irreversible colloid ²⁴³ Am _{irs} (decay to ²³⁹ Pu _{irs}) Transport fast irreversible colloid ²⁴³ Am _{irf} (decay to ²³⁹ Pu _{irf}) Transport reversible colloid and solute (decay to ²³⁹ Pu)	3-D transport of americium/plutonium slow irreversible colloid [SZ BTC 6] 3-D transport of americium/plutonium fast irreversible colloid [SZ BTC 10] 3-D transport of americium/thorium/protactinium	Dose from 3-D
¹⁴ C	Transport solute	Transport solute	3-D transport of nonsorbing solute [SZ BTC 1]	Dose from 3-D
³⁶ Cl	Transport solute	Transport solute	3-D transport of nonsorbing solute [SZ BTC 1]	Dose from 3-D
²⁴⁵ Cm ^e	Not transported (decay to ²⁴¹ Pu)	Not transported	Not transported	Dose not computed
¹³⁵ Cs	Transport reversible colloid and solute	Transport reversible colloid and solute	3-D transport of cesium colloid [SZ BTC3]	Dose from 3-D
¹³⁷ Cs	Transport reversible colloid and solute	Transport reversible colloid and solute	3-D transport of cesium colloid [SZ BTC 3]	Dose from 3-D
¹²⁹ I	Transport solute	Transport solute	3-D transport of nonsorbing solute [SZ BTC 1]	Dose from 3-D

Table 6.3.7-6. Disposition of Radionuclides for Groundwater Release Modeling Cases: Nominal, Igneous Intrusion, and Seismic (Continued)

Radionuclide (Table 6.3.7-2)	Disposition in WF, EBS, and UZ TSPA-LA Model Components (Section 6.3.7)	Disposition in 3-D UZ FEHM Submodel ^a (Section 6.3.9)	Disposition in SZ Submodels (3-D SZ_Convolute and 1-D Pipe) ^b (Section 6.3.10)	Disposition in Biosphere (Section 6.3.11)
²³⁷ Np	Transport solute (decay to ²³³ U)	Transport solute (decay to ²³³ U)	3-D transport of neptunium solute [SZ BTC 5], boosted ^c by ²⁴¹ Am _{irs} , ²⁴¹ Am _{iff} , and ²⁴¹ Am _{rev/sol}	Dose from 3-D
²³¹ Pa	Transport reversible colloid and solute (decay to ²²⁷ Ac)	Transport reversible colloid and solute (simple decay)	1-D transport reversible colloid and solute (decay to ²²⁷ Ac) [SZ BTC 2]	Dose from 1-D
²¹⁰ Pb ^f	Not explicitly included	Not explicitly included	Not explicitly included	Dose included with ²²⁶ Ra BDCF ^f
²³⁸ Pu	Transport embedded colloid ²³⁸ Pu _{emb} (decay to ²³⁴ U) Transport irreversible FeO colloid ²³⁸ Pu _{FeO} (decay to ²³⁴ U) Transport reversible colloid and solute (decay to ²³⁴ U)	Transport slow irreversible colloid ²³⁸ Pu _{irs} (decay to ²³⁴ U) Transport fast irreversible colloid ²³⁸ Pu _{iff} (decay to ²³⁴ U) Transport reversible colloid and solute (decay to ²³⁴ U)	3-D transport of americium/plutonium slow irreversible colloid [SZ BTC 6] 3-D transport of americium/plutonium fast irreversible colloid [SZ BTC 10] 3-D transport of plutonium reversible colloid [SZ-BTC 4]	Dose from 3-D
²³⁹ Pu	Transport embedded colloid ²³⁹ Pu _{emb} (decay to ²³⁵ U) Transport irreversible FeO colloid ²³⁹ Pu _{FeO} (decay to ²³⁵ U) Transport reversible colloid and solute (decay to ²³⁵ U)	Transport slow irreversible colloid ²³⁹ Pu _{irs} (decay to ²³⁵ U) Transport fast irreversible colloid ²³⁹ Pu _{iff} (decay to ²³⁵ U) Transport reversible colloid and solute (decay to ²³⁵ U)	3-D transport of americium/plutonium slow irreversible colloid [SZ BTC 6], boosted ^c by ²⁴³ Am _{irs} 3-D transport of americium/plutonium fast irreversible colloid [SZ BTC 10], boosted ^c by ²⁴³ Am _{iff} 3-D transport of plutonium reversible colloid [SZ BTC 4], boosted ^c by ²⁴³ Am _{rev/sol}	Dose from 3-D
²⁴⁰ Pu	Transport embedded colloid Pu _{emb} (decay to ²³⁶ U) Transport irreversible FeO colloid ²⁴⁰ Pu _{FeO} (decay to ²³⁶ U) Transport reversible colloid and solute (decay to ²³⁶ U)	Transport slow irreversible colloid ²⁴⁰ Pu _{irs} (decay to ²³⁶ U) Transport fast irreversible colloid ²⁴⁰ Pu _{iff} (decay to ²³⁶ U) Transport reversible colloid and solute (decay to ²³⁶ U)	3-D transport of americium/plutonium slow irreversible colloid [SZ BTC 6] 3-D transport of americium/plutonium fast irreversible colloid [SZ BTC 10] 3-D transport of plutonium reversible colloid [SZ BTC 4]	Dose from 3-D
²⁴¹ Pu ^e	Not transported (decay to ²⁴¹ Am)	Not transported	Not transported	Dose not computed

Table 6.3.7-6. Disposition of Radionuclides for Groundwater Release Modeling Cases: Nominal, Igneous Intrusion, and Seismic (Continued)

Radionuclide (Table 6.3.7-2)	Disposition in WF, EBS, and UZ TSPA-LA Model Components (Section 6.3.7)	Disposition in 3-D UZ FEHM Submodel ^a (Section 6.3.9)	Disposition in SZ Submodels (3-D SZ_Convolute and 1-D Pipe) ^b (Section 6.3.10)	Disposition in Biosphere (Section 6.3.11)
²⁴² Pu	Transport embedded colloid ²⁴² Pu _{emb} (decay to ²³⁸ U) Transport irreversible FeO colloid ²⁴² Pu _{FeO} (decay to ²³⁸ U) Transport reversible colloid and solute (decay to ²³⁸ U)	Transport slow irreversible colloid ²⁴² Pu _{irs} (decay to ²³⁸ U) Transport fast irreversible colloid ²⁴² Pu _{irf} (decay to ²³⁸ U) Transport reversible colloid and solute (decay to ²³⁸ U)	3-D transport ^d of americium/plutonium slow irreversible colloid [SZ BTC 6] 3-D transport ^d of americium/plutonium fast irreversible colloid [SZ BTC 10] 3-D transport ^d of plutonium reversible colloid [SZ BTC 4]	Dose from 3-D ^g
²²⁶ Ra	Transport solute (simple decay)	Transport solute (simple decay)	1-D transport of solute (simple decay) [SZ BTC 7]	Dose from 1-D ^g ; concentration from 1-D ^f
²²⁸ Ra	Not transported	Not transported	Not transported	Dose from 1-D ^g ; concentration from 1-D, both assuming secular equilibrium with ²³² Th
⁷⁹ Se	Transport solute	Transport solute	3-D transport of nonsorbing solute [SZ BTC 11]	Dose from 3-D
¹²⁶ Sn	Transport solute	Transport reversible colloid and solute	3-D transport of tin colloid [SZ BTC 12]	Dose from 3-D
⁹⁰ Sr	Transport solute	Transport solute	3-D transport of strontium solute [SZ BTC 8]	Dose from 3-D
⁹⁹ Tc	Transport solute	Transport solute	3-D transport of nonsorbing solute [SZ BTC 1]	Dose from 3-D
²²⁹ Th	Transport reversible colloid and solute (simple decay)	Transport reversible colloid and solute (simple decay)	1-D transport of reversible colloid and solute (simple decay) [SZ BTC 2]	Dose from 1-D
²³⁰ Th	Transport reversible colloid and solute (decay to ²²⁶ Ra)	Transport reversible colloid and solute (decay to ²²⁶ Ra)	1-D transport of reversible colloid and solute (decay to ²²⁶ Ra) [SZ BTC 2]	Dose from 1-D ^g ; concentration from 1-D
²³² Th	Transport reversible colloid and solute (decay to ²²⁸ Ra)	Transport reversible colloid and solute (simple decay)	1-D transport of reversible colloid and solute (decay to ²²⁸ Ra) [SZ BTC 2]	Dose from 1-D ^g ; concentration from 1-D
²³² U	Transport solute	Transport solute	3-D transport of ²³² U solute [SZ BTC 9]	Dose from 3-D
²³³ U	Transport solute (decay to ²²⁹ Th)	Transport solute (decay to ²²⁹ Th)	1-D transport of solute (decay to thorium) [SZ BTC 9]	Dose from 1-D

Table 6.3.7-6. Disposition of Radionuclides for Groundwater Release Modeling Cases: Nominal, Igneous Intrusion, and Seismic (Continued)

Radionuclide (Table 6.3.7-2)	Disposition in WF, EBS, and UZ TSPA-LA Model Components (Section 6.3.7)	Disposition in 3-D UZ FEHM Submodel ^a (Section 6.3.9)	Disposition in SZ Submodels (3-D SZ_Convolute and 1-D Pipe) ^b (Section 6.3.10)	Disposition in Biosphere (Section 6.3.11)
²³⁴ U	Transport solute (decay to ²³⁰ Th)	Transport solute (decay to ²³⁰ Th)	3-D transport of ²³⁴ U solute, [SZ BTC 9], boosted ^c by ²³⁸ U, ²³⁸ Pu _{irs} , ²³⁸ Pu _{irf} , and ²³⁸ Pu _{rev/sol}	Dose from 3-D
²³⁵ U	Transport solute (decay to ²³¹ Pa)	Transport solute (decay to ²³¹ Pa)	1-D transport of solute (decay to ²³¹ Pa) [SZ BTC 9]	Dose from 1-D ^g
²³⁶ U	Transport solute (decay to ²³² Th)	Transport solute (decay to ²³² Th)	3-D transport ^d of ²³⁶ U solute [SZ BTC 9], boosted ^c by ²⁴⁰ Pu _{irs} , ²⁴⁰ Pu _{irf} , and ²⁴⁰ Pu _{rev/sol}	Dose from 3-D
²³⁸ U	Transport solute (decay to ²³⁴ U)	Transport solute (decay to ²³⁴ U)	3-D transport of ²³⁸ U solute [SZ BTC 9], boosted ^c by ²⁴² Pu _{irs} , ²⁴² Pu _{irf} , and ²⁴² Pu _{rev/sol}	Dose from 3-D

NOTE:

Plutonium and americium isotopes are transported irreversibly on two different colloid types (minerals) in the EBS: FeO_x colloids (e.g., see ²³⁹Pu_{FeO} in the above table) and waste form colloids (e.g., see ²³⁹Pu_{emb} in the above table). However, at the EBS-UZ interface, the plutonium or americium mass associated with these two types of colloids is combined (effectively losing or ignoring the mineral specificity) and then resplit into slow-Transport and fast-Transport irreversible colloids in the natural system (e.g., see ²³⁹Pu_{irs} and ²³⁹Pu_{irf} in the above table). Thus, the specific radionuclides in GoldSim designated “Ic” and “If” are used differently in the EBS versus the natural system—in the EBS “Ic” stands for plutonium and americium mass transported in “embedded” colloids (i.e., the plutonium and americium mass is embedded in the mineral matrix of these colloid particles), and “If” stands for plutonium and americium mass sorbed irreversibly onto FeO_x colloids, whereas in the UZ (Section 6.3.9) and SZ (Section 6.3.10), “Ic” stands for plutonium and americium mass transported irreversibly on slow colloids, and “If” stands for plutonium or americium mass transported irreversibly on fast colloids.

Saturated Zone Breakthrough Curve and the associated number refers to the “Radionuclide Group Number” listed in the first column of Table 6.3.10-3 (see Section 6.3.10).

Boosting of a daughter (e.g., ²³⁹Pu) means that the injected mass of the daughter over any timestep at the UZ-SZ interface is increased by the maximum decay (over the remaining simulation time) of the designated parent (e.g., ²⁴³Am).

This nuclide could have been deleted from the 3-D SZ model (Section 6.3.10), because only the 1-D SZ transport results are used for the ingrowth of its daughter.

²⁴⁵Cm and ²⁴¹Pu were recommended for inclusion in TSPA-LA in *Radionuclide Screening* (SNL 2007 [DIRS 177424], Section 6.6.2 and Table 7-1) only to ensure that the effect of their decay on the inventories of ²⁴¹Am and ²³⁷Np are included in the model. They are not recommended for transport or dose consequences.

Though ²¹⁰Pb is not tracked, it is assumed to be in secular equilibrium with ²²⁶Ra; that is, the BDCF used for ²²⁶Ra is the summation of the BDCFs provided for ²²⁶Ra and ²¹⁰Pb.

Doses only calculated for million-year simulations (SNL 2007 [DIRS 177424], Table 7-1).

WF = waste form; SZ BTC = Saturated Zone Breakthrough Curve.

Table 6.3.7-7. Uncertainty Multipliers for Grams per Waste Package of Radionuclides for Each Waste Type

TSPA Parameter Name	CSNF	DSNF	HLW
	CSNF_Mass_Uncert_a	DSNF_Mass_Uncert_a	HLW_Mass_Uncert_a
Isotopes	All except ²³⁸ U	All except ²³⁸ U	All
Distribution	Uniform	Triangular	Triangular
Minimum	0.85	0.45	0.70
Most Likely	None	0.62	1
Maximum	1.4	2.9	1.5

Sources: DTN: SN0310T0505503.004_R0 [DIRS 168761]
Initial Radionuclide Inventories (SNL 2007 [DIRS 180472], Table 7-2).

Table 6.3.7-8. Summary of In-Package Chemistry Abstraction (Vapor or Liquid Influx)

Q (L/yr)	RH			
	<95%		≥95%	
	< 0.1	≥0.1	< 0.1	≥0.1
I (V) < I(L)	In-Package Chemistry Submodel Off	I(L)	I (V)	I (V), pH(L)
I (V) ≥ I(L)		pH(L)	pH(V)	I (L), pH(L)

Source: Modified from *In-Package Chemistry Abstraction* (SNL 2007 [DIRS 180506]) Table 6-23[a].

NOTE: Q is the water inflow rate; I(V) and I(L) are ionic strength given by the vapor influx abstraction and that given by the liquid influx abstraction, respectively; pH(V) and pH(L) are pH given by the vapor influx abstraction and that given by the liquid influx abstraction, respectively.

Table 6.3.7-9. In-Package Ionic Strength Abstraction for Vapor Influx Case

Cell	RH Range	A	B	Lower Uncertainty Factor (fmin)	Upper Uncertainty Factor (fmax)
CSNF Cell 1	95% ≤ RH < 98.3%	45.846	-45.525	0.5	1.5
	98.3% ≤ RH < 99.9%	64.0629	-64.0602		
	99.9% ≤ RH ≤ 100%	66.4312	-66.4308		
CDSP Cell 1A	95% ≤ RH < 97.2%	42.992	-42.654	0.5	1.5
	97.2% ≤ RH ≤ 100%	54.7803	-54.7776		
CDSP Cell 1B	95% ≤ RH < 98.33%	42.992	-42.654	0.5	1.5
	98.33% ≤ RH ≤ 100%	62.4136	-62.4112		

Source: DTN: SN0702PAIPC1CA.001_R2 [DIRS 180451], *Abstr CSNF No Drip Ion Str.xls*; *Abstr 2DHLW No Drip Ion Str.xls*; and *Abstr 2MCO No Drip Ion Str.xls*.

Table 6.3.7-10. In-Package Ionic Strength Abstraction for CSNF Cell 1 of Liquid Influx Case (log I (molal))

Log Time Since WP Breach (year)	Log Liquid Influx Rate (L/yr)					
	3	2	1	0	-0.3	-1
-1.75	-2.451	-2.433	-2.452	-2.454	-2.454	-2.455
-1.25	-2.501	-2.494	-2.501	-2.502	-2.502	-2.502
-0.75	-2.503	-2.506	-2.503	-2.502	-2.502	-2.502
-0.25	-2.466	-2.477	-2.456	-2.453	-2.453	-2.453
0.25	-2.390	-2.365	-2.320	-2.339	-2.311	-2.247
0.75	-2.317	-2.107	-2.004	-2.032	-1.982	-1.866
1.25	-2.306	-1.803	-1.608	-1.586	-1.585	-1.582
1.75	-2.305	-1.586	-1.178	-1.163	-1.160	-1.154
2.25	-2.305	-1.530	-0.786	-0.686	-0.677	-0.657
2.75	-2.305	-1.945	-1.106	-0.371	-0.320	-0.202
3.25	-2.305	-2.091	-1.634	-0.411	-0.178	0.366
3.75	-2.305	-2.091	-1.929	-0.987	-0.426	0.881
4.25	-2.305	-2.091	-2.095	-2.072	-1.540	-0.299
4.75	-2.305	-2.091	-2.095	-2.134	-2.131	-2.124
5.25	-2.305	-2.091	-2.095	-2.134	-2.134	-2.134
5.75	-2.305	-2.091	-2.095	-2.134	-2.134	-2.134
6.00	-2.305	-2.091	-2.095	-2.134	-2.134	-2.134

Source: DTN: SN0702PAIPC1CA.001_R2 [DIRS 180451], *Abstr CSNF Seepage Ion Str 2.xls*.

Table 6.3.7-11. In-Package Ionic Strength Abstraction for CDSP Cell 1A of Liquid Influx Case (log I (molal))

Log Time Since WP Breach (year)	Log Liquid Influx Rate (L/yr)				
	3	2	1	0	-1
-1.75	-2.391	-2.391	-2.391	-2.391	-2.391
-1.25	-2.391	-2.391	-2.391	-2.391	-2.391
-0.75	-2.391	-2.391	-2.391	-2.390	-2.390
-0.25	-2.391	-2.389	-2.389	-2.388	-2.388
0.25	-2.391	-2.386	-2.384	-2.380	-2.381
0.75	-2.391	-2.384	-2.369	-2.358	-2.360
1.25	-2.391	-2.384	-2.342	-2.296	-2.298
1.75	-2.391	-2.384	-2.319	-2.179	-2.162
2.25	-2.391	-2.384	-2.315	-2.021	-1.878
2.75	-2.391	-2.384	-2.315	-1.928	-1.551
3.25	-2.391	-2.384	-2.315	-1.917	-1.239
3.75	-2.391	-2.384	-2.315	-1.917	-1.088
4.25	-2.391	-2.384	-2.315	-1.917	-1.070
4.75	-2.391	-2.384	-2.315	-1.917	-1.070
5.25	-2.391	-2.384	-2.315	-1.917	-1.070
5.75	-2.391	-2.384	-2.315	-1.917	-1.070
6.00	-2.391	-2.384	-2.315	-1.917	-1.070

Source: DTN: SN0702PAIPC1CA.001_R2 [DIRS 180451],
Abstr 2DHLW Seepage Ion Str 2.xls.

Table 6.3.7-12. In-Package Ionic Strength Abstraction for CDSP Cell 1B of Liquid Influx Case (log I (molal))

Log Time Since WP Breach (year)	Log Liquid Influx Rate (L/yr)					
	3	2	1	0	-0.5	-1
-1.75	- 2.511	- -2.512	- -2.514	- -2.514	- -2.493	- -2.472
-1.25	- 2.505	- -2.509	- -2.515	- -2.515	- -2.515	- -2.515
-0.75	- 2.489	- -2.495	- -2.514	- -2.516	- -2.516	- -2.517
-0.25	- 2.462	- -2.448	- -2.508	- -2.514	- -2.514	- -2.515
0.25	- 2.448	- -2.315	- -2.493	- -2.512	- -2.513	- -2.515
0.75	- 2.447	- -2.087	- -2.446	- -2.506	- -2.510	- -2.515
1.25	- 2.491	- -1.912	- -2.309	- -2.486	- -2.501	- -2.515
1.75	- 2.514	- -2.477	- -2.019	- -2.444	- -2.491	- -2.538
2.25	- 2.514	- -2.512	- -1.702	- -2.208	- -2.286	- -2.364
2.75	- 2.514	- -2.513	- -2.467	- -1.374	- -1.688	- -2.003
3.25	- 2.514	- -2.513	- -2.505	- -1.242	- -1.088	- -0.935
3.75	- 2.514	- -2.513	- -2.505	- -2.144	- -0.690	- 0.763
4.25	- 2.514	- -2.513	- -2.505	- -2.157	- -1.663	- -1.169
4.75	- 2.514	- -2.513	- -2.505	- -2.157	- -1.675	- -1.194
5.25	- 2.514	- -2.513	- -2.505	- -2.157	- -1.675	- -1.192
5.75	- 2.514	- -2.513	- -2.505	- -2.157	- -1.675	- -1.192
6.00	- 2.514	- -2.513	- -2.505	- -2.157	- -1.675	- -1.675

Source: DTN: SN0702PAIPC1CA.001_R2 [DIRS 180451], *Abstr 2MCO Seepage Ion Str 2.xls*.

Table 6.3.7-13. In-Package Ionic Strength Deviation for CSNF Cell 1 of Liquid Influx Case (log I (molal))

Log Time Since WP Breach (year)	Log Liquid Influx Rate (L/yr)					
	3	2	1	0	-0.3	-1
-1.75	1.00	1.00	1.00	1.00	1.00	1.00
-1.25	1.00	1.00	1.00	1.00	1.00	1.00
-0.75	1.00	1.00	1.00	1.00	1.00	1.00
-0.25	1.00	1.00	1.00	1.00	1.00	1.00
0.25	1.00	1.00	1.00	1.00	1.00	1.05
0.75	1.00	1.00	1.00	1.00	1.00	1.08
1.25	1.00	1.00	1.00	1.00	1.00	1.00
1.75	1.00	1.00	1.00	1.00	1.00	1.00
2.25	1.00	1.00	1.00	1.00	1.00	1.01
2.75	1.00	1.00	1.00	1.00	1.00	1.08
3.25	1.00	1.00	1.00	1.00	1.00	1.39
3.75	1.00	1.00	1.00	1.00	1.00	1.93
4.25	1.00	1.00	1.00	1.00	1.00	1.89
4.75	1.00	1.00	1.00	1.00	1.00	1.01
5.25	1.00	1.00	1.00	1.00	1.00	1.00
5.75	1.00	1.00	1.00	1.00	1.00	1.00
6.00	1.00	1.00	1.00	1.00	1.00	1.00

Source: DTN: SN0702PAIPC1CA.001_R2 [DIRS 180451], *Abstr CSNF Seepage Ion Str 2.xls*.

Table 6.3.7-14. In-Package Ionic Strength Deviation for CDSP Cell 1A of Liquid Influx Case (log I (molal))

Log Time Since WP Breach (year)	Log Liquid Influx Rate (L/yr)				
	3	2	1	0	-1
-1.75	1.0	1.0	1.0	1.0	1.0
-1.25	1.0	1.0	1.0	1.0	1.0
-0.75	1.0	1.0	1.0	1.0	1.0
-0.25	1.0	1.0	1.0	1.0	1.0
0.25	1.0	1.0	1.0	1.0	1.0
0.75	1.0	1.0	1.0	1.0	1.0
1.25	1.0	1.0	1.0	1.0	1.0
1.75	1.0	1.0	1.0	1.0	1.0
2.25	1.0	1.0	1.0	1.0	1.0
2.75	1.0	1.0	1.0	1.0	1.0
3.25	1.0	1.0	1.0	1.0	1.0
3.75	1.0	1.0	1.0	1.0	1.0
4.25	1.0	1.0	1.0	1.0	1.0
4.75	1.0	1.0	1.0	1.0	1.0
5.25	1.0	1.0	1.0	1.0	1.0
5.75	1.0	1.0	1.0	1.0	1.0
6.00	1.0	1.0	1.0	1.0	1.0

Source: DTN: SN0702PAIPC1CA.001_R2 [DIRS 180451],
Abstr 2DHLW Seepage Ion Str 2.xls.

Table 6.3.7-15. In-Package Ionic Strength Deviation for CDSP Cell 1B of Liquid Influx Case (log I (molal))

Log Time Since WP Breach (year)	Log Liquid Influx Rate (L/yr)					
	3	2	1	0	-0.5	-1
-1.75	1.00	1.00	1.00	1.00	1.00	1.02
-1.25	1.00	1.00	1.00	1.00	1.00	1.00
-0.75	1.00	1.00	1.00	1.00	1.00	1.00
-0.25	1.00	1.00	1.00	1.00	1.00	1.00
0.25	1.00	1.00	1.00	1.00	1.00	1.00
0.75	1.00	1.00	1.00	1.00	1.00	1.00
1.25	1.00	1.00	1.00	1.00	1.00	1.01
1.75	1.00	1.00	1.00	1.00	1.00	1.05
2.25	1.00	1.00	1.00	1.00	1.00	1.08
2.75	1.00	1.00	1.00	1.00	1.00	1.31
3.25	1.00	1.00	1.00	1.00	1.00	1.15
3.75	1.00	1.00	1.00	1.00	1.00	2.45
4.25	1.00	1.00	1.00	1.00	1.00	1.49
4.75	1.00	1.00	1.00	1.00	1.00	1.48
5.25	1.00	1.00	1.00	1.00	1.00	1.48
5.75	1.00	1.00	1.00	1.00	1.00	1.48
6.00	1.00	1.00	1.00	1.00	1.00	1.24

Source: DTN: SN0702PAIPC1CA.001_R2 [DIRS 180451], *Abstr 2MCO Seepage Ion Str 2.xls*.

Table 6.3.7-16. Maximum pH for CSNF Cell 1 of Liquid Influx

pCO2 (bar)	Log Ionic Strength (molal)						
	-1.411	-0.162	-0.135	-0.059	0	0.5	1
4	9.07	8.90	8.90	8.90	8.90	8.90	8.90
3	8.32	8.14	8.13	8.13	8.13	8.13	8.13
2	7.55	7.22	7.21	7.19	7.19	7.19	7.19
1.5	7.17	6.82	6.81	6.79	6.79	6.79	6.79

Source: DTN: SN0702PAIPC1CA.001_R2 [DIRS 180451], *Abstr CSNF Seepage pH.xls*.

Table 6.3.7-17. Maximum pH for CDSP Cell 1A of Liquid Influx

pCO ₂ (bar)	Log Ionic Strength (molal)									
	-2.283	-1.516	-1.486	-1.418	-0.474	-0.406	-0.369	0	0.5	1
4	9.37	9.81	9.83	9.87	10.23	10.25	10.27	10.41	10.60	10.79
3	8.46	9.09	9.13	9.17	9.67	9.71	9.73	9.92	10.19	10.45
2	7.48	8.21	8.23	8.29	9.02	9.07	9.10	9.38	9.77	10.16
1.5	7.02	7.84	7.87	7.92	8.73	8.79	8.82	9.14	9.56	9.99

Source: DTN: SN0702PAIPC1CA.001_R2 [DIRS 180451], *Abstr 2DHLW Seepage pH.xls*.

Table 6.3.7-18. Maximum pH for CDSP Cell 1B of Liquid Influx

pCO ₂ (bar)	Log Ionic Strength (molal)									
	-2.409	-1.192	-1.166	-1.150	-0.128	-0.106	-0.014	0	0.5	1
4	8.99	9.06	9.06	9.06	8.89	8.89	8.89	8.89	8.89	8.89
3	8.15	8.30	8.31	8.31	8.12	8.11	8.11	8.11	8.11	8.11
2	7.21	7.55	7.54	7.53	7.21	7.20	7.17	7.17	7.17	7.17
1.5	6.78	7.17	7.16	7.15	6.81	6.80	6.77	6.77	6.77	6.77

Source: DTN: SN0702PAIPC1CA.001_R2 [DIRS 180451], *Abstr 2MCO Seepage pH.xls*.

Table 6.3.7-19. Minimum pH for CSNF Cell 1 of Liquid Influx

pCO ₂ (bar)	Log Ionic Strength (molal)				
	-1.531	-0.349	0	0.5	1
4	5.51	5.11	4.99	4.82	4.65
3	5.51	5.11	4.99	4.82	4.65
2	5.51	5.11	4.99	4.82	4.65
1.5	5.51	5.11	4.99	4.82	4.65

Source: DTN: SN0702PAIPC1CA.001_R2 [DIRS 180451],
Abstr CSNF Seepage pH.xls.

Table 6.3.7-20. Minimum pH for CDSP Cell 1A of Liquid Influx

pCO ₂ (bar)	Log Ionic Strength (molal)					
	-2.259	-1.416	-0.422	0	0.5	1
4	5.88	5.54	5.20	5.04	4.87	4.68
3	5.87	5.54	5.20	5.04	4.87	4.69
2	5.87	5.54	5.20	5.04	4.87	4.69
1.5	5.87	5.54	5.20	5.04	4.87	4.69

Source: DTN: SN0702PAIPC1CA.001_R2 [DIRS 180451], *Abstr 2DHLW Seepage pH.xls*.

Table 6.3.7-21. Minimum pH for CDSP Cell 1B of Liquid Influx

pCO2 (bar)	Log Ionic Strength (molal)					
	-2.448	-1.399	-0.396	0	0.5	1
4	6.02	5.59	5.23	5.07	4.89	4.69
3	6.01	5.59	5.23	5.07	4.89	4.70
2	5.97	5.59	5.23	5.08	4.90	4.72
1.5	5.96	5.59	5.23	5.09	4.91	4.73

Source: DTN: SN0702PAIPC1CA.001_R2 [DIRS 180451], *Abstr 2MCO Seepage pH.xls*.

Table 6.3.7-22. Maximum pH for CSNF Cell 1 of Vapor Influx

pCO2 (bar)	Log Ionic Strength (molal)						
	-1.198	-0.164	-0.138	-0.066	0	0.5	1
4	9.06	8.90	8.90	8.90	8.90	8.90	8.90
3	8.31	8.12	8.12	8.12	8.12	8.12	8.12
2	7.54	7.22	7.21	7.19	7.19	7.19	7.19
1.5	7.17	6.82	6.81	6.79	6.79	6.79	6.79

Source: DTN: SN0702PAIPC1CA.001_R2 [DIRS 180451], *Abstr CSNF No Drip pH.xls*.

Table 6.3.7-23. Maximum pH for CDSP Cell 1A of Vapor Influx

pCO2 (bar)	Log Ionic Strength (molal)									
	-2.287	-1.517	-1.486	-1.419	-0.474	-0.406	-0.369	0	0.5	1.5
4	9.37	9.81	9.83	9.87	10.23	10.26	10.27	10.41	10.60	10.98
3	8.46	9.09	9.13	9.17	9.67	9.71	9.73	9.92	10.19	10.72
2	7.47	8.21	8.23	8.29	9.02	9.07	9.10	9.38	9.77	10.54
1.5	7.02	7.84	7.87	7.92	8.73	8.79	8.82	9.14	9.56	10.42

Source: DTN: SN0702PAIPC1CA.001_R2 [DIRS 180451], *Abstr 2DHLW No Drip pH.xls*.

Table 6.3.7-24. Maximum pH for CDSP Cell 1B of Vapor Influx

pCO2 (bar)	Log Ionic Strength (molal)									
	-2.127	-1.193	-1.166	-1.150	-0.129	-0.107	-0.015	0	0.5	1
4	9.04	9.06	9.06	9.06	8.89	8.89	8.89	8.89	8.89	8.89
3	8.25	8.31	8.31	8.31	8.12	8.11	8.11	8.11	8.11	8.11
2	7.38	7.55	7.54	7.53	7.21	7.20	7.17	7.17	7.17	7.17
1.5	6.94	7.17	7.15	7.15	6.75	6.74	6.70	6.70	6.70	6.70

Source: DTN: SN0702PAIPC1CA.001_R2 [DIRS 180451], *Abstr 2MCO No Drip pH.xls*.

Table 6.3.7-25. Minimum pH for CSNF Cell 1 of Vapor Influx

pCO ₂ (bar)	Log Ionic Strength (molal)				
	-1.344	-0.350	0	0.5	1
4	5.44	5.11	4.99	4.82	4.65
3	5.44	5.11	4.99	4.82	4.65
2	5.44	5.11	4.99	4.82	4.65
1.5	5.44	5.11	4.99	4.82	4.65

Source: DTN: SN0702PAIPC1CA.001_R2 [DIRS 180451],
Abstr CSNF No Drip pH.xls.

Table 6.3.7-26. Minimum pH for CDSP Cell 1A of Vapor Influx

pCO ₂ (bar)	Log Ionic Strength (molal)					
	-2.318	-1.372	-0.365	0	0.5	1.5
4	5.84	5.46	5.12	4.98	4.81	4.45
3	5.84	5.46	5.12	4.98	4.81	4.45
2	5.83	5.46	5.12	4.98	4.81	4.45
1.5	5.83	5.46	5.12	4.98	4.81	4.45

Source: DTN: SN0702PAIPC1CA.001_R2 [DIRS 180451], *Abstr 2DHLW No Drip pH.xls*.

Table 6.3.7-27. Minimum pH for CDSP Cell 1B of Vapor Influx

pCO ₂ (bar)	Log Ionic Strength (molal)					
	-2.456	-1.351	-0.352	0	0.5	1
4	5.91	5.46	5.13	4.98	4.82	4.63
3	5.91	5.46	5.13	4.98	4.82	4.63
2	5.90	5.46	5.13	4.98	4.82	4.63
1.5	5.90	5.46	5.13	4.99	4.82	4.63

Source: DTN: SN0702PAIPC1CA.001_R2 [DIRS 180451], *Abstr 2MCO No Drip pH.xls*.

Table 6.3.7-28. Log K Temperature Interpolation Functions for Use in the Total Carbonate Concentration Abstraction

Log K Function of Temperature (°C)
$\text{Log}(K_1) = 7.0 \times 10^{-5} T^2 - 0.0159T - 1.1023$
$\text{Log}(K_2) = 5.0 \times 10^{-7} T^3 - 0.0002T^2 + 0.0132T - 6.5804$
$\text{Log}(K_3) = -8.0 \times 10^{-5} T^2 + 0.0128T - 10.618$

Source: DTN: SN0702PAIPC1CA.001_R2 [DIRS 180451],
worksheet Total Carbonate Validation in Total Carbonate and Eh Abstractions.xls.

Table 6.3.7-29. Initial Release Fraction Percentage Distributions

TSPA-LA Parameter Name	Model Abstraction Symbol	Description	Units	Distribution Type	Distribution Specification
Initial_Release_Frac_Cs_a	None	Cesium release fraction %	None	Triangular	Min = 0.39 Max = 11.06 Most likely = 3.63
Initial_Release_Frac_I_a	None	Iodine release fraction %	None	Triangular	Min = 2.04 Max = 26.75 Most likely = 11.24
Initial_Release_Frac_Tc_a	None	Technetium release fraction %	None	Triangular	Min = 0.01 Max = 0.26 Most likely = 0.10
Initial_Release_Frac_Sr_a	None	Strontium release fraction %	None	Triangular	Min = 0.02 Max = 0.25 Most likely = 0.09

Source: DTN: MO0404ANLSF001.001_R0 [DIRS 169007].

Table 6.3.7-30. Linear Regression Model Alkaline Case (pH ≥ 6.8)

TSPA-LA Parameter Name	Model Abstraction Symbol	Description	Units	Distribution Type	Distribution Specification
Log_Specific_SA_CSNF_a	$\log_{10}(A)$	Log of fuel specific surface area	None	Triangular	Min = -7.3 Max = -5.4 Most likely = -6.7
DR_CSNF_Alk_a0_mean	a_0	Constant coefficient in dissolution rate model	None	None (Uncertainty based on covariance matrix)	$\mu = 4.705$
DR_CSNF_Alk_a1_mean	a_1	Coefficient of inverse temperature in dissolution rate model	None	None (Uncertainty based on covariance matrix)	$\mu = -1093.826$
DR_CSNF_Alk_a2_mean	a_2	Coefficient of $\log_{10}TCC$ in dissolution rate model	None	None (Uncertainty based on covariance matrix)	$\mu = -0.102$
DR_CSNF_Alk_a3_mean	a_3	Coefficient of pO_2 in dissolution rate model	None	None (Uncertainty based on covariance matrix)	$\mu = -0.338$

Source: DTN: MO0404ANLSF001.001_R0 [DIRS 169007].

NOTE: Parameter $a_4 = 0$ under alkaline conditions.

Table 6.3.7-31. Linear Regression Model for Acid Case (pH < 6.8)

TSPA-LA Parameter Name	Model Abstraction Symbol	Description	Units	Distribution Type	Distribution Specification
Log_Specific_SA_CS NF_a	$\text{Log}_{10}(A)$	Log of fuel specific surface area	None	Triangular	Min = -7.3 Max = -5.4 Most likely = -6.7
DR_CS NF_Acid_a0_mean	a_0	Constant coefficient in dissolution rate model	None	None (Uncertainty based on covariance matrix)	$\mu = 6.60$
DR_CS NF_Acid_a1_mean	a_1	Coefficient of inverse temperature in dissolution rate model	None	None	$\mu = -1093.826$
DR_CS NF_Acid_a3_mean	a_3	Coefficient of pO_2 in dissolution rate model	None	None	$\mu = -0.338$
DR_CS NF_Acid_a4_mean	a_4	Coefficient of pH in dissolution rate model	None	None (Uncertainty based on covariance matrix)	$\mu = -0.340$

Source: DTN: MO0404ANLSF001.001_R0 [DIRS 169007].

NOTE: Parameter $a_2 = 0$ under acidic conditions.

Table 6.3.7-32. Dissolution Rate Parameters for High-Level Radioactive Waste Glass

TSPA-LA Parameter Name	Model Abstraction Symbol	Description	Units	Distribution Type/Uncertainty Type	Distribution Specification
Specific_Surface_Area_Glass	S_{sp}	Specific surface area for glass	m^2/kg	Single Value	2.70×10^{-3}
Rind_Porosity_CDSP	ϕ	Porosity of rind (alteration layer)	%	Single Value	17
HLW_Diss_Eta_Acidic	η_{acidic}	pH dependence coefficient acidic condition	None	Single Value	-0.49
HLW_Diss_Ea_Acidic	E_{a_acidic}	Effective activation energy acidic condition	kJ/mol	Single Value	31
HLW_Diss_kE_Acidic_a	k_{E_acid}	glass degradation rate coefficient for acidic solutions	$g/m^2/d$	Triangular	Min = 8.41×10^3 Max = 1.15×10^7 Most likely = 8.41×10^3
HLW_Diss_Eta_Alkaline	$\eta_{alkaline}$	pH dependence coefficient alkaline condition	None	Single Value	0.49
HLW_Diss_Ea_Alkaline	$E_{a_alkaline}$	Effective activation energy alkaline condition	kJ/mol	Single Value	69
HLW_Diss_kE_Alkaline_a	$k_{E_alkaline}$	glass degradation rate coefficient for alkaline solutions	$g/m^2/d$	Triangular	Min = 2.82×10^1 Max = 3.47×10^4 Most likely = 2.82×10^1
Exposure_Factor_a	$f_{exposure}$	Glass exposure factor	None	Triangular - Epistemic ^a	Min = 4 Max = 17 Most likely = 4
Glass_Log_Length_CDSP	L_o	Weighted average length of HLW glass	m	Single Value	3.9

Source: DTN: MO0502ANLGAMR1.016_R0 [DIRS 172830].

^a The DTN lists this parameter as an aleatory uncertain parameter, but it is treated as an epistemic uncertain parameter in the TSPA-LA Model.

Table 6.3.7-33. Solubility-Controlling Solid Phases Used in the Dissolved Concentration Limits Model Abstraction

Radionuclide	Solubility-Controlling Solid	Comments
Americium	AmOHCO ₃	None
Carbon	None	No solubility-controlling solid is expected to form under repository conditions.
Cesium	None	No solubility-controlling solid is expected to form under repository conditions.
Chlorine	None	No solubility-controlling solid is expected to form under repository conditions.
Iodine	None	No solubility-controlling solid is expected to form under repository conditions.
Neptunium	NpO ₂ Np ₂ O ₅ NaNpO ₂ CO ₃	NpO ₂ used within WPs while reductants remain. Np ₂ O ₅ used within WPs after reductants are consumed and for Invert. NaNpO ₂ CO ₃ used for high pH values.
Protactinium	No thermodynamic data available for Pa phases	Used calculated Np ₂ O ₅ solubility values as analogue for Pa.
Plutonium	PuO ₂ (hydrous, aged)	None
Radium	BaSO ₄	Radium solubility is based on calculated Ba solubility at 100°C using BaSO ₄ as the solubility controlling phase, which is a good analog for modeling radium solubility (SNL 2007 [DIRS 177418], Section 6.12). Since the solubility data of RaSO ₄ in the thermodynamic database (data0.ymp.R4) used in the solubility calculations does not have a temperature-dependent relationship, and the solubility data of BaSO ₄ indicates that BaSO ₄ solubility increases with temperature up to 100°C, calculated RaSO ₄ solubility could be no conservative. To be prudent, radium solubility is based on the conservative analog of RaSO ₄ ; i.e., BaSO ₄ solubility calculated at 100°C (SNL 2007 [DIRS 177418], Section 6.12).
Selenium	None	No solubility-controlling solid is expected to form under repository conditions.
Strontium	None	No solubility-controlling solid is expected to form under repository conditions.
Technetium	None	No solubility-controlling solid is expected to form under repository conditions.
Thorium	ThO ₂ (amorphous)	None
Tin	SnO ₂ (amorphous)	None
Uranium	Schoepite	Schoepite used for CSNF WPs in the Nominal and Seismic Scenario Classes.
Uranium	Schoepite Na-Boltwoodite Na ₄ UO ₂ (CO ₃) ₃	Schoepite used for lower pH values. Na-Boltwoodite used for higher pH values. Na ₄ UO ₂ (CO ₃) ₃ used only at high pH and log <i>f</i> CO ₂ values. This set of solubility-controlling solids is used for CSNF WPs in the Igneous Scenario Class, CDSP WPs in all scenarios and in all invert locations.

Source: *Dissolved Concentration Limits of Elements with Radioactive Isotopes* (SNL 2007 [DIRS 177418]).

Table 6.3.7-34. Base Americium Solubility Look-Up Table (log[Am], mg/L)

pH	log fco ₂ (bars)							
	-1.50	-2.00	-2.50	-3.00	-3.50	-4.00	-4.50	-5.00
5.50	2.40E+00	3.27E+00	500	500	500	500	500	500
5.75	1.53E+00	2.10E+00	2.80E+00	500	500	500	500	500
6.00	7.99E-01	1.30E+00	1.83E+00	2.43E+00	3.30E+00	500	500	500
6.25	1.60E-01	5.93E-01	1.07E+00	1.58E+00	2.14E+00	2.84E+00	500	500
6.50	-3.33E-01	-2.76E-02	3.88E-01	8.60E-01	1.36E+00	1.89E+00	2.50E+00	3.37E+00
6.75	-6.62E-01	-5.20E-01	-2.16E-01	1.98E-01	6.69E-01	1.16E+00	1.68E+00	2.25E+00
7.00	-9.13E-01	-8.85E-01	-7.05E-01	-3.84E-01	3.99E-02	5.14E-01	1.01E+00	1.52E+00
7.25	-1.11E+00	-1.16E+00	-1.08E+00	-8.65E-01	-5.11E-01	-6.96E-02	4.11E-01	9.07E-01
7.50	-1.20E+00	-1.36E+00	-1.38E+00	-1.25E+00	-9.73E-01	-5.76E-01	-1.14E-01	3.74E-01
7.75	-1.12E+00	-1.46E+00	-1.60E+00	-1.56E+00	-1.35E+00	-1.01E+00	-5.65E-01	-8.59E-02
8.00	-7.46E-01	-1.39E+00	-1.71E+00	-1.80E+00	-1.67E+00	-1.37E+00	-9.51E-01	-4.80E-01
8.25	-3.64E-02	-1.07E+00	-1.66E+00	-1.93E+00	-1.93E+00	-1.68E+00	-1.29E+00	-8.22E-01
8.50	8.95E-01	-4.41E-01	-1.38E+00	-1.90E+00	-2.10E+00	-1.95E+00	-1.58E+00	-1.13E+00
8.75	1.93E+00	4.47E-01	-8.11E-01	-1.66E+00	-2.12E+00	-2.16E+00	-1.86E+00	-1.41E+00
9.00	500	1.48E+00	3.02E-02	-1.15E+00	-1.92E+00	-2.26E+00	-2.09E+00	-1.68E+00
9.25	500	2.63E+00	1.06E+00	-3.53E-01	-1.46E+00	-2.14E+00	-2.27E+00	-1.93E+00
9.50	500	500	2.24E+00	6.65E-01	-7.01E-01	-1.74E+00	-2.28E+00	-2.15E+00
9.75	500	500	500	1.88E+00	3.08E-01	-1.02E+00	-1.98E+00	-2.28E+00
10.00	500	500	500	500	1.56E+00	-1.70E-02	-1.31E+00	-2.15E+00
10.25	500	500	500	500	500	1.25E+00	-3.16E-01	-1.57E+00
10.50	500	500	500	500	500	500	9.70E-01	-5.94E-01
10.75	500	500	500	500	500	500	500	7.01E-01

Source: DTN: MO0702PADISCON.001_R0 [DIRS 179358], Table 8.

NOTE: This look-up table is implemented in the TSPA-LA Model as parameter Sol_Am_LUT. Entries reported as "500" in the table indicate conditions for which a valid solubility value does not exist.

Table 6.3.7-35. Base Neptunium (Np₂O₅) Solubility Look-Up Table (log[Np], mg/L)

pH	log fco ₂ (bars)							
	-1.5	-2.0	-2.5	-3.0	-3.5	-4.0	-4.5	-5.0
3.00	4.38E+00	4.38E+00	4.38E+00	4.38E+00	4.38E+00	4.38E+00	4.38E+00	4.38E+00
3.25	4.10E+00	4.10E+00	4.10E+00	4.10E+00	4.10E+00	4.10E+00	4.10E+00	4.10E+00
3.50	3.82E+00	3.82E+00	3.82E+00	3.82E+00	3.82E+00	3.82E+00	3.82E+00	3.82E+00
3.75	3.55E+00	3.55E+00	3.55E+00	3.55E+00	3.55E+00	3.55E+00	3.55E+00	3.55E+00
4.00	3.29E+00	3.29E+00	3.29E+00	3.29E+00	3.29E+00	3.29E+00	3.29E+00	3.29E+00
4.25	3.03E+00	3.03E+00	3.03E+00	3.03E+00	3.03E+00	3.03E+00	3.03E+00	3.03E+00
4.50	2.77E+00	2.77E+00	2.77E+00	2.77E+00	2.77E+00	2.77E+00	2.77E+00	2.77E+00
4.75	2.52E+00	2.52E+00	2.52E+00	2.52E+00	2.52E+00	2.52E+00	2.52E+00	2.52E+00
5.00	2.26E+00	2.26E+00	2.26E+00	2.26E+00	2.26E+00	2.26E+00	2.26E+00	2.26E+00
5.25	2.01E+00	2.01E+00	2.01E+00	2.01E+00	2.01E+00	2.01E+00	2.01E+00	2.01E+00
5.50	1.76E+00	1.76E+00	1.76E+00	1.76E+00	1.76E+00	1.76E+00	1.76E+00	1.76E+00
5.75	1.51E+00	1.51E+00	1.51E+00	1.51E+00	1.51E+00	1.51E+00	1.51E+00	1.51E+00
6.00	1.26E+00	1.26E+00	1.26E+00	1.26E+00	1.26E+00	1.26E+00	1.26E+00	1.26E+00
6.25	1.01E+00	1.01E+00	1.01E+00	1.01E+00	1.01E+00	1.01E+00	1.01E+00	1.01E+00
6.50	7.66E-01	7.62E-01	7.61E-01	7.60E-01	7.60E-01	7.60E-01	7.60E-01	7.60E-01
6.75	5.35E-01	5.17E-01	5.12E-01	5.11E-01	5.10E-01	5.10E-01	5.10E-01	5.10E-01
7.00	3.46E-01	2.84E-01	2.68E-01	2.63E-01	2.61E-01	2.60E-01	2.60E-01	2.60E-01
7.25	2.41E-01	8.83E-02	3.52E-02	1.83E-02	1.28E-02	1.11E-02	1.05E-02	1.03E-02
7.50	2.76E-01	-1.94E-02	-1.63E-01	-2.14E-01	-2.31E-01	-2.37E-01	-2.39E-01	-2.39E-01
7.75	4.56E-01	8.77E-03	-2.77E-01	-4.12E-01	-4.64E-01	-4.81E-01	-4.87E-01	-4.89E-01
8.00	5.33E-01	1.71E-01	-2.53E-01	-5.29E-01	-6.61E-01	-7.13E-01	-7.31E-01	-7.37E-01
8.25	5.98E-01	4.49E-01	-9.89E-02	-5.11E-01	-7.78E-01	-9.11E-01	-9.63E-01	-9.81E-01
8.50	1.42E+00	1.00E+00	1.47E-01	-3.62E-01	-7.64E-01	-1.03E+00	-1.16E+00	-1.21E+00
8.75	500	1.06E+00	5.38E-01	-1.30E-01	-6.20E-01	-1.01E+00	-1.28E+00	-1.41E+00
9.00	500	500	7.93E-01	1.89E-01	-3.95E-01	-8.75E-01	-1.26E+00	-1.53E+00
9.25	500	500	500	8.19E-01	-1.08E-01	-6.54E-01	-1.12E+00	-1.51E+00
9.50	500	500	500	1.36E+00	3.72E-01	-3.81E-01	-9.10E-01	-1.37E+00
9.75	500	500	500	500	1.12E+00	2.16E-02	-6.44E-01	-1.16E+00
10.00	500	500	500	500	500	9.56E-01	-2.78E-01	-9.00E-01
10.25	500	500	500	500	500	1.96E+00	5.24E-01	-5.52E-01
10.50	500	500	500	500	500	500	1.76E+00	1.72E-01

Source: DTN: MO0702PADISCON.001_R0 [DIRS 179358], Table 3.

NOTE: This look-up table is implemented in the TSPA-LA Model as parameter Sol_Np2O5_LUT. Entries reported as "500" in the table indicate conditions for which a valid solubility value does not exist.

Table 6.3.7-36. Base Neptunium (NpO₂) Solubility Look-Up Table (log[Np], mg/L)

pH	log fCO ₂ (bars)							
	-1.5	-2.0	-2.5	-3.0	-3.5	-4.0	-4.5	-5.0
3.00	3.09E+00	3.09E+00	3.09E+00	3.09E+00	3.09E+00	3.09E+00	3.09E+00	3.09E+00
3.25	2.82E+00	2.82E+00	2.82E+00	2.82E+00	2.82E+00	2.82E+00	2.82E+00	2.82E+00
3.50	2.56E+00	2.56E+00	2.56E+00	2.56E+00	2.56E+00	2.56E+00	2.56E+00	2.56E+00
3.75	2.30E+00	2.30E+00	2.30E+00	2.30E+00	2.30E+00	2.30E+00	2.30E+00	2.30E+00
4.00	2.05E+00	2.05E+00	2.05E+00	2.05E+00	2.05E+00	2.05E+00	2.05E+00	2.05E+00
4.25	1.80E+00	1.80E+00	1.80E+00	1.80E+00	1.80E+00	1.80E+00	1.80E+00	1.80E+00
4.50	1.55E+00	1.55E+00	1.55E+00	1.55E+00	1.55E+00	1.55E+00	1.55E+00	1.55E+00
4.75	1.29E+00	1.29E+00	1.29E+00	1.29E+00	1.29E+00	1.29E+00	1.29E+00	1.29E+00
5.00	1.04E+00	1.04E+00	1.04E+00	1.04E+00	1.04E+00	1.04E+00	1.04E+00	1.04E+00
5.25	7.94E-01	7.94E-01	7.94E-01	7.94E-01	7.94E-01	7.94E-01	7.94E-01	7.94E-01
5.50	5.44E-01	5.44E-01	5.44E-01	5.44E-01	5.44E-01	5.44E-01	5.44E-01	5.44E-01
5.75	2.93E-01	2.94E-01						
6.00	4.37E-02	4.36E-02						
6.25	-2.05E-01	-2.06E-01						
6.50	-4.48E-01	-4.54E-01	-4.56E-01	-4.56E-01	-4.56E-01	-4.56E-01	-4.56E-01	-4.56E-01
6.75	-6.65E-01	-6.98E-01	-7.04E-01	-7.06E-01	-7.06E-01	-7.06E-01	-7.06E-01	-7.06E-01
7.00	-8.00E-01	-9.24E-01	-9.48E-01	-9.54E-01	-9.56E-01	-9.56E-01	-9.56E-01	-9.56E-01
7.25	-7.26E-01	-1.09E+00	-1.18E+00	-1.20E+00	-1.20E+00	-1.21E+00	-1.21E+00	-1.21E+00
7.50	-3.77E-01	-1.09E+00	-1.36E+00	-1.43E+00	-1.45E+00	-1.45E+00	-1.46E+00	-1.46E+00
7.75	2.05E-01	-8.33E-01	-1.41E+00	-1.62E+00	-1.68E+00	-1.70E+00	-1.70E+00	-1.71E+00
8.00	2.70E-01	-3.51E-01	-1.23E+00	-1.70E+00	-1.87E+00	-1.93E+00	-1.95E+00	-1.95E+00
8.25	5.98E-01	3.96E-01	-8.43E-01	-1.59E+00	-1.97E+00	-2.12E+00	-2.18E+00	-2.20E+00
8.50	1.42E+00	4.41E-01	-2.14E-01	-1.27E+00	-1.90E+00	-2.23E+00	-2.37E+00	-2.43E+00
8.75	500	1.06E+00	4.57E-01	-7.55E-01	-1.65E+00	-2.18E+00	-2.48E+00	-2.63E+00
9.00	500	500	7.93E-01	9.62E-02	-1.22E+00	-1.98E+00	-2.45E+00	-2.74E+00
9.25	500	500	500	1.33E+00	-5.02E-01	-1.63E+00	-2.27E+00	-2.71E+00
9.50	500	500	500	1.36E+00	6.43E-01	-1.03E+00	-1.98E+00	-2.55E+00
9.75	500	500	500	500	1.12E+00	2.13E-02	-1.48E+00	-2.29E+00
10.00	500	500	500	500	500	9.54E-01	-5.42E-01	-1.88E+00
10.25	500	500	500	500	500	1.96E+00	8.53E-01	-1.05E+00
10.50	500	500	500	500	500	500	1.76E+00	3.90E-01
10.75	500	500	500	500	500	500	500	1.61E+00

Source: DTN: MO0702PADISCON.001_R0 [DIRS 179358], Table 2.

NOTE: This look-up table is implemented in the TSPA-LA Model as parameter Sol_NpO₂_LUT. Entries reported as "500" in the table indicate conditions for which a valid solubility value does not exist.

Table 6.3.7-37. Base-Case Plutonium Solubility Look-Up Table (log[Pu], mg/L)

pH	log f_{CO_2} (bars)							
	-1.50	-2.00	-2.50	-3.00	-3.50	-4.00	-4.50	-5.00
2.00	4.53E+00	4.53E+00	4.53E+00	4.53E+00	4.53E+00	4.53E+00	4.53E+00	4.53E+00
2.25	3.84E+00	3.84E+00	3.84E+00	3.84E+00	3.84E+00	3.84E+00	3.84E+00	3.84E+00
2.50	3.19E+00	3.19E+00	3.19E+00	3.19E+00	3.19E+00	3.19E+00	3.19E+00	3.19E+00
2.75	2.62E+00	2.62E+00	2.62E+00	2.62E+00	2.62E+00	2.62E+00	2.62E+00	2.62E+00
3.00	2.14E+00	2.14E+00	2.14E+00	2.14E+00	2.14E+00	2.14E+00	2.14E+00	2.14E+00
3.25	1.74E+00	1.74E+00	1.74E+00	1.74E+00	1.74E+00	1.74E+00	1.74E+00	1.74E+00
3.50	1.38E+00	1.38E+00	1.38E+00	1.38E+00	1.38E+00	1.38E+00	1.38E+00	1.38E+00
3.75	1.04E+00	1.03E+00						
4.00	7.22E-01	7.12E-01	7.09E-01	7.08E-01	7.07E-01	7.07E-01	7.07E-01	7.07E-01
4.25	4.32E-01	4.12E-01	4.06E-01	4.04E-01	4.03E-01	4.03E-01	4.03E-01	4.03E-01
4.50	1.72E-01	1.35E-01	1.23E-01	1.19E-01	1.18E-01	1.17E-01	1.17E-01	1.17E-01
4.75	-5.78E-02	-1.22E-01	-1.45E-01	-1.52E-01	-1.54E-01	-1.55E-01	-1.55E-01	-1.55E-01
5.00	-2.54E-01	-3.60E-01	-3.99E-01	-4.12E-01	-4.17E-01	-4.18E-01	-4.19E-01	-4.19E-01
5.25	-4.13E-01	-5.75E-01	-6.42E-01	-6.65E-01	-6.73E-01	-6.75E-01	-6.76E-01	-6.76E-01
5.50	-5.33E-01	-7.62E-01	-8.70E-01	-9.11E-01	-9.25E-01	-9.29E-01	-9.30E-01	-9.31E-01
5.75	-6.17E-01	-9.17E-01	-1.08E+00	-1.15E+00	-1.17E+00	-1.18E+00	-1.18E+00	-1.18E+00
6.00	-6.73E-01	-1.03E+00	-1.27E+00	-1.37E+00	-1.41E+00	-1.43E+00	-1.43E+00	-1.43E+00
6.25	-7.07E-01	-1.12E+00	-1.42E+00	-1.58E+00	-1.65E+00	-1.67E+00	-1.68E+00	-1.69E+00
6.50	-7.28E-01	-1.17E+00	-1.54E+00	-1.77E+00	-1.88E+00	-1.92E+00	-1.93E+00	-1.93E+00
6.75	-7.39E-01	-1.21E+00	-1.62E+00	-1.92E+00	-2.08E+00	-2.15E+00	-2.18E+00	-2.18E+00
7.00	-7.44E-01	-1.23E+00	-1.67E+00	-2.04E+00	-2.27E+00	-2.38E+00	-2.42E+00	-2.43E+00
7.25	-7.44E-01	-1.24E+00	-1.70E+00	-2.12E+00	-2.42E+00	-2.58E+00	-2.65E+00	-2.67E+00
7.50	-7.32E-01	-1.24E+00	-1.72E+00	-2.17E+00	-2.53E+00	-2.76E+00	-2.87E+00	-2.91E+00
7.75	-6.64E-01	-1.23E+00	-1.72E+00	-2.20E+00	-2.61E+00	-2.91E+00	-3.08E+00	-3.15E+00
8.00	-2.26E-01	-1.17E+00	-1.71E+00	-2.20E+00	-2.65E+00	-3.02E+00	-3.25E+00	-3.37E+00
8.25	9.33E-01	-8.71E-01	-1.66E+00	-2.19E+00	-2.67E+00	-3.08E+00	-3.39E+00	-3.56E+00
8.50	2.39E+00	1.11E-01	-1.44E+00	-2.14E+00	-2.65E+00	-3.11E+00	-3.48E+00	-3.73E+00
8.75	500	1.50E+00	-6.37E-01	-1.96E+00	-2.59E+00	-3.09E+00	-3.51E+00	-3.84E+00
9.00	500	3.20E+00	6.73E-01	-1.31E+00	-2.43E+00	-3.01E+00	-3.49E+00	-3.88E+00
9.25	500	500	2.25E+00	-8.16E-02	-1.90E+00	-2.85E+00	-3.40E+00	-3.84E+00
9.50	500	500	500	1.46E+00	-7.69E-01	-2.41E+00	-3.22E+00	-3.74E+00
9.75	500	500	500	3.65E+00	7.62E-01	-1.39E+00	-2.86E+00	-3.56E+00
10.00	500	500	500	500	2.74E+00	1.24E-01	-1.96E+00	-3.24E+00

Table 6.3.7-37. Base-Case Plutonium Solubility Look-Up Table (log[Pu], mg/L)(Continued)

pH	log f_{CO_2} (bars)							
	-1.50	-2.00	-2.50	-3.00	-3.50	-4.00	-4.50	-5.00
10.25	500	500	500	500	500	2.10E+00	-4.65E-01	-2.47E+00
10.50	500	500	500	500	500	500	1.52E+00	-1.02E+00
10.75	500	500	500	500	500	500	500	9.86E-01

Source: DTN: MO0702PADISCON.001_R0 [DIRS 179358], Table 1.

NOTE: This look-up table is implemented in the TSPA-LA Model as parameter Sol_Pu_LUT. Entries reported as "500" in the table indicate conditions for which a valid solubility value does not exist.

Table 6.3.7-38. Base Protactinium Solubility Look-Up Table (log[Pa], mg/L)

pH	log f_{CO_2} (bars)							
	-1.50	-2.00	-2.50	-3.00	-3.50	-4.00	-4.50	-5.00
3.00	4.38E+00	4.38E+00	4.38E+00	4.38E+00	4.38E+00	4.38E+00	4.38E+00	4.38E+00
3.25	4.10E+00	4.10E+00	4.10E+00	4.10E+00	4.10E+00	4.10E+00	4.10E+00	4.10E+00
3.50	3.82E+00	3.82E+00	3.82E+00	3.82E+00	3.82E+00	3.82E+00	3.82E+00	3.82E+00
3.75	3.55E+00	3.55E+00	3.55E+00	3.55E+00	3.55E+00	3.55E+00	3.55E+00	3.55E+00
4.00	3.29E+00	3.29E+00	3.29E+00	3.29E+00	3.29E+00	3.29E+00	3.29E+00	3.29E+00
4.25	3.03E+00	3.03E+00	3.03E+00	3.03E+00	3.03E+00	3.03E+00	3.03E+00	3.03E+00
4.50	2.77E+00	2.77E+00	2.77E+00	2.77E+00	2.77E+00	2.77E+00	2.77E+00	2.77E+00
4.75	2.52E+00	2.52E+00	2.52E+00	2.52E+00	2.52E+00	2.52E+00	2.52E+00	2.52E+00
5.00	2.26E+00	2.26E+00	2.26E+00	2.26E+00	2.26E+00	2.26E+00	2.26E+00	2.26E+00
5.25	2.01E+00	2.01E+00	2.01E+00	2.01E+00	2.01E+00	2.01E+00	2.01E+00	2.01E+00
5.50	1.76E+00	1.76E+00	1.76E+00	1.76E+00	1.76E+00	1.76E+00	1.76E+00	1.76E+00
5.75	1.51E+00	1.51E+00	1.51E+00	1.51E+00	1.51E+00	1.51E+00	1.51E+00	1.51E+00
6.00	1.26E+00	1.26E+00	1.26E+00	1.26E+00	1.26E+00	1.26E+00	1.26E+00	1.26E+00
6.25	1.01E+00	1.01E+00	1.01E+00	1.01E+00	1.01E+00	1.01E+00	1.01E+00	1.01E+00
6.50	7.66E-01	7.62E-01	7.61E-01	7.60E-01	7.60E-01	7.60E-01	7.60E-01	7.60E-01
6.75	5.35E-01	5.17E-01	5.12E-01	5.11E-01	5.10E-01	5.10E-01	5.10E-01	5.10E-01
7.00	3.46E-01	2.84E-01	2.68E-01	2.63E-01	2.61E-01	2.60E-01	2.60E-01	2.60E-01
7.25	2.41E-01	8.83E-02	3.52E-02	1.83E-02	1.28E-02	1.11E-02	1.05E-02	1.03E-02
7.50	2.76E-01	-1.94E-02	-1.63E-01	-2.14E-01	-2.31E-01	-2.37E-01	-2.39E-01	-2.39E-01
7.75	4.56E-01	8.77E-03	-2.77E-01	-4.12E-01	-4.64E-01	-4.81E-01	-4.87E-01	-4.89E-01
8.00	5.33E-01	1.71E-01	-2.53E-01	-5.29E-01	-6.61E-01	-7.13E-01	-7.31E-01	-7.37E-01
8.25	5.98E-01	4.49E-01	-9.89E-02	-5.11E-01	-7.78E-01	-9.11E-01	-9.63E-01	-9.81E-01
8.50	1.42E+00	1.00E+00	1.47E-01	-3.62E-01	-7.64E-01	-1.03E+00	-1.16E+00	-1.21E+00
8.75	500	1.06E+00	5.38E-01	-1.30E-01	-6.20E-01	-1.01E+00	-1.28E+00	-1.41E+00
9.00	500	500	7.93E-01	1.89E-01	-3.95E-01	-8.75E-01	-1.26E+00	-1.53E+00
9.25	500	500	500	8.19E-01	-1.08E-01	-6.54E-01	-1.12E+00	-1.51E+00
9.50	500	500	500	1.36E+00	3.72E-01	-3.81E-01	-9.10E-01	-1.37E+00
9.75	500	500	500	500	1.12E+00	2.16E-02	-6.44E-01	-1.16E+00
10.00	500	500	500	500	500	9.56E-01	-2.78E-01	-9.00E-01
10.25	500	500	500	500	500	1.96E+00	5.24E-01	-5.52E-01
10.50	500	500	500	500	500	500	1.76E+00	1.72E-01

Source: DTN: MO0702PADISCON.001_R0 [DIRS 179358], Table 9.

NOTE: This look-up table is implemented in the TSPA-LA Model as parameter Sol_Pa_LUT. Entries reported as "500" in the table indicate conditions for which a valid solubility value does not exist.

Table 6.3.7-39. Base Thorium Solubility Look-Up Table (log[Th], mg/L)

pH	log f_{CO_2} (bars)							
	-1.50	-2.00	-2.50	-3.00	-3.50	-4.00	-4.50	-5.00
3.25	3.84E+00	3.84E+00	3.84E+00	3.84E+00	3.84E+00	3.84E+00	3.84E+00	3.84E+00
3.50	2.54E+00	2.54E+00	2.54E+00	2.54E+00	2.54E+00	2.54E+00	2.54E+00	2.54E+00
3.75	1.61E+00	1.61E+00	1.62E+00	1.62E+00	1.62E+00	1.62E+00	1.62E+00	1.62E+00
4.00	1.14E+00	1.14E+00	1.14E+00	1.14E+00	1.14E+00	1.14E+00	1.14E+00	1.14E+00
4.25	9.41E-01	9.41E-01	9.41E-01	9.41E-01	9.41E-01	9.41E-01	9.41E-01	9.41E-01
4.50	7.42E-01	7.42E-01	7.42E-01	7.42E-01	7.42E-01	7.42E-01	7.42E-01	7.42E-01
4.75	3.82E-01	3.82E-01	3.82E-01	3.82E-01	3.82E-01	3.82E-01	3.82E-01	3.82E-01
5.00	-2.92E-01	-2.94E-01	-2.95E-01	-2.95E-01	-2.95E-01	-2.95E-01	-2.95E-01	-2.95E-01
5.25	-1.17E+00	-1.20E+00	-1.21E+00	-1.21E+00	-1.22E+00	-1.22E+00	-1.22E+00	-1.22E+00
5.50	-1.75E+00	-1.99E+00	-2.10E+00	-2.14E+00	-2.16E+00	-2.16E+00	-2.16E+00	-2.16E+00
5.75	-1.69E+00	-2.13E+00	-2.50E+00	-2.73E+00	-2.84E+00	-2.88E+00	-2.89E+00	-2.90E+00
6.00	-1.46E+00	-1.94E+00	-2.39E+00	-2.75E+00	-2.99E+00	-3.10E+00	-3.14E+00	-3.16E+00
6.25	-1.22E+00	-1.70E+00	-2.17E+00	-2.60E+00	-2.91E+00	-3.09E+00	-3.17E+00	-3.20E+00
6.50	-9.69E-01	-1.46E+00	-1.94E+00	-2.40E+00	-2.77E+00	-3.02E+00	-3.15E+00	-3.19E+00
6.75	-7.16E-01	-1.22E+00	-1.70E+00	-2.18E+00	-2.60E+00	-2.92E+00	-3.10E+00	-3.18E+00
7.00	-4.60E-01	-9.69E-01	-1.46E+00	-1.94E+00	-2.40E+00	-2.78E+00	-3.03E+00	-3.15E+00
7.25	-2.02E-01	-7.16E-01	-1.22E+00	-1.70E+00	-2.18E+00	-2.60E+00	-2.92E+00	-3.10E+00
7.50	5.88E-02	-4.60E-01	-9.69E-01	-1.46E+00	-1.94E+00	-2.40E+00	-2.78E+00	-3.03E+00
7.75	3.22E-01	-2.02E-01	-7.15E-01	-1.22E+00	-1.70E+00	-2.18E+00	-2.60E+00	-2.92E+00
8.00	5.90E-01	5.91E-02	-4.60E-01	-9.69E-01	-1.46E+00	-1.94E+00	-2.40E+00	-2.78E+00
8.25	1.04E+00	3.23E-01	-2.01E-01	-7.15E-01	-1.22E+00	-1.70E+00	-2.18E+00	-2.60E+00
8.50	500	5.96E-01	6.01E-02	-4.59E-01	-9.68E-01	-1.46E+00	-1.94E+00	-2.40E+00
8.75	500	1.41E+00	3.25E-01	-2.00E-01	-7.14E-01	-1.22E+00	-1.70E+00	-2.18E+00
9.00	500	500	6.29E-01	6.31E-02	-4.57E-01	-9.67E-01	-1.47E+00	-1.94E+00
9.25	500	500	2.62E+00	3.33E-01	-1.96E-01	-7.12E-01	-1.22E+00	-1.70E+00
9.50	500	500	500	9.49E-01	7.17E-02	-4.53E-01	-9.65E-01	-1.47E+00
9.75	500	500	500	500	3.81E-01	-1.86E-01	-7.07E-01	-1.21E+00
10.00	500	500	500	500	500	9.60E-02	-4.41E-01	-9.58E-01
10.25	500	500	500	500	500	1.67E+00	-1.61E-01	-6.93E-01
10.50	500	500	500	500	500	500	6.41E-01	-4.13E-01
10.75	500	500	500	500	500	500	500	4.71E-03

Source: DTN: MO0702PADISCON.001_R0 [DIRS 179358], Table 7.

NOTE: This look-up table is implemented in the TSPA-LA Model as parameter Sol_Pa_LUT. Entries reported as "500" in the table indicate conditions for which a valid solubility value does not exist.

Table 6.3.7-40. Base Tin Solubility Look-Up Table (log[Sn], mg/L)

pH	log fCO ₂ (bars)							
	-1.5	-2.0	-2.5	-3.0	-3.5	-4.0	-4.5	-5.0
2.00	-2.38E+00	-2.38E+00	-2.38E+00	-2.38E+00	-2.38E+00	-2.38E+00	-2.38E+00	-2.38E+00
2.25	-2.38E+00	-2.38E+00	-2.38E+00	-2.38E+00	-2.38E+00	-2.38E+00	-2.38E+00	-2.38E+00
2.50	-2.39E+00	-2.39E+00	-2.39E+00	-2.39E+00	-2.39E+00	-2.39E+00	-2.39E+00	-2.39E+00
2.75	-2.39E+00	-2.39E+00	-2.39E+00	-2.39E+00	-2.39E+00	-2.39E+00	-2.39E+00	-2.39E+00
3.00	-2.39E+00	-2.39E+00	-2.39E+00	-2.39E+00	-2.39E+00	-2.39E+00	-2.39E+00	-2.39E+00
3.25	-2.39E+00	-2.39E+00	-2.39E+00	-2.39E+00	-2.39E+00	-2.39E+00	-2.39E+00	-2.39E+00
3.50	-2.39E+00	-2.39E+00	-2.39E+00	-2.39E+00	-2.39E+00	-2.39E+00	-2.39E+00	-2.39E+00
3.75	-2.39E+00	-2.39E+00	-2.39E+00	-2.39E+00	-2.39E+00	-2.39E+00	-2.39E+00	-2.39E+00
4.00	-2.39E+00	-2.39E+00	-2.39E+00	-2.39E+00	-2.39E+00	-2.39E+00	-2.39E+00	-2.39E+00
4.25	-2.39E+00	-2.39E+00	-2.39E+00	-2.39E+00	-2.39E+00	-2.39E+00	-2.39E+00	-2.39E+00
4.50	-2.39E+00	-2.39E+00	-2.39E+00	-2.39E+00	-2.39E+00	-2.39E+00	-2.39E+00	-2.39E+00
4.75	-2.39E+00	-2.39E+00	-2.39E+00	-2.39E+00	-2.39E+00	-2.39E+00	-2.39E+00	-2.39E+00
5.00	-2.38E+00	-2.38E+00	-2.38E+00	-2.38E+00	-2.38E+00	-2.38E+00	-2.38E+00	-2.38E+00
5.25	-2.38E+00	-2.38E+00	-2.38E+00	-2.38E+00	-2.38E+00	-2.38E+00	-2.38E+00	-2.38E+00
5.50	-2.38E+00	-2.38E+00	-2.38E+00	-2.38E+00	-2.38E+00	-2.38E+00	-2.38E+00	-2.38E+00
5.75	-2.38E+00	-2.38E+00	-2.38E+00	-2.38E+00	-2.38E+00	-2.38E+00	-2.38E+00	-2.38E+00
6.00	-2.37E+00	-2.37E+00	-2.37E+00	-2.37E+00	-2.37E+00	-2.37E+00	-2.37E+00	-2.37E+00
6.25	-2.37E+00	-2.37E+00	-2.37E+00	-2.37E+00	-2.37E+00	-2.37E+00	-2.37E+00	-2.37E+00
6.50	-2.35E+00	-2.35E+00	-2.35E+00	-2.35E+00	-2.35E+00	-2.35E+00	-2.35E+00	-2.35E+00
6.75	-2.33E+00	-2.33E+00	-2.33E+00	-2.33E+00	-2.33E+00	-2.33E+00	-2.33E+00	-2.33E+00
7.00	-2.29E+00	-2.29E+00	-2.29E+00	-2.29E+00	-2.29E+00	-2.29E+00	-2.29E+00	-2.29E+00
7.25	-2.22E+00	-2.22E+00	-2.22E+00	-2.22E+00	-2.22E+00	-2.22E+00	-2.22E+00	-2.22E+00
7.50	-2.12E+00	-2.12E+00	-2.13E+00	-2.13E+00	-2.13E+00	-2.13E+00	-2.13E+00	-2.13E+00
7.75	-1.98E+00	-1.99E+00	-1.99E+00	-1.99E+00	-2.00E+00	-2.00E+00	-2.00E+00	-2.00E+00
8.00	-1.81E+00	-1.82E+00	-1.83E+00	-1.83E+00	-1.83E+00	-1.83E+00	-1.83E+00	-1.83E+00
8.25	-1.60E+00	-1.62E+00	-1.63E+00	-1.63E+00	-1.63E+00	-1.64E+00	-1.64E+00	-1.64E+00
8.50	-1.37E+00	-1.39E+00	-1.41E+00	-1.41E+00	-1.42E+00	-1.42E+00	-1.42E+00	-1.42E+00
8.75	-1.12E+00	-1.14E+00	-1.16E+00	-1.18E+00	-1.18E+00	-1.19E+00	-1.19E+00	-1.19E+00
9.00	500	-8.70E-01	-9.03E-01	-9.26E-01	-9.36E-01	-9.40E-01	-9.42E-01	-9.42E-01
9.25	500	-5.82E-01	-6.18E-01	-6.55E-01	-6.76E-01	-6.84E-01	-6.87E-01	-6.88E-01
9.50	500	500	-2.98E-01	-3.55E-01	-3.94E-01	-4.13E-01	-4.20E-01	-4.22E-01
9.75	500	500	500	2.60E-03	-7.35E-02	-1.16E-01	-1.34E-01	-1.40E-01
10.00	500	500	500	500	3.29E-01	2.28E-01	1.85E-01	1.67E-01

Table 6.3.7-40. Base Tin Solubility Look-Up Table (log[Sn], mg/L) (Continued)

pH	log fCO2 (bars)							
	-1.5	-2.0	-2.5	-3.0	-3.5	-4.0	-4.5	-5.0
10.25	500	500	500	500	500	6.89E-01	5.71E-01	5.17E-01
10.50	500	500	500	500	500	500	1.08E+00	9.45E-01
10.75	500	500	500	500	500	500	500	1.51E+00

Source: DTN: MO0702PADISCON.001_R0 [DIRS 179358], Table 16.

NOTE: This look-up table is implemented in the TSPA-LA Model as parameter Sol_Sn_LUT. Entries reported as "500" in the table indicate conditions for which a valid solubility value does not exist.

Table 6.3.7-41. Uncertainty in Americium Solubility Model

TSPA-LA Model Name	Model Abstraction Symbol	Description	Units	Distribution Type	Distribution Specification
Am_Eps_1_low_a	ϵ_1	Uncertainties in log K below 1 molal ionic strength.	None	Truncated normal	$\mu = 0$ $\sigma = 1.0$ $2\sigma = \pm 2.0$
Am_Eps_1_high_a	ϵ_1	Uncertainties in log K at 1 to 3 molal ionic strength.	None	Truncated normal	$\mu = 0$ $\sigma = 1.04$ $2\sigma = \pm 2.08$
Am_Eps_2_Glass_Low_a	ϵ_2 ^{CSNF-low} ϵ_2 ^{CDSP-Glass} ϵ_2 ^{CDSP-F-low}	Fluoride Uncertainty, CSNF waste packages when I < 0.2m. CDSP packages, Cell 1b when I < 0.004m and Cell 1a.	None	Triangular	Min = 0 Max = 4.42 Most likely = 0
Am_Eps_2_CSNF_High_a	ϵ_2 ^{CSNF-high} ϵ_2 ^{CSNF-invert}	Fluoride Uncertainty, CSNF waste packages when I ≥ 0.2m and invert below CSNF waste packages.	None	Triangular	Min = 0 Max = 109.03 Most likely = 0
Am_Eps_2_CDSP_High_a	ϵ_2 ^{CDSP-F-high} ϵ_2 ^{CDSP-invert}	Fluoride Uncertainty, CDSP waste packages when I ≥ 0.004m and invert below CDSP waste packages.	None	Triangular	Min = 0 Max = 688.6 Most likely = 0

Source: DTN: MO0702PADISCON.001_R0 [DIRS 179358], Table 19; DTN: MO0702PAFLUORI.000_R1 [DIRS 181219], Table 13.

Table 6.3.7-42. Uncertainty in Neptunium (Np₂O₅) Solubility Model

TSPA-LA Model Name	Model Abstraction Symbol	Description	Units	Distribution Type	Distribution Specification
Np2O5_Eps_1_low_a	ϵ_1	Uncertainties in log K below 1 molal ionic strength.	None	Truncated normal	$\mu = 0$ $\sigma = 0.8$ $2\sigma = \pm 1.6$
Np2O5_Eps_1_high_a	ϵ_1	Uncertainties in log K at 1 to 3 molal ionic strength.	None	Truncated normal	$\mu = 0$ $\sigma = 0.85$ $2\sigma = \pm 1.7$
Np2O5_Eps_2_Glass_Low CSNF_High_a	ϵ_2 ^{CSNF-low} ϵ_2 ^{CDSP-Glass} ϵ_2 ^{CDSP-F-low}	Fluoride Uncertainty, CSNF waste packages when I < 0.2m. CDSP packages, Cell 1b when I < 0.004m and Cell 1a.	None	Triangular	Min = 0 Max = 11 Most likely = 0
Np2O5_Eps_2_CSNF_High_a	ϵ_2 ^{CSNF-high} ϵ_2 ^{CSNF-invert}	Fluoride Uncertainty, CSNF waste packages when I ≥ 0.2m and invert below CSNF waste packages.	None	Triangular	Min = 0 Max = 197 Most likely = 0
Np2O5_Eps_2_CDSP_High_a	ϵ_2 ^{CDSP-F-high} ϵ_2 ^{CDSP-invert}	Fluoride Uncertainty, CDSP waste packages when I ≥ 0.004m and invert below CDSP waste packages.	None	Triangular	Min = 0 Max = 853 Most likely = 0

Source: DTN: MO0702PADISCON.001_R0 [DIRS 179358], Table 19; DTN: MO0702PAFLUORI.000_R1 [DIRS 181219], Table 5.

Table 6.3.7-43. Uncertainty in Neptunium (NpO₂) Solubility Model

TSPA-LA Model Name	Model Abstraction Symbol	Description	Units	Distribution Type	Distribution Specification
NpO2_Eps_1_low_a	ϵ_1	Uncertainties in log K below 1 molal ionic strength.	None	Truncated normal	$\mu = 0$ $\sigma = 0.6$ $2\sigma = \pm 1.2$
NpO2_Eps_1_high_a	ϵ_1	Uncertainties in log K at 1 to 3 molal ionic strength.	None	Truncated normal	$\mu = 0$ $\sigma = 0.67$ $2\sigma = \pm 1.34$
NpO2_Eps_2_Glass_Low_a	ϵ_2 ^{CSNF-low} ϵ_2 ^{CDSP-Glass} ϵ_2 ^{CDSP-F-low}	Fluoride Uncertainty, CSNF waste packages when I < 0.2m. CDSP packages, Cell 1b when I < 0.004m and Cell 1a.	None	Triangular	Min = 0 Max = 14.1 Most likely = 0
NpO2_Eps_2_CSNF_High_a	ϵ_2 ^{CSNF-high} ϵ_2 ^{CSNF-invert}	Fluoride Uncertainty, CSNF waste packages when I ≥ 0.2m and invert below CSNF waste packages.	None	Triangular	Min = 0 Max = 255.8 Most likely = 0
NpO2_Eps_2_CDSP_High_a	ϵ_2 ^{CDSP-F-high} ϵ_2 ^{CDSP-invert}	Fluoride Uncertainty, CDSP waste packages when I ≥ 0.004m and invert below CDSP waste packages.	None	Triangular	Min = 0 Max = 1093.5 Most likely = 0

Source: DTN: MO0702PADISCON.001_R0 [DIRS 179358], Table 19; DTN: MO0702PAFLUORI.000_R1 [DIRS 181219], Table 3.

Table 6.3.7-44. Uncertainty in Plutonium Solubility Model

TSPA-LA Model Name	Model Abstraction Symbol	Description	Units	Distribution Type	Distribution Specification
Pu_Eps_1_low_a	ϵ_1	Uncertainties in log K below 1 molal ionic strength.	None	Truncated normal	$\mu = 0$ $\sigma = 0.7$ $2\sigma = 1.4$
Pu_Eps_1_high_a	ϵ_1	Uncertainties in log K at 1 to 3 molal ionic strength.	None	Truncated normal	$\mu = 0$ $\sigma = 0.76$ $2\sigma = 1.52$
Pu_Eps_2_Glass_Low_a	$\epsilon_2^{\text{CSNF-low}}$ $\epsilon_2^{\text{CDSP-Glass}}$ $\epsilon_2^{\text{CDSP-F-low}}$	Fluoride Uncertainty, CSNF waste packages when $I < 0.2\text{m}$. CDSP packages, Cell 1b when $I < 0.004\text{m}$ and Cell 1a.	None	Triangular	Min = 0 Max = 79 Most likely = 0
Pu_Eps_2_CSNF_High_a	$\epsilon_2^{\text{CSNF-high}}$ $\epsilon_2^{\text{CSNF-invert}}$	Fluoride Uncertainty, CSNF waste packages when $I \geq 0.2\text{m}$ and invert below CSNF waste packages.	None	Triangular	Min = 0 Max = 1374 Most likely = 0
Pu_Eps_2_CDSP_High_a	$\epsilon_2^{\text{CDSP-F-high}}$ $\epsilon_2^{\text{CDSP-invert}}$	Fluoride Uncertainty, CDSP waste packages when $I \geq 0.004\text{m}$ and invert below CDSP waste packages.	None	Triangular	Min = 0 Max = 5460 Most likely = 0

Source: DTN: MO0702PADISCON.001_R0 [DIRS 179358], Table 19; DTN: MO0702PAFLUORI.000_R1 [DIRS 181219], Table 1.

Table 6.3.7-45. Uncertainty in Protactinium Solubility Model

TSPA-LA Model Name	Model Abstraction Symbol	Description	Units	Distribution Type	Distribution Specification
Pa_Eps_1_a	ϵ_1	Uncertainties in analogue	None	Uniform	Min = -4.42 Max = -0.05
Pa_Eps_2_Glass_Low_a	$\epsilon_2^{\text{CSNF-low}}$ $\epsilon_2^{\text{CDSP-Glass}}$ $\epsilon_2^{\text{CDSP-F-low}}$	Fluoride Uncertainty, CSNF waste packages when $I < 0.2\text{m}$. CDSP packages, Cell 1b when $I < 0.004\text{m}$ and Cell 1a.	None	Triangular	Min = 0 Max = 11 Most likely = 0
Pa_Eps_2_CSNF_High_a	$\epsilon_2^{\text{CSNF-high}}$ $\epsilon_2^{\text{CSNF-invert}}$	Fluoride Uncertainty, CSNF waste packages when $I \geq 0.2\text{m}$ and invert below CSNF waste packages.	None	Triangular	Min = 0 Max = 197 Most likely = 0
Pa_Eps_2_CDSP_High_a	$\epsilon_2^{\text{CDSP-F-high}}$ $\epsilon_2^{\text{CDSP-invert}}$	Fluoride Uncertainty, CDSP waste packages when $I \geq 0.004\text{m}$ and invert below CDSP waste packages.	None	Triangular	Min = 0 Max = 853 Most likely = 0

Source: DTN: MO0702PADISCON.001_R0 [DIRS 179358], Table 19; DTN: MO0702PAFLUORI.000_R1 [DIRS 181219], Table 15.

Table 6.3.7-46. Uncertainty in Thorium Solubility Model

TSPA-LA Model Name	Model Abstraction Symbol	Description	Units	Distribution Type	Distribution Specification
Th_Eps_1_low_a	\mathcal{E}_1	Uncertainties in log K below 1 molal ionic strength.	None	Truncated normal	$\mu = 0$ $\sigma = 0.7$ $2\sigma = \pm 1.4$
Th_Eps_1_high_a	\mathcal{E}_1	Uncertainties in log K at 1 to 3 molal ionic strength.	None	Truncated normal	$\mu = 0$ $\sigma = 0.76$ $2\sigma = \pm 1.52$
Th_Eps_2_Glass_Low_a	$\mathcal{E}_2^{\text{CSNF-low}}$ $\mathcal{E}_2^{\text{CDSP-Glass}}$ $\mathcal{E}_2^{\text{CDSP-F-low}}$	Fluoride Uncertainty, CSNF waste packages when $I < 0.2\text{m}$. CDSP packages, Cell 1b when $I < 0.004\text{m}$ and Cell 1a.	None	Triangular	Min = 0 Max = 626.2 Most likely = 0
Th_Eps_2_CSNF_High_a	$\mathcal{E}_2^{\text{CSNF-high}}$ $\mathcal{E}_2^{\text{CSNF-invert}}$	Fluoride Uncertainty, CSNF waste packages when $I \geq 0.2\text{m}$ and invert below CSNF waste packages.	None	Triangular	Min = 0 Max = 7848.3 Most likely = 0
Th_Eps_2_CDSP_High_a	$\mathcal{E}_2^{\text{CDSP-F-high}}$ $\mathcal{E}_2^{\text{CDSP-invert}}$	Fluoride Uncertainty, CDSP waste packages when $I \geq 0.004\text{m}$ and invert below CDSP waste packages.	None	Triangular	Min = 0 Max = 23723.3 Most likely = 0

Source: DTN: MO0702PADISCON.001_R0 [DIRS 179358], Table 19; DTN: MO0702PAFLUORI.000_R1 [DIRS 181219], Table 11.

Table 6.3.7-47. Uncertainty in Tin Solubility Model

TSPA-LA Model Name	Model Abstraction Symbol	Description	Units	Distribution Type	Distribution Specification
Sn_Eps_low_a	\mathcal{E}_1	Uncertainties in log K below 1 molal ionic strength.	None	Truncated normal	$\mu = 0$ $\sigma = 0.45$ $2\sigma = 0.90$
Sn_Eps_high_a	\mathcal{E}_1	Uncertainties in log K at 1 to 3 molal ionic strength.	None	Truncated normal	$\mu = 0$ $\sigma = 0.54$ $2\sigma = 1.08$

Source: DTN: MO0702PADISCON.001_R0 [DIRS 179358], Table 19.

Table 6.3.7-48. Multiplication Factor, N(pH), Used to Modify Fluoride Concentration Uncertainty Terms (ϵ^2) for Americium

pH	Multiplication Factor for Fluoride Uncertainty		
	Glass, CSNF low, and CDSP low	CSNF high and CSNF invert	CDSP high and CDSP invert
6.00	1.00E+00	1.00E+00	1.00E+00
6.25	8.91E-02	1.45E-01	3.20E-01
6.50	1.30E-02	2.92E-02	7.24E-02
6.75	2.13E-03	5.61E-03	1.36E-02
7.00	3.44E-04	1.04E-03	2.47E-03
7.25	4.98E-05	1.98E-04	4.50E-04
7.50	3.39E-06	4.08E-05	8.39E-05
7.75	0.00E-00	1.04E-05	1.68E-05
8.00	0.00E-00	4.41E-06	4.13E-06
8.25	3.62E-06	2.41E-06	1.52E-06
8.50	3.39E-06	2.34E-06	1.36E-06
8.75	8.82E-06	6.00E-06	3.67E-06
9.00	3.69E-05	2.59E-05	1.65E-05
9.25	1.92E-04	1.36E-04	8.82E-05
9.50	1.13E-03	8.02E-04	5.23E-04
9.75	7.24E-03	5.10E-03	3.33E-03

Source: DTN: MO0702PAFLUORI.000_R1 [DIRS 181219], Table 14.

NOTE: These multiplication factors are implemented in the TSPA-LA Model as parameters Am_Eps_2_Glass_Low, Am_Eps_2_CS NF_High, Am_Eps_2_CDSP_High.

Table 6.3.7-49. Multiplication Factor, N(pH), Used to Modify Fluoride Concentration Uncertainty Terms (ϵ^2) for Neptunium (Np2O5)

pH	Multiplication Factor for Fluoride Uncertainty		
	Glass, CSNF low, and CDSP low	CSNF high and CSNF invert	CDSP high and CDSP invert
3.00	1.00E+00	1.00E+00	1.00E+00
3.25	7.27E-01	7.36E-01	7.63E-01
3.50	4.91E-01	5.09E-01	5.47E-01
3.75	3.18E-01	3.30E-01	3.60E-01
4.00	1.91E-01	2.01E-01	2.17E-01
4.25	1.09E-01	1.17E-01	1.41E-01
4.50	6.64E-02	6.66E-02	9.31E-02
4.75	3.82E-02	3.74E-02	5.70E-02
5.00	2.09E-02	2.08E-02	3.36E-02
5.25	1.18E-02	1.16E-02	1.94E-02
5.50	6.64E-03	6.51E-03	1.11E-02
5.75	3.73E-03	3.68E-03	6.28E-03
6.00	2.09E-03	2.15E-03	3.55E-03
6.25	1.18E-03	1.24E-03	2.00E-03
6.50	6.64E-04	7.13E-04	1.13E-03
6.75	3.73E-04	4.12E-04	6.37E-04
7.00	2.09E-04	2.41E-04	3.60E-04
7.25	1.18E-04	1.44E-04	2.04E-04
7.50	6.45E-05	8.96E-05	1.17E-04
7.75	3.45E-05	6.01E-05	6.97E-05
8.00	1.55E-05	4.81E-05	4.52E-05
8.25	4.64E-05	4.15E-05	3.37E-05
8.50	4.09E-05	3.80E-05	3.11E-05
8.75	5.45E-05	5.13E-05	4.43E-05
9.00	1.55E-04	1.55E-04	1.47E-04
9.25	1.34E-03	1.32E-03	1.29E-03

Source: DTN: MO0702PAFLUORI.000_R1 [DIRS 181219], Table 6.

NOTE: These multiplication factors are implemented in the TSPA-LA Model as parameters Np2O5_Eps_2_Glass_Low_N, Np2O5_CSNF_High_N, Np2O5_CDSP_High_N .

Table 6.3.7-50. Multiplication Factor, N(pH), Used to Modify Fluoride Concentration Uncertainty Terms (ϵ^2) for Neptunium (NpO₂)

pH	Multiplication Factor for Fluoride Uncertainty		
	Glass, CSNF low, and CDSP low	CSNF high and CSNF invert	CDSP high and CDSP invert
3.00	1.00E+00	1.00E+00	1.00E+00
3.25	5.77E-01	6.74E-01	7.77E-01
3.50	2.86E-01	4.12E-01	5.75E-01
3.75	1.23E-01	2.16E-01	3.77E-01
4.00	4.96E-02	9.57E-02	2.04E-01
4.25	1.92E-02	3.78E-02	9.00E-02
4.50	7.66E-03	1.42E-02	3.50E-02
4.75	3.26E-03	5.53E-03	1.31E-02
5.00	1.49E-03	2.26E-03	4.98E-03
5.25	7.09E-04	9.96E-04	2.01E-03
5.50	3.62E-04	4.71E-04	8.74E-04
5.75	1.91E-04	2.37E-04	4.10E-04
6.00	1.06E-04	1.24E-04	2.04E-04
6.25	5.74E-05	6.74E-05	1.07E-04
6.50	3.12E-05	3.74E-05	5.74E-05
6.75	1.84E-05	2.11E-05	3.15E-05
7.00	9.93E-06	1.22E-05	1.75E-05
7.25	5.53E-06	7.21E-06	9.88E-06
7.50	3.05E-06	4.45E-06	5.68E-06
7.75	1.49E-06	3.01E-06	3.46E-06
8.00	4.26E-07	2.82E-06	2.61E-06
8.25	4.40E-06	3.92E-06	3.22E-06
8.50	1.00E-05	9.27E-06	8.17E-06
8.75	4.75E-05	4.55E-05	4.40E-05
9.00	4.18E-04	4.07E-04	4.07E-04
9.25	5.53E-03	5.47E-03	5.48E-03

Source: DTN: MO0702PAFLUORI.000_R1 [DIRS 181219], Table 4.

NOTE: These multiplication factors are implemented in the TSPA-LA Model as parameters NpO₂_Glass_low_N, NpO₂_CSNF_High_N, NpO₂_CDSP_High_N.

Table 6.3.7-51. Multiplication Factor, N(pH), Used to Modify Fluoride Concentration Uncertainty Terms (ϵ^2) for Plutonium

pH	Multiplication Factor for Fluoride Uncertainty		
	Glass, CSNF low, and CDSP low	CSNF high and CSNF invert	CDSP high and CDSP invert
2.00	1.00E+00	1.00E+00	1.00E+00
2.25	7.67E-01	7.58E-01	7.42E-01
2.50	5.08E-01	4.98E-01	4.83E-01
2.75	3.50E-01	3.42E-01	3.33E-01
3.00	2.41E-01	2.40E-01	2.44E-01
3.25	1.48E-01	1.60E-01	1.81E-01
3.50	7.51E-02	9.41E-02	1.27E-01
3.75	3.18E-02	4.69E-02	7.81E-02
4.00	1.18E-02	1.96E-02	3.95E-02
4.25	4.06E-03	7.20E-03	1.64E-02
4.50	1.34E-03	2.45E-03	5.90E-03
4.75	4.32E-04	8.03E-04	1.98E-03
5.00	1.37E-04	2.58E-04	6.44E-04
5.25	4.32E-05	8.19E-05	2.07E-04
5.50	1.34E-05	2.58E-05	6.61E-05
5.75	4.08E-06	8.04E-06	2.12E-05
6.00	1.19E-06	2.47E-06	6.81E-06
6.25	3.29E-07	7.39E-07	2.22E-06
6.50	6.33E-08	2.12E-07	7.38E-07
6.75	0.00E+00	5.60E-08	2.54E-07
7.00	0.00E+00	1.34E-08	9.23E-08
7.25	0.00E+00	3.20E-09	3.64E-08
7.50	0.00E+00	2.04E-09	1.62E-08
7.75	0.00E+00	3.35E-09	9.16E-09
8.00	0.00E+00	7.71E-09	8.44E-09
8.25	1.90E-08	1.68E-08	1.43E-08
8.50	4.94E-08	4.79E-08	4.62E-08
8.75	2.91E-07	2.90E-07	3.07E-07
9.00	2.85E-06	2.91E-06	3.15E-06
9.25	3.85E-05	3.94E-05	4.24E-05
9.50	7.34E-04	7.44E-04	7.90E-04
9.75	6.33E-02	6.43E-02	6.90E-02

Source: DTN: MO0702PAFLUORI.000_R1 [DIRS 181219], Table 2.

NOTE: These multiplication factors are implemented in the TSPA-LA Model as parameters Pu_Glass_low_N, Pu_CSNF_High_N, Pu_CDSP_High_N.

Table 6.3.7-52. Multiplication Factor, N(pH), Used to Modify Fluoride Concentration Uncertainty Terms (ϵ^2) for Thorium

pH	Multiplication Factor for Fluoride Uncertainty		
	Glass, CSNF low, and CDSP low	CSNF high and CSNF invert	CDSP high and CDSP invert
3.25	1.00E+00	1.00E+00	1.00E+00
3.50	7.51E-02	1.01E-01	1.48E-01
3.75	2.70E-02	3.53E-02	4.75E-02
4.00	2.08E-02	2.74E-02	3.60E-02
4.25	1.76E-02	2.41E-02	3.19E-02
4.50	1.45E-02	2.15E-02	2.91E-02
4.75	1.05E-02	1.90E-02	2.67E-02
5.00	4.73E-03	1.59E-02	2.44E-02
5.25	8.99E-04	1.19E-02	2.17E-02
5.50	1.02E-04	6.88E-03	1.82E-02
5.75	1.04E-05	2.26E-03	1.32E-02
6.00	1.04E-06	3.40E-04	6.85E-03
6.25	1.03E-07	3.62E-05	1.77E-03
6.50	7.98E-09	3.65E-06	2.26E-04
6.75	0.00E-00	3.62E-07	2.34E-05
7.00	0.00E-00	3.25E-08	2.36E-06
7.25	0.00E-00	0.00E-00	2.63E-07
7.50	0.00E-00	4.33E-09	7.86E-08
7.75	0.00E-00	4.00E-08	1.08E-07
8.00	0.00E-00	1.73E-07	2.14E-07
8.25	2.87E-07	3.57E-07	3.72E-07
8.50	3.83E-07	5.08E-07	5.61E-07
8.75	5.11E-07	6.79E-07	7.91E-07
9.00	4.79E-07	8.28E-07	1.02E-06
9.25	7.98E-07	1.07E-06	1.42E-06
9.50	3.61E-05	5.21E-05	7.81E-05

Source: DTN: MO0702PAFLUORI.000_R1 [DIRS 181219], Table 12.

NOTE: These multiplication factors are implemented in the TSPA-LA Model as parameters Th_Glass_low_N, Th_CSNF_High_N, Th_CDSP_High_N.

Table 6.3.7-53. Uranium Solubility Look-Up Table (log[U], mg/L) for CSNF WPs Breached under Nominal Conditions or by Seismic Activity

pH	log fCO ₂ (bars)							
	-1.5	-2.0	-2.5	-3.0	-3.5	-4.0	-4.5	-5.0
3.50	4.41E+00	4.41E+00	4.41E+00	4.41E+00	4.41E+00	4.41E+00	4.41E+00	4.41E+00
3.75	3.55E+00	3.55E+00	3.55E+00	3.55E+00	3.55E+00	3.55E+00	3.55E+00	3.55E+00
4.00	2.87E+00	2.87E+00	2.87E+00	2.87E+00	2.87E+00	2.87E+00	2.87E+00	2.87E+00
4.25	2.33E+00	2.33E+00	2.33E+00	2.33E+00	2.33E+00	2.33E+00	2.33E+00	2.33E+00
4.50	1.93E+00	1.92E+00	1.92E+00	1.92E+00	1.92E+00	1.92E+00	1.92E+00	1.92E+00
4.75	1.62E+00	1.60E+00	1.60E+00	1.59E+00	1.59E+00	1.59E+00	1.59E+00	1.59E+00
5.00	1.35E+00	1.32E+00	1.31E+00	1.31E+00	1.30E+00	1.30E+00	1.30E+00	1.30E+00
5.25	1.10E+00	1.03E+00	1.00E+00	9.95E-01	9.93E-01	9.92E-01	9.92E-01	9.91E-01
5.50	9.31E-01	7.65E-01	6.97E-01	6.74E-01	6.66E-01	6.63E-01	6.63E-01	6.62E-01
5.75	9.05E-01	6.19E-01	4.67E-01	4.07E-01	3.86E-01	3.79E-01	3.77E-01	3.76E-01
6.00	1.03E+00	6.26E-01	3.76E-01	2.51E-01	2.03E-01	1.87E-01	1.82E-01	1.80E-01
6.25	1.25E+00	7.58E-01	4.13E-01	2.07E-01	1.17E-01	8.36E-02	7.27E-02	6.92E-02
6.50	1.52E+00	9.60E-01	5.30E-01	2.48E-01	9.90E-02	3.93E-02	1.87E-02	1.19E-02
6.75	1.86E+00	1.21E+00	7.12E-01	3.53E-01	1.32E-01	3.21E-02	-4.74E-03	-1.71E-02
7.00	2.33E+00	1.51E+00	9.38E-01	5.01E-01	2.11E-01	5.47E-02	-8.42E-03	-3.04E-02
7.25	500	1.89E+00	1.20E+00	6.98E-01	3.34E-01	1.09E-01	6.00E-03	-3.21E-02
7.50	500	2.54E+00	1.52E+00	9.32E-01	4.92E-01	2.00E-01	4.29E-02	-2.10E-02
7.55	500	2.90E+00	1.60E+00	9.95E-01	5.39E-01	2.24E-01	5.35E-02	-1.69E-02
7.75	500	500	1.98E+00	1.21E+00	6.96E-01	3.26E-01	1.09E-01	7.58E-03
7.90	500	500	2.51E+00	1.42E+00	8.48E-01	4.32E-01	1.66E-01	3.59E-02
8.00	500	500	500	1.58E+00	9.38E-01	4.97E-01	2.12E-01	6.04E-02
8.25	500	500	500	2.27E+00	1.24E+00	7.07E-01	3.47E-01	1.45E-01
8.30	500	500	500	2.58E+00	1.33E+00	7.66E-01	3.88E-01	1.66E-01
8.50	500	500	500	500	1.73E+00	9.65E-01	5.26E-01	2.59E-01
8.65	500	500	500	500	2.31E+00	1.19E+00	6.64E-01	3.56E-01
8.75	500	500	500	500	500	1.34E+00	7.47E-01	4.16E-01
9.00	500	500	500	500	500	2.11E+00	1.04E+00	6.11E-01
9.07	500	500	500	500	500	2.67E+00	1.18E+00	6.84E-01
9.25	500	500	500	500	500	500	1.58E+00	8.56E-01
9.50	500	500	500	500	500	500	500	1.24E+00
9.75	500	500	500	500	500	500	500	2.08E+00

Source: DTN: MO0702PADISCON.001_R0 [DIRS 179358], Table 4.

NOTE: This look-up table is implemented in the TSPA-LA Model as parameter Sol_U_LUT_Schoepite_CSNF. Entries reported as '500' in the table indicate conditions for which a valid solubility value does not exist.

Table 6.3.7-54. Uncertainty in Log K Values for Base-Case Uranium Solubility Model (CSNF WP Nominal and Seismic Scenario Classes)

TSPA-LA Model Name	Model Abstraction Symbol	Description	Units	Distribution Type	Distribution Specification
U_Eps_1_low_Nominal_a	ϵ_1	Uncertainties in log K (schoepite) below 1 molal ionic strength	None	Truncated normal	$\mu = 0$ $\sigma = 0.5$ $2\sigma = \pm 1.0$
U_Eps_1_high_Nominal_a	ϵ_1	Uncertainties in log K (schoepite) at 1 to 3 molal ionic strength	None	Truncated normal	$\mu = 0$ $\sigma = 0.6$ $2\sigma = \pm 1.2$
U_Eps_2_CSNF_Low_Nominal_a	ϵ_2 CSNF-low	Fluoride Uncertainty, CSNF waste packages when $I < 0.2m$.	None	Triangular	Min = 0 Max = 78 Most likely = 0
U_Eps_2_CSNF_High_Nominal_a	ϵ_2 CSNF-high ϵ_2 CSNF-invert	Fluoride Uncertainty, CSNF waste packages when $I \geq 0.2m$	None	Triangular	Min = 0 Max = 1361 Most likely = 0

Source: DTN: MO0702PADISCON.001_R0 [DIRS 179358], Table 19;
DTN: MO0702PAFLUORI.000_R1 [DIRS 181219], Table 7.

Table 6.3.7-55. Multiplication Factor, N(pH), Used to Modify Fluoride Concentration Uncertainty Terms (ϵ_2) for Uranium (CSNF WP, Nominal and Seismic Scenario Classes)

pH	Multiplication Factor for Fluoride Uncertainty	
	CSNF low	CSNF high
3.50	1.00E+00	1.00E+00
3.75	7.24E-01	7.03E-01
4.00	5.17E-01	4.85E-01
4.25	4.18E-01	3.73E-01
4.50	3.48E-01	2.99E-01
4.75	2.70E-01	2.41E-01
5.00	1.85E-01	1.92E-01
5.25	1.06E-01	1.45E-01
5.50	4.86E-02	9.86E-02
5.75	1.83E-02	5.67E-02
6.00	6.17E-03	2.63E-02
6.25	1.99E-03	1.01E-02
6.50	6.31E-04	3.42E-03
6.75	1.94E-04	1.11E-03
7.00	5.00E-05	3.49E-04
7.25	0.00E-00	1.07E-04
7.50	0.00E-00	4.64E-05
7.75	0.00E-00	1.67E-04
8.00	0.00E-00	2.01E-03
8.25	2.44E-02	2.51E-02

Source: DTN: MO0702PAFLUORI.000_R1 [DIRS 181219], Table 8.

NOTE: This multiplication factor is implemented in the TSPA-LA Model as parameters U_CS NF_Low_Nominal_N and U_CS NF_High_Nominal_N.

Table 6.3.7-56. Schoepite Controlled Uranium Solubility Look-Up Table (log[U], mg/L) for CDSP WPs Breached Under any Scenario, CSNF WPs Breached in by an Igneous Intrusion, and in the Invert (all locations and scenarios)

pH	log fco ₂ (bars)							
	-1.50	-2.00	-2.50	-3.00	-3.50	-4.00	-4.50	-5.00
3.50	4.41E+00	4.41E+00	4.41E+00	4.41E+00	4.41E+00	4.41E+00	4.41E+00	4.41E+00
3.75	3.55E+00	3.55E+00	3.55E+00	3.55E+00	3.55E+00	3.55E+00	3.55E+00	3.55E+00
4.00	2.86E+00	2.86E+00	2.86E+00	2.86E+00	2.86E+00	2.86E+00	2.86E+00	2.86E+00
4.25	2.33E+00	2.33E+00	2.33E+00	2.33E+00	2.33E+00	2.33E+00	2.33E+00	2.33E+00
4.50	1.92E+00	1.91E+00	1.91E+00	1.91E+00	1.91E+00	1.91E+00	1.91E+00	1.91E+00
4.75	1.61E+00	1.59E+00	1.59E+00	1.59E+00	1.59E+00	1.59E+00	1.59E+00	1.59E+00
5.00	1.34E+00	1.31E+00	1.30E+00	1.30E+00	1.30E+00	1.30E+00	1.30E+00	1.30E+00
5.25	1.10E+00	1.02E+00	9.94E-01	9.85E-01	9.83E-01	9.82E-01	9.81E-01	9.81E-01
5.50	9.24E-01	7.55E-01	6.86E-01	6.62E-01	6.54E-01	6.51E-01	6.51E-01	6.50E-01
5.75	9.10E-01	6.11E-01	4.57E-01	3.94E-01	3.73E-01	3.66E-01	3.64E-01	3.63E-01
6.00	1.04E+00	6.30E-01	3.68E-01	2.41E-01	1.92E-01	1.75E-01	1.70E-01	1.68E-01
6.25	1.25E+00	7.66E-01	4.09E-01	2.01E-01	1.09E-01	7.55E-02	6.43E-02	6.08E-02
6.50	1.52E+00	9.70E-01	5.37E-01	2.45E-01	9.45E-02	3.42E-02	1.33E-02	6.55E-03
6.75	1.86E+00	1.22E+00	7.22E-01	3.52E-01	1.30E-01	2.93E-02	-7.88E-03	-2.03E-02
7.00	2.33E+00	1.51E+00	9.48E-01	5.09E-01	2.10E-01	5.32E-02	-1.02E-02	-3.22E-02
7.25		1.89E+00	1.21E+00	7.08E-01	3.34E-01	1.08E-01	5.05E-03	-3.31E-02
7.50		2.54E+00	1.53E+00	9.44E-01	5.01E-01	2.00E-01	4.24E-02	-2.16E-02
7.75			1.98E+00	1.22E+00	7.07E-01	3.33E-01	1.09E-01	7.28E-03
8.00				1.57E+00	9.51E-01	5.06E-01	2.12E-01	6.02E-02

Source: DTN: MO0702PADISCON.001_R0 [DIRS 179358], Table 5.

NOTE: This look-up table is implemented in the TSPA-LA Model as parameter Sol_U_LUT_Schoepite. This solubility corresponds to schoepite saturation. The shaded area indicates the region where it is uncertain if uranium solubility is controlled by schoepite or Na-Boltwoodite.

Table 6.3.7-57. Na-Boltwoodite and Na₄UO₂(CO₃)₃ Controlled Uranium Solubility Look-Up Table (log[U], mg/L) for CDSP WPs Breached under Any Scenario, CSNF WPs Breached by an Igneous Intrusion, and in the Invert (all locations and scenarios)

pH	log fco ₂ (bars)							
	-1.50	-2.00	-2.50	-3.00	-3.50	-4.00	-4.50	-5.00
6.50	2.56E+00							
6.75	2.16E+00	2.00E+00	1.51E+00	1.07E+00	7.46E-01	5.56E-01	4.73E-01	4.43E-01
7.00	1.94E+00	1.82E+00	1.28E+00	8.21E-01	4.79E-01	2.77E-01	1.88E-01	1.56E-01
7.25	2.14E+00	1.51E+00	1.09E+00	5.88E-01	2.28E-01	2.04E-02	-7.08E-02	-1.04E-01
7.50	2.79E+00	1.55E+00	1.03E+00	3.97E-01	-9.31E-03	-2.29E-01	-3.23E-01	-3.56E-01
7.75	4.78E+00	1.98E+00	1.03E+00	3.18E-01	-2.14E-01	-4.68E-01	-5.67E-01	-6.01E-01
8.00	4.78E+00	2.76E+00	1.34E+00	4.67E-01	-3.27E-01	-6.84E-01	-8.00E-01	-8.35E-01
8.25	4.78E+00	4.78E+00	1.92E+00	7.59E-01	-2.27E-01	-8.41E-01	-1.01E+00	-1.05E+00
8.50	4.78E+00	4.78E+00	2.75E+00	1.25E+00	1.67E-01	-8.36E-01	-1.19E+00	-1.25E+00
8.75	4.78E+00	4.78E+00	4.77E+00	1.89E+00	6.32E-01	-5.27E-01	-1.27E+00	-1.41E+00
9.00	4.78E+00	4.78E+00	4.77E+00	2.75E+00	1.20E+00	3.81E-02	-1.13E+00	-1.51E+00
9.25	4.78E+00	4.78E+00	4.77E+00	4.76E+00	1.88E+00	5.47E-01	-6.60E-01	-1.51E+00
9.50	4.78E+00	4.78E+00	4.77E+00	4.76E+00	2.78E+00	1.15E+00	-9.89E-02	-1.26E+00
9.75	4.78E+00	4.78E+00	4.77E+00	4.76E+00	4.73E+00	1.89E+00	4.56E-01	-7.58E-01
10.00	4.78E+00	4.78E+00	4.77E+00	4.76E+00	4.73E+00	2.92E+00	1.13E+00	-2.57E-01
10.25	500	500	500	500	500	500	2.02E+00	3.92E-01

Source: DTN: MO0702PADISCON.001_R0 [DIRS 179358] Table 6.

NOTE: This look-up table is implemented in the TSPA-LA Model as parameter Sol_U_LUT_Boltwoodite. The upper shaded area indicates the region where it is uncertain if uranium solubility is controlled by schoepite or Na-Boltwoodite saturation. The lower shaded area is where solubility is controlled by Na₄UO₂(CO₃)₃. Entries reported as '500' indicate conditions for which a valid solubility value does not exist.

Table 6.3.7-58. Uncertainty in Uranium Solubility Model in CDSP WPs Breached Under Any Scenario, CSNF WPs Breached by an Igneous Intrusion, and in the Invert (all locations and scenarios)

TSPA-LA Model Name	Model Abstraction Symbol	Description	Units	Distribution Type	Distribution Specification
U_Eps_1_low_other_a	ϵ_1	Uncertainties in solubility (schoepite and Na-Boltwoodite) below 1 molal ionic strength; to be used in the colorless and shaded regions in Table 6.3.7-37 and upper shaded region in Table 6.3.7-38	None	Truncated normal	$\mu = 0$ $\sigma = 0.5$ $2\sigma = \pm 1.0$
U_Eps_1_high_other_a	ϵ_1	Uncertainties in solubility (schoepite and Na-Boltwoodite) at 1 to 3 molal ionic strength; uncertainties in log K ($\text{Na}_4\text{UO}_2(\text{CO}_3)_3$) below 3 molal ionic strength (blue regions in Table 6.3.7-38)	None	Truncated normal	$\mu = 0$ $\sigma = 0.6$ $2\sigma = \pm 1.2$
U_Eps_2_Schoepite_Glass_Low_a	ϵ_2 CSNF-low ϵ_2 CDSP-Glass ϵ_2 CDSP-F-low ϵ_2	Fluoride uncertainty, CSNF waste packages when $l < 0.2\text{m}$. CDSP packages, Cell 1b when $l < 0.004\text{m}$ and Cell 1a.	None	Triangular	Min = 0 Max = 78 Most likely = 0
U_Eps_2_Schoepite_CSNF_High_a	ϵ_2 CSNF-high ϵ_2 CSNF-invert ϵ_2	Fluoride uncertainty, CSNF waste packages when $l \geq 0.2\text{m}$ and invert below CSNF waste packages	None	Triangular	Min = 0 Max = 1361 Most likely = 0
U_Eps_2_Schoepite_CDSP_High_a	ϵ_2 CDSP-F-high ϵ_2 CDSP-invert ϵ_2	Fluoride uncertainty, CDSP waste packages when $l \geq 0.004\text{m}$ and invert below CDSP waste packages	None	Triangular	Min = 0 Max = 5385 Most likely = 0
U_Eps_2_Boltwoodite_Glass_Lo_a	ϵ_2 CSNF-high ϵ_2 CSNF-invert ϵ_2	Fluoride uncertainty, CSNF waste packages when $l < 0.2\text{m}$. CDSP packages, Cell 1b when $l < 0.004\text{m}$ and Cell 1a	None	Triangular	Min = 0 Max = 6.13 Most likely = 0
U_Eps_2_Boltwoodite_CSNF_Hig_a	ϵ_2 CSNF-high ϵ_2 CSNF-invert ϵ_2	Fluoride uncertainty, CSNF waste packages when $l \geq 0.2\text{m}$ and invert below CSNF waste packages	None	Triangular	Min = 0 Max = 57.01 Most likely = 0
U_Eps_2_Boltwoodite_CDSP_Hig_a	ϵ_2 CDSP-F-high ϵ_2 CDSP-invert ϵ_2	Fluoride uncertainty, CDSP waste packages when $l \geq 0.004\text{m}$ and invert below CDSP waste packages	None	Triangular	Min = 0 Max = 272.3 Most likely = 0
Schoepite_Boltwoodite_Interp_a	None	Used in the TSPA-LA Model to determine the fractional value that is used to interpolate between schoepite and Na-Boltwoodite look-up tables	None	Uniform	Min. = 0 Max = 1

Source: DTN: MO0702PADISCON.001_R0 [DIRS 179358], Table 19; DTN: MO0702PAFLUORI.000_R1 [DIRS 181219], Table 9.

NOTE: The parameter Schoepite_Boltwoodite_Interp_a was developed by TSPA based on information given in notes to Table 6 of DTN: MO0702PADISCON.001_R0 [DIRS 179358].

Table 6.3.7-59. Multiplication Factor, N(pH), Used to Modify Fluoride Concentration Uncertainty Terms (ϵ_2) for Uranium in CDSP WPs Breached under Any Scenario, CSNF Waste Packages Breached by an Igneous Intrusion and in the Invert (all locations and scenarios)

Glass, CSNF low, and CDSP low			CSNF high and CSNF invert			CDSP high and CDSP invert		
pH	Schoepite	Boltwoodite-Na	pH	Schoepite	Boltwoodite-Na	pH	Schoepite	Boltwoodite-Na
3.50	1.00E+00	None	3.50	1.00E+00	None	3.50	1.00E+00	None
3.75	7.24E-01	None	3.75	7.03E-01	None	3.75	6.68E-01	None
4.00	5.17E-01	None	4.00	4.85E-01	None	4.00	4.44E-01	None
4.25	4.18E-01	None	4.25	3.73E-01	None	4.25	3.34E-01	None
4.50	3.48E-01	None	4.50	2.99E-01	None	4.50	2.73E-01	None
4.75	2.70E-01	None	4.75	2.41E-01	None	4.75	2.31E-01	None
5.00	1.85E-01	None	5.00	1.92E-01	None	5.00	1.98E-01	None
5.25	1.06E-01	None	5.25	1.45E-01	None	5.25	1.68E-01	None
5.50	4.86E-02	None	5.50	9.86E-02	None	5.50	1.36E-01	None
5.75	1.83E-02	None	5.75	5.67E-02	None	5.75	1.03E-01	None
6.00	6.17E-03	None	6.00	2.63E-02	None	6.00	6.91E-02	None
6.25	1.99E-03	None	6.25	1.01E-02	None	6.25	3.93E-02	None
6.50	6.32E-04	6.36E-02	6.50	3.42E-03	3.62E-01	6.50	1.81E-02	1.00E+00
6.75	1.95E-04	1.89E-02	6.75	1.11E-03	7.86E-02	6.75	6.90E-03	3.30E-01
7.00	4.87E-05	7.98E-03	7.00	3.48E-04	1.79E-02	7.00	2.36E-03	7.49E-02
7.25	0.00E-00	4.36E-03	7.25	1.07E-04	5.52E-03	7.25	7.96E-04	1.55E-02
7.50	0.00E-00	3.13E-03	7.50	4.58E-05	2.88E-03	7.50	3.34E-04	4.08E-03
7.75	0.00E-00	3.82E-03	7.75	1.64E-04	3.25E-03	7.75	4.02E-04	2.75E-03
8.00	0.00E-00	9.87E-03	8.00	1.98E-03	8.60E-03	8.00	2.13E-03	6.92E-03
8.25	2.44E-02	4.89E-02	8.25	2.50E-02	2.56E-02	8.25	2.90E-02	1.93E-02
8.50	None	9.10E-02	8.50	None	6.80E-02	8.50	None	5.55E-02
8.75	None	2.40E-01	8.75	None	2.17E-01	8.75	None	1.82E-01
9.00	None	1.00E+00	9.00	None	1.00E+00	9.00	None	8.43E-01

Source: DTN: MO0702PAFLUORI.001_R1 [DIRS 181219], Table 10.

NOTE: These multiplication factors are implemented in the TSPA-LA Model as parameters: U_Schoepite_Glass_low_N, U_Schoepite_CSNF_High_N, U_Schoepite_CDSP_High_N, U_Boltwoodite_Glass_low_N, U_Boltwoodite_CSNF_High_N, and U_Boltwoodite_CDSP_High_N.

Table 6.3.7-60. Actinide Caps (mg/L) Between an Ionic Strength of 3 and 10 Molal for CSNF Packages

Controlling solid	Element	IS = 3	IS = 7	IS= 10
PuO ₂ (hyd,aged)	Pu	39487	92135	131622
NpO ₂	Np	981	2289	3270
Np ₂ O ₅	Np	1417	3306	4723
Schoepite	U	29698	69294	98992
ThO ₂ (am)	Th	1400	3266	4666
AmOHCO ₃	Am	1285	2999	4285
Np ₂ O ₅ (by analog)	Pa	1417	3306	4723

Source: DTN: MO0704PASOLCAP.000_R0 [DIRS 180389], Table 2.

NOTE: These caps are implemented in the TSPA-LA Model as parameters: CSNF_Pu_TypeIII_Cap, CSNF_NpO2_TypeIII_Cap, CSNF_Np2O5_TypeIII_Cap, CSNF_U_Schoepite_TypeIII_Cap, CSNF_Th_TypeIII_Cap, CSNF_Am_TypeIII_Cap, CSNF_Pa_TypeIII_Cap

IS = ionic strength in units of molal

Table 6.3.7-61. Actinide Caps (mg/L) Between an Ionic Strength of 3 and 10 Molal for CDSP Packages, Cell 1b

Controlling solid	Element	IS = 3	IS = 7	IS= 10
PuO ₂ (hyd,aged)	Pu	39487	92135	131622
NpO ₂	Np	981	2289	3270
Np ₂ O ₅	Np	1417	3306	4723
Schoepite*	U	29698	69294	98992
Na-Boltwoodite*	U	33636	61967	88524
ThO ₂ (am)	Th	1400	3266	4666
AmOHCO ₃	Am	1285	2999	4285
Np ₂ O ₅ (by analog)	Pa	1417	3306	4723

Source: DTN: MO0704PASOLCAP.000_R0 [DIRS 180389], Table 2.

NOTE: These caps are implemented in the TSPA-LA Model as parameters: CDSP_Pu_TypeIII_Cap, CDSP_NpO2_TypeIII_Cap, CDSP_Np2O5_TypeIII_Cap, CDSP_U_Schoepite_TypeIII_Cap, CDSP_U_Boltwoodite_TypeIII_Cap, CDSP_Th_TypeIII_Cap, CDSP_Am_TypeIII_Cap, CDSP_Pa_TypeIII_Cap.

When sampling between the schoepite and boltwoodite LUTs, use the schoepite values.

IS = ionic strength (molal).

Table 6.3.7-62. Parameters for TSPA-LA Glass Waste Form Colloid Abstraction

TSPA-LA Parameter Name	Model Abstraction Symbol	Description	Units	Distribution Type	Distribution Specification
DTN: MO0701PAGLASWF.000_R1 [DIRS 180393]					
CPu_Col_Wf_Embed_Sampled_a	<i>C_{RN, coll, DHLWG, embed, sampled}</i>	Concentration of irreversibly attached plutonium, associated with DHLWG colloids.	mol/L	Uniform	1.E-11 to 1.E-8
CPu_Col_Glass_Embed_Min	<i>C_{Rn, coll, DHLWG, embed, min}</i>	Lowest observed or expected concentration of irreversibly attached plutonium associated with DHLWG colloids.	mol/L	Single Value	1.E-13
CPu_Per_WF_Embed_Col_a	<i>C_{coll, DHLWG, sampled}</i>	Concentration of irreversibly attached plutonium per concentration of colloids.	(mol/L)/(mg/L)	Triangular Distribution	min 5×10^{-9} Mode 2×10^{-8} Max 2.5×10^{-8}
Smectite_ZPC	None	Smectite zero point of charge, pH below which the smectite does not sorb.	None	Single Value	1.5
Smectite_pH_hi	None	High pH for smectite ionic strength threshold fit.	None	Single Value	9
Coeff_pH_Sq_Smectite	None	Coefficient of pH squared term for fit of ionic strength threshold for smectite colloid stability.	None	Single Value	-0.008
Coeff_pH_Smectite	None	Coefficient of pH term for fit of ionic strength threshold for smectite colloid stability.	None	Single Value	0.12
Coeff_inter_Smectite	None	Intercept term for fit of ionic strength threshold for smectite colloid stability.	None	Single Value	0.03
Specific_SA_Smectite_Col_a	SA, Smectite, coll	Specific surface area for DHLWG (smectite) colloid.	M2/g	Uniform	10 to 100

Table 6.3.7-62. Parameters for TSPA-LA Glass Waste Form Colloid Abstraction (Continued)

TSPA-LA Parameter Name	Model Abstraction Symbol	Description	Units	Distribution Type	Distribution Specification	
Smectite_Site_Density	NS, Smectite, coll	Site density for DHLWG (smectite) colloid.	Sites/ nm ²	Single Value	2.3	
DTN: MO0701PASORPTN.000_R1 [DIRS 180391]						
Kd_Pu_Rev_Smectite_a	$K_{d,Pu,coll,wf}$	Distribution coefficient for reversible sorption of plutonium to smectite colloids.	mL/g	Cumulative Distribution Function	Prob Level	Value
					0	1×10^3
					0.45	5×10^3
					0.80	1×10^4
					0.95	5×10^4
1	1×10^5					
Kd_Am_Rev_Smectite_a Kd_Th_Rev_Smectite_a Kd_Pa_Rev_Smectite_a	$K_{d,Am,coll,wf}$ $K_{d,Th,coll,wf}$ $K_{d,Pa,coll,wf}$	Distribution coefficient for reversible sorption of americium, thorium, and protactinium to smectite colloids. Each distribution sampled independently.	mL/g	Cumulative Distribution Function	Prob Level	Value
					0	1×10^4
					0.07	5×10^4
					0.17	1×10^5
					0.4	5×10^5
					0.6	1×10^6
					0.92	5×10^6
1	1×10^7					
Kd-Cs_Rev_Smectite_a	$K_{d,Cs,coll,wf}$	Distribution coefficient for reversible sorption of cesium to smectite colloids.	mL/g	Cumulative Distribution Function	Prob Level	Value
					0	5×10^1
					0.05	1×10^2
					0.4	5×10^2
					0.7	1×10^3
1	5×10^3					
DTN: MO0701PAKDSUNP.000_R1 [DIRS 180392]						
Kd_Np_Rev_Smectite_a	$K_{d,Np,coll,Smectite}$	Distribution coefficient for reversible sorption of neptunium to smectite colloids.	mL/g	Log Uniform	1×10^1 to 5×10^2	
Kd_U_Rev_Smectite_a	$K_{d,U,coll,Smectite}$	Distribution coefficient for reversible sorption of tin to smectite colloids.	mL/g	Log Uniform	5×10^2 to 5×10^4	

Table 6.3.7-62. Parameters for TSPA-LA Glass Waste Form Colloid Abstraction (Continued)

TSPA-LA Parameter Name	Model Abstraction Symbol	Description	Units	Distribution Type	Distribution Specification
Kd_Sn_Rev_Smectite_a	$K_{d,Sn,coll,Smecti}$	Distribution coefficient for reversible sorption of uranium to smectite colloids.	mL/g	Log Uniform	1×10^5 to 1×10^6
Kd_Ra_Rev_Smectite_a	$K_{d,Ra,coll,Smecti}$	Distribution coefficient for reversible sorption of radium to smectite colloids.	mL/g	Log Uniform	1×10^2 to 5×10^3

Sources: DTN: MO0701PAGLASWF.000_R1 [DIRS 180393]; DTN: MO0701PASORPTN.000_R1 [DIRS 180391];
DTN: MO0701PAKDSUNP.000_R1 [DIRS 180392].

NOTE: Condition report 11424 describes the errata in the source documents.

Table 6.3.7-63. Parameters for TSPA-LA CSNF Waste Form Irreversible Colloid Abstraction

TSPA-LA Parameter Name	Model Abstraction Symbol	Description	Units	Distribution Type	Distribution Specification	
					Prob Level	Value
CPu_Col_CSNF_Sampled_a	$C_{RNcoll,SNF,embed}$	Concentration of irreversibly attached radionuclide element RN (plutonium, americium) associated with SNF colloids.	mol/L	Cumulative Distribution Function	0	1×10^{-10}
					0.05	5×10^{-10}
					0.1	1×10^{-9}
					0.15	5×10^{-9}
					0.2	1×10^{-8}
					0.3	5×10^{-8}
					0.5	1×10^{-7}
					0.7	5×10^{-7}
					0.9	1×10^{-6}
					1	5×10^{-6}
CPu_Col_CSNF_Min	$C_{RNcoll,SNF,min}$	Lowest observed or expected concentration of irreversibly attached plutonium associated with DHLWG colloids.	Mol/L	Single Value	1.E-13	
CPu_Per_CSNF_Embed_Col_a	$C_{coll,SNF,uniform}$	Concentration of Irreversibly attached plutonium per concentration of CSNF colloids.	(mol/L) / (mg/L)	Uniform Distribution	Min	5×10^{-7}
					Max	1×10^{-6}
CSNF_pH_lo	None	Lower limit of pH range for CSNF colloid stability data	None	Single Value	4	
CSNF_ZPC_lo	None	Lower limit of pH range for zero point of charge for CSNF colloid stability data.	None	Single Value	7	
CSNF_ZPC_hi	None	Upper limit of pH range for zero point of charge for CSNF colloid stability data.	None	Single Value	9.3	
CSNF_pH_hi	None	Upper limit of pH range for CSNF colloid stability data.	None	Single Value	10.6	
Coeff_pH_Cube_lo_CSNF	None	Coefficient of pH cubed term for fit of ionic strength threshold for CSNF colloid stability at low pH.	None	Single Value	0.0089	

Table 6.3.7-63. Parameters for TSPA-LA CSNF Waste Form Irreversible Colloid Abstraction (Continued)

TSPA-LA Parameter Name	Model Abstraction Symbol	Description	Units	Distribution Type	Distribution Specification
Coeff_pH_Sq_lo_CSNF	None	Coefficient of pH squared term for fit of ionic strength threshold for CSNF colloid stability at low pH.	None	Single Value	-0.1466
Coeff_pH_lo_CSNF	None	Coefficient of pH term for fit of ionic strength threshold for CSNF colloid stability at low pH.	None	Single value	0.7462
Coeff_inter_pH_lo_CSNF	None	Coefficient of intercept term for fit of ionic strength threshold for CSNF colloid stability at low pH.	None	Single value	-1.092
Coeff_pH_Cube_hi_CSNF	None	Coefficient of pH cubed term for fit of ionic strength threshold for CSNF colloid stability at high pH.	None	Single value	0.087362
Coeff_pH_Sq_hi_CSNF	None	Coefficient of pH squared term for fit of ionic strength threshold for CSNF colloid stability at high pH.	None	Single value	-2.4078
Coeff_pH_hi_CSNF	None	Coefficient of pH term for fit of ionic strength threshold for CSNF colloid stability at high pH.	None	Single value	22.126
Coeff_inter_pH_hi_CSNF	None	Coefficient of intercept term for fit of ionic strength threshold for CSNF colloid stability at high pH.	None	Single value	-67.791

Source: DTN: MO0701PACSNF.000_R1 [DIRS 180439].

NOTE: Condition report 11424 describes the errata in the source documents.

Table 6.3.7-64. Parameters for TSPA-LA SNF Waste Form Reversible Colloid Abstraction

TSPA-LA Parameter Name	Model Abstraction Symbol	Description	Units	Distribution Type	Distribution Specification	
					Prob Level	Value
Conc_Col_U_Sampled_a	$m_{coll,Uranophane,sampled}$	Expected mass of uranophane colloids per unit volume or mass of water.	mg/L	Cumulative Distribution Function	0	1×10^{-3}
					0.5	1×10^{-1}
					0.75	1×10^0
					0.90	1×10^1
					0.98	5×10^1
					1	2×10^2
Conc_Col_U_Min	$m_{coll,Uranophane,min}$	Lowest observed or expected mass of uranophane colloids per unit volume or mass of water.	mg/L	Single value	1×10^{-6}	
U_pH_lo	None	Lower limit of pH range for U colloid stability data.	None	Single value	4	
U_pH_hi	None	Upper limit of pH range for U colloid stability data.	None	Single value	9	
Coeff_pH_Sq_U	None	Coefficient of pH squared term for fit of ionic strength threshold for U colloid stability.	None	Single value	-0.008	
Coeff_pH_U	None	Coefficient of pH term for fit of ionic strength threshold for U colloid stability.	None	Single value	0.14	
Coeff_inter_U	None	Coefficient of intercept term for fit of ionic strength threshold for U colloid stability.	None	Single value	0.4	
Kd_Pu_Rev_U_Col_a	$K_{d,Pucoll,uranophane}$	Distribution coefficient for reversible sorption of plutonium onto uranophane colloids.	mL/g	Log Uniform	5×10^0 to 1×10^4	
Kd_Am_Rev_U_Col_a	$K_{d,Amcoll,uranophane}$	Distribution coefficient for reversible sorption of americium onto uranophane colloids.	mL/g	Log Uniform	5×10^0 to 1×10^4	
Kd_Th_Rev_U_Col_a	$K_{d,Thcoll,uranophane}$	Distribution coefficient for reversible sorption of thorium onto uranophane colloids.	mL/g	Log Uniform	5×10^0 to 1×10^4	

Table 6.3.7-64. Parameters for TSPA-LA SNF Waste Form Reversible Colloid Abstraction (Continued)

TSPA-LA Parameter Name	Model Abstraction Symbol	Description	Units	Distribution Type	Distribution Specification
Kd_Pa_Rev_U_Col_a	$K_{d,Pa_{coll},uranophane}$	Distribution coefficient for reversible sorption of Pa onto uranophane colloids.	mL/g	Log Uniform	5×10^0 to 1×10^4
Kd_Cs_Rev_U_Col_a	$K_{d,Cs_{coll},uranophane}$	Distribution coefficient for reversible sorption of cesium onto uranophane colloids.	mL/g	Log Uniform	1×10^1 to 1×10^3
Kd_Np_Rev_U_Col_a	$K_{d,Np_{coll},uranophane}$	Distribution coefficient for reversible sorption of neptunium onto uranophane colloids.	mL/g	Log Uniform	1×10^1 to 5×10^2 Note: incorrectly implemented as 1 to 5×10^2 ; see Appendix P Table P-6
Kd_Ra_Rev_U_Col_a	$K_{d,Ra_{coll},uranophane}$	Distribution coefficient for reversible sorption of radium onto uranophane colloids.	mL/g	Log Uniform	1×10^1 to 1×10^3
Kd_Sn_Rev_U_Col_a	$K_{d,Sn_{coll},uranophane}$	Distribution coefficient for reversible sorption of tin onto uranophane colloids.	mL/g	Log Uniform	1×10^0 to 1×10^2
Specific_SA_U_Col	$S_{A,uranophane,coll}$	Specific surface area for uranophane.	m ² /g	Single value	30
U_Site_Density	$N_{S,uranophane,coll}$	Site density for uranophane particle colloid.	Sites/nm ²	Single value	2

Source: DTN: MO0701PACSNF.000_R1 [DIRS 180439].

NOTE: Condition report 11424 describes the errata in the source documents.

Table 6.3.7-65. Parameters for TSPA-LA Iron Oxyhydroxide Colloid Abstraction

TSPA-LA Parameter Name	Model Abstraction Symbol	Description	Units	Distribution Type	Distribution Specification	
Conc_Col_FeOx_Min	$m_{coll,FeOx,min}$	Minimum concentration of FeOx colloids.	mg/L	Single value	1×10^{-6}	
Conc_Col_FeOx_CS_Sampled_a		Sampled FeOx colloid concentration when carbon steel is degrading.	mg/L	Truncated Log Normal	Mean = 03.69 Standard deviation = 2.79 Minimum 0.3 Maximum 30	
Conc_Col_FeOx_SS_Sampled_a	$m_{coll,FeOx,sampled}$	Sampled FeOx colloid concentration for locations containing degraded stainless steel.	mg/L	Cumulative Distribution Function	Prob Level	Value
					0	1×10^{-3}
					0.6	1×10^{-1}
					0.90	1×10^0
					0.95	1×10^1
1	3×10^1					
FeOx_pH_lo	None	Low pH for FeOx colloid ionic strength threshold fit.	None	Single value	4.5	
FeOx_ZPC_lo	None	Low end of zero point of charge range.	None	Single value	8.4	
FeOx_ZPC_hi	None	Low end of zero point of charge range.	None	Single value	9.4	
FeOx_pH_hi	None	Low pH for FeOx colloid ionic strength threshold fit.	None	Single value	10.4	
Coeff_pH_lo_FeOx	None	Coefficient of pH term for fit of ionic strength threshold for FeOx colloid stability at low pH.	None	Single value	-0.013	
Coeff_Inter_pH_lo_FeOx	None	Intercept term for fit of ionic strength threshold for FeOx colloid stability at low pH.	None	Single value	0.11	
Coeff_pH_sq_hi_FeOx	None	Coefficient of pH squared term for fit of ionic strength threshold for FeOx colloid stability at high pH.	None	Single value	0.0017	
Coeff_pH_hi_FeOx	None	Coefficient of pH term for fit of ionic strength threshold for FeOx colloid stability at high pH.	None	Single value	-0.0327	

Table 6.3.7-65. Parameters for TSPA-LA Iron Oxyhydroxide Colloid Abstraction (Continued)

TSPA-LA Parameter Name	Model Abstraction Symbol	Description	Units	Distribution Type	Distribution Specification
Coeff_inter_pH_hi_FeOx	None	Intercept term for fit of ionic strength threshold for FeOx colloid stability at high pH.	None	Single value	0.158
Min_Default_Fwd_Rate_Const	<i>k</i>	Minimum value for the log uniform default forward rate constant.	m ³ /m ² , yr	Single value	0.002
Max_Default_Fwd_Rate_Const	<i>k</i>	Maximum value for the log uniform default forward rate constant.	m ³ /m ² , yr	Single value	0.05
Default_Fwd_Rate_Const_a	<i>k</i>	Default forward rate constant	m ³ /m ² , yr	Log-uniform	Min = Min_Default_Fwd_Rate_Const (0.002) Max = Max_Default_Fwd_Rate_Const (0.05)
Target_Flux_Out_Ratio_a	F _{RN}	Target flux-out ratio: ratio of radionuclide mass associated with colloids (reversible and irreversible) to radionuclide mass associated with colloids and dissolved radionuclide mass.	None	Uniform	Min = 0.9 Max = 0.99

Source: DTN: MO0701PAIRONCO.000_R1 [DIRS 180440].

NOTE: Condition report 11424 describes the errata in the source documents.

Table 6.3.7-66. Parameters for TSPA-LA Groundwater Colloid Abstraction

TSPA-LA Parameter Name	Model Abstraction Symbol	Description	Units	Distribution Type	Distribution Specification	
Conc_Col_GW_Min	$m_{coll, gw, min}$	Minimum GW colloid concentration.	mg/L	Single value	1×10^{-6}	
Conc_Col_GW_Sampled_a	$m_{coll, gw, sampled}$	Sampled GW colloid concentration.	mg/L	Cumulative Distribution Function	Prob Level	Value
					0	0.001
					0.5	0.1
					0.75	1
					0.9	10
					0.98	50
1	200					
Kd_Pu_Rev_Smectite_a Kd_Am_Rev_Smectite_a Kd_Th_Rev_Smectite_a Kd_Pa_Rev_Smectite_a Kd-Cs_Rev_Smectite_a Kd_Np_Rev_Smectite_a Kd_U_Rev_Smectite_a Kd_Sn_Rev_Smectite_a Kd_Ra_Rev_Smectite_a	Table 6.3.7-62	Table 6.3.7-62	mL/g	Table 6.3.7-62	Table 6.3.7-62	
Smectite_ZPC Smectite_ph_hi Coeff_pH_Sq_Smectite Coeff_pH_Smectite Coeff_Inter_Smectite	None	Table 6.3.7-62	None	Single value	Table 6.3.7-62	

Source: DTN: MO0701PAGROUND.000_R0 [DIRS 179310].

Table 6.3.7-67. Alternative Conceptual Models Considered for In-Package Chemistry

Alternative Conceptual Model	Key Assumptions	Screening Assessment and Basis
Alternative Conceptual Model I	The WP is compositionally discrete.	The WVC model showed that the resulting chemical effects of individual WP components were comparable to that of their ensembles. See Section 6.5.1 in <i>In-Package Chemistry Abstraction</i> (SNL 2007 [DIRS 180506]).
Alternative Conceptual Model II	The composition of seepage entering a WP is likely to vary as a function of changing conditions in the UZ and drift environments.	The SDM showed that wide compositional ranges in the seepage composition had very little influence on the resulting in-package chemistry. See Section 6.5.2 in <i>In-Package Chemistry Abstraction</i> (SNL 2007 [DIRS 180506]).

Source: *In-Package Chemistry Abstraction* (SNL 2007 [DIRS 180506], Table 6-14).

Table 6.3.7-68. Alternative Conceptual Models Considered for CSNF Waste Form Degradation

Alternative Conceptual Model	Key Assumptions	Screening Assessment and Basis
Electrochemical	<p>The anodic Tafel lines can be extrapolated to the corrosion potential.</p> <p>The long-term corrosion behavior of commercial spent nuclear fuel is similar to that of unirradiated UO₂.</p> <p>Differences between the corrosion behavior of commercial spent nuclear fuel and unirradiated UO₂ are due to water radiolysis.</p>	<p>Do not incorporate into the TSPA-LA Model; data needed to apply the model can only be estimated.</p> <p>Use for Nominal Scenario Class model validation—particularly for validation of long-term extrapolation.</p>
Surface Complexation Model	<p>The overall rate of CSNF corrosion is controlled by the rate of surface complexation reactions.</p> <p>The long-term corrosion behavior of commercial spent nuclear fuel is similar to that of unirradiated UO₂.</p>	<p>Do not incorporate into TSPA-LA Model; data needed to apply the model can only be estimated from open literature.</p> <p>Use for Nominal Scenario Class model validation—particularly for validation of long-term extrapolation.</p>

Source: Table 6-13 in *CSNF Waste Form Degradation: Summary Abstraction* (BSC 2004 [DIRS 169987]).

Table 6.3.7-69. Alternative Conceptual Models Considered for High-Level Radioactive Waste Glass Degradation

Alternative Conceptual Model	Key Concepts	Screening Assessment and Basis
Diffusion-Controlled Release	Release rate of radionuclides determined by solid-state diffusion rates.	Not incorporated into TSPA-LA Model. Not supported by data for waste glasses.
Composition-Independent Effective Rate Constant	Intrinsic rate constants vary over a small interval for different compositions and the very low flow rates in the repository compared to those used in the laboratory mean that the affinity term will be low.	Not incorporated into TSPA-LA Model. Current approach provides a much more robust range of values for use in the TSPA-LA.

Source: *Defense HLW Glass Degradation Model* (BSC 2004 [DIRS 169988], Table 6-2).

Table 6.3.7-70. Alternative Conceptual Models Considered for Dissolved Concentration Limits

Element	Alternative Conceptual Model	Model Basis	Screening Assessment and Basis
Plutonium	The theoretical fO_2 model	$fO_2 = 0.2$ bars.	The results of this model differ significantly from experimental measurements.
	The empirical Eh model	$Eh = 1.04 - 0.0592 \cdot pH$.	The results of this model are lower than experimental results.
Neptunium	Neptunium incorporation into uranyl secondary phases	Neptunium concentration controlled by solid solution rather than by pure phases.	Experimental studies on whether secondary uranyl phase can incorporate neptunium and immobilize it during spent nuclear fuel corrosion do not provide a solid basis for recommending this model to be used in the TSPA-LA model.
Thorium	Solubility control by other thorium phases including ThO_2 (thorianite), $Th_{0.75}PO_4$, $Th(SO_4)_2$, ThF_4 , $ThF_4 \cdot 2H_2O$	Solubility of thermodynamically most-stable phase controls concentrations.	Solubilities calculated with $ThO_2(am)$ are consistent with measured thorium solubility in pure water. Other phases may be less soluble only under certain conditions or may be based on questionable data.
Americium	Solubility control by phase with properties between $Am(OH)_3(am)$ to $Am(OH)_3$	Initially formed $Am(OH)_3(am)$ will convert to more stable $Am(OH)_3$ with time. $Am(OH)_3$ stability decreases with time from self irradiation.	$AmOHCO_3$ is formed in americium solubility experiments under Yucca Mountain conditions. Under some conditions, $Am(OH)_3$ may be less soluble, but choosing $AmOHCO_3$ is, generally, conservative.
Radium	Solid solution (Ra, Ba, Sr, Ca) SO_4	None	Chemistry of in-package and invert waters are not so far outside the normal range of natural waters to cause different radium solubilities.
Technetium	Tc incorporation into epsilon or "5 metal" phases during CSNF corrosion	Tc in the epsilon particles may not be released when the fuel matrix corrodes.	Studies on fuel corrosion indicate the formation of Epsilon particles ("5 metal particles"). Tc in these particles may not be released when the fuel corrodes. Sparse data on this phenomenon, however, do not provide a solid basis for recommending this as a Tc model. Therefore, no solubility was defined, and inventory release should be in control.
Strontium	Solubility controlled by $SrCO_3$ or $SrSO_4$ or solid solution (Ra, Ba, Sr, Ca) SO_4	None	No solubility was defined, and inventory release should be in control. This is a conservative approach.
Tin	Solubility controlled by very insoluble crystalline phase cassiterite (SnO_2)	Solubility of thermodynamically most-stable phase controls concentrations	Solubilities calculated with $SnO_2(am)$ are consistent with measured Sn solubility in pure water. Other phases may form only under certain conditions.

Source: Modified from Table 6.23-1 in *Dissolved Concentration Limits of Radioactive Elements* (SNL 2007 [DIRS 177418]).

Table 6.3.7-71. Alternative Conceptual Models Considered for Colloids

Alternative Conceptual Model	Basis for Model	Screening Assessment
Kinetic Sorption	<p>This model provides a method for predicting sorption behavior beyond laboratory time scales. Allows interpretation of data from different time scales.</p> <p>Based on the model developed by Painter et al. (2002 [DIRS 174071]) and extended two- and three-site model developed by Wittman et al. (2005 [DIRS 174895]).</p>	<p>This ACM is screened out for the following reasons:</p> <ul style="list-style-type: none"> - Slow kinetic sorption rates are difficult to determine in laboratory tests that have been run for less than 150 days. - The lack of sufficient sorption data on colloids for sufficient time periods causes uncertainty in the extrapolation beyond the experimental times.
Rate of Colloid Generation	<p>Method for using markers for waste form corrosion for estimating colloid production.</p>	<p>This ACM is screened out for the following reasons:</p> <ul style="list-style-type: none"> - The model may overestimate colloid formation by not accounting for significant retention of actinides to the immobilized phase as has been observed in waste form corrosion experiments. - The model does not include colloids from CSNF and DSNF.
Mechanisms of Colloid Generation	<p>Mobile colloid generation will require large perturbations to the system that may not occur within the waste package. Furthermore, attachment of particles to air-water interfaces may limit mobile colloid generation.</p>	<p>This ACM is screened out for the following reasons:</p> <ul style="list-style-type: none"> - Data for Yucca Mountain related conditions are unavailable. - The process of attachment to air-water interfaces will depend on the degree of particle hydrophobicity. Smectite clays and iron oxyhydroxides in general will not attach to air-water interfaces but various oxides and U(VI) oxides phases may. - For flow rates similar to those anticipated in the repository waste package environment, there is no literature evidence to indicate mobile colloid generation.

Source: *Waste Form and In-Drift Colloids-Associated Radionuclide Concentrations: Abstraction and Summary* (SNL 2007 [DIRS 177423], Table 6-19).

NOTE: DHLWG = defense high-level waste glass.

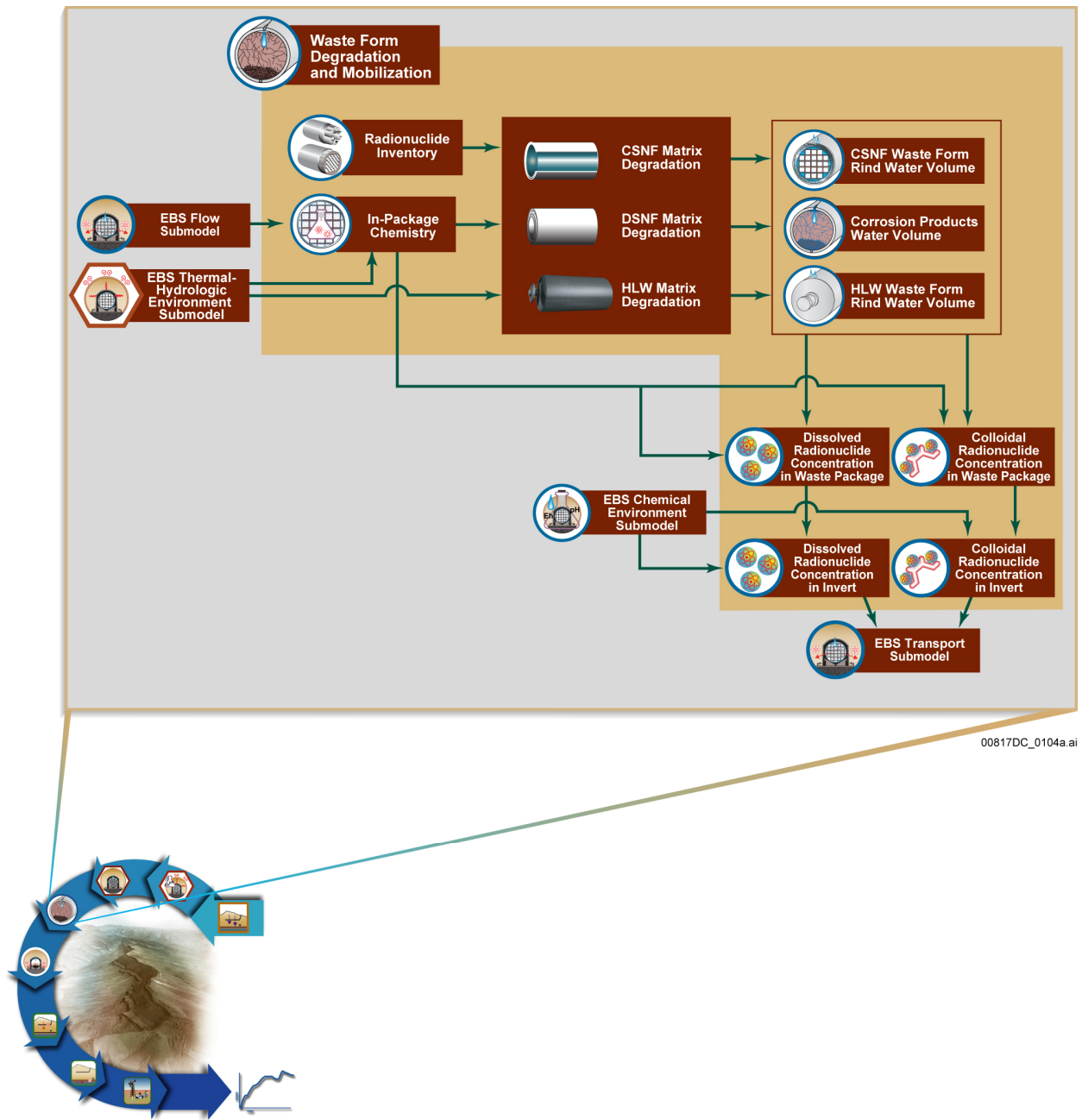


Figure 6.3.7-1. Information Flow Diagram for Waste Form Degradation and Mobilization

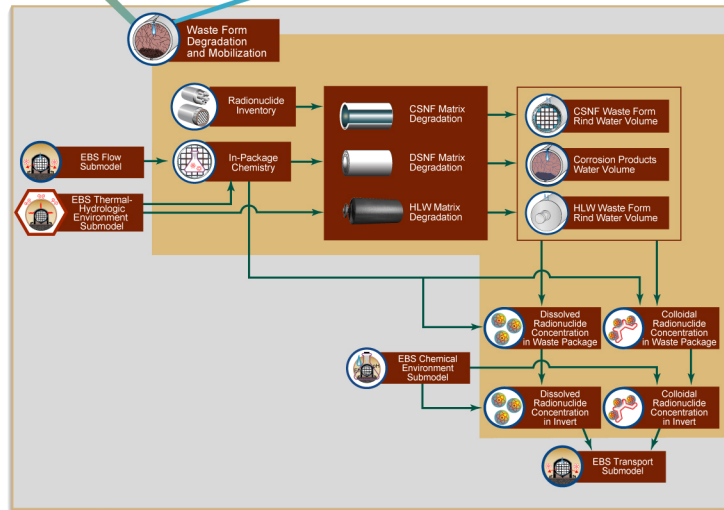
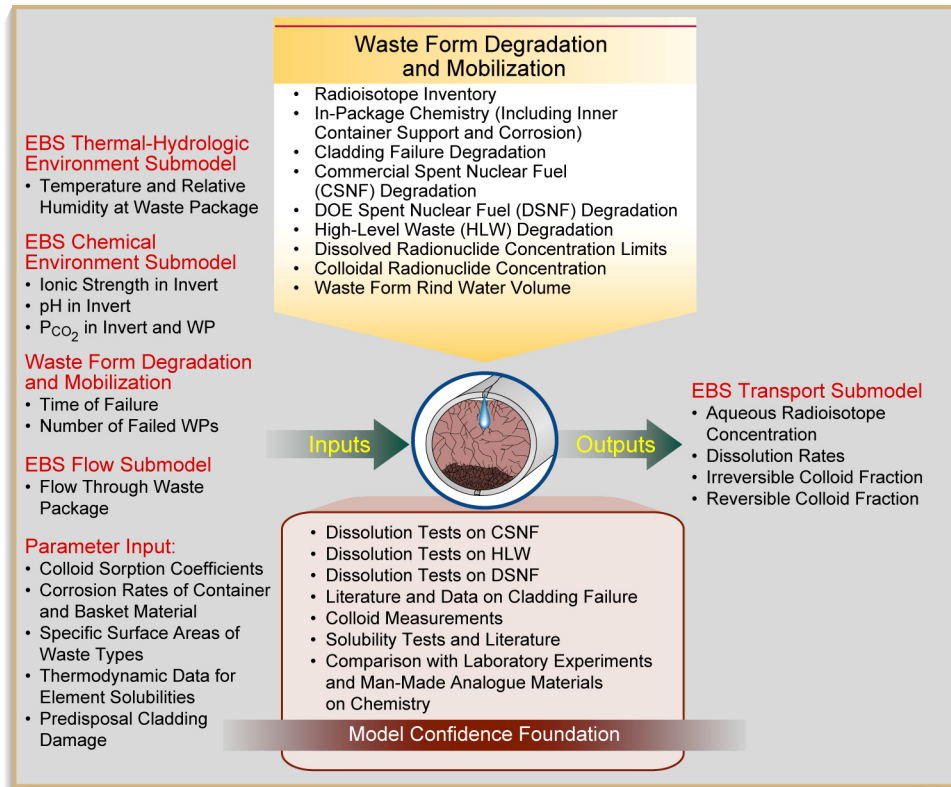
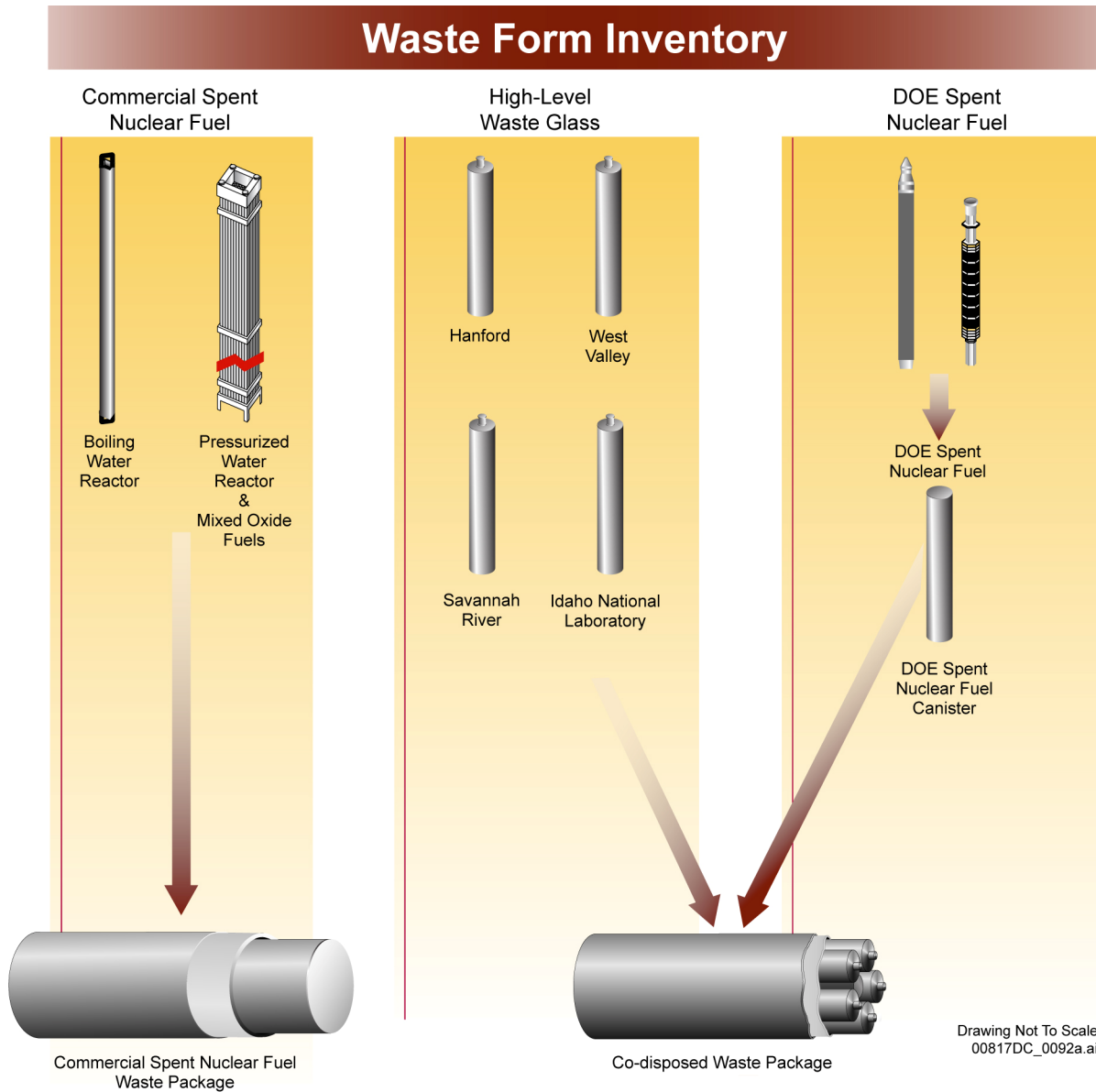


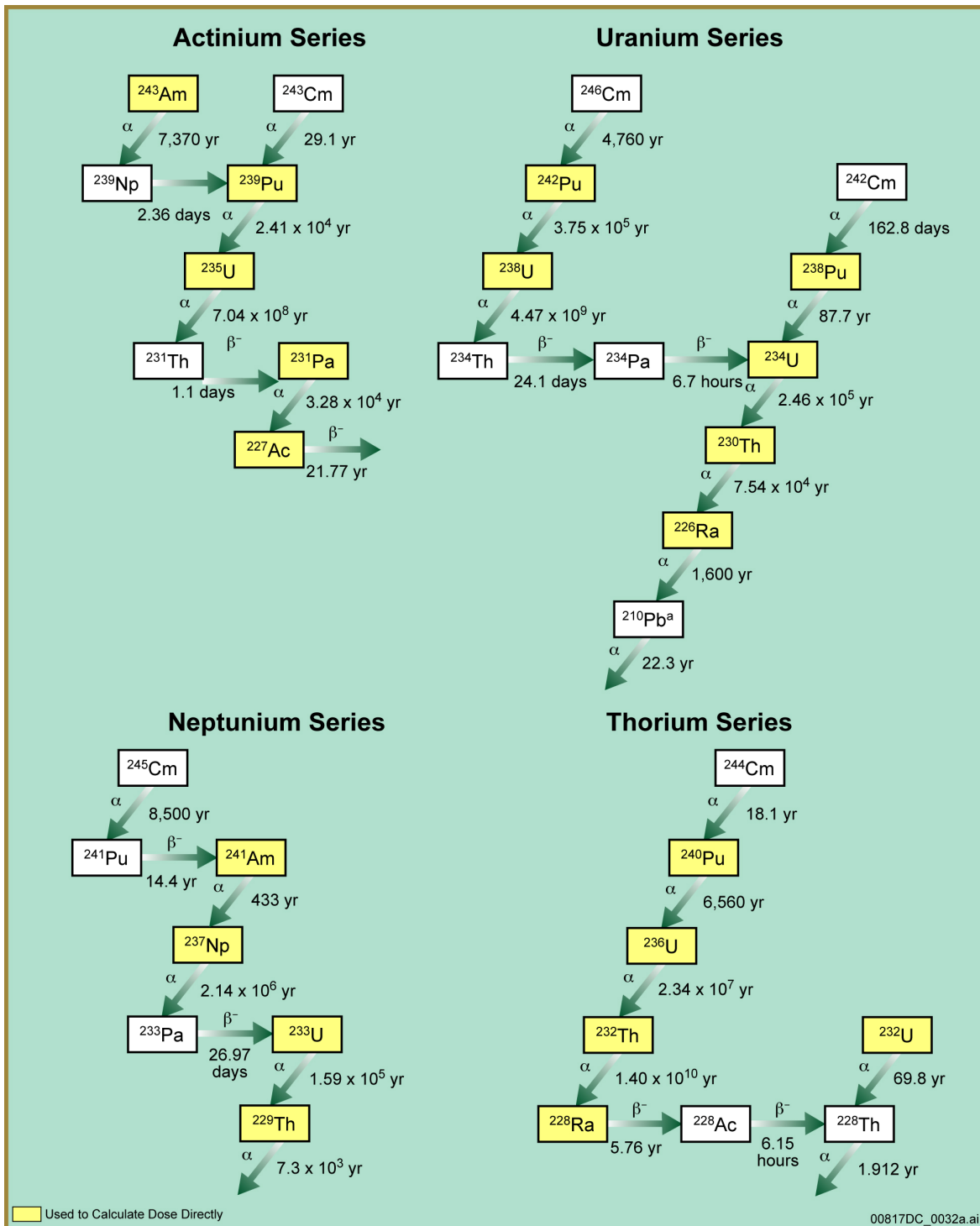
Figure 6.3.7-2. Inputs, Outputs, and Basis for Model Confidence for Waste Form Degradation and Mobilization



Source: Modified SNL 2007 [DIRS 180472], Figure 6-1.

NOTE: For modeling purposes, the naval waste packages are modeled as commercial waste packages.

Figure 6.3.7-3. Three Waste Types Grouped into Two Representative Waste Packages: CSNF and CDSP WPs



Source: Modified from Rechard 1993 [DIRS 147343], Volume 2 Appendices; and DTN: MO0702PASTREAM.001_R0 [DIRS 179925].

NOTE: Value listed under each radionuclide is the decay half-life for the radionuclide.

^a A series of short-lived daughters is between ^{226}Ra and ^{210}Pb . Also, ^{210}Pb is not used to calculate dose directly, but its biosphere dose conversion factor is included with that of ^{226}Ra .

Figure 6.3.7-4. Decay Chains of the Actinide Elements

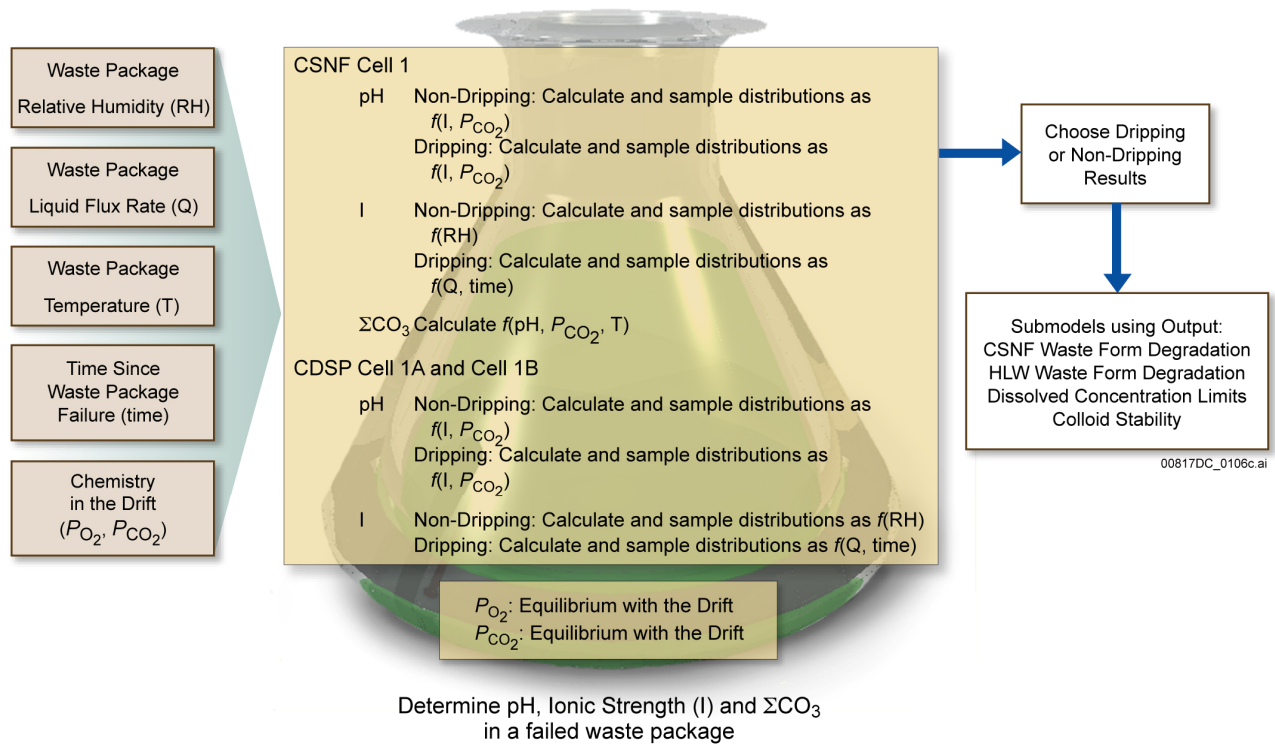


Figure 6.3.7-5. Implementation of the In-Package Chemistry Submodel

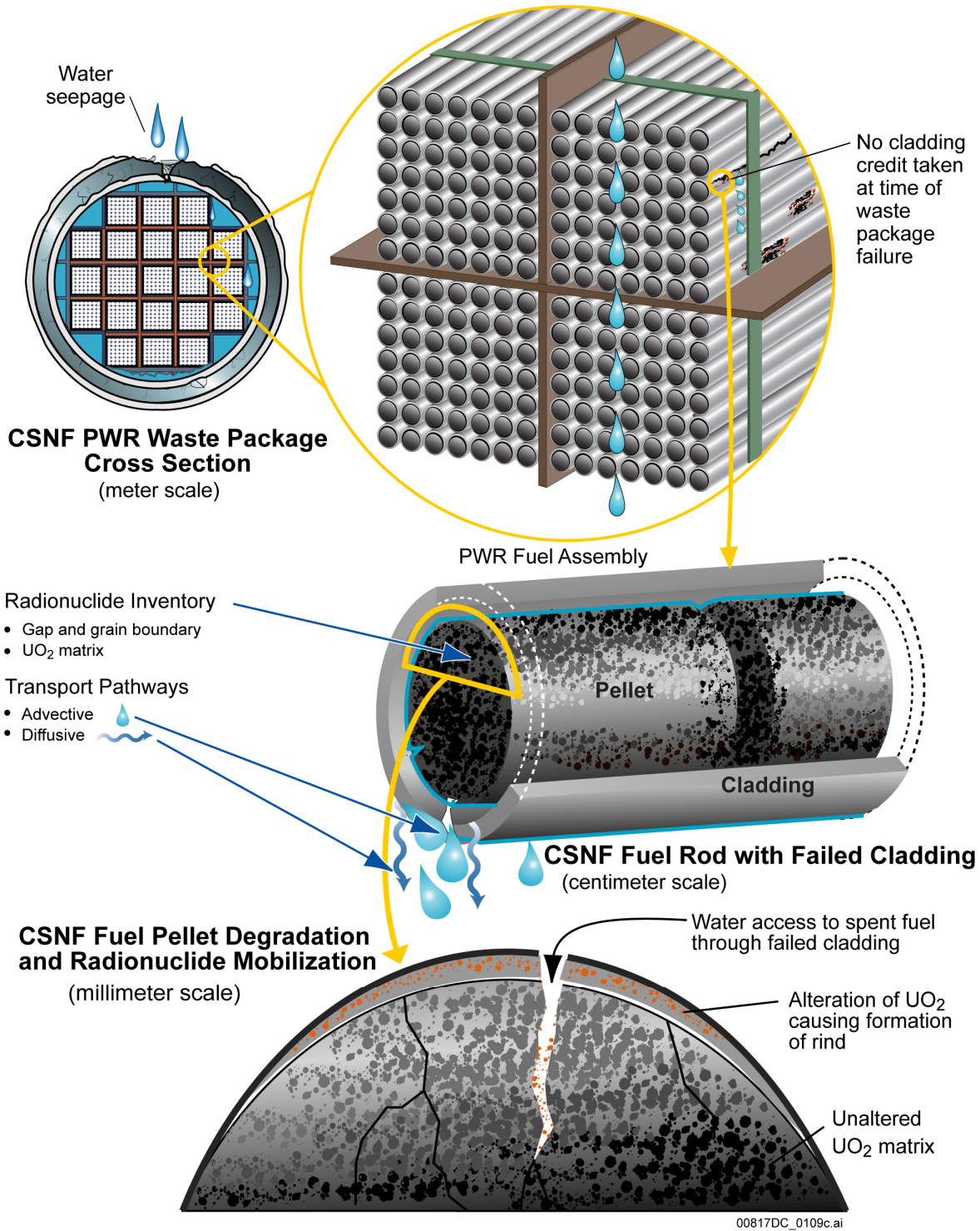


Figure 6.3.7-6. Schematic of CSNF Fuel Waste Form Degradation Mechanisms at Various Scales

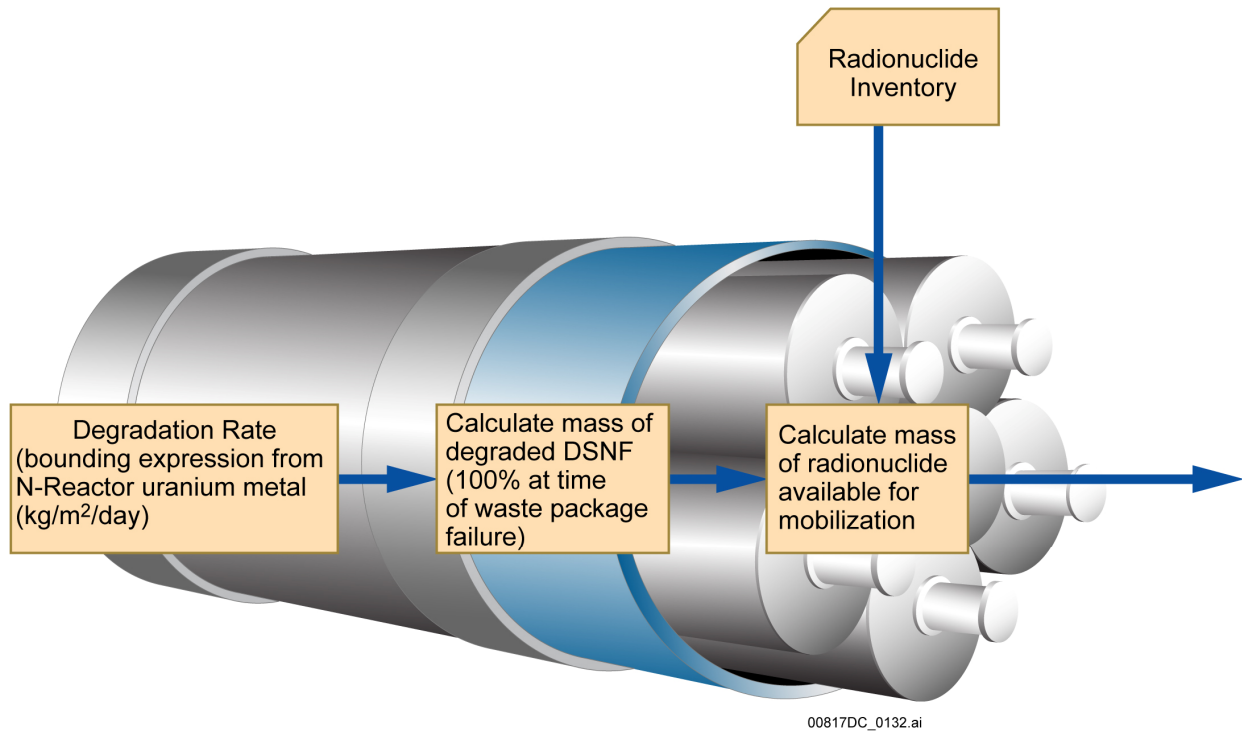


Figure 6.3.7-7. Implementation of the DSNF Degradation Submodel

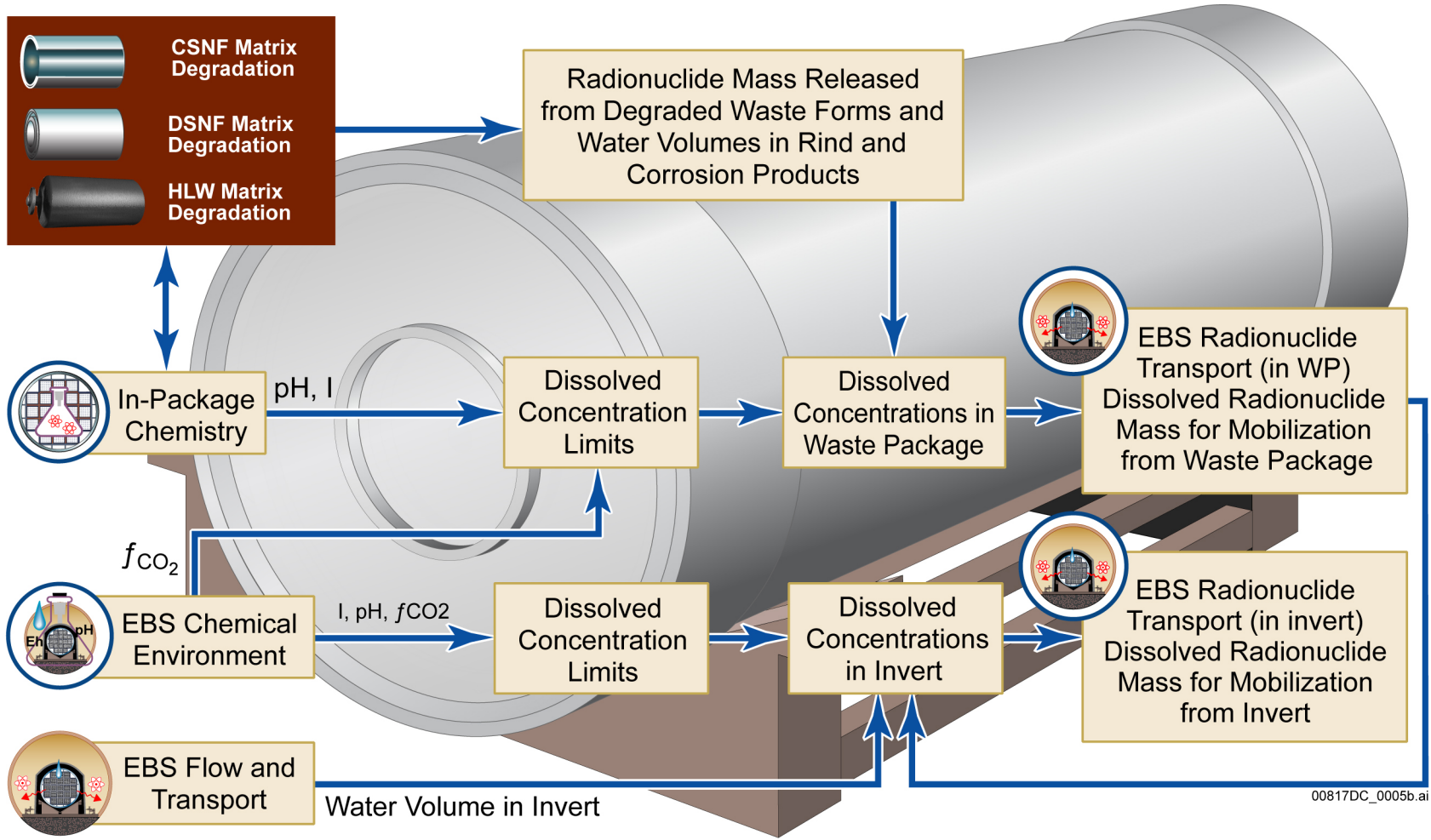
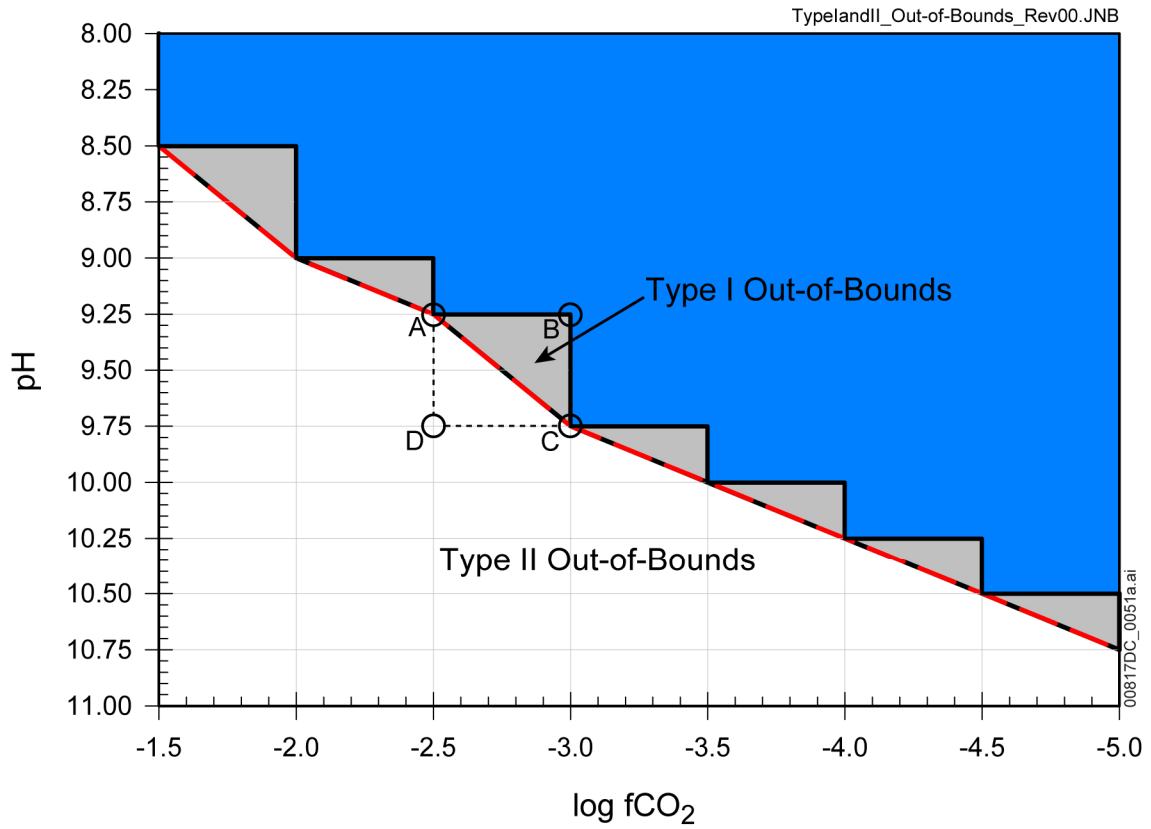
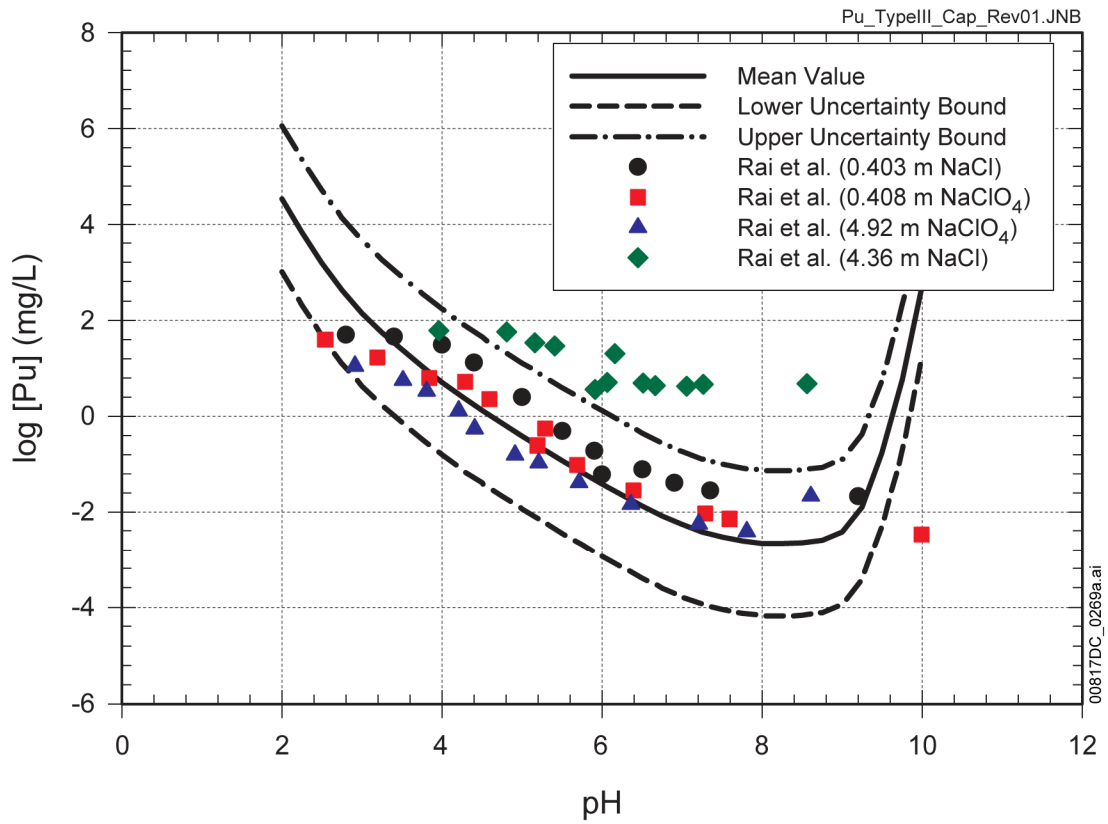


Figure 6.3.7-8. Connections between the Dissolved Concentrations Limits Submodel and Other TSPA-LA Submodels



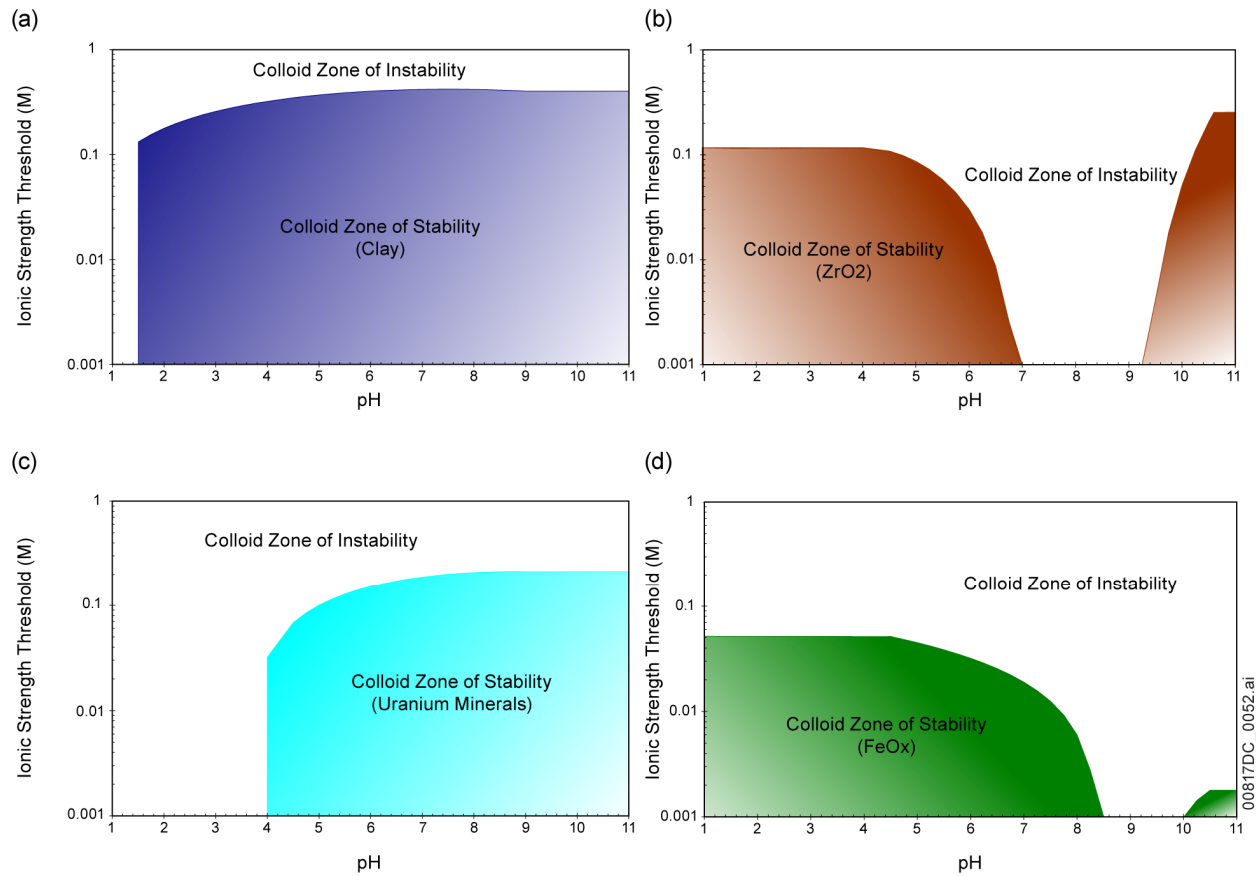
NOTE: Type I out-of-bounds can be removed by implementing a triangular interpolation scheme and a dynamic sampling approach for pH.

Figure 6.3.7-9. Illustration of Type I and Type II Out-of-Bound Conditions Using the Plutonium Solubility Model as an Example



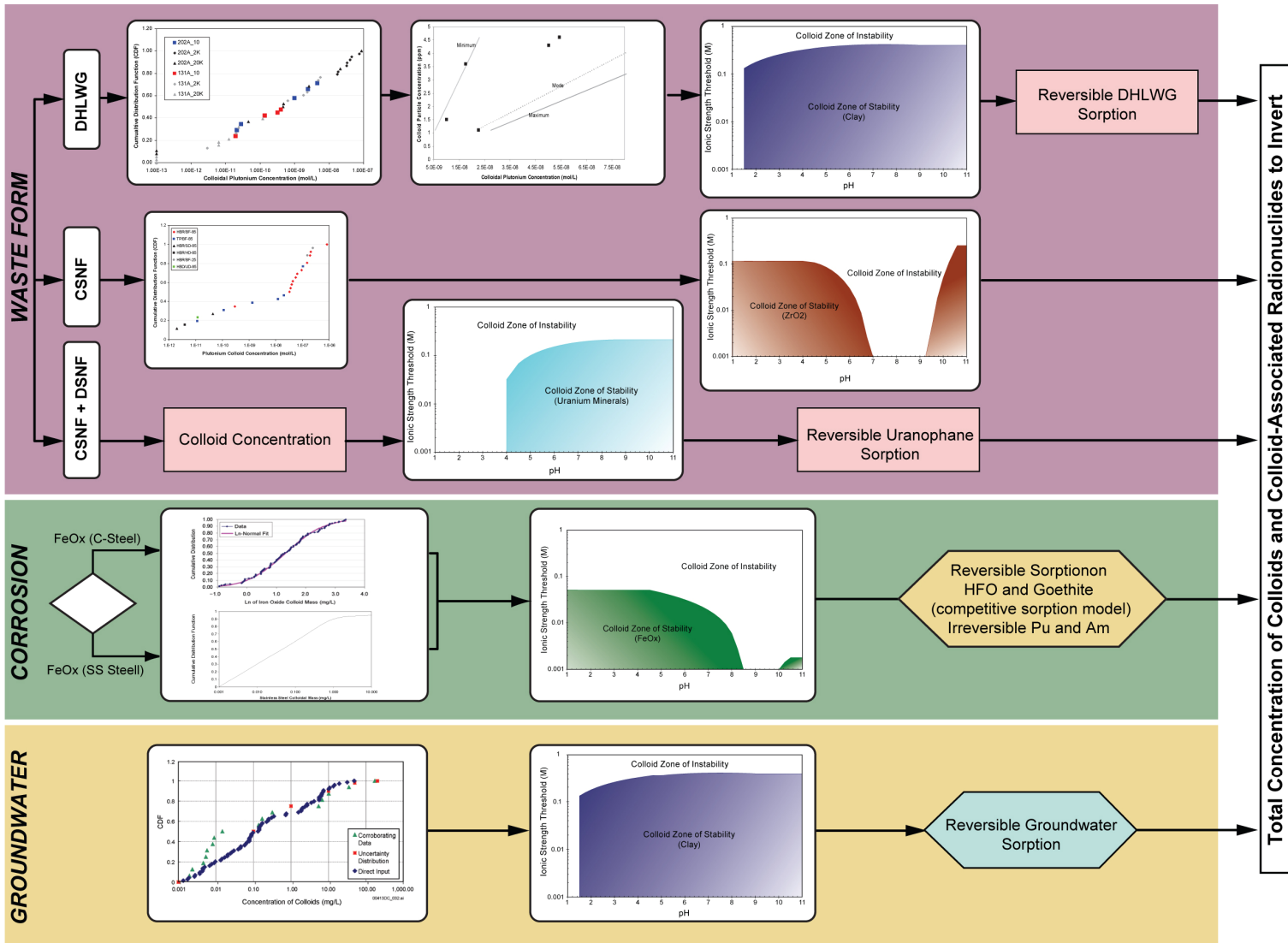
Sources: SNL 2007 [DIRS 177418], Table 6.5-1; and Rai et al. 2001 [DIRS 168392], Tables A.1 and A.2.

Figure 6.3.7-10. Comparison of the Solubility-Limited Dissolved Concentration Model for Plutonium



Source: Modified from SNL 2007 [DIRS 177423], Figures 6-9, 6-12, 6-14, and 6-5.

Figure 6.3.7-11. Schematic Representation of Colloid Suspension Stability as a Function of pH and Ionic Strength for (a) Groundwater and Glass Degradation Colloids (montmorillonite), (b) CSNF Residue Colloids (ZrO₂), (c) Uranium Mineral Colloids (meta-autunite), and (d) Steel Degradation Colloids (hematite)



Source: Modified from SNL 2007 [DIRS 177423], Figure 6-17.

Figure 6.3.7-12. Logic Diagram for Computing the Concentration and Stability of All Colloids in the Waste Package